UNIVERSIDADE DE LISBOA
FACULDADE DE CIÊNCIAS

Dissecting heat and drought tolerance in wheat and maize using plant systems biology

"Documento Definitivo"

Doutoramento em Biologia
Especialidade de Biologia de Sistemas

Pedro Miguel Pereira Correia

Tese orientada por:
Professor Doutor Jorge Marques da Silva e Professora Doutora Elizabete Carmo-Silva

Documento especialmente elaborado para a obtenção do grau de doutor

2021

UNIVERSIDADE DE LISBOA
FACULDADE DE CIÊNCIAS

Dissecting heat and drought tolerance in wheat and maize using plant systems biology

Doutoramento em Biologia

Especialidade de Biologia de Sistemas

Pedro Miguel Pereira Correia

Tese orientada por:

Professor Doutor Jorge Marques da Silva e Professora Doutora Elizabete Carmo-Silva

Júri:

Presidente:

- Doutor Rui Manuel dos Santos Malhó, Professor Catedrático e Presidente do Departamento de Biologia Vegetal, da Faculdade de Ciências da Universidade de Lisboa

Vogais:

- Doutor Mauro Guida dos Santos, Professor Associado do Centro de Biociências da Universidade Federal de Pernambuco, Brasil
- Doutora Elizabete Carmo-Silva, Senior Lecturer do Lancaster Environment Centre da Lancaster University, Reino Unido, orientadora
- Doutor Jaume Flexas Sans, Catedrático de universidad do Departamento de Biología da Universitat de les Illes Balears, Espanha
- Doutora Cristina Maria Nobre Sobral de Vilhena da Cruz Houghton, Professora Auxiliar com Agregação da Faculdade de Ciências da Universidade de Lisboa

PD/BD/130973/2017

Documento especialmente elaborado para a obtenção do grau de doutor

2021

Pedro Miguel Pereira Correia foi bolseiro de doutoramento no âmbito do programa doutoral BioSys - Sistemas Biológicos, Genómica Funcional & Integrativa da Faculdade de Ciências da Universidade de Lisboa (FCT/PD/00065/2012), financiado pela Fundação para a Ciência e Tecnologia do Ministério da Educação e Ciência, Bolsa PD/BD/130973/2017.

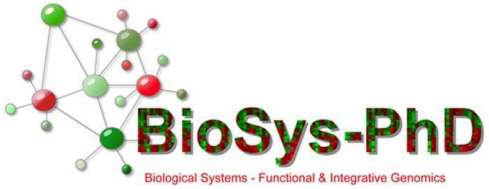

De acordo com o disposto no artigo 24º do Regulamento de Estudos de Pós-Graduação da Universidade de Lisboa, Despacho nº 7024/2017, publicado no diário da República – 2a Série – nº 155 – 11 de Agosto de 2017, foi incluído nesta dissertação dois artigos de científicos publicados:

Correia PMP, Silva AB, Roitsch T, Carmo-Silva E, Marques da Silva J, (2021) Photoprotection and optimization of sucrose usage contribute to faster recovery of photosynthesis after water deficit at high temperatures in wheat. Physiol Plant 172:615–628. https://doi.org/10.1111/ppl.13227

Correia PMP, da Silva AB, Vaz M, et al (2021) Efficient regulation of CO2 assimilation enables greater resilience to high temperature and drought in maize. Front Plant Sci 12:1505. https://doi.org/10.3389/FPLS.2021.675546

Um artigo científico submetido para publicação:
Correia PMP, Westergaard JC, da Silva AB, Roitsch T, Carmo-Silva E, Marques da Silva J, (2021) Functional high-throughput phenotyping for wheat resilience to high temperature and water deficit – em preparação para submissão no Journal of Experimental Botany

Durante o período de realização deste trabalho, Pedro Correia foi co-autor dos seguintes trabalhos, não incluído neste trabalho:

Marques Da Silva J, Correia P, Calejo Pires M, Soares Augusto J, Miguel Costa J, (2020) Interdisciplinarity in action: Using infrared thermography to teach plants' energy balance in secondary education. In: 15th Quantitative InfraRed Thermography Conference doi:10.21611/qirt.2020.062

Barradas A, Correia PMP, Silva S, et al (2021) Comparing Machine Learning Methods for Classifying Plant Drought Stress from Leaf Reflectance Spectra in Arabidopsis thaliana. Appl Sci 2021, Vol 11, Page 6392 11:6392. https://doi.org/10.3390/APP11146392.

No cumprimento do disposto da referida deliberação, o autor esclarece serem da sua responsabilidade, exceto quando referido o contrário, a execução das experiências que permitiram a elaboração dos resultados apresentados, assim como da interpretação e discussão dos mesmos. Os resultados obtidos por outros autores foram incluídos com a autorização dos mesmos para facilitar a compreensão dos trabalhos e estão assinalados nas respetivas figuras e metodologias.

Acknowledgements

I would like to express my gratitude to those people who have contributed to this great experience, in which I was able to grow both as a scientist and as a person.

Aos meus orientadores, **Professores Jorge Marques da Silva** e **Elizabete Carmo-Silva**, por me proporcionarem esta inestimável oportunidade de prosseguir o meu caminho como investigador científico, por todo o suporte e apoio, pela disponibilidade e tempo dispensado, por reverem inúmeros relatórios, posters, manuscritos e a tese e pela atenção ao detalhe. À **Professora Anabela Bernardes da Silva,** por ter sempre seguido o meu trabalho de perto, por todo o apoio, disponibilidade para discutir os meus resultados e partilhar o seu vasto conhecimento científico. To our collaborators at Copenhagen University – A special thank you goes to **Professor Thomas Roitsch,** for welcoming me into his research group. **Rene Hvidberg Petersen,** for the support in plant growth. **Mengistu Mekureyaw** and **Daniel Amby,** for the assistance in the lab. **Jesper Cairo Westergaard,** for the support in image analysis. To the **Photosynthesis group at the Lancaster Environment Centre,** for sharing much of their practical knowledge in diverse techniques with me, so essential at the beginning of my PhD. À **Professora Isabel Abreu,** pelo feedback crítico enquanto membro do meu do meu comité científico de tese. Aos meus colegas de laboratório, **Hamilton Chiango** e **André Cartaxana**, por toda a ajuda essencial em projetos paralelos, por tornarem o tempo passado no lab/gabinete mais agradável, por todas as discussões nos mais diversos temas e companhia nas caminhadas e almoços na "Velha". Às minhas colegas no projeto Optimal, **Juliana Melo** e **Mafalda Pastaneira,** pela agradável companhia no laboratório e nas saídas de campo aos pomares de Alcobaça. À **"Dona" Manuela Lucas**, pelo seu sentido de organização laboratorial que a bem ou mal nos incutiu, pelo seu enorme sentido prático e capacidade de "desenrascanço", por me ter "valido" imensas vezes e por todos os cafés da manhã. Aos meus colegas da **4ª edição do BioISI**, por todos os finais de tarde nos 100 Montaditos, jantares, noites bem passadas e incríveis retiros "científicos". Por fim à **minha família**, por todo o apoio e a quem devo grande parte dos meus princípios e valores humanos. **À Filipa,** estes caracteres nunca serão suficientes para agradecer todo o apoio nos momentos mais negros e todo o companheirismo nos bons momentos.

I am also highly grateful for the public funding that directly or indirectly allowed me to have time and resources to do my research, through the **Fundação para a Ciência e a Tecnologia** (Portugal), **EPPN2020** (EU), **Danish National Research Foundation** (DK) and **Biotechnology and Biological Sciences Research Council** (UK).

OBRIGADO! THANK YOU!

Summary

Population growth and climate change pose serious threats to food security. Heat and drought are major abiotic constraints to crop production and their co-occurrence will increase during the cropping season in several regions. However, there is a lack of studies investigating their combined effect in crop physiological and biochemical processes. Aiming to close this gap, two of the main crops were investigated, wheat and maize, under these conditions.

In the **first results chapter,** it is shown that these co-occurring stresses equally affect the photosynthetic efficiency of genotypes adapted to Mexico (Sokoll) and the UK (Paragon). However, Paragon recovered faster upon stress relief due to an increased PSII photoprotection and cytosolic Invertase activity, suggesting that optimal sucrose export/utilization and increased electron transport machinery photoprotection are essential to limit wheat yield fluctuations under these conditions.

In the **second results chapter**, by studying maize genotypes with contrasting drought or heat tolerance, it was observed that limited transpiration under high temperature allowed water saving upon deficit without decreasing photosynthetic efficiency. This was sustained by higher phosphorylated PEPC and electron transport rate. Limited transpiration rate and synchronized regulation of the C_4 carbon assimilation metabolism showed to be key traits for drought and heat tolerance in maize.

In the **third results chapter**, by screening ten wheat genotypes with different tolerance to drought or heat, it was observed that leaf temperature and evapotranspiration expressed significant genotype-environment interactions. Low leaf number and transpiration efficiency were essential to balance water-saving strategies and biomass production. Changes in the carbohydrate (cytosolic Invertase, Hexokinase, Phosphofructokinase) and antioxidant metabolism (Peroxidases, phenolic compounds) were associated with tolerance mechanisms.

Altogether, these results expand our knowledge about crops metabolic responses to high temperature and water deficit. These findings can be further explored in breeding programs to improve crop resilience to climate change and meet food security.

Key words: drought tolerance, global warming, heat tolerance, maize, *Triticum aestivum*, water deficit, wheat, *Zea mays*.

Resumo

O crescimento acentuado da população humana tem aumentado a procura de alimentos e de novas áreas aráveis, levando ao desgaste dos ecossistemas e diminuição da biodiversidade. Paralelamente, o aumento do uso de combustíveis fosseis após a revolução industrial e as mudanças de estilo de vida levaram ao aumento da poluição, incluindo a subida da concentração de CO_2 atmosférico. A acumulação destas pressões antropogénicas estão a levar a alterações climáticas significativas, ao nível global. Neste cenário, torna-se um desafio muito exigente garantir a segurança alimentar para a crescente população humana. Para alcançá-lo, é necessário aumentar a produtividade das principais culturas agrícolas e a sua tolerância aos fatores climáticos adversos, evitando ampliar a área atualmente cultivada.

De entre as alterações climáticas, as ondas de calor e episódios de seca são as que têm causado mais dano na produção agroalimentar nas últimas décadas. O aumento da temperatura a nível global e da frequência e intensidade de ondas calor e de episódios de seca são esperados, tornando imperativo estudar os efeitos do stresse térmico e do stresse hídrico nas plantas. Apesar da ocorrência simultânea destes stresses em algumas das principais regiões agrícolas do mundo, existem poucas investigações que estudem o efeito da sua coocorrência. O impacto da combinação destas duas pressões ambientais não pode ser visto como a simples soma da resposta aos estímulos singulares, pois têm efeitos sinergéticos ou antagónicos e a resposta combinada poderá requerer mecanismos compensatórios únicos e a interação cruzada entre diferentes vias metabólicas a diferentes níveis, tornando essencial investigar a resposta ao stresse combinado.

A fotossíntese é um processo chave na fisiologia das plantas, servindo de sensor a stresses abióticos, e sendo um dos principais fatores determinantes para a produtividade das plantas. O impacto de stresses abióticos, e a concomitante resposta fisiológica, está dependente do equilíbrio entre os processos fotossintéticos que ocorrem ao nível dos tilacoides (transporte eletrónico) e a fixação de carbono, bem como da resposta de vias metabólicas acessórias, tais como a síntese e partição de hidratos de carbono e a resposta antioxidante. Consequentemente, alterações no crescimento e desenvolvimento, bem como na aclimatação ao stresse, estão diretamente interligadas com ajustes metabólicos nestas vias, tornando imperativo investigar o impacto do stresse combinado de seca e elevadas temperaturas.

Neste contexto, este trabalho debruça-se sobre o efeito do défice hídrico a elevadas temperaturas em duas das plantas agrícolas mais produzidas a nível global, o milho (*Zea mays* L.) e o trigo (*Triticum aestivum* L.). Estas plantas foram selecionadas pois, além da relevância na produção alimentar, utilizam dois mecanismos fotossintéticos diferentes, C_3 em

trigo e C_4 em milho. O principal objetivo desta tese é o de contribuir para uma melhor compreensão dos mecanismos de tolerância a seca em elevadas temperaturas, com especial atenção aos processos fotossintéticos. Para isso, estudaram-se as estratégias de resposta de genótipos adaptados a diferentes climas ou com diferentes níveis de tolerância a seca ou elevadas temperaturas, submetendo-os a duas temperaturas diferentes (25ºC vs 38ºC) com ou sem défice hídrico.

O **primeiro capítulo de resultados** deste trabalho teve como intuito comparar a eficiência fotossintética de dois cultivares de trigo, Sokoll e Paragon, adaptados ao clima do México e do Reino Unido, respetivamente, quando sujeitos a condições de seca e elevadas temperaturas. Para esse efeito, estes foram expostos na fase vegetativa a uma semana de défice hídrico (suspendendo a rega mas mantendo no mínimo 30% de água no solo comparativamente à capacidade de campo) e elevadas temperaturas (25ºC vs 38ºC), isoladamente ou em efeito combinado. Nos genótipos, quando sujeitos a seca em elevadas temperaturas, as principais limitações fotossintéticas resultaram da diminuição da condutância estomática e da taxa de transporte eletrónico. Os parâmetros de fluorescência da clorofila *a* indicaram claramente diferenças entre os genótipos nos mecanismos de fotoproteção do fotossistema II sob o stresse combinado. Especificamente, Paragon evidenciou uma maior capacidade de dissipação de energia durante o stresse e uma mais rápida recuperação após a remoção deste. A atividade de Invertase citosólica durante o stresse combinado está fortemente relacionada com a rápida recuperação de Paragon. Os resultados sugerem que uma exportação e/ou utilização otimizada de sacarose e um aumento da fotoproteção do fotossistema II são componentes importantes para limitar as flutuações de rendimento de trigo associadas a condições de seca a elevadas temperaturas.

No **segundo capítulo de resultados** foi testado se a tolerância a condições de seca em elevadas temperaturas, em milho, é regulada por um sistema fotossintético mais eficiente, relacionado com o mecanismo de concentração de CO_2 existente em plantas C_4. Para tal, dois genótipos de milho com diferentes níveis de tolerância a seca e a elevadas temperaturas (B73, sensível, e P0023, tolerante) foram sujeitos a uma semana de défice hídrico (mantendo no mínimo 30% de água no solo comparativamente à capacidade de campo) e elevadas temperaturas (25ºC vs 38ºC), isoladamente ou em efeito combinado, na fase vegetativa. Ambos os genótipos aclimatizaram com sucesso a condições de elevadas temperaturas, mas através de mecanismos diferentes. Enquanto B73 manteve a mesma taxa fotossintética aumentando a condutância estomática, P0023 manteve a taxa fotossintética limitando a taxa de transpiração. Quando as plantas foram submetidas a condições de elevadas temperaturas combinadas com seca, a transpiração limitada de P0023 permitiu reduzir a perda de água atuando como um mecanismo de evasão à seca. A eficiência fotossintética de P0023 foi sustentada por altos níveis de fosforilação de PEPC e da taxa de transporte eletrónico nos

cloroplastos de células próximas dos feixes vasculares, taxa essa capaz de fornecer energia essencial para o correto funcionamento do mecanismo de concentração de CO_2. Os resultados sugerem que as características-chave para tolerância à seca a elevadas temperaturas em milho são uma limitação da taxa de transpiração, em condições de elevada demanda transpiratória, o nível de fosforilação de PEPC e o controlo da atividade de PSII nos cloroplastos de células próximas dos feixes vasculares. As descobertas deste capítulo poderão ser exploradas em futuros programas de melhoramento de milho com o intuito de aumentar a tolerância deste a condições de seca em elevadas temperaturas.

No **terceiro capítulo de resultados** foi realizada uma monotorização do crescimento na fase vegetativa de dez genótipos de trigo com diferentes níveis de tolerância a seca ou calor numa estação de alto-débito de fenotipagem, em condições de elevadas temperaturas (38ºC) com ou sem deficit hídrico (induzido por suspensão da rega, mas mantendo no mínimo 30% de água no solo comparativamente à capacidade de campo). Com o objetivo de encontrar características fenotípicas que conferem respostas adaptativas ao stresse em trigo, os genótipos foram classificados segundo o seu uso de água e dinâmicas de crescimento. As características relacionadas com a temperatura das folhas e evapotranspiração demonstraram uma interação genótipo-ambiente significativa ao longo da progressão do stresse, indicando maior plasticidade. Características como baixo número de folhas e eficiência transpiratória foram identificadas como essenciais para a manutenção do balanço entre estratégias de poupança de água e produção de biomassa. Para estabelecer uma interação entre a regulação do metabolismo dos hidratos de carbono e antioxidante e a tolerância ao stresse, no final do ensaio foi avaliada a atividade enzimática de algumas enzimas-chave destas vias metabólicas. A tolerância ao stresse foi relacionada com alterações na atividade de enzimas das vias sucrolítica (Invertase citosólica), glicolítica (Hexocinase e Fosfofrutocinase) e antioxidante (Peroxidases) e com o aumento da produção de compostos fenólicos.

Em suma, este trabalho fornece uma visão integrada dos mecanismos de resposta a seca a elevada temperatura em trigo e milho, contribuindo desta forma para uma melhor compreensão dos processos essenciais envolvidos na tolerância ao stresse. Além disso, estes resultados podem ser explorados em programas de melhoramento de variedades agrícolas, tornando-as mais resilientes às alterações climáticas, e ajudando, assim, a garantir a segurança alimentar.

Main table of contents

List of tables

List of figures

List of abbreviations

2-PG - 2-phospho-glycolate

3-PGA - 3-phosphoglycerate

A - CO_2 assimilation rate

ABTS - 2,2′-Azino-bis (3-ethylbenzothiazoline-6-sulfonic acid) diammo-nium salt

AerialDW - aboveground biomass

AGPase- ADP-glucose pyrophosphorylase

Ald - Aldolase

AOI - area of interest

APX - Ascorbate peroxidase

area.low - area exposed extracted from images

ATPase - ATP-synthase

BMV ETR - between mid-vein ETR

BGLM - Bayesian Generalized Linear Model

BLASSO - Bayesian Lasso

BSC - bundle sheath cells

CA - Carbonic anhydrase

CAT - Catalase

CBBC - Calvin-Benson-Bassham cycle

CCM - CO_2 concentrating mechanism

CIMMYT - International Maize and Wheat Improvement Center

Cytb$_6$f - cytochrome b_6f

cytINV - cytosolic Invertase

DAS - days after sowing,

DTT - 1,4-dithiothreitol

DW - dry weight

E - transpiration rate

E4P - erythrose-4-phosphate

EDTA – ethylenediamine tetraacetic acid

ETR - electron transport rate

ETRmax - maximum ETR

Evap - evapotranspiration

FBP - fructose-1,6-bisphosphate

FBPase - Fructose-1,6-bisphosphatase

Fdr - Benjamini-Hochberg false discovery rate

Fm - maximal chlorophyll *a* fluorescence

Fo - minimal chlorophyll *a* fluorescence

FRAP - ferric reducing antioxidant power

Fv/Fm - maximum quantum efficiency of PSII

FW - fresh weight

G3P - glyceraldehyde-3-phosphate

G6PDH - Glucose-6-phosphate dehydrogenase

GLM - Generalized Linear Model

GLMNET - Elastic-Net Regularized Generalized Linear Models

GOD - Glucose oxidase from *Aspergillus niger*

GPDH - Glycerol-3-phosphate dehydrogenase

GP-Poly - Gaussian Process with Polynomial Kernel

GPX - Glutathione peroxidase

GR - Glutathione reductase

gs - stomatal conductance

GST - Glutathione S transferase

GxE - genotype-environment interaction

HXK - Hexokinase

IC50 - half-maximal inhibitory concentration

INV - Invertase

IPCC - Intergovernmental Panel for Climate Change

IRGA - infra red gas analyzer

J^{ABS} - absorbed photon flux

J^{DI} - dissipated energy flux

J_o^{RE1} - electron transport flux until PSI acceptors

J_o^{TR} - maximum trapped exciton flux

L ETR - total leaf area ETR

LASSO - Lasso Model

LDW - leaf dry weight

LeafT - leaf temperature

LHCII - light-harvesting complex from PSII

LOD - log probability of corrected P-value

LRWC - leaf relative water content

LTW - leaf turgid weight

LWP - leaf water potential

MC - mesophyll cells

MLR - Multivariate Linear Regression

MRSRE - root mean squared relative error

MV ETR- midvein ETR

NAD-ME - NAD-dependent malic enzyme

NADP-ME - NADP-dependent malic enzyme

nCDA - normalized Canonical Discriminant Analysis

NPQ - non-photochemical quenching

OEC - oxygen-evolving complex

PCC - Pearson correlation coefficient

PEP - phosphoenolpyruvate

PEPC - Phosphoenolpyruvate carboxylase

PEPCK - Phosphoenolpyruvate carboxykinase

PFK - Phosphofructokinase

PGI - Phosphoglucoisomerase

PGM - Phosphoglucomutase

PI^{ABS} - performance index for energy conservation from photons absorbed by PSII antenna to the reduction of QB

PI^{TOTAL} - performance index for energy conservation from photons absorbed by PSII antenna until the reduction of PSI acceptors

PLS-DA - partial least squares-discriminant analysis

PMSF - phenylmethylsulfonyl fluoride

POD - Peroxidase from horseradish

POX - Peroxidase

PPDK - Pyruvate orthophosphate dikinase

PPFD - photosynthetic photon flux density

PRK - Phosphoribulokinase

PsbS - PSII subunit S

PSI - photosystem I

PSII - photosystem II

PVP - polyvinylpyrrolidone

qE - energy-dependent quenching

qI - photoinhibitory quenching

qN - non-photochemical quenching

qT - state-transition quenching

R5P - ribose-5-phosphate

RCA - Rubisco activase

Reflect - reflectance

RGR - relative growth rate

RH - relative humidity

RIDGE - Ridge Regression

RLCs - chlorophyll *a* fluorescence rapid light curves

ROI - region of interest

RootDW - root dry biomass

ROS - reactive oxygen species

RPE - Ribulose-5-phosphate epimerase

RPI - Ribose-5-phosphate isomerase

Rubisco - Ribulose-1,5-bisphosphate carboxylase/oxygenase

RuBP - ribulose-1,5-bisphosphate

RWD38°C - recovery from well-watered at 38ºC

RWW38°C - recovery from water deficit at 38ºC

S7P - sedoheptulose-7-phosphate

SATYN - Stress Adapted Trait Yield Nurseries trial

SBP - Sedoheptulose-1,7-bisphosphate

SBP ald - Sedoheptulose-1,7-bisphosphate aldolase

SBPase - Sedoheptulose-1,7-bisphosphatase

SDW - soil dry weight

SFC - soil field capacity

Sm - number of electron carriers per electron transport chain

SOD - Superoxide dismutase

SRWC - soil relative water content

Svm - support vector machine

SVM-Linear - SVM with Linear Kernel

TEAC - trolox equivalents antioxidant capacity

TK - Transketolase

Tmax - time point of maximum biomass

TPTZ - 2,4,6-tripyridyl-s-triazine

Trolox - 6-hydroxy-2,5,7,8-tetramethylchroman-2-carboxylic acid

TSP - total soluble protein

vacINV - vacuole Invertase

Vi - Rubisco initial activity

VIFs - variance inflation factors

Vmax - enzyme maximal activity

Volumepyr - plant pyramidal volume

VPD – vapour-pressure deficit

Vphysiol - enzyme physiological activity

Vt - Rubisco total activity

WD - water deficit

WD25 - water deficit at 25ºC

WD25ºC - water deficit at 25ºC

WD38 - water deficit at 38ºC

WD38ºC - water deficit at 38ºC

WUE - water use efficiency

WW - well-watered

WW25 - well-watered at 25ºC

WW25°C - well-watered at 25ºC

WW38 - well-watered at 38ºC

WW38°C - well-watered at 38ºC

Xu5P - xylulose-5-phosphate

ΔChlF - variable chlorophyll *a* fluorescence

μ - predictive bias

ΦPSII - effective quantum efficiency of PSII

Chapter I

General introduction and research objectives

Table of Contents – Chapter I

1.1 Food security and sustainable land use

The world's population at the end of 2020 surpassed 7.8 billion people (Worldometers.info 2020), and at this rate, around 10 billion will live on our planet by 2050 (Figure 1.1A) (United Nations, Department of Economic and Social Affairs 2019). However, the global increase masks the differences between regions. In particular, while Europe, North America and Oceania stabilised their population since the beginning of the century, South America and Asia will only reach their population peak at the middle of the century. Furthermore, the population increase in the Near East and North Africa will only halt near the end of the century, whereas the Sub-Saharan Africa population will continuously increase until the end of the century (Figure 1.1B) (FAO 2017). The regions where the population is growing faster are associated with low-income countries where most of the population have unreliable food availability and health care, causing a serious threat to food security. The populational growth in these regions is expected to lead to migratory fluxes, already experienced in Europe and North America, competition, overexploitation, and unsustainable use of natural resources (Alexandratos and Bruinsma 2012). Increased resource competition and migration can also catalyse conflict (Hendrix and Glaser 2007; Mbow et al. 2019). Consequently, this cannot be regarded as a regional problem as these socioeconomic and environmental pressures will have global repercussions.

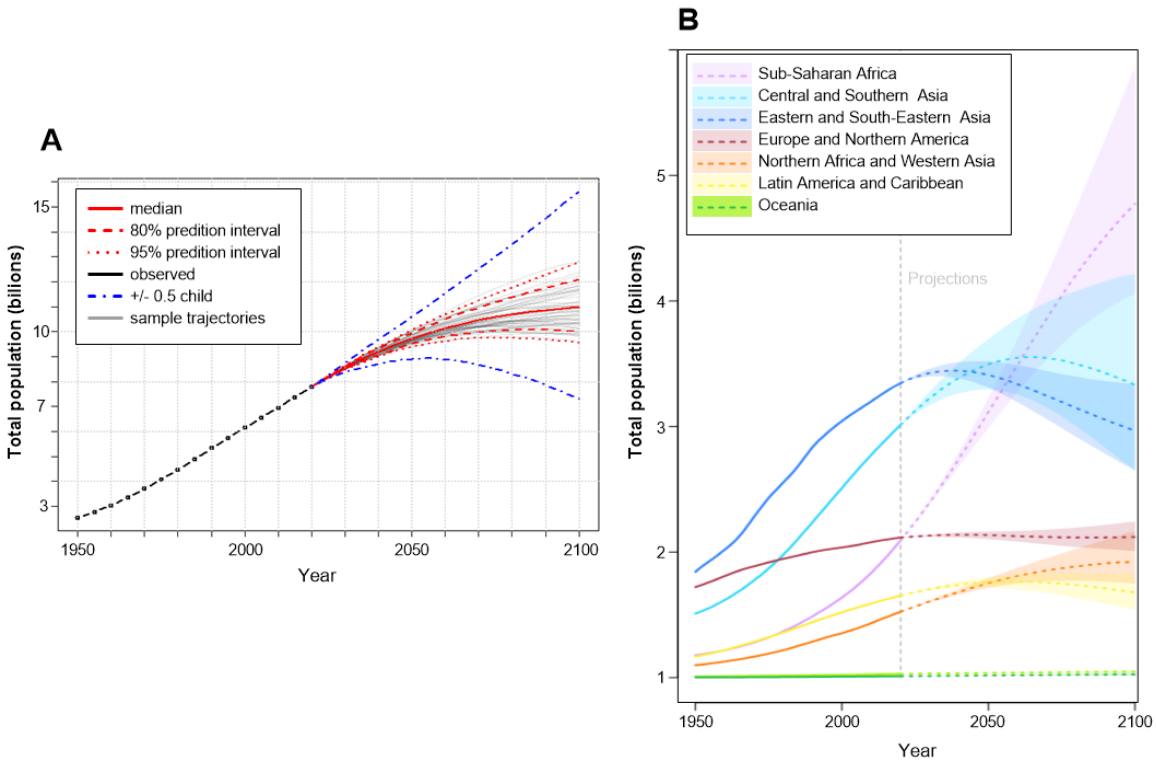

Figure 1.1 – Estimates and probabilistic projections of population growth. **(A)** World total population. **(B)** Population by regional Region. Adapted from ONU 2019.

Moreover, along with population increase, lifestyle changes and the increase in the prevalence of more caloric and protein-rich diets in high and middle-income countries contributes to an additional increase in agricultural demand for food production and animal feeding (Mbow et al. 2019). Over the last 50 years, the global cultivated area has grown by 12%, however, this has been mainly done with the degradation of ecosystems (biomass, carbon storage, soil health, biodiversity, water storage and supply, Figure 1.2) (FAO 2017). Consequently, to overcome food insecurity and undernourishment, future agricultural production will have to occur mainly on existing agricultural land. Therefore, improvement has to come from increased crop productivity and agricultural systems efficiency, allied with progress in other processes unrelated to food production (e.g. storage and distribution) (Mbow et al. 2019).

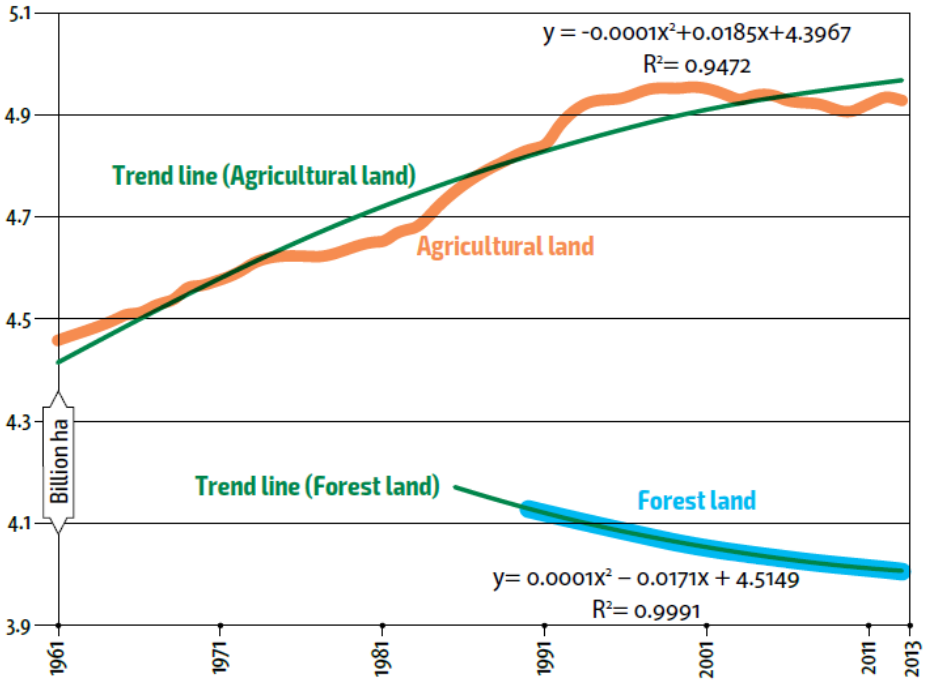

Figure 1.2 – Land use from 1961 to 2013. Source: FAO 2017

1.2 Climate change and impact on crop production

Air temperature has been increasing across the entire earth (Stocker et al. 2013), predominantly since the late 1970s (0.267 ± 0.054°C per decade), mainly due to anthropogenic activities, such as the increment in fossil fuel emissions since the industrial revolution (Figure 1.3A) (Hansen et al. 2010). Global air temperatures are predicted to rise on average 0.3-0.6°C per decade, and hot extremes are expected to increase in intensity, duration and frequency during the 21st century (Russo et al. 2014; Schär 2016). Global warming increases moisture evaporation from land to the atmosphere (Trenberth et al. 2007). As precipitation distribution is controlled primarily by atmospheric circulation patterns, the general tendency is for precipitation to increase in regions where it is high and decrease where

evaporation is high, wet regions becoming wetter and dry regions become drier (Allen and Ingram 2002; Kumar et al. 2014). Trends of increase in intensity and frequency in drought episodes are evident in several regions, such as the Mediterranean, Middle East, central China, India, Southern Amazon, North America, Eastern Australia, North Africa, and some regions of sub-Saharan Africa (Jia et al. 2019). Even though long-term global drought predictions are challenging to establish, due to its natural variability and quality/availability of data, increased drying over these regions is expected during the 21st century (Figure 1.3B) (Hoegh-Guldberg et al. 2018). Moreover, as in several of these regions changes in regional temperature are often related with changes in precipitation, drought is more likely to coincide with elevated temperatures (Trenberth and Shea 2005; Tricker et al. 2018).

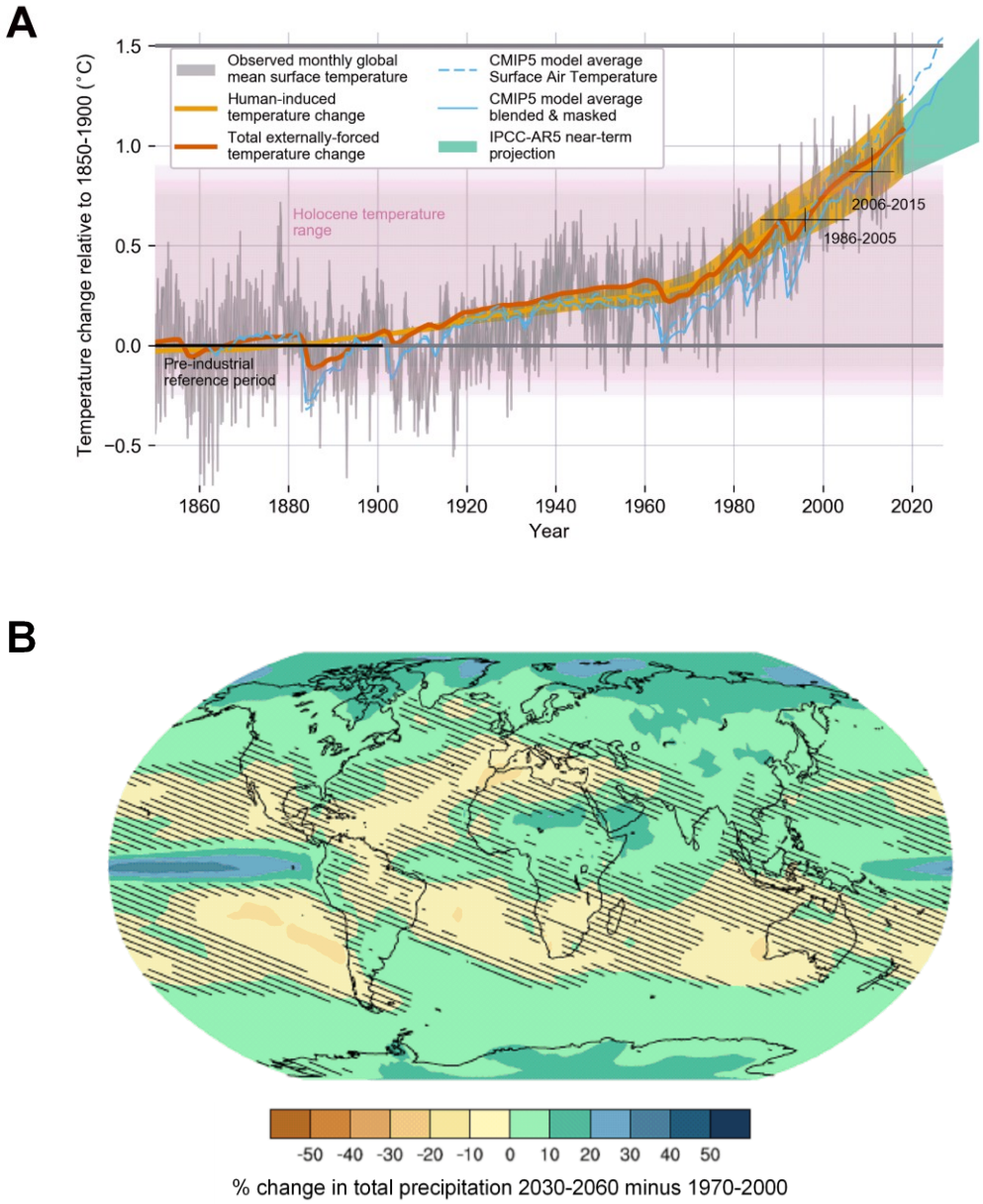

Figure 1.3 – Changes in surface temperature and precipitation. (A) Evolution of global mean surface temperature (1840-2018) and models projections. Source: Hoegh-Guldberg et

al. 2018. **(B)** Atlas data from a multimodel average per cent change in total annual precipitation (rain and snow) between 1970-2000 and 2030-260. The hatching represents areas where the signal is smaller than one standard deviation of natural variability. Source: KNMI 2013.

Plants, as sessile organisms, are not able to move, and environmental variability can pose a significant challenge to their ability to grow and reproduce (Walters 2005). Thus, to respond to changes in the environment, plants relied upon adjustments in pre-existing components (short-term/reversible acclimation) or more pronounced adjustments involving reallocation of resources and morphological changes (long-term/developmental acclimation). Both types of acclimation are dependent on plants' physiological and morphological plasticity. On the other hand, the environment poses selective pressures that may lead to slow adaptation processes, covering multiple generations and conferring new genetic attributes (Demmig-Adams et al. 2008). However, when climatic changes are more suddenly, or environmental changes occur in plants not adapted to these conditions, plants may not adjust their performance and experience growth and development impairment and eventually death (Mathur et al. 2014; Zampieri et al. 2017).

At the global scale, several studies indicated that climatic changes experienced between 1980 and 2010 decreased global mean yields in the major crops, relative to the climatic conditions prior to industrialisation (Lobell et al. 2011; Moore and Lobell 2015; Iizumi et al. 2018). Particularly, Zampieri et al. (2017) analysed wheat production anomalies from 1980 to 2010, concluding that heat and drought are accountable for more than 50% of the global inter-annual fluctuations. Moreover, several studies predicted the influence of climate change in crop production and global yields of the principal crops, attempting to characterize key dynamic processes affecting yields (Deryng et al. 2014; Lobell and Asseng 2017; Zhao et al. 2017). Notably, Deryng et al. (2014), predicted that maize yield decreases when average global temperature exceeds the normal value from 1ºC up to 4.8ºC, and extreme heat stress at anthesis decreased the predicted yield in wheat and soybean. These results demonstrate that extreme heat stress adversely affects the reproduction growth phase and seed production in the major crops. Zhao et al. (2017) compiled extensive published results, and applied four analytical methods, showing consistently negative temperature impacts on yields of four major crops, maize, wheat, rice and soybean. They predicted that without effective adaptation, and genetic improvement, each degree-Celsius increase in global mean temperature would, on average, lead to a reduction of 6% in wheat, 3.2% in rice, 7.4% in maize, 3.1% in soybean production. In a parallel study, Lobell and Asseng (2017) compared several published studies predicting sensitivities to temperature, precipitation, and carbon dioxide changes. Generally, they found a systematic concordance to the unfavourable impact of temperature change up to +2ºC. However, for precipitation, the few estimates available demonstrate some differences in the prediction.

In summary, studies assessing the effect of climate change on crop production indicated that global warming progress is detrimental, and impacts vary depending on precipitation patterns at the regional level and the incidence of extremes. Furthermore, the probability of crops encountering a more severe combination of abiotic stresses is likely to increase in the following decades. Therefore, climate change becomes a serious threat to crop production, and we must mitigate the impact of a warming and drier climate to increase crop productivity and achieve global food security. To increase crop productivity, we have to understand the mechanisms involved in plant response and identify traits conferring stress resistance, to be included in breeding programmes so that crops can continue to be productive, even in the presence of environmental stress.

1.3 Water relations under water deficit and high temperature

To maintain tissue hydration and photosynthesis, plants pull water from the soil, that moves radially through root cell layers, and then axially in a hydraulic continuum through xylem flow from roots to stems and leaves and finally through leaf tissues from xylem to stomata air spaces (Figure 1.4) (Tyree 1997; Steudle 2001). Water moves in plants by capillary action of cell walls, powered by the surface tension at evaporating surfaces of leaves. Water transfer depends on the gradient of water potential multiplied by the hydraulic conductance between two points (Figure 1.4) (Tardieu 2013; Lourenço et al. 2016). Thus, plant water status is a dynamic system, depending on soil water availability, the roots capacity to supply water, and the transpiration rate, which combines evaporative demand and canopy architecture (Tardieu et al. 2018).

Stomatal control is one of the key mechanisms allowing plants to regulate and optimise CO_2 assimilation versus evaporative water loss. Generically, stomatal closure results from a turgor loss in guard cells, which involves ion channels and aquaporins, mediated by hydraulic and hormonal signals (Comstock 2002; Maurel et al. 2016). Abscisic acid (ABA) is considered the primary plant hormone involved in stomatal regulation (Luan 2002; Pantin et al. 2013). Genetic variation in the control of plant water status by stomata has been observed across and within species, and can be divided into two categories depending on stomatal regulation of water status, labelled as isohydric or anisohydric (Sade et al. 2012; Tardieu et al. 2018). Generally, plants with isohydric behaviour exhibit change in stomatal conductance according to soil water status before they experience any substantial change in leaf water potential. This behaviour appears to be a conservative mechanism that is favourable under conditions of drought and high evaporative demand (Sade et al. 2012; Tardieu et al. 2018). On the other hand, anisohydric performance is a more risk-taken behaviour that may be favourable under milder conditions but is more predisposed to the occurrence of embolism in the xylem

elements, hydraulic failure and xylem function loss under more severe circumstances (Sade et al. 2012; Tardieu et al. 2018).

Plants use evaporative cooling, driven by transpiration, as their primary mechanism to decrease internal temperatures under warm conditions, which could otherwise be detrimental to several physiological processes (Machado and Paulsen 2001; Carmo-Silva et al. 2012; Lawson et al. 2018). In tobacco plants, Rizhsky et al. (2002) observed that when subjected to the combination of high temperature and drought, plants exhibited higher temperature than plants only exposed to warm conditions. Similarly, when comparing drought response versus the combination with heat in Arabidopsis and citrus plants, Rizhsky et al. (2004) and Zandalinas et al. (2016), respectively, observed that stomatal conductance decreased in co-occurrence. Heat increases stomatal conductance, whereas drought has the opposite effect, therefore these results suggest that stomata control under drought condition could prevail over evaporative demand. The ability to tolerate the combination of drought and heat due to different transpiration rates also varies among different genotypes of a specific plant species (Aprile et al. 2013; Zandalinas et al. 2016; Medina et al. 2019; El Habti et al. 2020). Consequently, an optimal balance between evaporative cooling and water-saving mechanisms, and consequently water use efficiency (WUE) is even more critical to crop production under water deficit and high temperature.

WUE can be defined as the ratio of carbon capture to water consumption by a plant. WUE may be instantaneous (when measured at leaf level by gas exchange methods) or integrated over the crop cycle (when it takes into account a longer period and including organs at several plant levels) (Tambussi et al. 2007; Tardieu 2013; Tardieu et al. 2018). Selecting crops based only on intrinsic low water consumption (the low denominator of WUE), achieved by low transpiration rate/stomatal conductance, has been argued to lead to the selection of small plants with low biomass accumulation and light interception. Ultimately, this results in loss of sink strength and yield penalties over all the crop season and evaporative cooling under high temperature (Blum 2009; Tricker et al. 2018). These plants may be adequate to grow in more extreme conditions and useful to escape a complete loss of production when the selection is associated with other tolerance mechanisms, but not in most agricultural systems (Tardieu 2012). On the other hand, fine control of water relations through timely modifications in stomatal conductance/transpiration, according to critical stages during the day or growing cycle, are seen as good strategies to maintain high yields (Tardieu et al. 2018; Tricker et al. 2018). Avoidance mechanisms as high stomata density (Vile et al. 2012; Roche 2015; Shahinnia et al. 2016), patchy stomatal closure (Vadez et al. 2014), a partial decrease of transpiration in response to high evaporation demand associated with high temperature (high vapour pressure deficit (VPD)) (Schoppach et al. 2016; Sinclair 2017) were previously associated to high yielded crops.

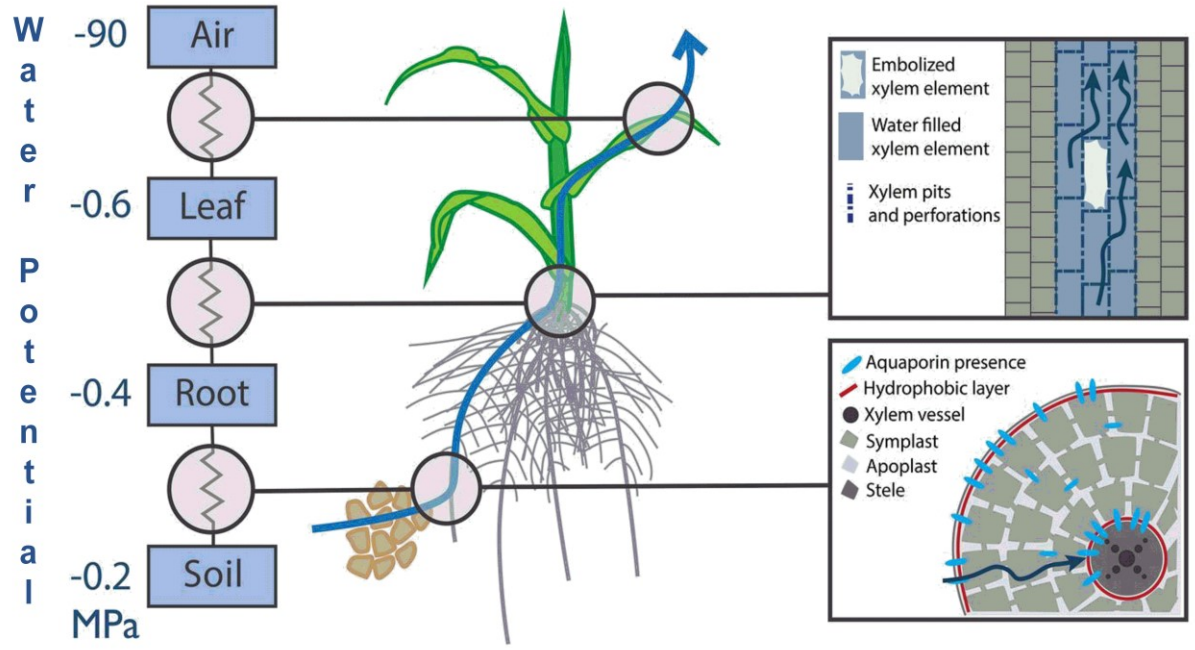

Figure 1.4 – Water flow in the plant driven by water potential differences and regulated by hydraulic conductivity between soil, root, shoot and atmosphere. Water flow (blue arrows) is influenced radially by the anatomy of the root and axially by the anatomy of the xylem and the occurrence of cavitation. Adapted from Lobet et al. (2014).

1.4 The combined effect of water deficit and high temperature in photosynthesis

Photosynthesis is a key process in plant physiology and serves as a sensor of abiotic stresses. It is inhibited before other cell functions and has long been recognised as one of the most heat-sensitive plant processes and a primary factor determining crop productivity (Berry and Bjorkman 1980; Long and Ort 2010). Major stress-targets on the photosynthetic apparatus are the photosystems, mainly photosystem II (PSII), and the carbon assimilation process (Allakhverdiev et al. 2008).

1.4.1 Light reactions

Photosynthetic electron transport incorporates the two photosystems (PSII and PSI), the cytochrome b_6f ($cytb_6f$) complex and the free electron carriers plastoquinone and plastocyanin, that lead to the production of NADPH and proton-motive force, the latter being afterwards used for ATP production by ATP-synthase (ATPase) (Figure 1.5). Briefly, the process starts when light energy is trapped by the light-harvesting complex of PSII and PSI (containing chlorophylls and other pigments), which funnel its energy to photosystems reaction centres. In PSII, more specifically in the oxygen-evolving complex (OEC) water is oxidised to O_2 and 4 protons. The electrons extracted are then shuttled through a quinone pool and the $cytb_6f$ complex to

plastocyanin. In PSI, the light energy induces the translocation of an electron from plastocyanin to ferredoxin, and the reduced ferredoxin is subsequently used for NADPH production (Figure 1.5) (Nelson and Ben-Shem 2004; Eberhard et al. 2008).

Imbalances between CO_2 assimilation and the rate of light capture usually lead to an excess of energy in the system that can result in reactive oxygen species (ROS) formation and photoinhibition (qI), if the capacity of dissipation, scavenging, and repairing is exceeded (Yamamoto 2016). Thus, photoprotective mechanisms are employed to reduce light absorption. Among the main energy dissipation mechanisms are the non-photochemical quenching (qN, generally compartmented in three major components, energy-dependent quenching, qE, state-transition quenching, qT, and photoinhibition quenching, qI), and alternative electron sinks, such as cyclic electron flow around PSI, chlororespiration and the Mehler- Ascorbate peroxidase pathway (Asada 2000; Rumeau et al. 2007; Ruban 2016; Wang and Fu 2016).

Some studies have shown that, under abiotic stress, PSI is more stable than PSII and inactivation of PSII can be caused by a series of independent or interconnected events. The main processes involved are the damage of the oxygen-evolving complex (Heckathorn et al., 1998; Tiwari et al., 2008; Chen et al., 2016), the degradation and aggregation of the D1 protein (Kamata et al., 2005; Komayama et al., 2007; Allakhverdiev et al., 2008; Takahashi and Murata, 2008) and changes on the membrane fluidity (Gounaris et al., 1983, Aronsson et al., 2008, Yamamoto, 2016). Chlorophyll *a* fluorescence, an indicator of the fate of excitation energy in the photosynthetic apparatus, has been used in several studies to quantify PSII damage in response to high temperature and water deficit (Sainz et al. 2010; Perdomo et al. 2015; Zandalinas et al. 2016; Sehgal et al. 2017). In citrus plants, Zandalinas et al. (2016) observed that a combination of heat for ten days and drought stress during 24h had a more detrimental effect on the effective quantum efficiency (ΦPSII) and maximum quantum efficiency of PSII (Fv/Fm) than isolated stresses. Investigating contrasting heat and drought sensitivity of lentil genotypes sensitivity (>30/20ºC, day/night, and 50% field capacity for 15 days), Sehgal et al. (2017) also observed that tolerant genotypes had significantly higher Fv/Fm than sensitive genotypes. Similarly, in *Lotus japonicus*, Sainz et al. (2010) found that Fv/Fm was only affected when plants were simultaneously subjected to four days without irrigation and four hours at 42ºC each day. Perdomo et al. (2015) investigated individual and combined effects of high temperature and water deficit on maize, rice, and wheat, and observed that wheat was the most affected crop with a substantial Fv/Fm decreased under combined stress. In summary, the combination of these two abiotic stresses was more detrimental to PSII efficiency than single stresses.

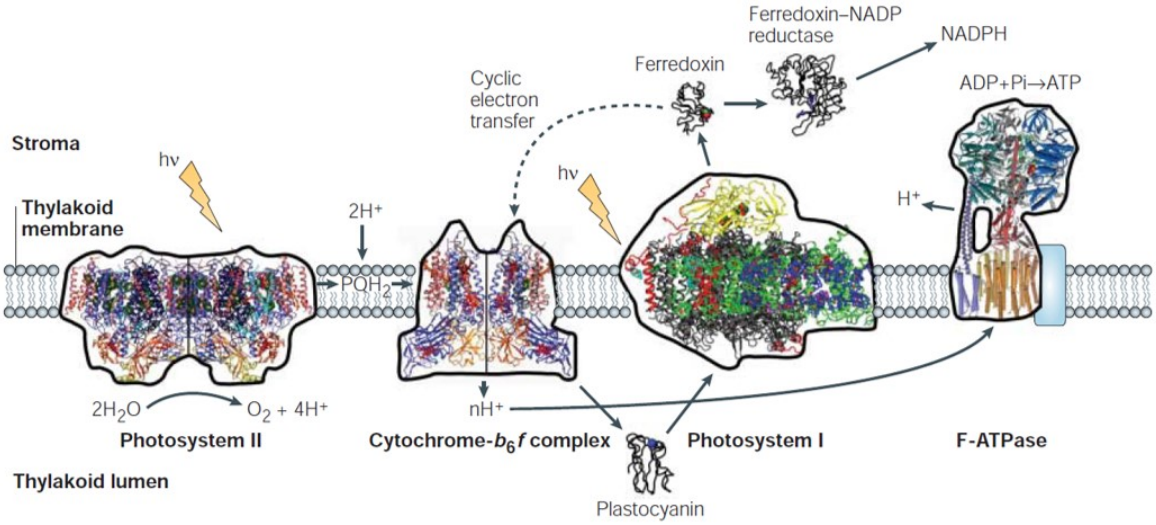

Figure 1.5 – Schematic representation of photosynthetic electron transport. Structures of the four major transmembrane protein complexes (Photosystem II, cytochrome b6f, Photosystem I, and ATPase) and electron donors and acceptors (plastocyanin, ferredoxin) (Nelson and Ben-Shem 2004). Solid arrows indicate the principal electron and proton pathways, and the cyclic electron-transfer pathway is indicated by a dashed arrow. hν, light quanta. Adapted from Nelson and Ben-Shem (2004).

1.4.2 Carbon fixation

In the form of NADPH and ATP, reducing power and energy generated by chloroplast electron transport in the thylakoid membranes are afterwards consumed in the pathway of carbon fixation in the chloroplast stroma, the Calvin-Benson-Bassham cycle (CBBC). Generically, the CBBC can be divided into three phases: carboxylation, reduction and regeneration (Figure 1.6). During the carboxylation reaction, Ribulose-1,5-bisphosphate carboxylase/oxygenase (Rubisco), the enzyme responsible for CO_2 fixation in photosynthetic organisms, uses ribulose-1,5-bisphosphate (RuBP) and CO_2 to generate two 3-phosphoglycerate (3-PGA) (Figure 1.6). In the reduction phase, 3-PGA is converted into glyceraldehyde-3-phosphate (G3P), most of the G3P is used to regenerate RuBP via multiple pathways catalysed by nine enzymatic reactions (regeneration phase) and another part to make complex carbohydrates like starch and sucrose (Figure 1.6).

Rubisco can also catalyse an oxygenase reaction, producing 3-PGA and 2-phosphoglycolate (2-PG). Since 2-PG is toxic, recycling 2-PG involves a complex pathway in chloroplasts, peroxisomes, mitochondria, and cytosol, called photorespiration. This process is energy demanding and leads to loss of carbon in the form of CO_2. High temperature decreases CO_2 solubility relative to O_2 and the specificity of Rubisco for CO_2 relative to O_2, favouring oxygenation of RuBP over carboxylation (Berry and Bjorkman 1980). An increase in photorespiration was observed in different crops, either in drought or heat stress (Long and

Ort 2010; Walker et al. 2016). Photorespiration, as a high energetic cost process, has been regarded as detrimental for crop production and a target for crop improvement. However, recent studies suggest that reducing photorespiration may not always have beneficial effects (Betti et al. 2016; Eisenhut et al. 2017; Baslam et al. 2020).

In addition to the increase of photorespiration, the decrease in Rubisco's carboxylation activity was observed in different crops under high temperature and water deficit (Carmo-Silva et al. 2012; Zandalinas et al. 2014; Perdomo et al. 2017). For Rubisco to function, the enzyme active site requires carbamylation. When RuBP binds the carbamylated active site, it is available for catalysis. However, when RuBP binds to an uncarbamylated site or other sugar-phosphates bind to a carbamylated site, Rubisco becomes inhibited and forms a dead-end complex (Parry et al. 2008). A decrease of Rubisco's carboxylation activity under high temperature and water deficit was associated with decreased activation state and increased catalytic misfire events (Salvucci and Crafts-Brandner 2004; Carmo-Silva et al. 2012; Perdomo et al. 2017). Rubisco activase (RCA) uses the energy from ATP hydrolysis to remove inhibitory sugar phosphates from the catalytic site of both the carbamylated and decarbamylated forms of Rubisco, and is essential to Rubisco catalytic activity. Some studies have reported that high temperature inactivates RCA, attributed to aggregation of the protein (Feller et al. 1998; Salvucci et al. 2001; Crafts-Brandner and Salvucci 2002; Barta et al. 2010). Bioengineering approaches aiming to enhance the Rubisco activity by increasing the thermotolerance of RCA have been suggested for improving tolerance to higher temperatures (Carmo-Silva et al. 2015; Shivhare and Mueller-Cajar 2017; Scafaro et al. 2019; Degen et al. 2020). Some authors suggested that impairment of ATP synthesis (as described in section 1.4.1), which is essential for RCA function and RuBP regeneration, as well as decrease of CO_2 availability (as described in section 1.3) under drought and high temperature, can be metabolic factors decreasing photosynthesis (Tezara et al. 1999; Crafts-Brandner and Salvucci 2002; Flexas et al. 2004; Lawlor and Tezara 2009).

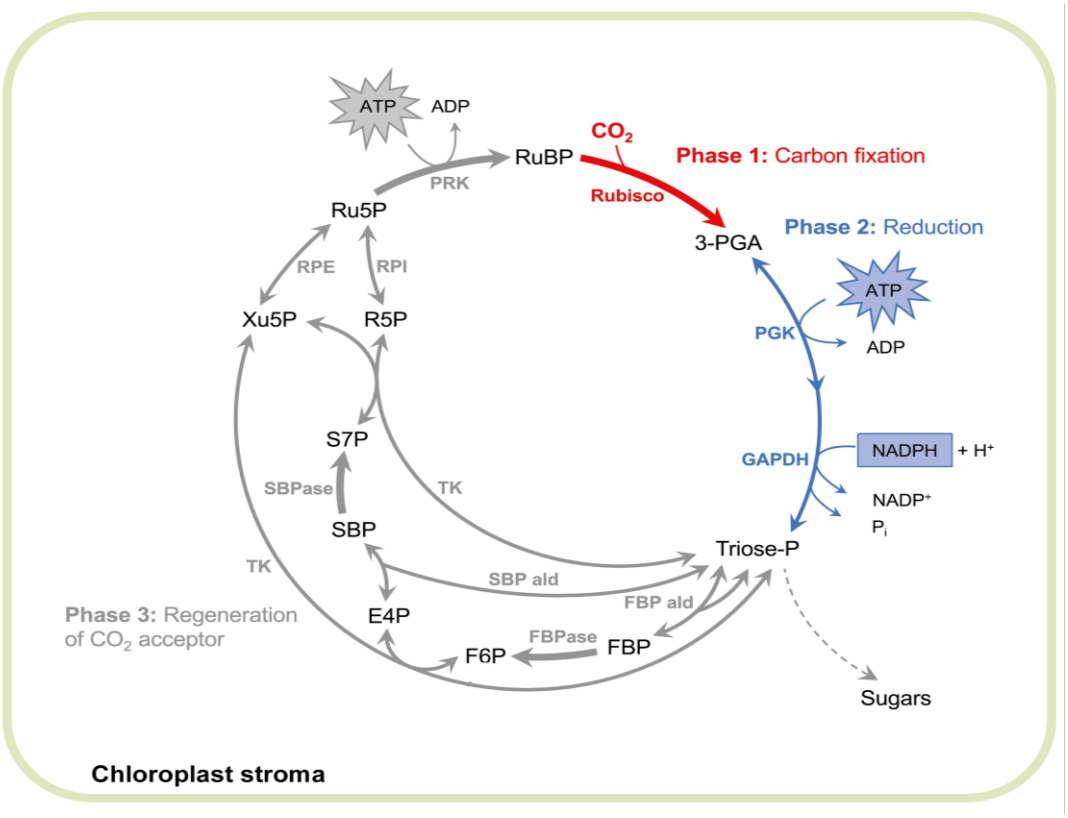

Figure 1.6 – Schematic representation of the Calvin-Benson-Bassham cycle (CBBC). CBBC is composed of three phases: (1) carbon fixation /carboxylation (in red), (2) reduction (in blue) and (3) regeneration of the CO_2 acceptor (in grey). Abbreviations: Erythrose-4-phosphate (E4P), fructose-1,6-bisphosphate (FBP), Fructose-1,6-bisphosphatase (FBPase), Phosphoribulokinase (PRK), ribose-5-phosphate (R5P), Ribulose-5-phosphate epimerase (RPE), Ribose-5-phosphate isomerase (RPI), ribulose-5-phosphate (Ru5P), Sedoheptulose-7-phosphate (S7P), Sedoheptulose-1,7-bisphosphate aldolase (SBP ald), sedoheptulose-1,7-bisphosphate (SBP), Sedoheptulose-1,7-bisphosphatase (SBPase), sedoheptulose-7-phosphate (S7P), Transketolase (TK), xylulose-5-phosphate (Xu5P). Bold arrows highlights enzymes catalysing irreversible reactions. Adapted from Schreier and Hibberd (2019).

1.4.3 C_3 vs C_4 photosynthetic pathways

Some important crops such as maize, sorghum, and sugarcane, use C_4 photosynthetic pathway, whereas wheat, rice and soybean utilise the C_3 pathway. C_3 and C_4 pathways differ in the way that CO_2 arrives at chloroplasts, where carbon fixation is achieved. In both C_3 and C_4 plants, CO_2 diffuses through the stomata and the intercellular air spaces to the mesophyll cells. However, a biochemical CO_2 concentrating mechanism (CCM) is present in C_4 plants that increases CO_2 concentrations at the catalytic sites of Rubisco (Furbank and Hatch 1987). The establishment of C_4 photosynthesis includes several biochemical and anatomical modifications. In C_4 crops, the CCM is achieved by the compartmentalisation of photosynthesis between two different leaf cell types, the mesophyll cells (MC) and bundle sheath cells (BSC) (Figure 1.7). Briefly, CO_2 is converted into bicarbonate by Carbonic anhydrase (CA) in MC,

afterwards fixed by Phosphoenolpyruvate carboxylase (PEPC) (Figure 1.7). The resulting oxaloacetate is then converted into a more stable C_4 acid (malate or aspartate) that diffuses until the BSC (Figure 1.7). There, CO_2 is released by the action of a decarboxylating enzyme, Phosphoenolpyruvate carboxykinase (PEPCK), NADP-dependent malic enzyme (NADP-ME) or NAD-dependent malic enzyme (NAD-ME), depending on the biochemical subtype (Figure 1.7). The CO_2 released is then refixed in CBBC through Rubisco (as described in section 1.4.2). Finally, the C_3 compound resulting from the decarboxylation is recycled to phosphoenolpyruvate (PEP) in the MC, by the action of Pyruvate orthophosphate dikinase (PPDK) in an energy-dependent reaction (Figure 1.7) (Hatch 1987; Edwards et al. 2004; Sage et al. 2014). Anatomically, a typical C_4 crop leaf follows a Kranz anatomy with an outer layer of MC, and an inner layer of larger BSC surrounding the vascular tissue (Figure 1.7), some times suberised (Sage 2004). Differentiation between MC and BSC localisation and functions also altered their specific energy requirement, with depletion or enhancement of PSII in BSC associated with the primary decarboxylating process used and the shuttle of reducing power along with the C_4 acid (Meierhoff and Westhoff 1993; Rao and Dixon 2016).

It is generally accepted that plants with C_4 photosynthesis evolved from C_3 plants in response to the increase of temperature, decreased CO_2 concentration in the atmosphere and episodes of drought or salinity (Edwards et al. 2001, 2004b; Sage 2004). A previous study showed that C_4 species had higher temperature optima of photosynthesis but were less plastic (e.g. less able to acclimate photosynthesis to varying growth temperatures). On the other hand, C_3 species tended to adapt the photosynthetic rate across a range of growth temperatures (Yamori et al. 2014). The development of CCM in C_4 plants allowed the decrease of the oxygenation activity of Rubisco, and consequently, photorespiration (Sage et al. 2010), in large part by surpassing the decrease in CO_2 solubility relative to O_2 caused by high temperature (Sage and Kubien 2007; Dwyer et al. 2007). Additionally, it also allowed a decrease in Rubisco concentration since it operates only in BSC at high CO_2 concentrations, leading to better nitrogen-use efficiency of C_4 compared to C_3 plants. Ultimately, the CCM enables C_4 plants to increase the ratio of CO_2 fixed per water loss through transpiration (Ghannoum et al. 2010; Osborne and Sack 2012). Some authors also suggested that under varying environmental conditions, as high temperature and drought, some C_4 crops showed some flexibility in their decarboxylation pathway, adjusting the CCM to the environmental condition and working more efficiently (Furbank 2011; von Caemmerer and Furbank 2016; Arrivault et al. 2017). However, as in C_3 crops, high temperature and water deficit can also impair the physical integrity of the electron transport components in C_4 crops limiting photosynthetic efficiency (Crafts-Brandner and Salvucci 2002). Impairment of ATP and reducing power synthesis, essential for the fine-tuning of the CCM, and CO_2 leakage from the

BSC under drought and high temperature are also suggested to decrease photosynthesis in C_4 crops (Hatch et al. 1995; Kromdijk et al. 2014).

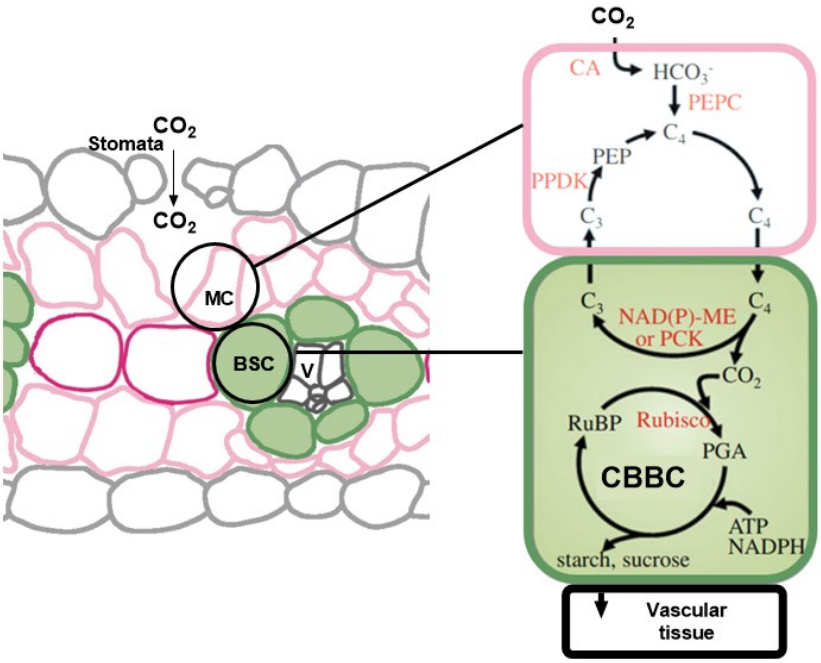

Figure 1.7 – C_4 photosynthesis. Schematic representation of a longitudinal cross-section of a leaf showing a Kranz anatomy and C_4 photosynthetic pathway major reactions. Abbreviations: bundle sheath cells (BSC), Carbonic anhydrase (CA), mesophyll cell (MC), NAD-dependent malic enzyme (NAD-ME), NADP-dependent malic enzyme (NADP-ME), Phosphoenolpyruvate carboxykinase (PCK), phosphoenolpyruvate (PEP), phosphoglycerate (PGA), Phosphoenolpyruvate carboxykinase (PEPCK), ribulose-1,5-bisphosphate (RuBP), vascular tissue (V). Adapted fromYamori et al. (2014) and Sedelnikova et al. (2018).

1.5 Antioxidant response under water deficit and high temperature

Abiotic stresses commonly induce ROS overproduction in the chloroplast, mitochondria, peroxisome and apoplast (Choudhury et al. 2017). Therefore, plants can perceive an increase of intracellular levels of ROS as a signature of specific stress that will result in a corresponding acclimation response. However, as ROS are highly reactive and toxic, overexposure disrupting the cellular redox homeostasis can damage proteins, lipids, carbohydrates, and DNA, ultimately resulting in oxidative stress (Foyer and Noctor 2005). The balance between the ROS damage and their signalling role under stress is dependent on the plant's capacity to maintain ROS homeostasis, as the trade-off between production and detoxification (Choudhury et al. 2017). ROS detoxification is generally conducted enzymatically and by producing several low molecular weight antioxidants, such as flavonoids, terpenoids, carotenoids, ascorbate and glutathione (Mittler et al. 2004; Foyer 2018).

In some crops, tolerance to drought or heat stress was associated with increased antioxidant capacity and reduced oxidative damage (Sairam et al. 2000; Suzuki et al. 2014; Ahmed et al. 2015; Zhang et al. 2017). Recent studies also highlight the importance of modulation of ROS scavenging, where some pathways were induced explicitly by combined stress (Rizhsky et al. 2002; Koussevitzky et al. 2008; Bi et al. 2016; Zandalinas et al. 2017). Rizhsky et al. (2002) observed differences in the type of ROS detoxification induced by an individual or combined stresses in tobacco plants. While drought resulted in the induction of Catalase (CAT) and Glutathione peroxidase (GPX), heat induced Peroxidases (APX and TPX). On the other hand, the combinatory effect induced the transcription of Glutathione reductase and S transferase (GR and GST, respectively) and Superoxide dismutase (SOD). Koussevitzky et al. (2008) conducted a functional analysis with mutants of Arabidopsis and found that APX could play a key role in the acclimation of plants to a combination of drought and heat stress. In citrus plants, increased levels of secondary metabolites such as phenylpropanoid, precursors of lignins, flavonols, and flavones were observed in response to drought and temperature stresses (Zandalinas et al. 2017). In general, heat and drought combination generate singular ROS signatures apart from drought and heat individually. Induction of ROS detoxification enzymes and metabolites was a general response among plant species suggesting that a higher antioxidant capacity is associated with the tolerance of plants to stress combination.

1.6 Changes in the carbohydrate metabolism under water deficit and high temperature

Carbohydrates are by-products of photosynthesis and play an essential role in plant growth and development. Therefore their synthesis and concentration/partition upon stress imposition make them crucial for plant tolerance (Gangola and Ramadoss 2018). Carbohydrates provide cells with the building material and energy for cell component synthesis and, along with hormones, play a crucial role in long-distance signalling (Krasavina et al. 2014; Ljung et al. 2015). Sucrose and hexoses are the major contributors to the carbohydrates pool in plant cells (Roitsch 1999; Koch 2004). Sucrose, being a nonreducing carbohydrate with restricted chemical activity, is the major transport and storage molecule and can be translocated symplastically or apoplastically to the phloem cells and sink tissues (Roitsch and González 2004; Gangola and Ramadoss 2018). Its accumulation is determined by the balance between sucrose synthesis and degradation into hexoses. Hexoses serve as a substrate for glycolysis, and their products are used in essential anabolic processes, including synthesis of fatty acids, amino acids, riboses and reducing equivalents (Krasavina et al. 2014).

An astonishing large fraction of carbohydrates assimilated by plants (25-70%) are consumed by respiration on the same day (Lambers et al. 2005). Heat increases respiration, and when in combination, drought may exacerbate the effect of heat stress-induced increases in respiration (Atkin et al. 2005; Tricker et al. 2018). Plant productivity depends on the whole balance between photosynthesis and respiration (Flexas et al. 2005). Stored carbohydrates consumed in respiration are less available for partition between source and sink tissues affecting plant growth and development (Roitsch 1999). Therefore, tolerance to drought and heat stress will depend on the concentration of carbohydrates available to export and the use of these reserves for respiration.

Combination of drought and high temperature can also exacerbate cells dehydration and osmotic stress, causing disruption of hydrophilic interactions and consequently leading to protein denaturation, destabilisation of membranes, and ultimately organelles collapse (Gangola and Ramadoss 2018). To protect cells from dehydration and maintain turgor pressure, plants generally increase the concentration of osmoprotectants. Along with some soluble amino acids and derivates (e.g proline, glycine betaine), carbohydrates as hexoses (e. g. glucose and fructose), disaccharides (sucrose, trehalose) and oligosaccharides (e.g. raffinose) are important osmoprotectants (Krasavina et al. 2014). Proline accumulation has been reported in Arabidopsis and *Portulaca oleracea* upon heat or drought stress but not in combined stress (Rizhsky et al. 2004; Jin et al. 2016). Along with the increase of sucrose concentration when plants were subject to stress combination, Rizhsky et al. (2004) suggested that sucrose could replace proline as the main osmoprotectant in Arabidopsis under these conditions.

In summary, carbohydrates play diverse roles during plant growth and development, and their metabolic regulation is crucial for plants response and acclimation to abiotic stresses, particularly those associated with high temperature and drought.

1.7 Growth and development under water deficit and high temperatures

Plants readjust their performance to transient changes in the environmental conditions through acclimation processes. Alternatively to short term acclimation changes (occurring within minutes and relying on changes on pre-existing components), long-term acclimation involves altered patterns of gene expression, reallocation of resources and morphological changes (Walters 2005). These responses are not immediately reversible and usually lead to growth and development changes, resulting in a different phenotype. However, the ability to adapt and acclimate to given stress varies between species and even between genotypes of

the same species, suggesting that these processes must carry advantages at some cost (Athanasiou et al. 2010).

Water stress generally reduces crops growth at the morphological level through reduced tillering and/or leaf expansion, whereas high temperature accelerates plant growth and shortens developmental stages. Under combined stress, crops generally reduce organ elongation rates, producing less biomass and flowering earlier than under single stress (Acevedo et al. 1971; Parent and Tardieu 2012; Tricker et al. 2018). Plants response to stress also depends on their developmental stage. Generally, reproductive tissues are more sensitive to drought, heat and their combination than vegetative tissues (Barnabás et al. 2008). However, combined effects are more remarkable than single stress, reducing the size and weight of individual grains and shortening the grain filling duration (Barnabás et al. 2008; Fábián et al. 2019; Pennacchi et al. 2019; El Habti et al. 2020).

To cope with decreased water availability in soil, crops generally allocate more photo-assimilates to underground tissues to develop a more extensive root system, increasing the root to shoot ratio (Boyer 1982; Lopes et al. 2012). On the other hand, several authors observed a reduction in the carbon partitioned to underground parts in warmer conditions (Batts et al. 1998; Vile et al. 2012; Pinto and Reynolds 2015). Furthermore, delayed senescence and a "stay-green" phenotype were associated with drought or heat tolerance without water deficit through a functional root system accessing water reserves in deep soils (Kumari et al. 2007; Pinto et al. 2010). However, under the combination of stresses, water deficit can be exacerbated, and the contribution of root growth to tolerance is uncertain if water reserves are available for continuous water use (Tricker et al. 2018).

In summary, morphological changes express adjustments in physiological and biochemical processes (discussed in the previous sections), and the process to acclimate to drought and high temperature differ from those activated by single acclimation. Combined stress might require conflicting or antagonistic responses, and acclimation might require compensatory mechanisms and cross-talk between co-activated pathways at different levels. Future climatic scenarios predict that global temperature will increase, and the occurrence of extremely high temperatures with simultaneous water shortage phenomena is likely to increase in frequency, causing damage to crop production. Therefore, it is imperative to increase our knowledge of essential crop metabolic response processes, such as the photosynthetic, carbohydrate, and antioxidant metabolisms under high temperature and water deficit conditions.

1.8 Research objectives

To improve food production, it is essential to develop crops with increased tolerance to drought and high temperatures, which are among the major abiotic stresses. The main goal of this project was to improve the understanding of the impact of heatwaves and water scarcity on crop physiological and biochemical processes, and response mechanisms associated with improved performance. To this end, wheat and maize were used as model crops, as they represent two of the most important cereal crops globally for food production, with contrasting photosynthetic metabolisms (C_3 and C_4, respectively). To achieve this general goal, three specific objectives were defined, each one corresponding to a results chapter of this work:

1. Characterise the photosynthetic constraints of wheat genotypes adapted to distinct climate conditions, under water deficit and high temperature, and determine which factors are responsible for photosynthetic performance and recovery from these conditions.

2. Characterise the combined effects of water deficit and high temperature on maize photosynthesis. Assess the role of the CO_2 concentrating mechanism in the tolerance to these conditions and unravel mechanisms that can help the improvement of maize growth under high temperatures and extended drought.

3. Optimize high-throughput methods to phenotype plants under controlled water deficit and high temperature and identify wheat phenotypic traits conferring adaptative stress responses.

1.9 References

Acevedo E, Hsiao TC, Henderson DW (1971) Immediate and Subsequent Growth Responses of Maize Leaves to Changes in Water Status. Plant Physiol 48:631–636. https://doi.org/10.1104/pp.48.5.631

Ahmed IM, Nadira UA, Bibi N, et al (2015) Secondary metabolism and antioxidants are involved in the tolerance to drought and salinity, separately and combined, in Tibetan wild barley. Environ Exp Bot 111:1–12. https://doi.org/10.1016/j.envexpbot.2014.10.003

Alexandratos N, Bruinsma J (2012) World agriculture towards 2030/2050: the 2012 revision. Rome

Allakhverdiev SI, Kreslavski VD, Klimov V V., et al (2008) Heat stress: An overview of molecular responses in photosynthesis. Photosynth Res 98:541–550. https://doi.org/10.1007/s11120-008-9331-0

Allen MR, Ingram WJ (2002) Constraints on future changes in climate and the hydrologic cycle. Nature 419:642

Aprile A, Havlickova L, Panna R, et al (2013) Different stress responsive strategies to drought and heat in two durum wheat cultivars with contrasting water use efficiency. BMC Genomics 14:821. https://doi.org/10.1186/1471-2164-14-821

Arrivault S, Obata T, Szecówka M, et al (2017) Metabolite pools and carbon flow during C_4 photosynthesis in maize: 13CO 2 labeling kinetics and cell type fractionation. J Exp Bot 68:283–298. https://doi.org/10.1093/jxb/erw414

Asada K (2000) The water-water cycle as alternative photon and electron sinks. https://doi.org/10.1098/rstb.2000.0703

Athanasiou K, Dyson BC, Webster RE, Johnson GN (2010) Dynamic acclimation of photosynthesis increases plant fitness in changing environments. Plant Physiol 152:366–373. https://doi.org/10.1104/pp.109.149351

Atkin OK, Bruhn D, Tjoelker MG (2005) Response of Plant Respiration to Changes in Temperature: Mechanisms and Consequences of Variations in Q10 Values and Acclimation. In: Plant Respiration. Springer-Verlag, pp 95–135

Awasthi R, Kaushal N, Vadez V, et al (2014) Individual and combined effects of transient drought and heat stress on carbon assimilation and seed filling in chickpea. In: Functional Plant Biology. CSIRO, pp 1148–1167

Barnabás B, Jäger K, Fehér A (2008) The effect of drought and heat stress on reproductive processes in cereals. Plant, Cell Environ 31:11–38. https://doi.org/10.1111/j.1365-3040.2007.01727.x

Barta C, Dunkle AM, Wachter RM, Salvucci ME (2010) Structural changes associated with the acute thermal instability of Rubisco activase. Arch Biochem Biophys 499:17–25.

https://doi.org/10.1016/j.abb.2010.04.022

Baslam M, Mitsui T, Hodges M, et al (2020) Photosynthesis in a Changing Global Climate: Scaling Up and Scaling Down in Crops. Front. Plant Sci. 11:882

Batts GR, Ellis RH, Morison JIL, et al (1998) Yield and partitioning in crops of contrasting cultivars of winter wheat in response to CO_2 and temperature in field studies using temperature gradient tunnels. J Agric Sci 130:17–27. https://doi.org/10.1017/S0021859697005017

Berry J, Bjorkman O (1980) Photosynthetic Response and Adaptation to Temperature in Higher Plants. Annu Rev Plant Physiol 31:491–543. https://doi.org/10.1146/annurev.pp.31.060180.002423

Betti M, Bauwe H, Busch FA, et al (2016) Manipulating photorespiration to increase plant productivity: Recent advances and perspectives for crop improvement. J. Exp. Bot. 67:2977–2988

Bi A, Fan J, Hu Z, et al (2016) Differential acclimation of enzymatic antioxidant metabolism and photosystem II photochemistry in tall fescue under drought and heat and the combined stresses. Front Plant Sci 7:453. https://doi.org/10.3389/fpls.2016.00453

Blum A (2009) Effective use of water (EUW) and not water-use efficiency (WUE) is the target of crop yield improvement under drought stress. F. Crop. Res. 112:119–123

Boyer JS (1982) Plant Productivity and Environment. Science (80-) 218:443–448. https://doi.org/10.1126/science.218.4571.443

Carmo-Silva AE, Gore MA, Andrade-Sanchez P, et al (2012) Decreased CO 2 availability and inactivation of Rubisco limit photosynthesis in cotton plants under heat and drought stress in the field. Environ Exp Bot 83:1–11. https://doi.org/10.1016/j.envexpbot.2012.04.001

Carmo-Silva E, Scales JC, Madgwick PJ, Parry MAJ (2015) Optimizing Rubisco and its regulation for greater resource use efficiency. Plant, Cell Environ 38:1817–1832. https://doi.org/10.1111/pce.12425

Choudhury FK, Rivero RM, Blumwald E, Mittler R (2017) Reactive oxygen species, abiotic stress and stress combination. Plant J 90:856–867. https://doi.org/10.1111/tpj.13299

Comstock JP (2002) Hydraulic and chemical signalling in the control of stomatal conductance and transpiration. J Exp Bot 53:195–200. https://doi.org/10.1093/jexbot/53.367.195

Crafts-Brandner SJ, Salvucci ME (2002) Sensitivity of Photosynthesis in a C_4 Plant, Maize, to Heat Stress. Plant Physiol 129:

Degen GE, Worrall D, Carmo-Silva E (2020) An isoleucine residue acts as a thermal and regulatory switch in wheat Rubisco activase. Plant J 103:742–751. https://doi.org/10.1111/tpj.14766

Demmig-Adams B, Dumlao MR, Herzenach MK, Adams WW (2008) Acclimation. In: Encyclopedia of Ecology, Five-Volume Set. Elsevier Inc., pp 15–23

Deryng D, Conway D, Ramankutty N, et al (2014) Global crop yield response to extreme heat stress under multiple climate change futures. Environ Res Lett 9:034011. https://doi.org/10.1088/1748-9326/9/3/034011

Eberhard S, Finazzi G, Wollman FA (2008) The dynamics of photosynthesis. Annu. Rev. Genet. 42:463–515

Edwards GE, Franceschi VR, Voznesenskaya E V. (2004) Single-cell C_4 photosynthesis versus the dual-cell (Kranz) paradigm. Annu. Rev. Plant Biol. 55:173–196

Eisenhut M, Bräutigam A, Timm S, et al (2017) Photorespiration Is Crucial for Dynamic Response of Photosynthetic Metabolism and Stomatal Movement to Altered CO_2 Availability. Mol Plant 10:47–61. https://doi.org/10.1016/j.molp.2016.09.011

El Habti A, Fleury D, Jewell N, et al (2020) Tolerance of Combined Drought and Heat Stress Is Associated With Transpiration Maintenance and Water Soluble Carbohydrates in Wheat Grains. Front Plant Sci 11:1555. https://doi.org/10.3389/fpls.2020.568693

Fábián A, Sáfrán E, Szabó-Eitel G, et al (2019) Stigma functionality and fertility are reduced by heat and drought co-stress in wheat. Front Plant Sci 10:. https://doi.org/10.3389/fpls.2019.00244

FAO (2017) The future of food and agriculture – Trends and challenges. Rome

FAOSTAT (2019) Food and Agriculture Organization of the United Nations. http://www.fao.org/faostat/en/#data. Accessed 13 Jul 2020

Feller U, Crafts-Brandner SJ, Salvucci ME (1998) Moderately High Temperatures Inhibit Ribulose-1,5-Bisphosphate Carboxylase/Oxygenase (Rubisco) Activase-Mediated Activation of Rubisco. Plant Physiol 116:539–46. https://doi.org/10.1104/PP.116.2.539

Flexas J, Bota J, Loreto F, et al (2004) Diffusive and metabolic limitations to photosynthesis under drought and salinity in C_3 plants. Plant Biol. 6:269–279

Flexas J, Galmes J, Ribas-Carbo M, Medrano H (2005) The Effects of Water Stress on Plant Respiration. In: Plant Respiration. Springer-Verlag, pp 85–94

Foyer CH (2018) Reactive oxygen species, oxidative signaling and the regulation of photosynthesis. Environ. Exp. Bot. 154:134–142

Foyer CH, Noctor G (2005) Oxidant and antioxidant signalling in plants: A re-evaluation of the concept of oxidative stress in a physiological context. Plant, Cell Environ. 28:1056–1071

Furbank RT (2011) Evolution of the C 4 photosynthetic mechanism: Are there really three C 4 acid decarboxylation types? J. Exp. Bot. 62:3103–3108

Furbank RT, Hatch MD (1987) Mechanism of C_4 photosynthesis: the size and composition of the inorganic carbon pool in bundle sheath cells. Plant Physiol 85:958–64. https://doi.org/10.1104/PP.85.4.958

Gangola MP, Ramadoss BR (2018) Sugars play a critical role in abiotic stress tolerance in plants. In: Biochemical, Physiological and Molecular Avenues for Combating Abiotic

Stress in Plants. Elsevier, pp 17–38

Hansen J, Ruedy R, Sato M, Lo K (2010) GLOBAL SURFACE TEMPERATURE CHANGE. Rev Geophys 48:RG4004. https://doi.org/10.1029/2010RG000345

Hatch MD (1987) C_4 photosynthesis: a unique elend of modified biochemistry, anatomy and ultrastructure. BBA Rev. Bioenerg. 895:81–106

Hatch MD, Agostino A, Jenkins CL (1995) Measurement of the leakage of CO_2 from bundle-sheath cells of leaves during C_4 photosynthesis. Plant Physiol 108:173–181. https://doi.org/10.1104/pp.108.1.173

Hendrix CS, Glaser SM (2007) Trends and triggers: Climate, climate change and civil conflict in Sub-Saharan Africa. Polit Geogr 26:695–715. https://doi.org/10.1016/j.polgeo.2007.06.006

Hoegh-Guldberg O, Jacob D, Taylor M, et al (2018) : Impacts of 1.5ºC Global Warming on Natural and Human Systems. In: Masson-Delmotte V, Zhai P, H.-O. Pörtner, et al. (eds) Global Warming of 1.5°C. An IPCC Special Report on the impacts of global warming of 1.5°C above pre-industrial levels and related global greenhouse gas emission pathways, in the context of strengthening the global response to the threat of climate change.

Iizumi T, Shiogama H, Imada Y, et al (2018) Crop production losses associated with anthropogenic climate change for 1981–2010 compared with preindustrial levels. Int J Climatol 38:5405–5417. https://doi.org/10.1002/joc.5818

Jia G, Shevliakova E, Artaxo P, et al (2019) Land-climate interactions. In: Shukla P, Skea J, Calvo Buendia E, et al. (eds) Climate Change and Land: an IPCC special report on climate change, desertification, land degradation, sustainable land management, food security, and greenhouse gas fluxes in terrestrial ecosystems

Jin R, Wang Y, Liu R, et al (2016) Physiological and metabolic changes of purslane (Portulaca oleracea L.) in response to drought, heat, and combined stresses. Front Plant Sci 6:1123. https://doi.org/10.3389/fpls.2015.01123

KNMI (2013) KNMI Climate Change Atlas. KNMI Clim. Explor.

Koch K (2004) Sucrose metabolism: Regulatory mechanisms and pivotal roles in sugar sensing and plant development. Curr. Opin. Plant Biol. 7:235–246

Koussevitzky S, Suzuki N, Huntington S, et al (2008) Ascorbate peroxidase 1 plays a key role in the response of *Arabidopsis thaliana* to stress combination. J Biol Chem 283:34197–34203. https://doi.org/10.1074/jbc.M806337200

Krasavina MS, Burmistrova NA, Raldugina GN (2014) The Role of Carbohydrates in Plant Resistance to Abiotic Stresses. In: Emerging Technologies and Management of Crop Stress Tolerance: Biological Techniques. Elsevier Inc., pp 229–270

Kromdijk J, Ubierna N, Cousins AB, Griffiths H (2014) Bundle-sheath leakiness in C_4 photosynthesis: A careful balancing act between CO_2 concentration and assimilation. J.

Exp. Bot. 65:3443–3457

Kumar S, Lawrence DM, Dirmeyer PA, Sheffield J (2014) Less reliable water availability in the 21st century climate projections. Earth's Futur 2:152–160. https://doi.org/10.1002/2013ef000159

Lambers H, Robinson SA, Ribas-Carbo M (2005) Regulation of Respiration In Vivo. In: Plant Respiration. Springer-Verlag, pp 1–15

Lawlor DW, Tezara W (2009) Causes of decreased photosynthetic rate and metabolic capacity in water-deficient leaf cells: A critical evaluation of mechanisms and integration of processes. Ann. Bot. 103:561–579

Lawson T, Terashima I, Fujita T, Wang Y (2018) Coordination Between Photosynthesis and Stomatal Behavior. pp 141–161

Ljung K, Nemhauser JL, Perata P (2015) New mechanistic links between sugar and hormone signalling networks. Curr. Opin. Plant Biol. 25:130–137

Lobell DB, Asseng S (2017) Comparing estimates of climate change impacts from process-based and statistical crop models. Environ Res Lett 12:15001. https://doi.org/10.1088/1748-9326/aa518a

Lobell DB, Schlenker W, Costa-Roberts J (2011) Climate trends and global crop production since 1980. Science (80-) 333:616–620. https://doi.org/10.1126/science.1204531

Lobet G, Couvreur V, Meunier F, et al (2014) Plant water uptake in drying soils. Plant Physiol 164:1619–1627. https://doi.org/10.1104/pp.113.233486

Long SP, Ort DR (2010) More than taking the heat: crops and global change. Curr Opin Plant Biol 13:240–247. https://doi.org/10.1016/j.pbi.2010.04.008

Lopes MS, Reynolds MP, Jalal-Kamali MR, et al (2012) The yield correlations of selectable physiological traits in a population of advanced spring wheat lines grown in warm and drought environments. F Crop Res 128:129–136. https://doi.org/10.1016/j.fcr.2011.12.017

Lourenço TF, Barros PM, Saibo NJM, et al (2016) Genomics of drought. In: Plant Genomics and Climate Change. Springer New York, pp 85–135

Luan S (2002) Signalling drought in guard cells. Plant, Cell Environ 25:229–237. https://doi.org/10.1046/j.1365-3040.2002.00758.x

Machado S, Paulsen GM (2001) Combined effects of drought and high temperature on water relations of wheat and sorghum. Plant Soil 233:179–187. https://doi.org/10.1023/A:1010346601643

Mathur S, Agrawal D, Jajoo A (2014) Photosynthesis: Response to high temperature stress. J Photochem Photobiol B Biol 137:116–126. https://doi.org/10.1016/J.JPHOTOBIOL.2014.01.010

Maurel C, Verdoucq L, Rodrigues O (2016) Aquaporins and plant transpiration. Plant Cell

Environ. 39:2580–2587

Mbow C, Rosenzweig C, Barioni LG, et al (2019) Food Security. In: Shukla PR, Skea J, Calvo Buendia E, et al. (eds) Climate Change and Land: an IPCC special report on climate change, desertification, land degradation, sustainable land management, food security, and greenhouse gas fluxes in terrestrial ecosystems

Medina S, Vicente R, Nieto-Taladriz MT, et al (2019) The plant-transpiration response to vapor pressure deficit (VPD) in durum wheat is associated with differential yield performance and specific expression of genes involved in primary metabolism and water transport. Front Plant Sci 9:1994. https://doi.org/10.3389/fpls.2018.01994

Meierhoff K, Westhoff P (1993) Differential biogenesis of photosystem II in mesophyll and bundle-sheath cells of monocotyledonous NADP-malic enzyme-type C_4 plants: the non-stoichiometric abundance of the subunits of photosystem II in the bundle-sheath chloroplasts and the translational. Planta 191:23–33. https://doi.org/10.1007/BF00240892

Mittler R, Vanderauwera S, Gollery M, Van Breusegem F (2004) Reactive oxygen gene network of plants. Trends Plant Sci. 9:490–498

Moore FC, Lobell DB (2015) The fingerprint of climate trends on european crop yields. Proc Natl Acad Sci U S A 112:2970–2975. https://doi.org/10.1073/pnas.1409606112

Nelson N, Ben-Shem A (2004) The complex architecture of oxygenic photosynthesis. Nat. Rev. Mol. Cell Biol. 5:971–982

Pantin F, Monnet F, Jannaud D, et al (2013) The dual effect of abscisic acid on stomata. New Phytol 197:65–72. https://doi.org/10.1111/nph.12013

Parant A (1990) Les perspectives demographiques mondiales. Futuribles 49–78. https://doi.org/10.3406/tiers.1983.4290

Parent B, Tardieu F (2012) Temperature responses of developmental processes have not been affected by breeding in different ecological areas for 17 crop species. New Phytol 194:760–774. https://doi.org/10.1111/j.1469-8137.2012.04086.x

Parry MAJ, Keys AJ, Madgwick PJ, et al (2008) Rubisco regulation: A role for inhibitors. In: Journal of Experimental Botany. Oxford Academic, pp 1569–1580

Pennacchi JP, Carmo-Silva E, Andralojc PJ, et al (2019) Stability of wheat grain yields over three field seasons in the UK. Food Energy Secur 8:e00147. https://doi.org/10.1002/fes3.147

Perdomo JA, Capó-Bauçà S, Carmo-Silva E, Galmés J (2017) Rubisco and Rubisco Activase Play an Important Role in the Biochemical Limitations of Photosynthesis in Rice, Wheat, and Maize under High Temperature and Water Deficit. Front Plant Sci 8:490. https://doi.org/10.3389/fpls.2017.00490

Perdomo JA, Conesa M, Medrano H, et al (2015) Effects of long-term individual and combined

water and temperature stress on the growth of rice, wheat and maize: Relationship with morphological and physiological acclimation. Physiol Plant 155:149–165. https://doi.org/10.1111/ppl.12303

Pinto RS, Reynolds MP (2015) Common genetic basis for canopy temperature depression under heat and drought stress associated with optimized root distribution in bread wheat. Theor Appl Genet 128:575–585. https://doi.org/10.1007/s00122-015-2453-9

Rao X, Dixon RA (2016) The differences between NAD-ME and NADP-ME subtypes of C_4 photosynthesis: More than decarboxylating enzymes. Front. Plant Sci. 7:1525

Rizhsky L, Liang H, Mittler R (2002) The combined effect of drought stress and heat shock on gene expression in tobacco. Plant Physiol 130:1143–1151. https://doi.org/10.1104/pp.006858

Rizhsky L, Liang H, Shuman J, et al (2004) When defense pathways collide. The response of arabidopsis to a combination of drought and heat stress 1[w]. Plant Physiol 134:1683–1696. https://doi.org/10.1104/pp.103.033431

Roche D (2015) Stomatal Conductance Is Essential for Higher Yield Potential of C_3 Crops. CRC Crit Rev Plant Sci 34:429–453. https://doi.org/10.1080/07352689.2015.1023677

Roitsch T (1999) Source-sink regulation by sugar and stress. Curr Opin Plant Biol 2:198–206. https://doi.org/10.1016/S1369-5266(99)80036-3

Roitsch T, González MC (2004) Function and regulation of plant Invertases: Sweet sensations. Trends Plant Sci. 9:606–613

Ruban A V. (2016) Nonphotochemical chlorophyll fluorescence quenching: Mechanism and effectiveness in protecting plants from photodamage. Plant Physiol. https://doi.org/10.1104/pp.15.01935

Rumeau D, Peltier G, Cournac L (2007) Chlororespiration and cyclic electron flow around PSI during photosynthesis and plant stress response. Plant, Cell Environ. 30:1041–1051

Russo S, Dosio A, Graversen RG, et al (2014) Magnitude of extreme heat waves in present climate and their projection in a warming world. J Geophys Res Atmos 119:12,500-12,512. https://doi.org/10.1002/2014JD022098

Sade N, Gebremedhin A, Moshelion M (2012) Risk-taking plants: anisohydric behavior as a stress-resistance trait. Plant Signal. Behav. 7:767–770

Sage RF (2004) The evolution of C_4 photosynthesis. New Phytol. 161:341–370

Sage RF, Khoshravesh R, Sage TL (2014) From proto-Kranz to C_4 Kranz: building the bridge to C_4 photosynthesis. J Exp Bot 65:3341–3356. https://doi.org/10.1093/jxb/eru180

Sainz M, Díaz P, Monza J, Borsani O (2010) Heat stress results in loss of chloroplast Cu/Zn superoxide dismutase and increased damage to Photosystem II in combined drought-heat stressed Lotus japonicus. Physiol Plant 140:46–56. https://doi.org/10.1111/j.1399-3054.2010.01383.x

Sairam RK, Srivastava GC, Saxena DC (2000) Increased antioxidant activity under elevated temperatures: A mechanism of heat stress tolerance in wheat genotypes. Biol Plant 43:245–251. https://doi.org/10.1023/A:1002756311146

Salvucci ME, Crafts-Brandner SJ (2004) Mechanism for deactivation of Rubisco under moderate heat stress. Physiol Plant 122:513–519. https://doi.org/10.1111/j.1399-3054.2004.00419.x

Salvucci ME, Osteryoung KW, Crafts-Brandner SJ, Vierling E (2001) Exceptional sensitivity of Rubisco activase to thermal denaturation in vitro and in vivo. Plant Physiol 127:1053–64. https://doi.org/10.1104/PP.010357

Scafaro AP, Bautsoens N, den Boer B, et al (2019) A Conserved Sequence from Heat-Adapted Species Improves Rubisco Activase Thermostability in Wheat. Plant Physiol 181:43–54. https://doi.org/10.1104/pp.19.00425

Schär C (2016) Climate extremes: The worst heat waves to come. Nat. Clim. Chang. 6:128–129

Schoppach R, Taylor JD, Majerus E, et al (2016) High resolution mapping of traits related to whole-plant transpiration under increasing evaporative demand in wheat. J. Exp. Bot. 67:2847–2860

Schreier TB, Hibberd JM (2019) Variations in the Calvin-Benson cycle: Selection pressures and optimization? J Exp Bot 70:1697–1701. https://doi.org/10.1093/jxb/erz078

Sedelnikova O V., Hughes TE, Langdale JA (2018) Understanding the genetic basis of c 4 Kranz anatomy with a view to engineering c 3 crops. Annu. Rev. Genet. 52:249–270

Sehgal A, Sita K, Kumar J, et al (2017) Effects of drought, heat and their interaction on the growth, yield and photosynthetic function of lentil (Lens culinaris medikus) genotypes varying in heat and drought sensitivity. Front Plant Sci 8:1776. https://doi.org/10.3389/fpls.2017.01776

Shahinnia F, Roy J Le, Laborde B, et al (2016) Genetic association of stomatal traits and yield in wheat grown in low rainfall environments. BMC Plant Biol 16:150. https://doi.org/10.1186/s12870-016-0838-9

Shivhare D, Mueller-Cajar O (2017) In vitro characterization of thermostable CAM Rubisco activase reveals a Rubisco interacting surface loop. Plant Physiol 174:1505–1516. https://doi.org/10.1104/pp.17.00554

Sinclair TR (2017) Limited-Transpiration Rate Under Elevated Atmospheric Vapor Pressure Deficit. Springer, Cham, pp 11–16

Steudle E (2001) The cohesion-tension mechanism and the acquisition of water by plant roots. Annu Rev Plant Biol 52:847–875

Stocker TF, Qin D, Plattner G-K, et al (2013) Climate Change 2013: The Physical Science Basis Working Group I Contribution to the Fifth Assessment Report of the

Intergovernmental Panel on Climate Change

Suzuki N, Rivero RM, Shulaev V, et al (2014) Abiotic and biotic stress combinations. New Phytol 203:32–43. https://doi.org/10.1111/nph.12797

Tambussi EA, Bort J, Araus JL (2007) Water use efficiency in C_3 cereals under Mediterranean conditions: A review of physiological aspects. Ann Appl Biol 150:307–321. https://doi.org/10.1111/j.1744-7348.2007.00143.x

Tardieu F (2013) Plant response to environmental conditions: Assessing potential production, water demand, and negative effects of water deficit. Front Physiol 4 FEB:1–11. https://doi.org/10.3389/fphys.2013.00017

Tardieu F (2012) Any trait or trait-related allele can confer drought tolerance: Just design the right drought scenario. J Exp Bot 63:25–31. https://doi.org/10.1093/jxb/err269

Tardieu F, Simonneau T, Muller B (2018) The Physiological Basis of Drought Tolerance in Crop Plants: A Scenario-Dependent Probabilistic Approach. Annu. Rev. Plant Biol. 69:733–759

Tezara W, Mitchell VJ, Driscoll SD, Lawlor DW (1999) Water stress inhibits plant photosynthesis by decreasing coupling factor and ATP. Nature 401:914–917. https://doi.org/10.1038/44842

Trenberth KE, Jones PD, Ambenje P, et al (2007) Observations: Surface and Atmospheric Climate Change Coordinating Lead Authors: Lead Authors: Review Editors: This chapter should be cited as. In: Solomon S, Qin D, Manning M, et al. (eds) Climate Change 2007: The Physical Science Basis. Contribution of Working Group I to the Fourth Assessment Report of the Intergovernmental Panel on Climate Change. Cambridge University Press, Cambridge, United Kingdom and New York, NY, USA

Trenberth KE, Shea DJ (2005) Relationships between precipitation and surface temperature. Geophys Res Lett 32:1–4. https://doi.org/10.1029/2005GL022760

Tricker PJ, Elhabti A, Schmidt J, Fleury D (2018) The physiological and genetic basis of combined drought and heat tolerance in wheat. J. Exp. Bot. 69:3195–3210

Tyree MT (1997) The Cohesion-Tension theory of sap ascent: Current controversies. J. Exp. Bot. 48:1753–1765

United Nations, Department of Economic and Social Affairs PD (2019) World Population Prospects 2019: Highlights (ST/ESA/SER.A/423)

Vadez V, Kholova J, Medina S, et al (2014) Transpiration efficiency: New insights into an old story. J. Exp. Bot. 65:6141–6153

Vile D, Pervent M, Belluau M, et al (2012) Arabidopsis growth under prolonged high temperature and water deficit: Independent or interactive effects? Plant, Cell Environ 35:702–718. https://doi.org/10.1111/j.1365-3040.2011.02445.x

von Caemmerer S, Furbank RT (2016) Strategies for improving C_4 photosynthesis. Curr. Opin.

Plant Biol. 31:125–134

Walker BJ, VanLoocke A, Bernacchi CJ, Ort DR (2016) The Costs of Photorespiration to Food Production Now and in the Future. Annu Rev Plant Biol 67:107–129. https://doi.org/10.1146/annurev-arplant-043015-111709

Walters RG (2005) Towards an understanding of photosynthetic acclimation. In: Journal of Experimental Botany. Oxford Academic, pp 435–447

Wang D, Fu A (2016) The Plastid Terminal Oxidase is a Key Factor Balancing the Redox State of Thylakoid Membrane. In: Enzymes. Academic Press, pp 143–171

Worldometers.info (2020) Worldometers. http://www.worldometers.info/faq/. Accessed 12 Dec 2020

Yamamoto Y (2016) Quality Control of Photosystem II: The Mechanisms for Avoidance and Tolerance of Light and Heat Stresses are Closely Linked to Membrane Fluidity of the Thylakoids. Front Plant Sci 7:1136. https://doi.org/10.3389/fpls.2016.01136

Yamori W, Hikosaka K, Way DA (2014) Temperature response of photosynthesis in C_3, C_4, and CAM plants: Temperature acclimation and temperature adaptation. Photosynth Res 119:101–117. https://doi.org/10.1007/s11120-013-9874-6

Zampieri M, Ceglar A, Dentener F, Toreti A (2017) Wheat yield loss attributable to heat waves, drought and water excess at the global, national and subnational scales. Environ Res Lett 12:. https://doi.org/10.1088/1748-9326/aa723b

Zandalinas SI, Balfagón D, Arbona V, Gómez-Cadenas A (2017) Modulation of Antioxidant Defense System Is Associated with Combined Drought and Heat Stress Tolerance in Citrus. Front Plant Sci 8:953. https://doi.org/10.3389/fpls.2017.00953

Zandalinas SI, Rivero RM, Martínez V, et al (2016) Tolerance of citrus plants to the combination of high temperatures and drought is associated to the increase in transpiration modulated by a reduction in abscisic acid levels. BMC Plant Biol 16:105. https://doi.org/10.1186/s12870-016-0791-7

Zhang G, Zhang M, Zhao Z, et al (2017) Wheat TaPUB1 modulates plant drought stress resistance by improving antioxidant capability. Sci Rep 7:1–13. https://doi.org/10.1038/s41598-017-08181-w

Zhao C, Liu B, Piao S, et al (2017) Temperature increase reduces global yields of major crops in four independent estimates. Proc Natl Acad Sci U S A 114:9326–9331. https://doi.org/10.1073/pnas.1701762114

Chapter II

Photoprotection and optimization of sucrose usage contribute to faster recovery of photosynthesis after water deficit at high temperatures in wheat

Data presented in this chapter was included in the following work:

Correia PMP, Silva AB, Roitsch T, Carmo-Silva E, Marques da Silva J, (2021) Photoprotection and optimization of sucrose usage contribute to faster recovery of photosynthesis after water deficit at high temperatures in wheat. Physiol Plant 172:615–628. https://doi.org/10.1111/ppl.13227

Table of Contents – Chapter II

Abstract

Plants are increasingly exposed to events of elevated temperature and water deficit, which threaten crop productivity. Understanding the ability to rapidly recover from abiotic stress, restoring carbon assimilation and biomass production, is important to unravel crop climate resilience. This study compared the photosynthetic performance of two *Triticum aestivum* L. cultivars, Sokoll and Paragon, adapted to the climate of Mexico and UK, respectively, exposed to one week water deficit and high temperatures, in isolation or combination. Measurements included photosynthetic assimilation rate, stomatal conductance, in vitro activities of Rubisco (EC 4.1.1.39) and Invertase (INV, EC 3.2.1.26), antioxidant capacity and chlorophyll *a* fluorescence. In both genotypes, under elevated temperatures and water deficit (WD38ºC), the photosynthetic limitations were mainly due to stomatal restrictions and to a decrease in the electron transport rate. Chlorophyll *a* fluorescence parameters clearly indicate differences between the two genotypes in the photoprotection when subjected to WD38ºC and showed faster recovery of Paragon after stress relief. The activity of the cytosolic Invertase (cytINV) under these stress conditions was strongly related to the fast photosynthesis recovery of Paragon. Taken together, the results suggest that optimal sucrose export/utilization and increased photoprotection of the electron transport machinery are important components to limit yield fluctuations due to water shortage and elevated temperatures.

2.1 Introduction

Global warming is a serious threat to crop production. Wheat is the world's most harvested crop per area, however, wheat yield is below the average of the other major crops (e.g. maize and rice) being therefore only the second most-produced cereal grain, with 26% of the world share (FAOSTAT 2017). Around 40% of the global wheat yield fluctuations are explained by climatic variation, and heatwaves and drought are among the principal stressors (Deryng et al. 2014, Zampieri et al. 2017). Each degree-Celsius increase in global mean temperature reduces, on average, the global yield of wheat by 6% (Zhao et al. 2017). To improve wheat yield in a changing climate, and ensure food security for an increasing world population, it is essential to comprehend how wheat plants respond to fluctuations in temperature and water availability, and the mechanisms involved in fast recovery of plant growth upon relief from high temperatures and extended drought.

When subjected to high temperatures, plants usually use evaporative cooling to reduce leaf temperature (Carmo-Silva et al. 2012, Costa et al. 2013). However, in response to water shortage, higher plants close the stomata to limit water loss by transpiration. When both conditions are present, stomatal closure reduces transpiration and consequently the plant temperature rises and intercellular CO_2 concentration decreases (Chaves et al. 2003, Carmo-Silva et al. 2012, Duque et al. 2013) . High temperatures and drought negatively affect photosynthetic CO_2 fixation at different levels, depending on the stress intensity, decreasing biomass accumulation (Zandalinas et al. 2018, Lamaoui et al. 2018, Tricker et al. 2018, Raja et al. 2020). Even if high temperature increases the maximum rate (Vmax) of the primary carboxylation enzyme of C_3 photosynthesis (Rubisco, EC 4.1.1.39), it also increases the inhibition of Rubisco by sugar phosphate derivatives and thus Rubisco activation state decreases (Salvucci and Crafts-Brandner, 2004a,b). The efficiency of Rubisco depends on the activity of Rubisco's catalytic chaperone, Rubisco activase (RCA), to promote the release of inhibitory sugar phosphates from active sites. However, RCA is extremely thermal sensitive and depends on the redox status and ADP/ATP ratio (Carmo-Silva et al. 2015). To improve plant tolerance to increased temperatures, bioengineering approaches aiming to enhance Rubisco activity by increasing the thermotolerance of RCA have been suggested (Scafaro et al. 2016, Mueller-Cajar 2017, Shivhare and Mueller-Cajar 2017, Scafaro et al. 2019, Degen et al. 2020). Lower internal CO_2 concentration and high temperatures also reduce Rubisco specificity for CO_2 relative to O_2, resulting in an increase of photorespiration, which leads to the release of previous fixed CO_2 and higher demand for ATP (Walker et al. 2016).

Moreover, imbalances between CO_2 assimilation and the rate of light capture usually lead to an excess of energy in the system that can result in reactive oxygen species (ROS) formation and photoinhibition if the capacities of dissipation, scavenging and repairing are

exceeded (Yamamoto 2016). Among the main energy dissipation mechanisms are the non-photochemical quenching (qN, generally compartmented in three major components, energy-dependent quenching, qE , state-transition quenching, qT, and photoinhibition quenching, qI), cyclic electron flow around photosystem I and chlororespiration (Rumeau et al. 2007, Ruban 2016, Wang and Fu 2016). ROS detoxification is generally conducted enzymatically and by the production of several antioxidant compounds (Mittler et al. 2004; Foyer 2018; Begum et al. 2019) When energy dissipation and ROS detoxification fails, oxidative damage occurs. Many studies reported the reduction of the electron transfer from water to $NADP^+$, due to reversible and irreversible inhibition of photosystem II (PSII) caused by oxidative stress in face of elevated temperatures and/or drought. The main processes involved are the damage of the oxygen-evolving complex (Heckathorn et al. 1998, Tiwari et al. 2008, Chen et al. 2016), the degradation and aggregation of the D1 protein (Kamata et al. 2005, Komayama et al. 2007, Allakhverdiev et al. 2008, Takahashi and Murata 2008) and changes on the membrane fluidity (Gounaris et al. 1983, Aronsson et al. 2008, Yamamoto 2016).

Therefore, when photosynthetic performance and plant growth are challenged by water shortage and elevated temperatures, optimization of sucrose export, uptake, and utilization, e.g. through adjustment of source – sink relations via Invertase activity (INV, EC 3.2.1.26), can contribute to reducing yield fluctuations. Invertases mediate the hydrolytic cleavage of sucrose into hexose monomers and are involved in regulating carbohydrate partitioning, developmental processes, hormone responses and biotic and abiotic interactions (Roitsch and González 2004). Invertases localized in the vacuole (vacINVs) play a major role in the osmotic regulation (Nägele et al. 2010, Ruan 2014, Weiszmann et al. 2018), while cytosolic Invertases (cytINVs) control sugar homeostasis and the maintenance of constant glucose levels to sustain cellular functions (Ruan et al. 2010, Lunn 2016, Figueroa and Lunn 2016).

The aims of the present study were to (1) characterise the photosynthetic limitations of two wheat genotypes, Paragon and Sokoll, adapted to distinct climate conditions, under water deficit and/or high temperature, and (2) to determine which factors are responsible for photosynthetic performance and recovery from high temperature in the absence or presence of water deficit. To test the hypothesis that the UK-adapted cultivar Paragon would be less resistant to heat stress and water deficit compared to the Mexican-adapted cultivar Sokoll, the two genotypes were subject to water deficit and elevated temperatures, in isolation or in combination, and compared for net assimilation rate, stomatal conductance, Rubisco and Invertase in vitro activities, antioxidant capacity and chlorophyll *a* fluorescence.

2.2 Materials and methods

2.2.1 Plant growth conditions

Two *Triticum aestivum* L. (wheat) genotypes were selected on the basis that these are adapted to distinct climate conditions: Paragon is a traditional UK spring wheat elite cultivar, while Sokoll is a synthetic-derived cultivar developed by the International Maize and Wheat Improvement Centre (CMMYT, Mexico). Plants of both genotypes were grown from seeds in a controlled environment chamber (Fitoclima 5000 EH, Aralab) in 1 L pots containing horticultural substrate (Compo Sana Universal, Compo Sana). Light was provided by fluorescent lamps (Osram Lumilux L 58W/840 cool white lamps) placed at specific distances from the plants to obtain an average photosynthetic photon flux density (PPFD) of 300 µmol m^{-2} s^{-1} at the top of the canopy, with a photoperiod of 16 h. Due to space constraints, temperature assays were performed in two consecutive experiments. After full germination, all plants were initially grown under a control temperature (25/18°C day/night), with 50% relative humidity (RH) for 21 days.

For experiments under control temperature, plants remained at 25/18°C (day/night) with 50% RH throughout the experiment. Three weeks post-germination plants were randomly assigned to two irrigation treatments: five plants per cultivar were maintained well-watered (WW; minimum 80% field capacity, WW25°C) throughout the experiment and five plants were subject to water deficit (WD, 30±5% field capacity, WD25°C) for 7 days. For experiments under elevated temperature, 21-day-old plants were also exposed to high temperatures (38/31°C day/night) with 60% RH and randomly assigned to the irrigation treatments: ten plants per cultivar were maintained WW (80±5% field capacity, WW38°C) and ten plants were subject to WD (30±5% field capacity, WD38°C) for 5 days. From the 10 plants allocated to WW38°C or WD38°C, 5 were randomly selected for recovery after 5 days of stress, re-watered and maintained at control temperatures for 7 days. WD was established by withholding watering and sustaining a minimum of 30±5% field capacity. The soil water content was determined gravimetrically by weighing the pots, and irrigation was provided to compensate evapotranspiration and keep the field capacity in the WW and WD pots. Leaf samples for biochemical analyses were collected at the end of the respective temperature and irrigation treatment, 5-7 h after the beginning of the photoperiod, frozen into liquid nitrogen and stored at -80°C.

2.2.2 Leaf and soil water status

Plant water status was estimated by leaf relative water content (LRWC) following the methodology described by Čatský (1960). Fresh leaf samples from the flag leaf (1-2 cm^2) were collected, fresh weight was immediately measured in an electronic scale (Sartorius BP221S), turgid weight (LTW) was determined after saturating samples by immersion in deionized water overnight, and dry weight (LDW) was measured after oven-drying samples at

70°C for 48 h. Soil relative water content (SRWC) was determined by following a similar procedure; although soil field capacity (SFC) was achieved by watering the pots to saturation and allowing water drainage for 2 hours, and dry weight (SDW) was measured after oven-drying samples at 110°C for 36 h. Leaf water potential was measured with a C-52 thermocouple chamber (Wescor), 20 mm^2 leaf discs were cut and equilibrated for 30 min in the chamber before the readings were recorded by a PSYPRO water potential datalogger (Wescor) in the psychrometric mode.

$$\mathrm{LRWC} = \frac{(\mathrm{LFW}-\mathrm{LDW})}{(\mathrm{LTW}-\mathrm{LDW})}.$$

2.2.3 Thermal imaging

Thermal images were obtained using a thermal camera (Flir 50bx, FLIR Systems Inc.) with emissivity set at 0.95 and approximately 1 m distance from the plants. Before each set of measurements, background temperature was determined by measuring the temperature of a crumpled sheet of aluminum foil in a similar position to the leaves of interest with the emissivity set at 1.0 following the methodology described by Costa et al. (2013). Thermal images were analysed with the software FLIR Tools (FLIR Systems, Inc.). The temperature of each plant was determined from the temperature of five leaves using the function “area”. Visible images (RGB) were collected to complement the analysis of thermal images.

2.2.4 Gas exchange and chlorophyll *a* fluorescence steady-state measurements

Parallel measurements of photosynthetic gas exchange and chlorophyll *a* fluorescence were performed in a non-detached fully expanded leaf from each plant using a gas exchange system (IRGA LCpro+, ADC BioScientific) combined with a chlorophyll fluorescence imaging system (Imaging-PAM Chlorophyll Fluorometer M-series Mini version, Heinz Walz GmbH). Control air temperature was set to 25°C, PPFD at the leaf level set to 226 µmol m^{-2} s^{-1} and the CO_2 concentration in the leaf chamber set to 400 µmol CO_2 mol^{-1} air allowing the leaf to reach steady-state assimilation rate (A) and stomatal conductance (gs). A and gs were calculated by the LCpro+ software according to von Caemmerer and Farquhar (1981). Chlorophyll *a* steady-state fluorescence was analysed using the Imaging Win analytical software (Heinz Walz GmbH). PSII effective quantum yield (*Φ*PSII) was obtained according to Genty et al. (1989), photochemical (qP) and non-photochemical (qN) quenching were calculated according to Oxborough and Baker (1997) and total non-photochemical fluorescence quenching (NPQ) was calculated using the Stern-Volmer approach (Krause and Jahns 2007). Electron transport rate (ETR) was then calculated as:

$$\mathrm{ETR} = 0.5\Phi\mathrm{PSII} \times \mathrm{PPFD} \times \mathrm{abs},$$

, where absorptivity (abs) was measured for each leaf before the chlorophyll *a* fluorescence measurement.

2.2.5 Chlorophyll *a* fluorescence induction

The kinetics of the rapid fluorescence induction rise was recorded on fully expanded dark-adapted leaves (10 minutes) exposed to a saturating light pulse (3500 µmol m^{-2} s^{-1}) for 1 second to obtain the OJIP Chl *a* fluorescence transient rise (Handy PEA, Hansatech Instruments). Fluorescence parameters derived from the extracted data, namely specific energy fluxes per QA-reducing PSII reaction center and photosynthetic performance indexes were calculated according to Strasser and collaborators (Strasser et al. 2004, Tsimilli-Michael and Strasser 2008) with the nomenclature presented in Stirbet and Govindjee (2011).

2.2.6 Antioxidant capacity

Antioxidant metabolites were extracted from frozen leaf samples (0.1-0.3 g FW) by homogenisation in pure methanol with 1.4 mm zirconium oxide beads (Precellys) in a tissue homogenizer (Precellys Evolution, Precellys) and then centrifuged at 20 000 *g* for 5 min. Trolox equivalents antioxidant capacity (TEAC) and ferric reducing antioxidant power (FRAP) were measured in the supernatant using a 96-well microtiter plate. TEAC was determined by the reaction of sample supernatant and 2,2′-Azino-bis (3-ethylbenzothiazoline-6-sulfonic acid) diammonium salt (ABTS), solution 1:20 in phosphate buffer pH 7.4 (0.7-0.8 optical density). The reaction mixtures were incubated 6 min at room temperature before measuring absorbance at 734 nm (ELx808, BioTek Instruments, Inc.). 6-hydroxy-2,5,7,8-tetramethylchroman-2-carboxylic acid (Trolox) standards (0-0.8 mM in 96% ethanol) were measured alongside the samples and used to prepare the respective calibration curve. FRAP was measured by the reaction of the sample supernatant with a solution consisting of 0.3 mM acetate buffer, 10 mM 2,4,6-tripyridyl-s-triazine (TPTZ) and 20 mM $FeCl_3$. The reaction mixtures were incubated 4 min at room temperature before measuring the absorbance at 593nm (ELx808, BioTek Instruments Inc.). $FeSO_4$ standards (0-1.0 mM) in ddH_2O were measured alongside the samples and used to prepare the respective calibration curves. Samples and standards were measured in triplicate alongside blanks containing no sample.

2.2.7 Rubisco activity

Rubisco was extracted from the leaves by grinding frozen samples (0.1-0.3 g FW) in a cold mortar with quartz sand, 1% (w/v) insoluble polyvinylpyrrolidone (PVP), ice-cold extraction medium (1/10 FW per mL) containing 50 mM Bicine-KOH pH 8.0, 1 mM ethylenediaminetetraacetic acid (EDTA), 5% (w/v) polyvinylpyrrolidone (PVP25000), 6% polyethylene glycol (PEG_{4000}), 10 mM 1,4-dithiothreitol (DTT), 50 mM β-mercaptoethanol and 1% (v/v) protease inhibitor cocktail for plant extracts (Sigma-Aldrich), adapted from Carmo-Silva et al. (2010). Leaf extracts were then centrifuged at 14 000 *g* and 4°C for 5 min. The supernatant was kept at 4°C and used immediately for measurement of Rubisco activities by the incorporation of

$^{14}CO_2$ into acid-stable products at 25 and 38ºC, following the protocol described in Parry et al. (1997) with modifications. The reaction mixture contained 100 mM Bicine-NaOH pH 8.2, 40 mM $MgCl_2$, 10 mM $NaH^{14}CO_3$ (7.4 kBq µmol^{-1}) and 0.4 mM ribulose 1,5-bisphosphate(RuBP). Rubisco initial activity (Vi) was determined by adding the supernatant to the mixture and stopping the reaction after 60-180s with 10 M HCOOH. Total activity (Vt) was measured after incubating the same volume of extract for 3 min with all the reaction mixture components except RuBP, to allow carbamylation of all the Rubisco available catalytic sites. The reaction was then started by adding RuBP and stopped as above. All measurements were carried out in triplicate and control reactions were quenched with HCOOH prior to the addition of RuBP. The mixtures were completely dried at 70°C overnight and the residues re-hydrated in 0.5 mL ddH_2O, then mixed with 5 mL scintillation cocktail (Ultima Gold, Perkin-Elmer). Radioactivity due to ^{14}C incorporation in the acid-stable products was measured by liquid scintillation counting (LS7800, Beckman). The activation state of Rubisco was calculated as the ratio,

$$\text{Activation state Rubisco} = \frac{\text{Vi}}{\text{Vt}} \times 100.$$

Total soluble protein (TSP) content was determined according to the Bradford method (Bradford 1976) using BSA Fraction V as standard protein.

2.2.8 Invertase activity

Cytosolic Invertase (cytInv) and vacuolar Invertase (vacInv) were extracted from the leaves by grinding frozen samples (0.1-0.3 g FW) in a cold mortar with quartz sand, 1% (w/v) PVPP, ice-cold extraction medium containing 40 mM TRIS-HCl pH 7.6, 3 mM $MgCl_2$, 1 mM EDTA, 0.1 mM phenylmethylsulfonyl fluoride (PMSF), 1 mM benzamidine, 14 mM β-mercaptoethanol, 24 µM nicotinamide adenine dinucleotide phosphate ($NADP^+$), according to Jammer et al. (2015), with modifications. Leaf extracts were then centrifuged at 20 000 *g* for 10 min at 4°C. The supernatant was kept at 4°C and dialysed overnight with 20 mM potassium phosphate buffer pH 7.4 at 4°C in a dark room. Extracts were aliquoted, frozen in liquid nitrogen and stored at -20°C. The activities were measured in thawed samples using 96-well microtiter plates. Reaction mixtures containing 10 mM sucrose and dialysed protein extract were incubated for 30 min at 37°C, cooled for 5 min on ice to stop the reaction, and then incubated for 30 min at room temperature with GOD-POD reagent (10 U mL^{-1} of Glucose oxidase from *Aspergillus niger* (GOD), 0.8 U mL^{-1} Peroxidase from horseradish (POD) and 0.8 mg mL^{-1} ABTS in 0.1 M potassium phosphate buffer (pH 7.0). The amount of liberated glucose was determined by measurement of absorbance at 405 nm at 30°C (ELx808, BioTek Instruments Inc.). Glucose standards (0-50 nmol) were measured alongside the samples and used to prepare the respective calibration curves. All measurements were carried out in triplicate alongside blanks containing no sucrose. TSP content was determined according to the Bradford method (Bradford 1976) using BSA Fraction V as standard protein.

2.2.9 Statistical analysis

The statistical significance of trait variation was tested by factorial ANOVA, with cultivars, irrigation and temperature regimes as fixed factors. Post-hoc comparison between treatments was performed with Duncan test ($P < 0.05$) using IBM SPSS Statistics, Version 25 (IBM, USA). Multivariate analysis was performed with MixOmics R package (Rohart et al. 2017) using Rstudio software.

2.3 Results

2.3.1 Leaf and soil water relations under drought and high temperatures

To characterise the leaf and soil water status of Sokoll and Paragon plants, leaf and soil relative water content (LRWC and SRWC, respectively) and leaf water potential (LWP) were estimated at the end of each experimental condition (Table 2.1). Well-watered (WW) plants presented LRWC and LWP around or above 80% and -1 M Pa, respectively, suggesting good cellular hydration. On the other hand, water deficit (WD) conditions led to a decrease in LRWC and LWP values (lower than 70% and -1 MPa, respectively), revealing a reduction in hydration and a considerable driving force for water movement through the plant. Under WD25°C, Paragon presented higher LRWC than Sokoll, even though no significant differences were found for LWP and soil relative water content (SRWC), showing the capacity of this genotype to maintain cellular hydration under these conditions. The canopy temperature (Tcanopy) increased in both cultivars when subject to high temperatures. Under WW38°C, Tcanopy was significantly lower in Sokoll compared to Paragon, indicating the ability of Sokoll to avoid heat and maintain optimal cell temperature. No differences were observed between the genotypes when subjected to WD38ºC, the observed LRWC under 50% and low LWP indicate severe drought stress, and Tcanopy was also highest in these plants.

Table 2.1 – Leaf and soil water status, and canopy temperature of Paragon and Sokoll wheat plants exposed to a combination of high temperature and water deficit and recovery from high temperature conditions. Plants were grown for 3 weeks, then exposed to high temperature (38°C versus control, 25°C), water deficit (WD versus well-watered, WW) and re-watered at control temperature (25°C) after high temperature conditions (RWW38°C and RWD38°C). Values are means ± SD (n = 5 biological replicates). Different letters denote statistically significant differences between treatments (Duncan analysis, $P<0.05$). LRWC- leaf relative water content; LWP- leaf water potential; SRWC- soil relative water content; Tcanopy- canopy temperature.

Treatment		Genotype	LRWC (% H_2O)	LWP (MPa)	SRWC (% H_2O)	Tcanopy (°C)
25 °C	WW	Paragon	90.11 ± 8.82 c	-0.50 ± 0.08 c	88.45 ± 5.84 c	26.87 ± 0.65 a
		Sokoll	90.20 ± 1.73 c	-0.81 ± 0.12 bc	80.11 ± 4.88 b	26.33 ± 0.19 a

	WD	**Paragon**	68.24 ± 12.45 b	-1.16 ± 0.16 ab	26.74 ± 4.84 a	28.79 ± 0.62 b
		Sokoll	31.89 ± 8.87 a	-1.39 ± 0.10 a	29.12 ± 0.92 a	27.89 ± 1.10 b
38 °C	**WW**	**Paragon**	78.60 ± 8.47 bc	-0.82 ± 0.06 bc	87.57 ± 2.11 c	35.04 ± 0.98 c
		Sokoll	80.38 ± 4.74 bc	-0.77 ± 0.09 bc	75.02 ± 5.32 b	33.37 ± 0.40 d
	WD	**Paragon**	39.60 ± 17.71 a	-1.30 ± 0.59 a	30.44 ± 1.69 a	36.95 ± 0.74 e
		Sokoll	43.06 ± 26.64 a	-1.55 ± 0.58 a	28.42 ± 2.72 a	37.52 ± 0.47 e
Recovery	**RWW 38 °C**	**Paragon**	86.46 ± 1.36 c	-0.76 ± 0.03 bc	90.13 ± 5.25 c	25.71 ± 0.3 a
		Sokoll	94.91 ± 4.82 cd	-0.74 ± 0.05 bc	91.69 ± 6.14 c	25.58 ± 0.4 a
	RWD 38 °C	**Paragon**	90.83 ± 3.42 c	-0.72 ± 0.1 bc	88.96 ± 4.1 c	26.33 ± 0.44 a
		Sokoll	78.31 ± 21.18 bc	-0.98 ± 0.16 ab	89.3 ± 3.22 c	26.43 ± 0.21 a

2.3.2 Effects of drought and high temperatures on photosynthesis

WD plants had significantly lower net photosynthesis assimilation rate (A), stomatal conductance (gs) and electron transport rate (ETR) compared to WW plants, except for Paragon at 25ºC (Figure 2.1A-C). Steady-state photosynthetic gas-exchanges were comparable for both genotypes under WW conditions. A strong positive relationship between A and gs was observed (r=0.914, P<0.0001 and r=0.974 P<0.0001, Paragon and Sokoll respectively,Table S2.1), suggesting a possible stomatal limitation to photosynthesis, and between A and ETR (r= 0.966, P<0.0001 and r=0.797, P<0.0001, Table S2.1), suggesting limitations at the photosystems level.

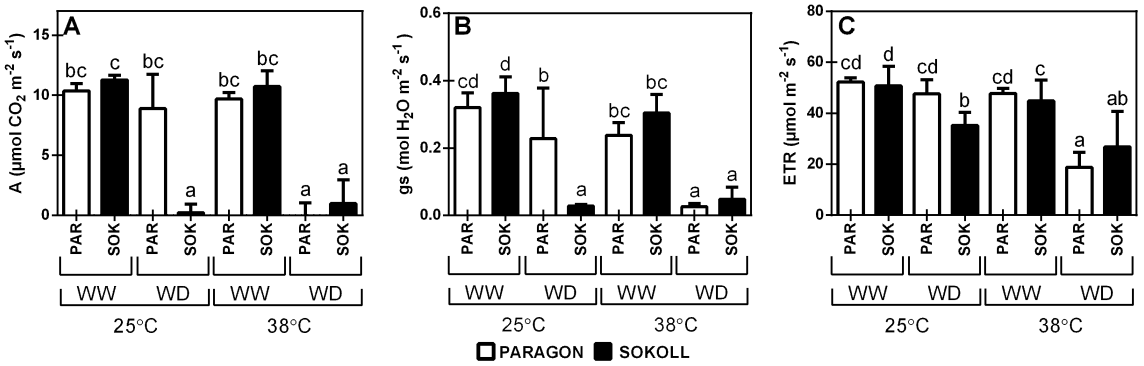

Figure 2.1 – Steady-state photosynthesis of Paragon (PAR) and Sokoll (SOK) wheat plants exposed to a combination of high temperature and water deficit. (A) Net CO_2 assimilation, **(B)** stomatal conductance (gs) and **(C)** electron transport rate (ETR) were measured at growth light and ambient CO_2 in fully expanded leaves of wheat 3-week-old plants under well-watered (WW) and water deficit (WD) conditions and exposed to control (25°C)

and high temperature conditions (38°C). Values are means ± SD (n = 5 biological replicates). Different letters denote statistically significant differences between treatments (Duncan analysis, P<0.05).

2.3.3 Effect of water deficit and high temperatures on Rubisco in vivo activities measured at control and high temperatures

To verify if the limitations in the carbon fixation found under stress conditions were a result of an imbalance in the Calvin-Benson-Bassham cycle, the in vivo Rubisco activity was assessed at the two growth temperatures. When Rubisco activity was measured at 25ºC, the initial and total velocities decreased significantly under WD (WD25ºC and WD38ºC) and elevated temperatures (WW38ºC) (Figure 2.2A-B). However, the activation state of Rubisco remained largely unchanged between the various conditions (Figure 2.2C). When Rubisco assays were performed at 38ºC, activities were higher compared to measurements at 25ºC, although the increase of initial velocity was higher than in total velocity (Figure 2.2D-E). A significant difference was also observed between plants grown at 38ºC under different irrigation regimes. No significant differences were observed in Rubisco activation state when measured at this temperature (Figure 2.2F). The lack of differences in net photosynthetic assimilation rate of WW38ºC plants (Figure 2.1A) would indicate that even the reduced level of Rubisco activity in these plants (~10 µmol CO_2 m^{-2} s^{-1}, Figure S2.1D) is sufficient to support photosynthesis at the growth light levels (PPFD <300 µmol photons m^{-2} s^{-1}).

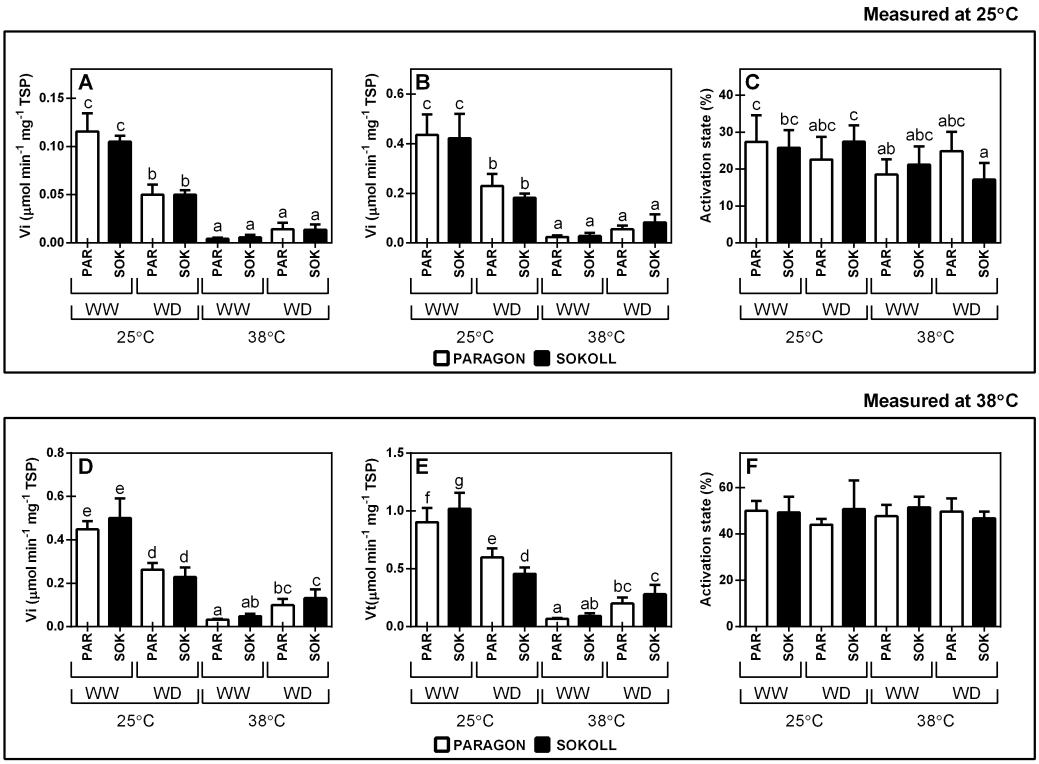

Figure 2.2 – Effect of high temperature and drought on Rubisco activity (expressed by total soluble protein, TSP) and activation state in two wheat genotypes, Paragon (PAR)

and Sokoll (SOK). (A-C) Rubisco initial (Vi) and total (Vt) activities and activation state were measured at 25°C and **(D-F)** 38°C in extracts of fully expanded leaves from 3-week-old wheat plants under well-watered (WW) and water deficit (WD) conditions and exposed to control (25°C) and high temperature conditions (38°C). Values are means ± SD (n = 4-5 biological replicates). Different letters denote statistically significant differences between treatments (Duncan analysis, $P<0.05$).

2.3.4 Effect of water deficit and high temperatures on the antioxidant capacity and chlorophyll *a* fluorescence

To analyse how both genotypes cope with possibly harmful consequences caused by energy excess under stress, chlorophyll *a* fluorescence and two dissipation mechanisms, ROS scavenging and non-photochemical dissipation, were quantified. A decrease of photochemical quenching (qP) was observed in Sokoll WD25ºC and in both genotypes at WD38ºC (Figure 2.3B). Under the same conditions, non-photochemical quenching (qN, NPQ) increased (Figure 2.3C-D). Moreover, the two genotypes showed an increase in the antioxidant capacity (FRAP and TEAC) under drought at both temperatures (Figure 2.3E, F). In order to thoroughly understand how the different biochemical processes in the photosystems are affected by stress conditions, the chlorophyll *a* kinetic parameters were correlated with the antioxidant capacity and NPQ, and ETR (Figure 2.4). A positive correlation was observed between the antioxidant capacity and NPQ, as well as an inverse correlation to ETR. In all conditions, Sokoll showed a stronger correlation between the number of electron carriers per electron transport chain (S_m) and ETR than Paragon. The strength of the correlation between energy fluxes (J^{ABS}, J^{DI}, J_o^{ET2} and J_o^{RE1}), ETR and NPQ changed for both genotypes under WD (Figure 2.4A,C). This was particularly the case in Paragon in WD38ºC (Figure 2.4C, Figure S2.2 and Table S2.2), supported by the increase of J^{ABS}, J^{DI} and J_o^{RE1} to control conditions. In Sokoll the positive correlation between ETR and both electron transport fluxes (J_o^{ET2} and J_o^{RE1}, Figure 2.4C) indicated a decrease of electron transport rate on the entire flux until photosystem I.

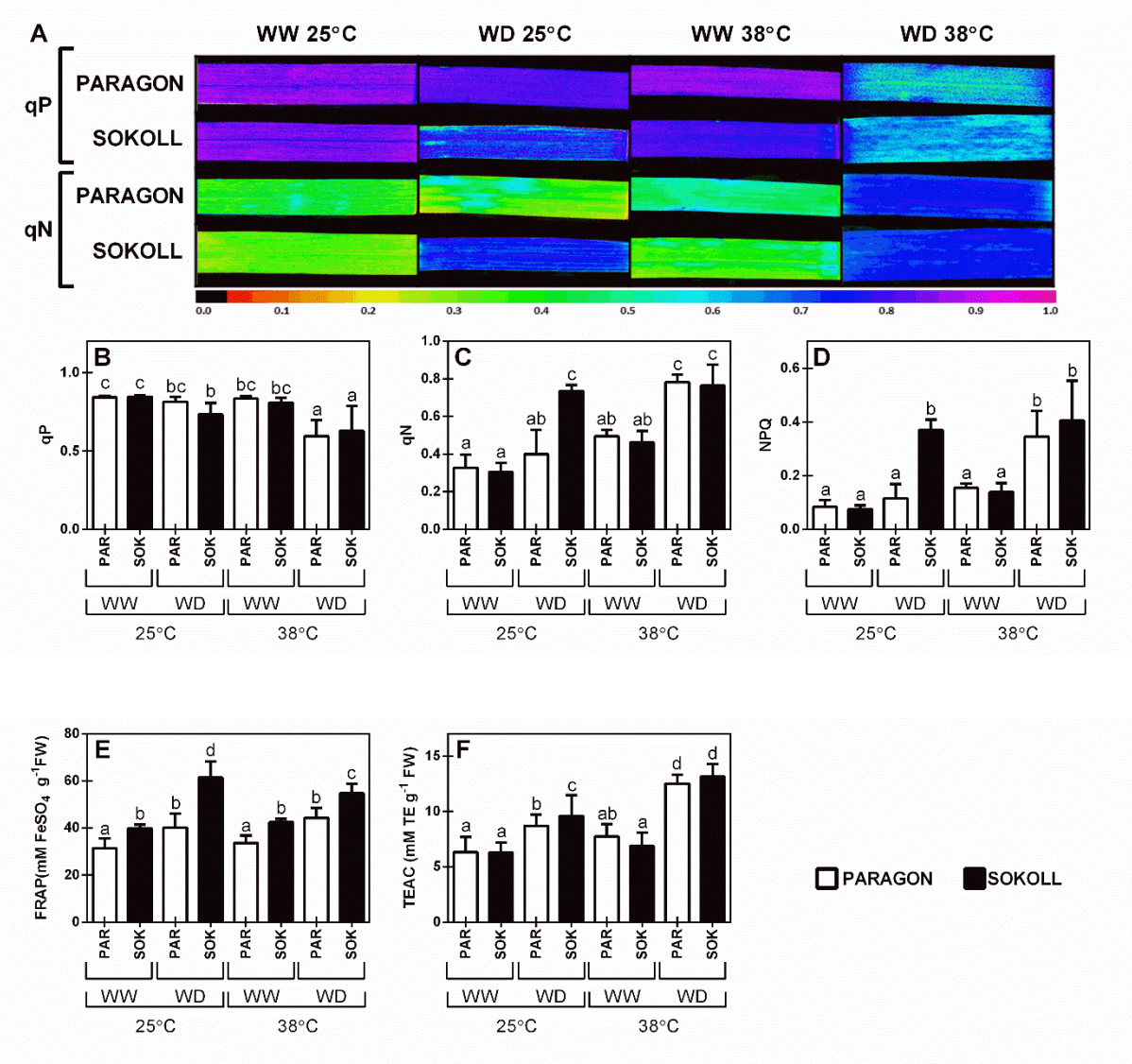

Figure 2.3 – Effect of high temperature and drought on chlorophyll *a* fluorescence and the antioxidant scavenging capacity in two wheat genotypes, Paragon (PAR) and Sokoll (SOK). (A) Chlorophyll *a* fluorescence imaging of the photochemical (qP) and non-photochemical (qN) quenching components in representative leaves. **(B)** Photochemical quenching (qP), **(C)** non-photochemical quenching (qN) **(D)** total non-photochemical quenching (NPQ), **(E)** ferric reducing antioxidant power (FRAP) and **(F)** trolox equivalents antioxidant capacity (TEAC) in fully expanded leaves of 3-week-old wheat plants under well-watered (WW) and water deficit (WD) conditions and exposed to control (25°C) and high temperature conditions (38°C). Values are means ± SD (n = 4-5 biological replicates). Different letters denote statistically significant differences between treatments (Duncan analysis, P<0.05).

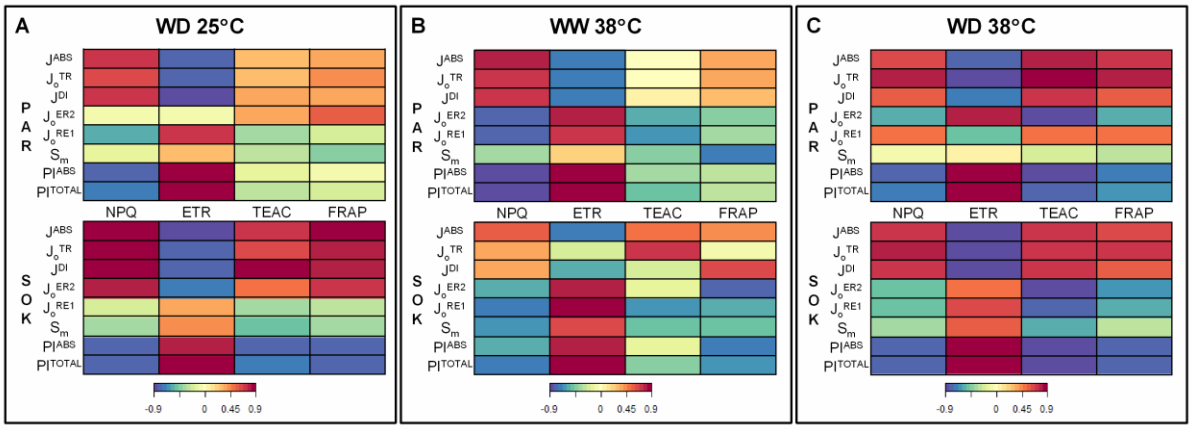

Figure 2.4 – Heatmap representation of the correlation between chlorophyll *a* fluorescence kinetics (OJIP parameters) and antioxidant capacity or steady-state chlorophyll *a* fluorescence of two wheat genotypes, Paragon (PAR) and Sokoll (SOK), under different stresses. Canonical correlations were determined according to the effect of **(A)** water deficit (at 25°C, WD25°C), **(B)** high temperatures (well-watered, WW38°C), and **(C)** water deficit combined with high temperatures (WD38°C) relative to control plants (WW25°C). All parameters were measured in fully expanded leaves of 3-week-old plants. OJIP parameters included are: absorbed photon flux (J^{ABS}); maximum trapped exciton flux (J_o^{TR}); dissipated energy flux (J^{DI}); electron transport flux from QA to QB (J_o^{ER2}); electron transport flux until PSI acceptors (J_o^{RE1}); number of electron carriers per electron transport chain (Sm); performance index for energy conservation from photons absorbed by PSII antenna to the reduction of QB (PI^{ABS}) and until the reduction of PSI acceptors (PI^{TOTAL}). Mean values ± sd (n = 5 biological replicates) are in supplementary data (Table S2.2). Steady-state chlorophyll *a* fluorescence parameters are non-photochemical quenching (NPQ) and electron transport rate (ETR). Antioxidant capacity was determined by trolox equivalents antioxidant capacity (TEAC) and ferric reducing antioxidant power (FRAP). Different colors denote positive (red) or negative (blue) correlations between variables (n = 5 biological replicates)

2.3.5 Recovery from high temperatures conditions

Following 5 days of exposure to high temperatures and/or drought, wheat plants were allowed to recover for 7 days (at 25ºC and WW) and their photosynthetic performance was compared by measuring chlorophyll *a* fluorescence, net photosynthetic assimilation and stomatal conductance. Even though no differences were detected on the fraction of open PSII reaction centres (qP, Figure 2.5A,B), a significant increase on the non-photochemical quenching was observed relative to control (qN, NPQ, Figure 2.5A,C,D). The increase in NPQ was only accompanied by a decrease in the electron transport rate of Sokoll recovering from WD38ºC (Figure 2.5E). Paragon presented higher LRWC and LWP when recovering from WD38ºC than Sokoll (Table 2.1), even though no significant differences were found, indicating a higher capacity of this genotype to return to control cellular hydration and recover the driving force for water movement through the plant. Slower recovery of Sokoll ETR and higher NPQ suggest that WD is promoting photoinhibition in Sokoll. The photosynthetic assimilation rate and stomatal conductance (Figure 2.5F-G) increased in Paragon plants recovered after

growing at 38ºC in WW and WD conditions relative to control. However, in Sokoll, the photosynthetic assimilation rate decreased significantly in recovery from WD38ºC and gs decreased when recovering from both conditions. All parameters reflecting the photosynthetic capacity revealed a better recovery from WD38ºC in Paragon compared to Sokoll. Once again, results suggest that stomatal conductance impairment and recovery are a limiting factor for photosynthesis rate under water deficit and high temperature.

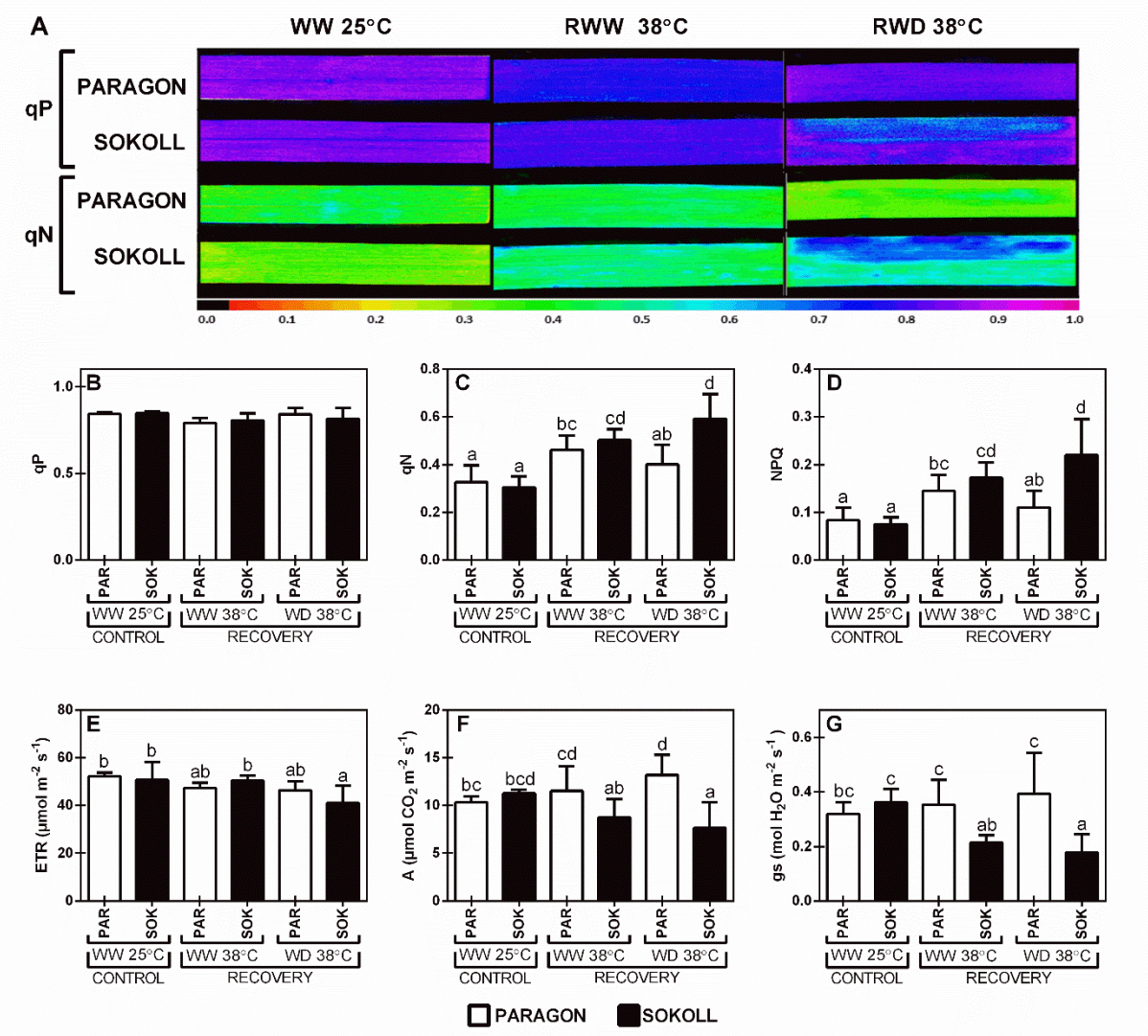

Figure 2.5 – Recovery of the photochemistry and stomatal function of two wheat genotypes, Paragon (PAR) and Sokoll (SOK), after exposure to high temperatures and water deficit. (A) Chlorophyll *a* fluorescence imaging of the photochemical (qP) and non-photochemical (qN) quenching components in representative leaves. **(B)** Photochemical quenching (qP), **(C)** non-photochemical quenching (qN), **(D)** total non-photochemical quenching (NPQ), **(E)** electron transport rate (ETR), **(F)** net photosynthetic assimilation rate (A), **(G)** stomatal conductance (gs). Measurements at growth PPFD in fully expanded leaves of 33-day-old wheat plants recovering for 7 days under well-watered (WW) conditions and 25ºC after exposure to WW (RWW38°C) or water deficit (RWD38°C) conditions and high temperature (38°C)

for 5 days. Values are means ± SD (n=5 biological replicates). Different letters denote statistically significant differences between treatments (Duncan analysis, P<0.05).

2.3.6 Invertase in vivo activities under water deficit and high temperatures

To verify if other sources of energy were used to cope with stress besides the direct usage of photoassimilates, the activity of Invertases isoenzymes (located in the cytosol and vacuole) were measured. Results showed that the activity of vacINV was higher in Paragon for all the conditions compared to Sokoll (Figure 2.6A). However, modulation of cytINV was observed according to different stress conditions (Figure 2.6B): the cytINV activity increased in plants growing at 38ºC with an interesting difference between WD38ºC to WW38ºC and WW25ºC in Paragon. Even though the cytINV activity slightly increased, no significant differences were found for all conditions in Sokoll (Fig 6B). Overall, in Paragon, cytINV was negatively correlated to the assimilation rate (r=-0.774, P<0.0001, Table S2.1). Together with the previous results that showed a better recovery of this genotype after the combination of water deficit and high temperature, these data suggest that an increase of sucrose catabolism, when the production of photosynthetic assimilates decreases, improved wheat recovery from stress conditions.

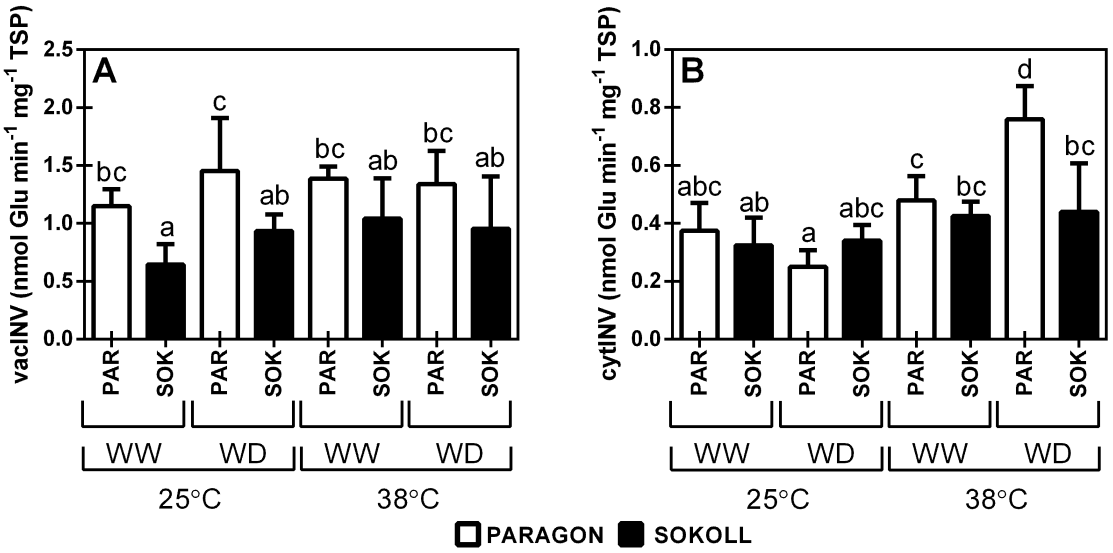

Figure 2.6 – Effect of high temperature and water deficit on cytoplasmic and vacuolar Invertases activities in two wheat genotypes, Paragon (PAR) and Sokoll (SOK). (A) Vacuolar Invertase (vacINV) and **(B)** cytoplasmic Invertase (cytINV) activities were measured at 30°C in fully expanded leaves of 3-week-old wheat plants under well-watered (WW) and water deficit (WD) conditions and exposed to control (25°C) and high temperatures (38°C). Values are means ± SD (n=4-5 biological replicates). Different letters denote statistically significant differences between treatments (Duncan analysis, P<0.05).

2.4 Discussion

Two wheat cultivars, Paragon and Sokoll, were studied for their ability to withstand water deficit and high temperatures, in isolation or in combination. Paragon is a traditional UK spring wheat elite cultivar (Moore 2015), while Sokoll is a synthetic-derived cultivar developed by the International Maize and Wheat Improvement Centre (CIMMYT, Mexico), known to show good productivity under elevated temperatures (Solís Moya and Camacho Casas 2016). As these genotypes are adapted to distinct environmental conditions, it is of relevance to determine which factors are responsible for their photosynthetic performance. Therefore, the present study aimed to first characterise the photosynthetic limitations of the two genotypes under water deficit and/or high temperature and then to assess photosynthetic recovery from high temperature in the absence or presence of drought. To achieve this goal, Paragon and Sokoll were compared using several established parameters, namely net assimilation rate, stomatal conductance, Rubisco and Invertase in vitro activities, antioxidant capacity and chlorophyll *a* fluorescence.

Under increased temperatures a natural heat avoidance strategy of plants is to decrease leaf temperature through increased transpiration (Carmo-Silva et al. 2012, Zandalinas et al. 2018). Albeit at 25ºC, both genotypes showed a mean leaf temperature slightly higher than the atmospheric temperature (Paragon = 26.87ºC; Sokoll = 26.33ºC), when subjected to 38ºC both genotypes showed a decrease of leaf temperature relative to atmospheric temperature, which was statistically significant in Sokoll at WW38ºC (Table 2.1). Additionally, both genotypes maintained similar photosynthetic assimilation and electron transport rates compared to control conditions (Figure 2.1A,C). However, in vitro Rubisco activity decreased more than 10-fold (Figure 2.2), in agreement with previous reports (Galmés et al. 2013, Perdomo et al. 2016, 2017). The maintenance of assimilation rates despite this abrupt decline in Rubisco activity can be explained by the increase in catalytic rate under increased temperature. When measured at 38ºC, the initial activity was 5 times higher than when measured at 25ºC (Figure 2.2A,D) and showed rates comparable to the rates of photosynthesis in the same plants. In vivo, the Rubisco chaperone (RCA) helps to overcome possible dead-end inhibition of Rubisco by promoting ATP-dependent conformational changes at the closed sites of Rubisco (Feller, Crafts-Brandner and Salvucci, 1998, Crafts-Brandner and Salvucci, 2000, Salvucci and Crafts-Brandner, 2004) and may contribute to sustaining Rubisco activities at adequate levels to support carbon assimilation (Perdomo et al. 2017). Under our experimental conditions and without water restrictions, photosynthesis occurred at sufficient rates to supply carbon for cellular growth and metabolic energy.

Despite no direct impact of high temperatures was found on photosynthetic assimilation, stomatal conductance and electron transport rate, and in spite of the better performance of

Paragon at WD25ºC, no differences between genotypes were observed at WD38ºC, since these parameters significantly decreased in both Paragon and Sokoll (Figure 2.1A,C). These results illustrate that when combined, water deficit and high temperatures have a synergistic effect, both genotypes showed severe leaf dehydration (LRWC> 50%, Table 2.1) and a serious reduction of stomatal conductance (less than 15% of control values, Figure 2.1B). Under such stress conditions, photosynthesis no longer provides a source of carbon and other mechanisms are required to enable plants' intense reprogramming effort to acclimatise, survive and, mostly, to recover physiological functions after re-watering. Various stress conditions result in the coordinated regulation of both source - sink relations and direct defence responses (Roitsch 1999, Jan et al. 2019, Kosar et al. 2020). Notably, the activities of the different Invertase isoenzymes are affected by drought and heat stress (Albacete et al. 2011). Paragon recovered faster from high temperatures and water deficit conditions (Figure 2.5) presented higher activity of cytINV and slightly higher activity of vacINV (Figure 2.6A,B). These results are suggesting that genotypes with high capacity to hydrolyse sucrose recover faster from episodes of high temperatures combined with drought and therefore reduce the impact of climate fluctuation in yield. Marques da Silva and Arrabaça (2004), in the C_4 grass *Setaria sphacelata*, found that the higher amount of soluble carbohydrates and the lower amount of starch in leaves exposed to long-term water deficit played a minor role on the osmoregulation against desiccation, suggesting that high availability of hexoses is mainly due to changes on the sucrose metabolism to support other cellular functions. Pinheiro and Chaves (2011) also suggested a connection between cytINV and ABA, sucrose, starch, and ROS metabolism in response to acute drought stress. Higher activity of vacINV has been reported in maize leaves under water deprivation conditions (Pelleschi et al. 1997, Trouverie et al. 2003), although in sugarcane (Wang et al. 2017), cytINV was also shown to play a more prominent role than vacINV under abiotic stress. In barley, activities of both vacINV and cytINV were repressed after a heat stress episode (Antonio Cuesta-Seijo et al. 2019). In tomato, ectopic expression of cell wall Invertases resulted in drought tolerance that was accompanied by also changes in cytINV and vacINV (Albacete et al. 2015). Barratt et al. (2009) demonstrated that cytINV may be the primary route by which carbon from sucrose is supplied to non-photosynthetic tissues in Arabidopsis, suggesting, in concordance to our results, that it would grant a source of carbon to feed cellular functions when photosynthesis is impaired. Secchi and Zwieniecki (2012, 2016) suggested that, under severe drought, high levels of sugar accumulation and Invertase activity could prime the xylem for the accelerated restoration of xylem function upon return to hydrated conditions. The authors proposed that the reduction of stomatal conductance and embolism reduces the transpiration flow, subsequently changing the balance of carbohydrate fluxes in xylem instigating the accumulation of sucrose in the apoplast. That mechanism can trigger a cellular stress response promoting starch

degradation, leading to the increase of cellular soluble sugar concentration and membrane sucrose gradient. The suggested model is in accordance to our results, Paragon showed high activity of Invertases under severe drought (WD38ºC, Figure 2.6) and the resuming high osmotic level could help xylem embolism refilling and the recovery of transport. When water is delivered from roots, the fast recovery of transpiration could consequently help to explain the faster recovery of photosynthesis, leaf water potential and leaf hydration (Figure 2.5 and Table 2.1). The observed evidence highlighted the role of sucrolytic enzymes in the supply of carbon from sucrose needed to the massive metabolic reorganization employed to tolerate stress, helping plants to recover faster and being less affected by heat and water deficit episodes.

In the present study, WD38ºC affected the photochemical capacity in both genotypes, increasing NPQ and qN (Figure 2.3B,C) and decreasing qP (Figure 2.3A), followed by a decrease of ETR (Figure 2.1C). Generally, in higher plants, qE is assumed as the major component of qN, as a short time adaptation to deal with the overproduction of ATP and NADPH and the accumulation of protons in the thylakoid lumen when CO_2 fixation decreases (Krause and Jahns 2007, Takahashi and Murata 2008). Generally, if the energy dissipation mechanisms (qE, qT) and ROS detoxification fail, oxidative damage occurs, leading to photoinhibition (Murata et al. 2007, Yamamoto 2016). The increase in the ROS scavenging activity was observed in both genotypes under WD38ºC (Figure 2.3E,F). In Paragon, an increase of the absorbed photon flux (J^{ABS}) was not followed by an increase in the maximum trapped flux (J_o^{TR}) and the electron transport from Q_A to Q_B (J_o^{ET2}), probably because of the observed increase in the dissipated energy flux (J^{DI}) (Figs 4, S2 and Table S2.2), which avoid the overreduction of the electron transport chain. Additionally, the photochemical function of this genotype fully recovered upon stress release, as shown by the recovery of qP and ETR to values similar to control conditions (Figure 2.5B,E). The increase in dissipated energy flux may be related to a photoprotective mechanism based on the aggregation and detachment of the light-harvesting complex II (LHCII) from the reaction center of PSII (Ruban et al. 2012; Ruban 2016). In higher plants, LHCII aggregates are common sites of energy dissipation facilitated by PsbS (qE) or induced by redox-controlled LHCII phosphorylation (qT) (Minagawa 2011). This mechanism was observed in plants under CO_2 starvation and heat stress (Šiffel and Vácha 1998, Šiffel and Braunová 1999, Tang et al. 2007). On the other hand, in Sokoll, the reduction of ETR highly correlates to the decrease of both electron transport fluxes (JoET2 and JoRE1, Figure 2.4 WD38ºC), and despite the full recovery of qP, NPQ levels remained at high levels and ETR stayed below control condition, indicating slower and limited recovery (Figure 2.5). Chlorophyll fluorescence parameters clearly indicate differences in photoprotection when both genotypes were subjected to WD38ºC and faster recovery of Paragon after stress relief.

Modulation of the cytosolic Invertase was observed and suggests a relationship between an increase of cytINV activity under stress and the recovery of photosynthesis upon high temperatures and water deficit conditions. Upon water shortage and elevated temperatures, when photosynthetic performance and growth priorities are altered, optimization of sucrose export and utilization in conjunction with increased photoprotection of the electron transport machinery could contribute to the recovery of photosynthetic capacity, and consequently to reduce yield fluctuations under climate change. The integration of cell physiological phenotyping via the semi-highthroughput determination of enzyme activity signatures (Jammer et al. 2015) with ecophysiological measurements proved to be a powerful holistic phenomics approach (Großkinsky et al. 2015).

2.5 Supplementary data

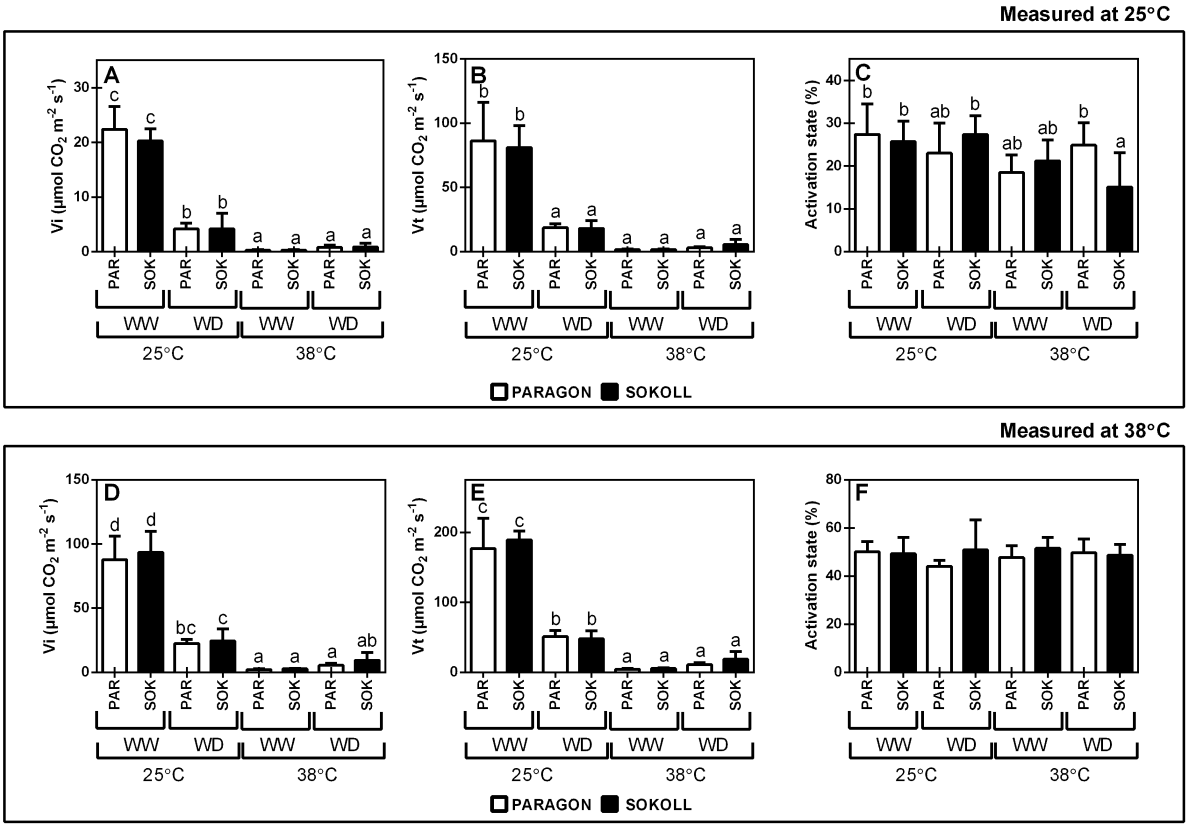

Figure S2.1 – Effect of high temperature and drought on Rubisco activity (expressed by leaf area) and activation state in two wheat genotypes, Paragon (PAR) and Sokoll (SOK). (A-C) Rubisco initial (Vi) and total (Vt) activities and activation state were measured at 25°C and **(D-F)** 38°C in extracts of fully expanded leaves of 3-week-old wheat plants under well-watered (WW) and water deficit (WD) conditions and exposed to control (25°C) and high temperature conditions (38°C). Values are means ± SD (n = 4-5 biological replicates). Different letters denote statistically significant differences between treatments (Duncan analysis, $P<0.05$).

Table S2.1 – Pearson correlation matrix between net photosynthetic assimilation rate (A), stomatal conductance (gs), electron transport rate (ETR) and cytoplasmic Invertase (cytINV) in two wheat genotypes, Paragon and Sokoll, under well-watered (WW) and water deficit (WD) conditions and exposed to control (25°C) and high temperatures (38°C). Values are correlation coefficients (r), the number of asterisks denotes the significance of the correlation: * P<0.05, **P<0.01.

Paragon				
	A	gs	ETR	cytINV
A	1			
gs	0.914**	1		
ETR	0.966**	0.840**	1	
cytINV	-0.774**	-0.621*	-0.811**	1
Sokoll				
	A	gs	ETR	cytINV
A	1			
gs	0.974**	1		
ETR	0.797**	0.750**	1	
cytINV	-0.145	-0.144	-0.445*	1

Table S2.2 – OJIP parameters of Paragon and Sokoll wheat plants exposed to a combination of high temperature and water deficit. Plants were grown for 3 weeks, then exposed to high temperature (38°C versus control, 25°C) and water deficit (WD versus well-watered WW) and then recovered from high temperatures conditions (recovered well-watered, RWW; recovered water deficit, RWD). OJIP parameters included are: absorbed photon flux (J^{ABS}); maximum trapped exciton flux ($J_o^{TR)}$; dissipated energy flux(J^{DI}); electron transport flux from Q_A to Q_B (J_o^{ET2}); electron transport flux until PSI acceptors (J_o^{RE1}); number of electron carriers per electron transport chain (S_m); performance index for energy conservation from photons absorbed by PSII antenna, to the reduction of QB (PI^{ABS}) and until the reduction of PSI acceptors (PI^{TOTAL}). Values are means ± SD (n = 5 biological replicates).

Treatment		Genotype	JABS	JoTR	JDI	JoET2	JoRE1	Sm	PIABS	PITOTAL
25°C	WW	Paragon	1.93 ± 0.06	1.58 ± 0.05	0.36 ± 0.02	0.94 ± 0.03	0.32 ± 0.03	24.41 ± 3.26	3.41 ± 0.47	1.79 ± 0.41
		Sokoll	1.91 ± 0.03	1.58 ± 0.02	0.33 ± 0.01	0.91 ± 0.02	0.35 ± 0.03	26.89 ± 3.20	3.38 ± 0.32	2.16 ± 0.35
	WD	Paragon	2.06 ± 0.23	1.66 ± 0.16	0.41 ± 0.08	0.98 ± 0.05	0.30 ± 0.05	23.33 ± 6.71	3.10 ± 0.89	1.46 ± 0.58
		Sokoll	2.24 ± 0.01	1.81 ± 0.03	0.43 ± 0.03	1.03 ± 0.03	0.34 ± 0.04	25.00 ± 3.11	2.46 ± 0.28	1.25 ± 0.30
38°C	WW	Paragon	2.14 ± 0.18	1.71 ± 0.11	0.43 ± 0.08	0.82 ± 0.06	0.21 ± 0.02	18.06 ± 2.34	1.90 ± 0.63	0.65 ± 0.21
		Sokoll	2.01 ± 0.04	1.59 ± 0.08	0.42 ± 0.04	0.79 ± 0.04	0.25 ± 0.05	21.75 ± 4.32	1.87 ± 0.18	0.87 ± 0.27
	WD	Paragon	3.73 ± 0.62	2.36 ± 0.07	1.37 ± 0.56	0.75 ± 0.08	0.42 ± 0.10	22.51 ± 5.18	0.28 ± 0.17	0.33 ± 0.09
		Sokoll	2.44 ± 0.33	1.91 ± 0.18	0.54 ± 0.15	0.80 ± 0.05	0.25 ± 0.04	22.04 ± 4.35	1.26 ± 0.61	0.59 ± 0.31
Recovery	RWW	Paragon	2.03 ± 0.04	1.66 ± 0.05	0.37 ± 0.04	0.93 ± 0.02	0.32 ± 0.07	23.78 ± 7.42	2.90 ± 0.26	1.58 ± 0.50
		Sokoll	1.84 ± 0.08	1.56 ± 0.11	0.28 ± 0.03	0.92 ± 0.04	0.35 ± 0.04	25.06 ± 1.69	4.35 ± 0.39	2.74 ± 0.54
	RWD	Paragon	2.23 ± 0.24	1.80 ± 0.19	0.43 ± 0.07	0.95 ± 0.04	0.33 ± 0.08	21.43 ± 8.61	2.29 ± 0.81	1.38 ± 0.83
		Sokoll	2.27 ± 0.19	1.81 ± 0.15	0.47 ± 0.09	0.96 ± 0.06	0.44 ± 0.08	26.39 ± 5.73	2.07 ± 0.52	1.68 ± 0.30

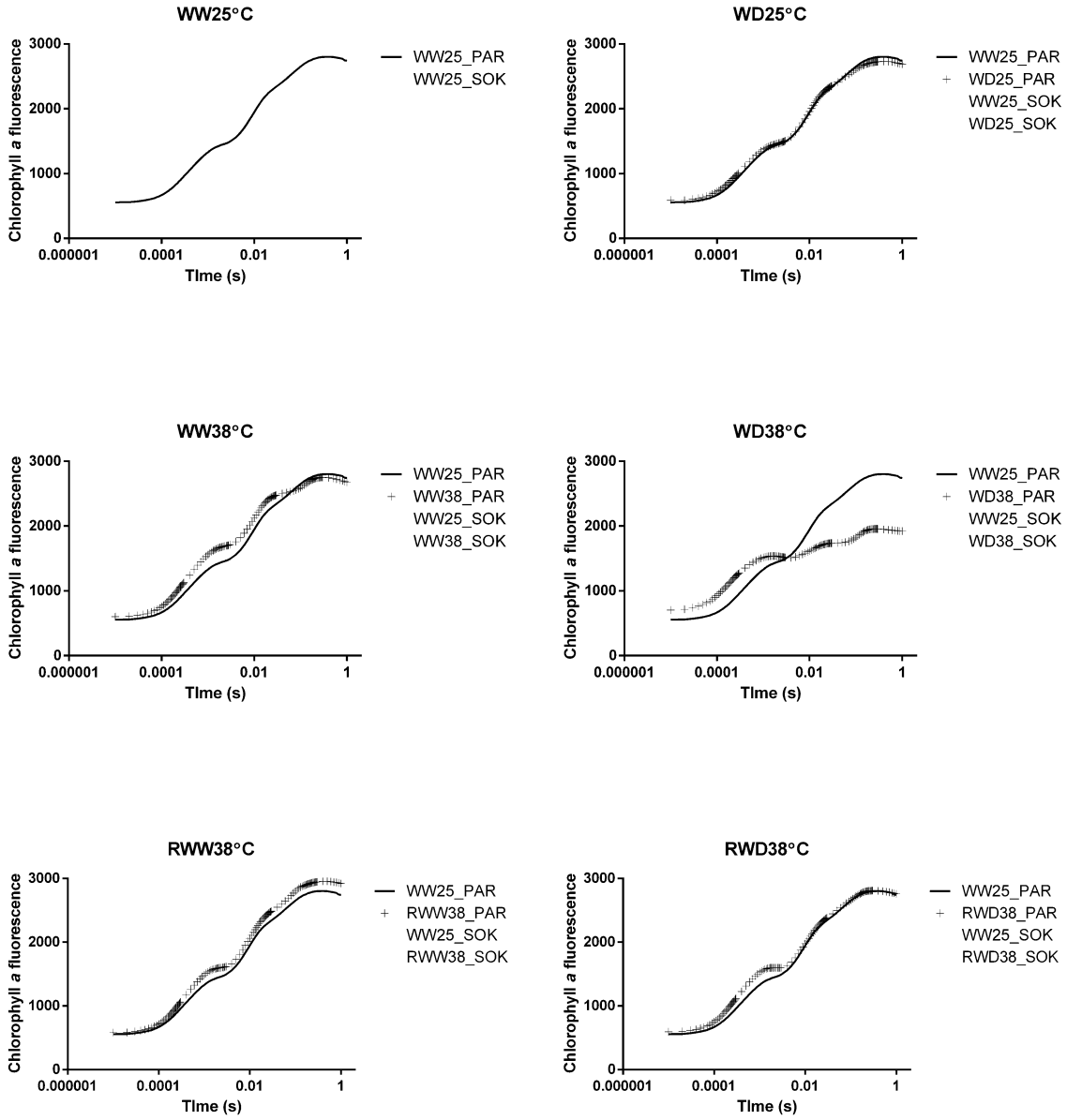

Figure S2.2 – Chlorophyll *a* fluorescence induction curves (OJIP curves) of Paragon and Sokoll wheat plants exposed to water deficit, high temperature, a combination of high temperature and water deficit and recovered under well-watered conditions. Plants were grown for 3 weeks, then exposed to water deficit (WD25°C) to high temperature (38°C,) under well-watered (WW38°C) and water deficit (WD38°C), and recovered under well-watered conditions for 7 days (RWW38°C, RWD38°C) Values are means of (n = 4-5 biological replicates), time is represented as a logarithmic scale. For contrast proposes WW25°C is present in all the charts.

2.6 References

Albacete A, Cantero-Navarro E, Großkinsky DK, Roitsch T (2015) Ectopic overexpression of the cell wall Invertase gene CIN1 leads to dehydration avoidance in tomato. J Exp Bot 66: 863–878

Albacete A, Großkinsky DK, Roitsch T (2011) Trick and treat: a review on the function and regulation of plant Invertases in the abiotic stress response. Phyton Annales Rei Botanicae 50: 181-204

Allakhverdiev SI, Kreslavski VD, Klimov VV, Los DA, Carpentier R, Mohanty P (2008) Heat stress: An overview of molecular responses in photosynthesis. Photosynth Res 98: 541–550

Cuesta-Seijo AJ, De Porcellinis AJ, Valente AH, Striebeck A, Voss C, Marri L, Hansson A, Jansson AM, Dinesen MH, Fangel JU, Harholt J, Popovic M, Thieme M, Hochmuth A, Zeeman SC, Mikkelsen TN, Jørgensen RB, Roitsch T, Lindberg MB, Braumann I (2019) Amylopectin chain length dynamics and activity signatures of key carbon metabolic enzymes highlight early maturation as culprit for yield reduction of barley endosperm starch after heat stress. Plant Cell Physiol 60: 2692–2706

Aronsson H, Schöttler MA, Kelly AA, Sundqvist C, Dörmann P, Karim S, Jarvis P (2008) Monogalactosyldiacylglycerol deficiency in Arabidopsis affects pigment composition in the prolamellar body and impairs thylakoid membrane energization and photoprotection in leaves. Plant Physiol 148: 580–592

Barratt DHP, Derbyshire P, Findlay K, Pike M, Wellner N, Lunn J, Feil R, Simpson C, Maule AJ, Smith AM, (2009) Normal growth of Arabidopsis requires cytosolic Invertase but not sucrose synthase. Proc Natl Acad Sci USA 106: 13124–13129

Begum N, Ahanger MA, Su Y, Lei Y, Mustafa NSA, Ahmad P, Zhang L (2019) Improved drought tolerance by AMF inoculation in maize (*Zea mays*) involves physiological and biochemical implications. Plants 8: 579

Bradford MM (1976) A rapid and sensitive method for the quantitation of microgram quantities of protein utilizing the principle of protein-dye binding. Anal Biochem 72: 248–254

Carmo-Silva AE, Gore MA, Andrade-Sanchez P, French NA, Hunsaker DJ, Salvucci ME (2012) Decreased CO_2 availability and inactivation of Rubisco limit photosynthesis in cotton plants under heat and drought stress in the field. Environ Exp Bot 83: 1–11

Carmo-Silva AE, Keys AJ, Andralojc PJ, Powers SJ, Arrabaça MC, Parry MAJ (2010) Rubisco activities, properties, and regulation in three different C_4 grasses under drought. J Exp Bot 61: 2355–2366

Carmo-Silva E, Scales JC, Madgwick PJ, Parry MAJ (2015) Optimizing Rubisco and its regulation for greater resource use efficiency. Plant, Cell Environ 38: 1817–1832

Čatský J (1960) Determination of water deficit in disks cut out from leaf blades. Biol Plant 2:76–78

Chaves MM, Maroco JP, Pereira JS (2003) Understanding plant responses to drought - from genes to the whole plant. Funct Plant Biol 30: 239

Chen YE, Liu WJ, Su YQ, Cui JM, Zhang ZW, Yuan M, Zhang HY, Yuan S (2016) Different response of photosystem II to short and long-term drought stress in *Arabidopsis thaliana*. Physiol Plant 158: 225–235

Costa JM, Grant OM, Chaves MM (2013) Thermography to explore plant-environment interactions. J Exp Bot 64: 3937–3949

Crafts-Brandner SJ, Salvucci ME (2000) Rubisco activase constrains the photosynthetic potential of leaves at high temperature and CO_2. Proc Natl Acad Sci USA 97: 13430–13435

Degen GE, Worrall D, Carmo-Silva E (2020) An isoleucine residue acts as a thermal and regulatory switch in wheat Rubisco activase. Plant J 103: 742–751

Deryng D, Conway D, Ramankutty N, Price J, Warren R (2014) Global crop yield response to extreme heat stress under multiple climate change futures. Environ Res Lett 9: 034011

Duque AS, de Almeida AM, Bernardes da Silva A, Marques da Silva J, Farinha PA, Santos D, Fevereiro P, Araújo SS (2013) Abiotic Stress Responses in Plants: Unraveling the Complexity of Genes and Networks to Survive. InTech 3: 49-101

Feller U, Crafts-Brandner SJ, Salvucci ME (1998) Moderately High Temperatures Inhibit Ribulose-1,5-Bisphosphate Carboxylase/Oxygenase (Rubisco) Activase-Mediated Activation of Rubisco. Plant Physiol 116: 539–46

Figueroa CM, Lunn JE (2016) A tale of two sugars: Trehalose 6-phosphate and sucrose. Plant Physiol 172: 7–27

Foyer CH (2018) Reactive oxygen species, oxidative signaling and the regulation of photosynthesis. Environ Exp Bot 154: 134–142

Galmés J, Aranjuelo I, Medrano H, Flexas J (2013) Variation in Rubisco content and activity under variable climatic factors. Photosynth. Res 117: 73–90

Genty B, Briantais JM, Baker NR (1989) The relationship between the quantum yield of photosynthetic electron transport and quenching of chlorophyll fluorescence. Biochim Biophys Acta 990:87–92

Gounaris K, Brain APR, Quinn PJ, Williams WP (1983) Structural and functional changes associated with heat-induced phase-separations of non-bilayer lipids in chloroplast thylakoid membranes. FEBS Letters 153: 47-52

Großkinsky DK, Svensgaard J, Christensen S, Roitsch T (2015) Plant phenomics and the need for physiological phenotyping across scales to narrow the genotype-to-phenotype knowledge gap. J Exp Bot 66: 5429-40

Heckathorn SA, Coleman JS, Hallberg RL (1998) Recovery of net CO_2 assimilation after heat stress is correlated with recovery of oxygen-evolving-complex proteins in *Zea mays* L. Photosynthetica 34: 13–20

Jammer A, Gasperl A, Luschin-Ebengreuth N, Heyneke E, Chu H, Cantero-Navarro E, Großkinsky DK, Albacete AA, Stabentheiner E, Franzaring J, Fangmeier A, Graaff E, Roitsch T (2015) Simple and robust determination of the activity signature of key carbohydrate metabolism enzymes for physiological phenotyping in model and crop plants. J Exp Bot 66: 5531–5542

Jan S, Abbas N, Ashraf M, Ahmad P (2019) Roles of potential plant hormones and transcription factors in controlling leaf senescence and drought tolerance. Protoplasma 256: 313–329

Kamata T, Hiramoto H, Morita N, Shen JR, Mann NH, Yamamoto Y (2005) Quality control of photosystem II: An FtsH protease plays an essential role in the turnover of the reaction center D1 protein in Synechocystis PCC 6803 under heat stress as well as light stress conditions. Photochem Photobiol Sci 4: 983–990

Komayama K, Khatoon M, Takenaka D, Horie J, Yamashita A, Yoshioka M, Nakayama Y, Yoshida M, Ohira S, Morita N, Velitchkova M, Enami I, Yamamoto Y (2007) Quality control of Photosystem II: Cleavage and aggregation of heat-damaged D1 protein in spinach thylakoids. Biochim Biophys Acta - Bioenerg 1767: 838–84

Kosar F, Akram NA, Ashraf M, Ahmad A, Alyemeni MN, Ahmad P (2020) Impact of exogenously applied trehalose on leaf biochemistry, achene yield and oil composition of sunflower under drought stress. Physiol Plant https://doi.org/10.1111/ppl.13155

Krause GH, Jahns P (2007) Non-photochemical Energy Dissipation Determined by Chlorophyll Fluorescence Quenching: Characterization and Function. In: Papageorgiou G.C., Govindjee (eds) Chlorophyll *a* Fluorescence. Advances in Photosynthesis and Respiration, vol 19. Springer, Dordrecht 463–495

Lamaoui M, Jemo M, Datla R, Bekkaoui F (2018) Heat and drought stresses in crops and approaches for their mitigation. Front Chem 6: 26

Lunn JE (2016) Sucrose Metabolism. In: eLS. John Wiley & Sons, Ltd, Chichester, UK, pp 1–9

Marques da Silva J, Arrabaça MC (2004) Contributions of soluble carbohydrates to the osmotic adjustment in the C_4 grass *Setaria sphacelata*: A comparison between rapidly and slowly imposed water stress. J Plant Physiol 161: 551–555

Minagawa J (2011) State transitions-the molecular remodeling of photosynthetic supercomplexes that controls energy flow in the chloroplast. Biochim Biophys Acta - Bioenerg. 1807: 897–905

Mittler R, Vanderauwera S, Gollery M, Van Breusegem F (2004) Reactive oxygen gene

network of plants. Trends Plant Sci 9: 490–498

Moore G (2015) Strategic pre-breeding for wheat improvement. Nat Plants 1: 15018

Mueller-Cajar O (2017) The diverse AAA+ machines that repair inhibited Rubisco active sites. Front Mol Biosci 4

Murata N, Takahashi S, Nishiyama Y, Allakhverdiev SI (2007) Photoinhibition of photosystem II under environmental stress. Biochim Biophys Acta - Bioenerg. 1767: 414–421

Nägele T, Henkel S, Hörmiller I, et al (2010) Mathematical modeling of the central carbohydrate metabolism in arabidopsis reveals a substantial regulatory influence of vacuolar Invertase on whole plant carbon metabolism. Plant Physiol 153: 260–272

Oxborough K, Baker NR (1997) Resolving chlorophyll *a* fluorescence images of photosynthetic efficiency into photochemical and non-photochemical components - Calculation of qP and Fv'/Fm' without measuring Fo'. Photosynth Res 54: 135–142

Parry MAJ, Andralojc PJ, Parmar S, Keys AJ, Habash D, Paul, MJ, Alred R, Quick WP, Servaites JC (1997) Regulation of Rubisco by inhibitors in the light. Plant, Cell Environ 20: 528–534

Pelleschi S, Rocher JP, Prioul JL (1997) Effect of water restriction on carbohydrate metabolism and photosynthesis in mature maize leaves. Plant, Cell Environ 20: 493–503

Perdomo JA, Capó-Bauçà S, Carmo-Silva E, Galmés J (2017) Rubisco and Rubisco Activase Play an Important Role in the Biochemical Limitations of Photosynthesis in Rice, Wheat, and Maize under High Temperature and Water Deficit. Front Plant Sci 8: 490

Perdomo JA, Carmo-Silva E, Hermida-Carrera C, Flexas J, Galmés J (2016) Acclimation of Biochemical and Diffusive Components of Photosynthesis in Rice, Wheat, and Maize to Heat and Water Deficit: Implications for Modeling Photosynthesis. Front Plant Sci 7: 1–16

Pinheiro C, Chaves MM (2011) Photosynthesis and drought: Can we make metabolic connections from available data? J Exp Bot 62: 869–882

Raja V, Qadir SU, Alyemeni MN, Ahmad P (2020) Impact of drought and heat stress individually and in combination on physio-biochemical parameters, antioxidant responses, and gene expression in *Solanum lycopersicum*. 3 Biotech 10:208

Rohart F, Gautier B, Singh A, Lê Cao K-A (2017) mixOmics: An R package for 'omics feature selection and multiple data integration. PLOS Comput Biol 13: e1005752

Roitsch T (1999) Source-sink regulation by sugar and stress. Curr Opin Plant Biol 2: 198–206

Roitsch T, González MC (2004) Function and regulation of plant Invertases: Sweet sensations. Trends Plant Sci 9: 606–613

Ruan Y-L (2014) Sucrose Metabolism: Gateway to Diverse Carbon Use and Sugar Signaling. Annu Rev Plant Biol 65: 33-67

Ruan YL, Jin Y, Yang YJ, Li GJ, Boyer JS (2010) Sugar input, metabolism, and signaling

mediated by Invertase: Roles in development, yield potential, and response to drought and heat. Mol Plant 3: 942–955

Ruban AV (2016) Nonphotochemical chlorophyll fluorescence quenching: Mechanism and effectiveness in protecting plants from photodamage. Plant Physiol 170: 1903-16

Ruban A V., Johnson MP, Duffy CDP (2012) The photoprotective molecular switch in the photosystem II antenna. Biochim Biophys Acta - Bioenerg 1817: 167–181

Rumeau D, Peltier G, Cournac L (2007) Chlororespiration and cyclic electron flow around PSI during photosynthesis and plant stress response. Plant, Cell Environ 30: 1041–1051

Salvucci ME, Crafts-Brandner SJ (2004a) Inhibition of photosynthesis by heat stress: the activation state of Rubisco as a limiting factor in photosynthesis. Physiol Plant 120: 179–186

Salvucci ME, Crafts-Brandner SJ (2004b) Mechanism for deactivation of Rubisco under moderate heat stress. Physiol Plant 122: 513–519

Salvucci ME, Crafts-Brandner SJ (2004c) Inhibition of photosynthesis by heat stress: The activation state of Rubisco as a limiting factor in photosynthesis. Physiol Plant 120: 179–186

Scafaro AP, Bautsoens N, den Boer B, Van Rie J, Gallé A (2019) A Conserved Sequence from Heat-Adapted Species Improves Rubisco Activase Thermostability in Wheat. Plant Physiol 181: 43–54

Scafaro AP, Gallé A, Van Rie J, Carmo-Silva E, Salvucci ME, Atwell BJ (2016) Heat tolerance in a wild Oryza species is attributed to maintenance of Rubisco activation by a thermally stable Rubisco activase ortholog. New Phytol 211: 899–911

Secchi F, Zwieniecki MA (2016) Accumulation of sugars in the xylem apoplast observed under water stress conditions is controlled by xylem pH. Plant Cell Environ 39: 2350–2360

Secchi F, Zwieniecki MA (2011) Sensing embolism in xylem vessels: The role of sucrose as a trigger for refilling. Plant, Cell Environ 34: 514–524

Shivhare D, Mueller-Cajar O (2017) In vitro characterization of thermostable CAM Rubisco activase reveals a Rubisco interacting surface loop. Plant Physiol 174: 1505–1516

Šiffel P, Braunová Z (1999) Release and aggregation of the light-harvesting complex in intact leaves subjected to strong CO_2 deficit. Photosynth Res 61: 217–226

Šiffel P, Vácha F (1998) Aggregation of the Light-Harvesting Complex in Intact Leaves of Tobacco plants stressed by CO_2 deficit. Photochem Photobiol 67: 304–311

Solís Moya E, Camacho Casas MA (2016) Evaluation of the Stress Adaptive Trait Yield Nursery (SATYN) in irrigated wheat growing locations in Mexico during the 2015-16 growing season. Proc 2nd Int TRIGO Yield Potential 10–14

Stirbet A, Govindjee (2011) On the relation between the Kautsky effect (chlorophyll *a* fluorescence induction) and Photosystem II: Basics and applications of the OJIP

fluorescence transient. J Photochem Photobiol B Biol 104: 236–257

Strasser RJ, Tsimilli-Michael M, Srivastava A (2004) Analysis of the Chlorophyll *a* Fluorescence Transient. In: Papageorgiou GC, Govindjee (eds) Chlorophyll *a* Fluorescence. Advances in Photosynthesis and Respiration, vol 19. Springer, Dordrecht

Takahashi S, Murata N (2008) How do environmental stresses accelerate photoinhibition? Trends Plant Sci 13: 178–182

Tang Y, Wen X, Lu Q, Yang Z, Cheng Z, Lu C (2007) Heat stress induces an aggregation of the light-harvesting complex of photosystem II in spinach plants. Plant Physiol 143: 629–38.

Tiwari A, Jajoo A, Bharti S (2008) Heat-induced changes in the EPR signal of tyrosine D (Y(D)OX) a possible role of Cytochrome b559. J Bioenerg Biomembr 40: 237–243

Tricker PJ, Elhabti A, Schmidt J, Fleury D (2018) The physiological and genetic basis of combined drought and heat tolerance in wheat. J Exp Bot 69: 3195–3210

Trouverie J, Thévenot C, Rocher JP, Sotta B, Prioul JL (2003) The role of abscisic acid in the response of a specific vacuolar Invertase to water stress in the adult maize leaf. J Exp Bot 54: 2177–2186

Tsimilli-Michael M, Strasser RJ (2008) In vivo assessment of stress impact on plant's vitality: Applications in detecting and evaluating the beneficial role of mycorrhization on host plants. In: Mycorrhiza: State of the Art, Genetics and Molecular Biology, Eco-Function, Biotechnology, Eco-Physiology, Structure and Systematics, 3rd edn. Springer-Verlag Berlin Heidelberg, pp 679–703

von Caemmerer S, Farquhar GD (1981) Some relationships between the biochemistry of photosynthesis and the gas exchange of leaves. Planta 153: 376–387

Walker BJ, VanLoocke A, Bernacchi CJ, Ort DR (2016) The Costs of Photorespiration to Food Production Now and in the Future. Annu Rev Plant Biol 67: 107–129

Wang D, Fu A (2016) The Plastid Terminal Oxidase is a Key Factor Balancing the Redox State of Thylakoid Membrane. In: Enzymes. Academic Press, pp 143–171

Wang L, Zheng Y, Ding S, Zhang Q, Chen Y, Zhang J (2017) Molecular cloning, structure, phylogeny and expression analysis of the Invertase gene family in sugarcane. BMC Plant Biol 17: 109

Weiszmann J, Fürtauer L, Weckwerth W, Nägele T (2018) Vacuolar sucrose cleavage prevents limitation of cytosolic carbohydrate metabolism and stabilizes photosynthesis under abiotic stress. FEBS J 285: 4082–4098

Yamamoto Y (2016) Quality Control of Photosystem II: The Mechanisms for Avoidance and Tolerance of Light and Heat Stresses are Closely Linked to Membrane Fluidity of the Thylakoids. Front Plant Sci 7: 1136

Zampieri M, Ceglar A, Dentener F, Toreti A (2017) Wheat yield loss attributable to heat waves,

drought and water excess at the global, national and subnational scales. Environ Res Lett 12

Zandalinas SI, Mittler R, Balfagón D, ArbonaV, Gómez-Cadenas A (2018) Plant adaptations to the combination of drought and high temperatures. Physiol Plant 162: 2–12

Zhao C, Liu B, Piao S, et al (2017) Temperature increase reduces global yields of major crops in four independent estimates. Proc Natl Acad Sci USA 114: 9326–9331

FAOSTAT Statistical Database; 2017; Food and Agriculture Organization of the United Nations; Rome

Chapter III

Efficient regulation of CO_2 assimilation enables greater resilience to high temperature and drought in maize

Data presented in this chapter was included in the following work:

Correia PMP, da Silva AB, Vaz M, Carmo-Silva E, Marques da Silva J, (2021) Efficient regulation of CO_2 assimilation enables greater resilience to high temperature and drought in maize. Front Plant Sci – submitted, under review.

Table of Contents – Chapter III

Abstract

Increasing temperatures and extended drought episodes are among the major constraints affecting food production. Maize has a relatively high temperature optimum for photosynthesis, however the response of this important C_4 crop to the combination of heat and drought stress is poorly understood. Here, we hypothesised that resilience to high temperature combined with water deficit would require efficient regulation of maize photosynthetic traits, including the C_4 CO_2 concentrating mechanism. Two maize genotypes with contrasting levels of drought and heat tolerance, B73 and P0023, were acclimatized at high temperature (38 vs 25°C) under well-watered or water deficit conditions. Photosynthesis performance was evaluated by gas-exchange and chlorophyll *a* fluorescence, and *in vitro* activities of key enzymes for carboxylation (phosphoenolpyruvate carboxylase), decarboxylation (NADP-malic enzyme), and carbon fixation (Rubisco). Both genotypes successfully acclimatized to high temperature, although with different mechanisms: while B73 maintained photosynthetic rates by increasing stomatal conductance (gs), P0023 maintained gs and showed limited transpiration. When water deficit was experienced in combination with high temperatures, limited transpiration allowed water-savings and acted as a drought stress avoidance mechanism. Photosynthetic efficiency in P0023 was sustained by higher phosphorylated PEPC and electron transport rate near vascular tissues, supplying chemical energy for an effective CO_2 concentrating mechanism. These results suggest that the key traits for drought and heat tolerance in maize are limited transpiration rate, allied with a synchronized regulation of carbon assimilation metabolism. These findings can be exploited in future breeding efforts aimed at improving maize resilience to climate change.

3.1 Introduction

Maize is one of the most important crops worldwide, representing 39% of the total cereal production and 27% of the total grain crops harvest area (FAOSTAT, 2018). According to the intergovernmental panel for climate change (IPCC), water restrictions and heat waves are among the main regional risks for food production in some of the most populated areas around the globe (IPCC 2014). Without major crop improvements, each degree-Celsius increase in global mean temperature can reduce, on average, the global yield of maize by 7.2% (Zhao et al. 2017). To improve maize yield in a changing climate, and ensure food security for an increasing world population, it is essential to comprehend how maize plants respond to fluctuations in temperature and water availability, unravel the traits that confer resilience to heat and drought stress, and develop genotypes expressing those traits.

Crop production is intimately dependent on a fine-tuned stomatal regulation since a trade-off between carbon uptake and water saving is always present. Furthermore, when subjected to high temperatures, plants usually use evaporative cooling to reduce leaf temperature, that otherwise could be detrimental to photosynthetic processes (Carmo-Silva et al. 2012; Costa et al. 2013; Lawson et al. 2018). However, in response to water shortage, higher plants close stomata to limit water losses by transpiration (Chaves et al. 2003; Nunes et al. 2009; Duque et al. 2013). It is generally accepted that plants with C_4 photosynthesis, as maize, evolved from C_3 plants in response to the increase of temperature, a decrease of CO_2 concentration in the atmosphere and episodes of drought or salinity (Edwards et al. 2001, 2004; Sage 2004). The revolutionary factor that allowed the success of C_4 plants under these conditions was the anatomical and biochemical differentiation that led to the development of a CO_2 concentrating mechanism (CCM) that increases CO_2 concentrations at the catalytic sites of Rubisco (Edwards et al. 2001, 2004; Sage 2004). This development allowed firstly the increase of photosynthetic efficiency by decreasing the oxygenation activity of Rubisco, and consequently photorespiration (Sage et al. 2010). Secondly, the increase of the optimum photosynthetic temperature, in large part by surpassing the decrease in CO_2 solubility relative to O_2 caused at high temperature (Sage and Kubien 2007; Dwyer et al. 2007). Ultimately, this enables C_4 plants to use low stomatal conductance (gs) as a water-conservative mechanism, by increasing the ratio of CO_2 fixated per water loss through transpiration (Ghannoum et al. 2010; Osborne and Sack 2012).

Maize uses mainly a NADP-malic enzyme type C_4 photosynthesis, where CO_2 is fixed in the mesophyll cells (MC) by Phosphoenolpyruvate carboxylase (PEPC, EC 4.1.1.31), leading to the formation of oxaloacetate, afterwards reduced to malate and transported into the bundle sheath cells (BSC). There, CO_2 is released by the NADP-malic enzyme (NADP-ME, EC 4.1.1.31) for refixation in the Calvin-Benson-Bassham cycle (CBBC) through ribulose-

bisphosphate carboxylase/oxygenase (Rubisco, EC 2.1.1.127) (Hatch 1987; Edwards et al. 2004). The regulatory and catalytic properties of enzymes involved in the CO_2 concentrating mechanism contribute to the acclimation and optimization of photosynthetic efficiency when exposed to high temperatures and drought. The activation state of C_4-PEPC generally increases when plants are exposed to water deficit (Foyer et al. 1998; Bernardes da Silva et al. 2004; Marques da Silva and Arrabaça 2004; Silva 2008) and the sensitivity to L-malate decreases (Carmo-Silva et al. 2008). Conversely, under high temperature PEPC activity is generally not affected (Crafts-Brandner and Salvucci 2002a; Dwyer et al. 2007) and the sensitivity to L-malate slightly increases (Crafts-Brandner and Salvucci 2002b). Usually, C_4-NADP-ME activity decreases or is not affected under water deficit (Du et al. 1996; Marques da Silva and Arrabaça 2004; Carmo-Silva et al. 2008). The activation state of Rubisco was reported to decrease mainly at high temperature, in isolation or combination to water deficit (Crafts-Brandner and Salvucci 2002b; Salvucci and Crafts-Brandner 2004a; Perdomo et al. 2017). The decline is mainly due to the thermal sensitivity of Rubisco's catalytic chaperone, Rubisco activase (Rca), that otherwise promotes the release of inhibitory sugar phosphates from active sites of Rubisco (Portis 2003; Salvucci and Crafts-Brandner 2004a; Carmo-Silva and Salvucci 2011; Carmo-Silva et al. 2015).

Differentiation between MC and BSC localization and functions also altered their specific energy requirement. MC are characterized by high grana-containing chloroplasts with higher PSII activities and linear electron flow, producing ATP and most of the reducing power (NADPH). BSC produce primarily the ATP required in the CBBC, via cyclic electron flow around PSI, and grana stacks are rare in these chloroplasts (Woo et al. 1970; Walker and Izawa 1979; von Caemmerer and Furbank 2016). Environmental regulation of PSII levels in BSC chloroplasts has not been extensively examined (Meierhoff and Westhoff 1993; Omoto et al. 2009). However, balancing the energetic capacity of the two compartments might be a requirement for the plasticity of the decarboxylating process under varying environmental conditions (Chapman and Hatch 1981; Furbank 2011; von Caemmerer and Furbank 2016; Arrivault et al. 2017). Effects of high temperature and water deficit on the electron transport capacity can also limit the photosynthetic efficiency mainly by the impairment of the physical integrity of electron transport components of the photosynthetic apparatus (Salvucci and Crafts-Brandner 2004a)

Previous studies focused on C_4 photosynthesis under isolated or rapidly imposed stresses. Thus, there is scarce information about the regulation of CCM in acclimatized plants under high temperature in isolation or combination to water deficit. Moreover, as great diversity is observed between C_4 metabolic types (Carmo-Silva et al. 2008; Furbank 2011; Rao and Dixon 2016), and even between genotypes of the same species, depending on breeding history and

genome-environmental interactions (Lopes et al. 2011; Khoshravesh et al. 2020), it is crucial to study the response of genotypes with contrasting behaviour.

In this study, contrasting levels of tolerance to drought and heat of two maize genotypes, B73 and P0023, were explored to (1) characterize the combined effects of high temperature and water deficit on maize photosynthesis, (2) test the hypothesis that the CO_2 concentrating mechanism efficiency is a major player in the tolerance to these conditions, and (3) ultimately unravel mechanisms that can help the improvement of maize growth under high temperatures and extended drought. B73 is heat and drought-sensitive (Petolino et al. 1990; Chen et al. 2012; Yang et al. 2018), the most widely used inbred line in breeding programs (Duvick et al. 2010; Chen et al. 2012) and one of the first maize genotypes sequenced (Schnable et al. 2009; Jiao et al. 2017). P0023 is a drought-tolerant Pioneer Optimum AQUAmax^{TM} hybrid line (DuPont Pioneer). The AQUAmax hybrids were developed in a long-term improvement program to increase maize yield for the US corn-belt, by applying multi-environment phenotyping and molecular markers-based selection (Cooper et al. 2014; Gaffney et al. 2015). The effects of long-term growth under drought (WD25), high temperature (WW38) and their combination (WD38) on the photosynthetic efficiency was assessed by steady-state gas-exchange and chlorophyll *a* fluorescence and related to (1) biomass production, (2) leaf evaporative colling system and water balance, (3) the catalytic activity of key enzymes involved in maize CCM, (4) kinetics of photosynthetic electron transport and (5) leaf tissue spatial heterogeneity of PSII activity.

3.2 Materials and methods

3.2.1 Plant material and growth conditions

Two *Zea mays* L. (maize) genotypes were selected, based on the evidence of contrasting drought and heat tolerance in previous studies (Chen et al. 2012; Cooper et al. 2014; Gaffney et al. 2015; Yang et al. 2018): B73, a heat and drought-sensitive line, and P0023, a drought-tolerant Pioneer Optimum AQUAmax^{TM} hybrid line (DuPont Pioneer). Plants of both genotypes were grown from seeds in a controlled environment chamber (Fitoclima 5000 EH, Aralab) in 2 L pots containing horticultural substrate (Compo Sana Universal, Compo Sana). The light was provided by fluorescent lamps (Osram Lumilux L 58W/840 cool white lamps) placed at specific distances from the plants to obtain an average photosynthetic photon flux density (PPFD) of ~300 µmol m^{-2} s^{-1} at the top of the canopy, with a photoperiod of 16 h. All plants were initially grown under a control temperature (25/18°C day/night), with 50% relative humidity (RH) for 21 days (21 days after sowing, DAS). For experiments under control temperature, plants remained at 25/18°C (day/night) with 50% RH throughout the experiment. Following 21 DAS plants were randomly assigned to two irrigation treatments: five plants per cultivar were maintained well-watered (WW; minimum 80% field capacity, WW25) throughout the experiment and five plants were subject to water deficit (WD, WD25) for 7 days. For experiments under elevated temperature, at 21 DAS plants were also exposed to high temperatures (38/31°C day/night) with 60% RH and randomly assigned to the irrigation treatments: five plants per cultivar were maintained WW (80±5% field capacity, WW38) and five plants were subject to WD (WD38), for 5 days. WD was established by withholding watering and sustaining a minimum of 30±5% field capacity. The water stress period was reduced to 5 days under high temperature to compensate the higher evapotranspiration demand. The soil water content was determined gravimetrically by weighing the pots, and irrigation was provided to compensate evapotranspiration and maintain field capacity in the WW and WD pots. Leaf samples collection for biochemical analyses occurred at the end of the respective temperature and irrigation treatment, 5-7 h after the beginning of the photoperiod. Samples were rapidly frozen into liquid nitrogen and stored at -80°C.

3.2.2 Leaf water status

Plant water status was estimated by leaf relative water content (LRWC) following the methodology described by Čatský (1960). A fresh leaf sample (3-4 cm^2) was collected, leaf fresh weight (LFW) was immediately measured in an electronic scale (Sartorius BP221S), leaf turgid weight (LTW) was determined after saturating samples by immersion in deionized water overnight, and leaf dry weight (LDW) was measured after oven drying samples at 70°C for 48 h, and LRWC calculated as follows:

$$\mathrm{LRWC} = \frac{(\mathrm{LFW}-\mathrm{LDW})}{(\mathrm{LTW}-\mathrm{LDW})}.$$

Leaf water potential (LWP) was measured with a C-52 thermocouple chamber (Wescor), 20 mm^2 leaf discs were cut and equilibrated for 30 min in the chamber before the readings were recorded by a water potential datalogger (PSYPRO, Wescor) operating in the psychrometric mode.

3.2.3 Above-ground biomass and growth rate

At the end of the experiment, plants were harvested to measure above-ground biomass in the form of fresh weight (FW) and dry weight (DW). FW was directly measured in an electronic scale (Sartorius BP221S) and DW measured after oven drying samples at 70°C for 52 h. Additionally, to assess the relative growth rate during the acclimatization period above-ground biomass was measured in a random group of plants before stress imposition (21 DAS, n=5). The relative growth rate for each plant, based on the DW, was estimated as:

$$\mathrm{RGR} = ln\frac{(\mathrm{W2}/\mathrm{W1})}{(\mathrm{T2}-\mathrm{T1})},$$

where w1 and w2 are DW of each plant at time points T1 (21 DAS) and T2 at the end of the acclimatization period.

3.2.4 Thermal imaging

Thermal images were obtained using a thermal camera (Flir 50bx, FLIR Systems Inc.) with emissivity set at 0.95 and approximately 1 m distance from the plants. Prior to each set of measurements, background temperature was determined by measuring the temperature of a crumpled sheet of aluminum foil in a similar position to the leaves of interest with the emissivity set at 1.0 following the methodology described by Costa et al. (2013). Thermal images were analysed with the software FLIR Tools (FLIR Systems, Inc.). The temperature of each plant was determined from the temperature of five leaves using the function *area*.

3.2.5 Steady-state gas exchange and chlorophyll *a* fluorescence

Parallel measurements of photosynthetic gas exchange and chlorophyll *a* fluorescence were performed in a non-detached fully expanded leaf from each plant with a portable fluorescence and gas exchange system (Li-6400-40, Li-Cor Inc.), at the climatic growth chamber. The control air temperature was set to the growth temperature, 25°C (WW25 and WD25) or 38°C (WW38 and WD38), PPFD at the leaf level set to 600 µmol m^{-2} s^{-1} and the CO_2 concentration in the leaf chamber set to 400 µmol CO_2 mol^{-1}, allowing the leaf to reach steady-state assimilation rate (A) and stomatal conductance (gs). All the photosynthetic parameters were calculated by the Li-6400-40 software. A, gs and transpiration rate (E) were calculated according to von Caemmerer and Farquhar (1981). PSII effective quantum yield

(*Φ*PSII) was obtained according to Genty et al. (1989) and electron transport rate (ETR) was then calculated as:

$$\mathrm{ETR} = 0.5\Phi\mathrm{PSII} \times \mathrm{PPFD} \times 0.84.$$

3.2.6 Chlorophyll *a* fluorescence induction

The kinetics of the rapid fluorescence induction rise was recorded on fully expanded dark-adapted leaves (10 minutes) exposed to a saturating light pulse (3,500 µmol m^{-2} s^{-1}) for 1 s, in order to obtain the OJIP Chl *a* fluorescence transient rise (Handy PEA, Hansatech Instruments). Fluorescence parameters derived from the extracted data, namely specific energy fluxes per QA-reducing PSII reaction centre and photosynthetic performance indexes were calculated according to Strasser and collaborators (Strasser et al., 2004, Tsimilli-Michael and Strasser, 2008) with the nomenclature presented in Stirbet and Govindjee (2011).

3.2.7 Chlorophyll *a* fluorescence imaging and rapid light curves

Chlorophyll *a* fluorescence rapid light curves (RLCs) were measured with a chlorophyll fluorescence imaging system (Imaging-PAM M-series Mini version, Heinz Walz GmbH) and images analysed using the Imaging Win analytical software (Heinz Walz GmbH). Measurements were recorded in full dark-adapted leaves (10 minutes) with an eight-step protocol (0, 43, 111, 223, 402, 624, 782, 996 µmol m^{-2} s^{-1}) with light irradiance increasing by 90 seconds intervals. ETR values were extracted from representative areas of interest (AOI) for the total leaf area (L ETR), midveins (MV ETR) and regions between mid-veins (BMV ETR). Data was fitted to a three-parameter photosynthesis-irradiance model (Platt et al. 1982) using a derivative-free optimization by quadratic approximation algorithm (bobyqa) in the R package phytotools (Silsbe and Malkin 2015). The maximum ETR (ETRmax) was estimated by the following equation:

$$\mathrm{ETRmax} = \mathrm{P_s}\,[\alpha/(\alpha+\beta)][\beta/(\alpha+\beta)]^{\beta/\alpha},$$

where Ps is a scaling factor defined as the maximum potential ETR, α the initial slope of the RLC before the onset of saturation and β the slope of the downturn of the curve characterised by photoinhibition. As leaf ETR was extracted in an AOI exclusively containing MV and BMV, the contribution of MV and BMV ETR to the leaf ETR was calculated by normalizing the data to Leaf ETR under WW25 and expressed as a relative percentage (% of WW25 L ERT).

3.2.8 Enzymes extraction

Soluble enzymes were extracted by grinding frozen leaf samples (0.1-0.3 g FW) in a cold mortar with quartz sand, 1% (w/v) insoluble polyvinylpyrrolidone (PVP), ice-cold extraction medium (1/10 FW per mL) containing 50 mM Bicine-KOH pH 8.0, 1 mM ethylenediaminetetraacetic acid (EDTA), 5% (w/v) polyvinylpyrrolidone (PVP25000), 6% (w/v) polyethylene glycol (PEG_{4000}), 10 mM 1,4-dithiothreitol (DTT), 50 mM β-mercaptoethanol and

1% (v/v) protease inhibitor cocktail for plant extracts (Sigma-Aldrich), as described in Carmo-Silva et al. (2008). Leaf extracts were then centrifuged at 14,000 *g* and 4°C for 3 min, supernatants were used for enzymatic activity assays and maintained on ice until all measurements were completed. Total soluble protein (TSP) content was quantified according to the Bradford method (Bradford 1976) using BSA Fraction V as standard protein.

3.2.9 PEPC activity and sensitivity to malate inhibition

PEPC activity was measured by coupling the carboxylase reaction with malate dehydrogenase (MDH) NADH-dependent, as described by Carmo-Silva et al. (2008). The maximal activity (Vmax), was determined under optimal pH (pH 8.0), saturating substrates and cofactor conditions, and 5-20 µL of leaf extract. The physiological activity (Vphysiol) was determined under similar conditions but at sub-optimal pH (pH 7.3) and PEP concentration (2.5 mM PEP). The reaction mixtures, with all the components except NADH and extract, were allowed to equilibrate at 25ºC or 38ºC; then the enzyme extract was added, and the reaction started by the addition of NADH. The activation state of PEPC was calculated as,

$$\text{Activation state} = \frac{\text{Vphysiol}}{\text{Vmax}} \times 100.$$

For the determination of PEPC sensitivity to L-malate inhibition, a sub-sample of protein extract was desalted by gel filtration (Sephadex G-25, Sigma-Aldrich) and assayed in the same conditions as described for the Vphysiol, with 40-60 µL of the desalted extract and by measuring the activity in the absence and increasing concentrations of L-malate. Malate sensitivity was estimated by the calculation of half-maximal inhibitory concentration (IC50) and used to evaluate PEPC phosphorylation state. Reactions were measured in continuous assays by monitoring absorbance at 340 nm and carried out in triplicates.

3.2.10 NADP-ME activity

NADP-ME activity was determined, according to Carmo-Silva et al. (2008). The maximal activity (Vmax), was determined under optimal pH (pH 8.0), saturating substrates and cofactor conditions, and 10-20 µL of leaf extract. The physiological activity (Vphysiol) was determined under similar conditions but with the leaf extract L-malate endogenous concentration. The reaction mixture, with all the components except $NADP^+$ (Sigma-Aldrich), L-malate and extract, was allowed to equilibrate at 25ºC and 38ºC. Then the protein extract and $NADP^+$ was added and the reaction started by the addition of L-malate (Vmax) or by the endogenous L-malate (Vphysiol). The activation state of NADP-ME was calculated as the ratio of Vphysiol to Vmax, as previously presented for PEPC. Reactions were measured in continuous assays by monitoring absorbance at 340 nm and carried out in triplicates.

$$\text{Activation state} = \frac{\text{Vphysiol}}{\text{Vmax}} \times 100.$$

3.2.11 Rubisco activity

Rubisco activities were measured by the incorporation of $^{14}CO_2$ into acid-stable products at 25°C and 38ºC, following the protocol described in Parry et al. (1997) with modifications. The reaction mixture contained 100 mM Bicine-NaOH pH 8.2, 40 mM $MgCl_2$, 10 mM $NaH^{14}CO_3$ (7.4 kBq µmol^{-1}) and 0.4 mM ribulose 1,5-bisphosphate (RuBP, Sigma-Aldrich). Rubisco initial activity (Vi) was determined by adding the supernatant to the mixture and stopping the reaction after 60s with 10 M HCOOH. Total activity (Vt) was measured after incubating the same volume of extract for 1 min with all the reaction mixture components except RuBP in order to allow carbamylation of all the Rubisco available catalytic sites. The reaction was then started by adding RuBP and stopped as above. All measurements were carried out in triplicate, and control reactions were quenched with HCOOH prior to the addition of RuBP. The mixtures were completely dried at 70°C overnight and the residues re-hydrated in 0.5 mL ddH_2O, then mixed with 5 mL scintillation cocktail (Ultima Gold, Perkin-Elmer). Radioactivity due to ^{14}C incorporation in the acid-stable products was measured by liquid scintillation counting (LS7800, Beckman). The activation state of Rubisco was calculated as the ratio,

$$\text{Activation state Rubisco} = \frac{\text{Vi}}{\text{Vt}} \times 100.$$

All measurements were carried out in triplicate.

3.2.12 Statistical analysis

The statistical significance of trait variation was tested by factorial ANOVA, and post-hoc comparison between treatments was performed with Duncan test ($P < 0.05$) using IBM SPSS Statistics, Version 25 (IBM, USA). T-test ($P < 0.05$) was used to analyse significant differences between experimental temperatures in the same genotypes and condition. The multivariate canonical correlation analysis was performed with MixOmics R package (Rohart et al. 2017) using Rstudio software.

3.3. Results

3.3.1 Effects of drought and high temperature on maize photosynthetic efficiency

Steady-state photosynthetic gas-exchanges and chlorophyll *a* fluorescence were assessed to quantify the photosynthetic performance of B73 and P0023 under high temperature and drought. WD plants had significantly lower net photosynthesis assimilation rate (A), stomatal conductance (gs) and electron transport rate (ETR) compared to WW plants (Figure 3.1A-C). However, under WW the genotypes modulated gs/A differently in response to high temperature. B73 increased gs to maintain A at similar levels as control (WW25) when the temperature increased and P0023 could achieve similar assimilation, as control, maintaining the same gs (Figure 3.1A-B). Under WD38 P0023 demonstrated slightly higher A and significantly greater

ETR than B73 (Figure 3.1B-C). The maximal quantum efficiency of PSII (Fv/Fm) was highly affected by the increase of temperature in both genotypes (Figure 3.1D), but mostly in B73. In this genotype, the decrease in FV/Fm with temperature was more pronounced under water deficit (WD38), whereas in P0023 Fv/Fm decreased similarly in both irrigation regimes at 38ºC (Figure 3.1D).

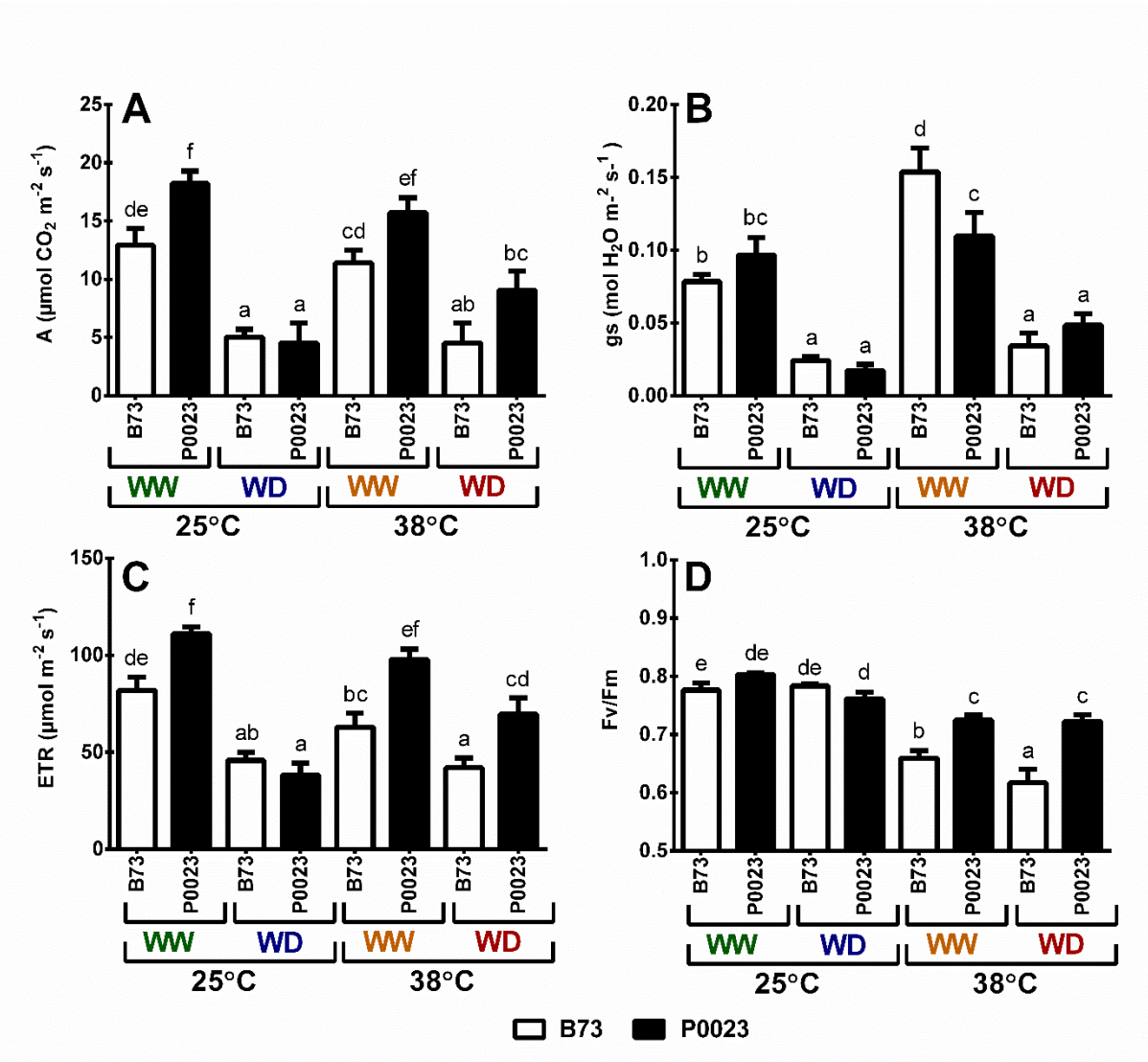

Figure 3.1 – Steady-state photosynthesis in two maize genotypes (B73, P0023) grown under well-watered (WW) and water deficit (WD) conditions and acclimatized to 25ºC or 38ºC. **(A)** Net CO_2 assimilation, **(B)** stomatal conductance, **(C)** electron transport rate (ETR) and **(D)** maximum quantum yield of primary PSII photochemistry (Fv/Fm) were measured at 600 µmol m^{-2} s^{-1} and 400 µmol CO_2 mol^{-1} in fully expanded leaves of maize 4-week-old plants. Values are means ± SEM (n = 5 biological replicates). Different letters denote statistically significant differences between treatments (Duncan analysis, $p < 0.05$).

3.3.2 Leaf water status and biomass allocation under drought and high temperatures

To characterise the water status of B73 and P0023 plants, leaf relative water content (LRWC) and leaf water potential (LWP) were estimated at the end of each experimental condition (Figure 3.2A-B). Well-watered (WW) plants presented leaf relative water content (Figure 3.2A) and leaf water potential (Figure 3.2B) around or above 80% and -1 M Pa, respectively, suggesting good cellular hydration. Water deficit (WD) conditions led to a decrease in LRWC and LWP values (lower than 70% and -1 MPa, respectively, Figure 3.2A-B), revealing a decrease in hydration and a considerable driving force for water uptake by the plant. Under WD38, P0023 presented higher LRWC than B73, even though no significant differences were found for LWP, showing the capacity of this genotype to maintain cellular hydration under these conditions. The above ground biomass was higher in P0023 in all the conditions and increased in both cultivars when subject to high temperatures (WW38, Figure 3.2C). Under WD25 biomass decreased in both genotypes, however, under WD38 only P0023 showed a decrease in biomass relatively to WW25 (Figure 3.2C). To assess the biomass allocation under stress conditions, the relative growth rate (RGR) between the first day of stress and the end of the experiment was determined. RGR was higher in P0023 in all well-watered conditions and decreased under WD to a similar magnitude in both genotypes.

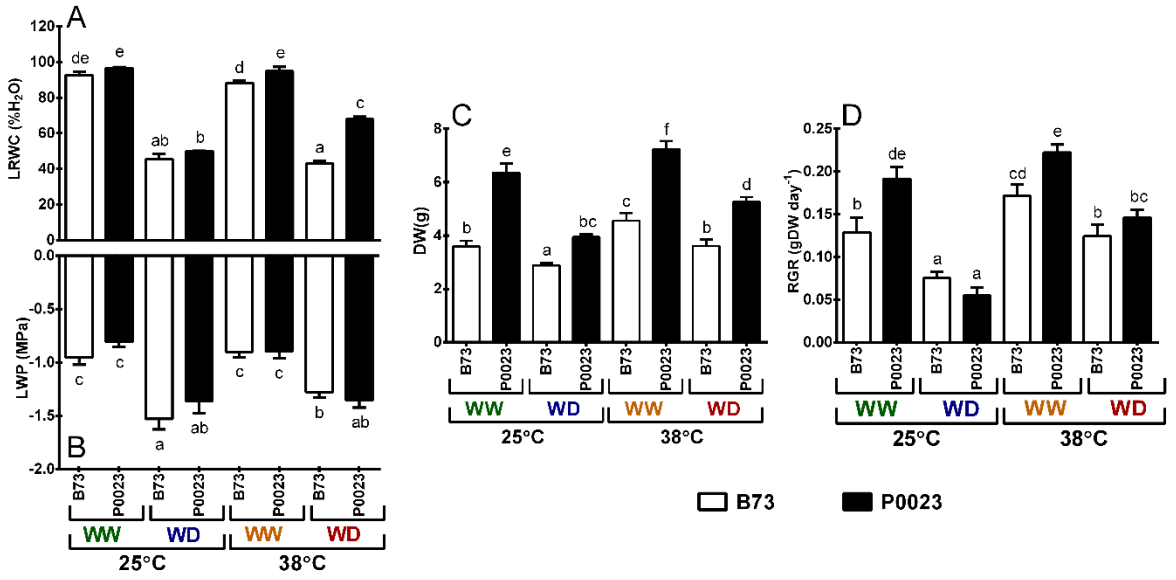

Figure 3.2 – Water status and biomass of two maize genotypes (B73, P0023) grown under well-watered (WW) and water deficit (WD) conditions and acclimatized to 25ºC or 38ºC. (A) Relative water content (LRWC), **(B)** water potential (LWP) of fully expanded leaves, and **(C)** above-ground biomass of 4-week-old maize plants. **(D)** Relative growth rate (RGR) during the acclimatization period. Values are mean ± SEM (n = 5 biological replicates). Different letters denote statistically significant differences between treatments (Duncan analysis, $p < 0.05$).

3.3.3 Effects of drought and high temperature on the leaf evaporative cooling system

To understand the effect of stress conditions on the leaf evaporative colling system, transpiration rate (E) and leaf temperature (LeafT) were measured at end of the experimental conditions. Leaf transpiration decreased significantly under WD conditions and was higher under elevated temperature (WW38, Figure 3.3A), in accordance with soil water availability and stomatal conductance, as assessed by leaf temperature (Figure 3.3B). The leaf temperature increased significantly in both genotypes under WD (Figure 3.3B-E) and increased in both cultivars when subject to high temperatures (Figure 3.3C). Under 25ºC P0023 showed a lower LeafT than B73 in all conditions (Figure 3.3B), although the temperature increased relatively to B73 at 38ºC (Figure 3.3C), in accordance with the decrease of transpiration (Figure 3.3A). However, the increase of leaf temperature in P0023 at 38ºC did not impair assimilation rate (Figure 3.1A) and ETR (Figure 3.1C).

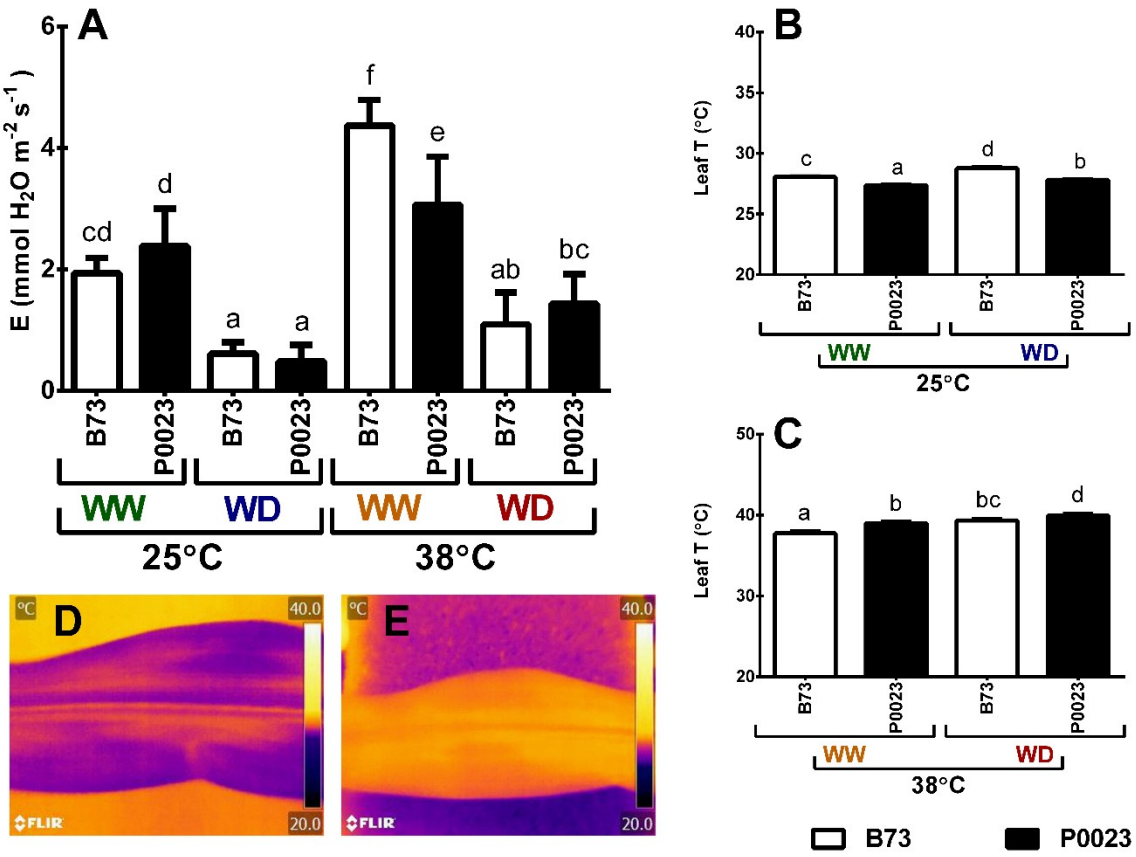

Figure 3.3 – Leaf evaporative cooling system of two maize genotypes (B73, P0023) grown under well-watered (WW) and water deficit (WD) conditions and acclimatized to 25ºC or 38ºC. (A) Transpiration rate, **(B)** leaf temperature at 25ºC and **(C)** leaf temperature at 38ºC. **(D-E)** Representative thermographic images from maize leaves of 4-week-old plants under well-watered (WW, D) and water deficit (WD, E) conditions, exposed to 25ºC.

Values are mean ± SEM (n = 5 biological replicates). Different letters denote statistically significant differences between treatments (Duncan analysis, $p < 0.05$).

3.3.4 Effects of drought and high temperature on the CO_2 concentration mechanism and Calvin-Benson-Bassham cycle

To characterize the combined effects of increased temperatures and water deficit on the CCM and CBBC, the activity of key photosynthetic enzymes was assessed, namely Phosphoenolpyruvate carboxylase (PEPC), NADP-malic enzyme (NADP-ME) and Rubisco (Figure S3.1-S3). A correlation analysis was then used to correlate enzyme activity (maximal/total activity and activation state) with photosynthetic activity and stomatal conductance (A, gs, Fv/Fm, ETR) (Figure 3.4 and Figure 3.5).

Maximal/total activity of carboxylation and decarboxylation enzymes (Figure 3.4) were used as proxy of CCM and CBBC capacity and to highlight the difference between B73 and P0023 genotypes in response to drought and high temperature. Under WD25, PEPC and NADP-ME capacities decreased more extensively in P0023 than in B73, while Rubisco total activity increased in both genotypes, but more significantly in B73 (93% and 68%, Figure 3.4A-B). The strongest correlations to the gas-exchange parameters and PSII capacity (Fv/Fm) were observed in B73 with Rubisco activity (negative) and in P0023 with PEPC and NADP-ME capacities (positive) (Figure 3.4A-B). The enzymes capacity always increased with high temperature (WW38 and WD38, Figure 3.4C-F). Under WW38, this increase was more pronounced in B73 than in P0023 (Figure 3.4C-D). A high positive correlation was identified between gs and PEPC activity in B73, and between gs and NADP-ME in both genotypes (Figure 3.4C-D). A strong negative correlation was observed between the Fv/Fm and PEPC capacity in both genotypes and NADP-ME in B73 (Figure 3.4C-D). Under WD38, the changes in PEPC capacity were similar between genotypes, however, variations in NADP-ME were more robust in B73 (64%) than in P0023 (29%), whereas Rubisco total activity was higher in P0023 (Figure 3.4E-F). The correlation between enzymes activity and photosynthetic parameters were similar for both genotypes, with a strong negative correlation for PEPC and NADP-ME activity and weak correlation to Rubisco activity (Figure 3.4E-F).

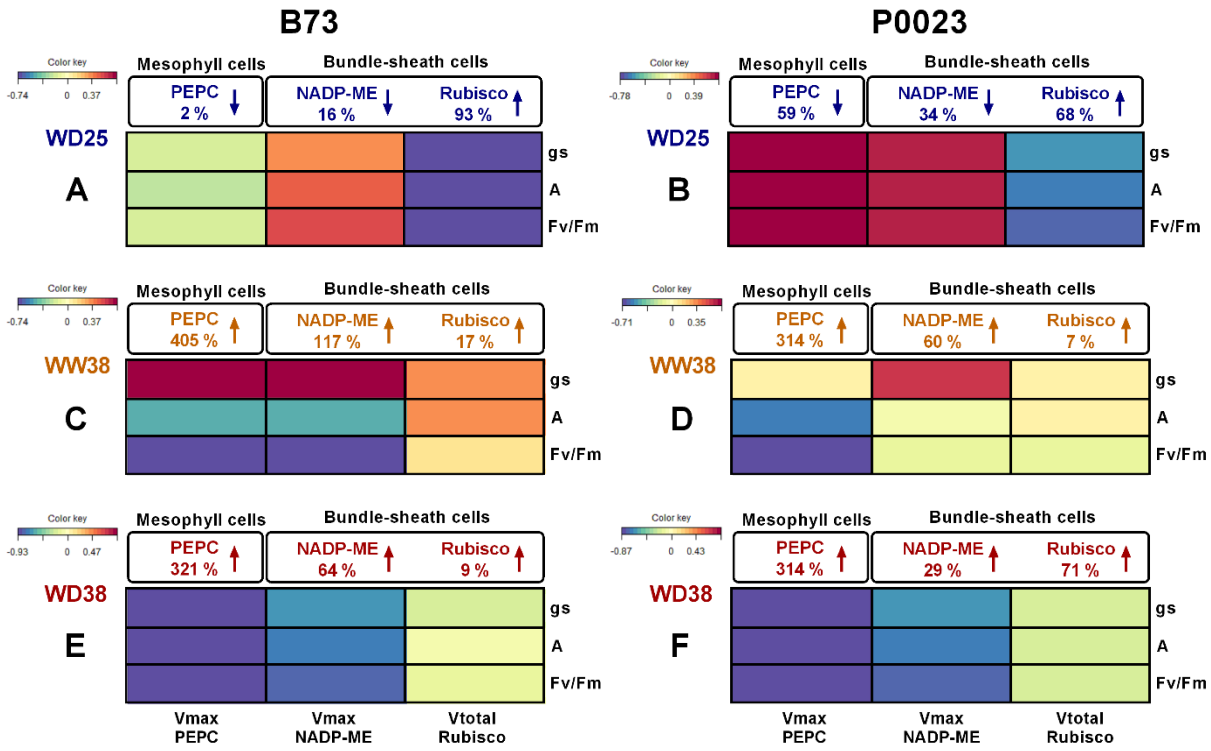

Figure 3.4 – PEPC, NADP-ME and Rubisco maximal capacity of two maize genotypes (B73, P0023) grown under well-watered (WW) and water deficit (WD) conditions and acclimatized to 25ºC or 38ºC. Heatmap represents the correlation between maximal/total activity (Vmax/Vtotal) of key photosynthetic enzymes and steady-state chlorophyll *a* fluorescence or gas-exchange parameters of two maize genotypes (B73, P0023). Canonical correlations were determined according to the effect of (**A-B**) water deficit at 25 ºC (WD25), (**C-D**) high temperatures (well-watered at 38ºC, WW38) and (**E-F**) water deficit combined with high temperatures (WD38) relative to control plants (WW25). Vmax PEPC, Vmax NADP-ME (Vmax), Total Rubisco activity (Vtotal), gs, A and ETR were measured in extracts or fully expanded leaves of 4-week-old plants. Differences in the catalytic activity are represented as percentages to the control activity (WW25), and arrows direction indicate activity increase or decrease. Different colours denote positive (red) or negative (blue) correlations between variables (n = 4-5 biological replicates).

The ratio of physiological activity to enzyme capacity was used as a proxy of the adjustment of CCM and CBBC function in response to drought and high temperature (Figure 3.5, Figure S3.1-Figure S3.3). Under WD25, the PEPC activation state increased in both genotypes at different rates, leading to a negative correlation to the photosynthetic parameters (Figure 5A-B). While B73 showed an increase in PEPC activation state (37%, Figure 5A), by maintaining a similar Vmax (Figure 3.4A) and increasing Vphysiol (Figure S3.1B), P0023 increased the PEPC activation state (76%, Figure 3.5B) by a more pronounced decrease of Vmax (59%, Figure 3.4B) relatively to Vphysiol (Figure S3.1B). On the other hand, both genotypes decreased the activation state of NADP-ME (Figure 3.5A-B) by a marked decrease of Vphysiol (Figure S3.2B) and a minor decrease of Vmax (Figure 3.4A-B). Regarding Rubisco, B73 and

P0023 increased its activation state (Figure 3.5A-B) by a more marked increase of Vinitial (Figure S3.3B) than Vtotal (Figure 3.4A-B). Overall, B73 showed a higher positive correlation between NADP-ME activation state (Figure 3.5A) and the decrease of the photosynthetic parameters (Figure 3.1A-C). In comparison, P0023 showed a stronger negative correlation between the activation state of PEPC (Figure 3.5B) and gs (Figure 3.1B). Under WW38, both genotypes showed a decrease of the activation state in the carboxylation and decarboxylation enzymes (Figure 3.5C-D), as Vphysiol increased less than Vmax (Figure S3.1 and Figure S3.2). Minor changes were also observed in Rubisco activation state in both genotypes (Figure 3.5C-D). Strong positive correlations were observed between ETR and the activation states of PEPC in B73 (Figure 3.5C) and Rubisco in P0023 (Figure 3.5D). Moreover, a strong negative correlation was identified between gs and NADP-ME in B73 (Figure 3.5C). Under WD38, a different regulation of the enzymes operating in the mesophyll or bundle-sheath cells was observed between genotypes. P0023 increased PEPC activation state to a greater extent than B73 (50% and 15%, respectively, Figure 3.5E-F), with a stronger negative correlation to the decrease of photosynthetic parameters. Both genotypes decreased NADP-ME and Rubisco activation state, however, B73 showed a higher correlation to the photosynthetic parameters (Figure 3.5A-F).

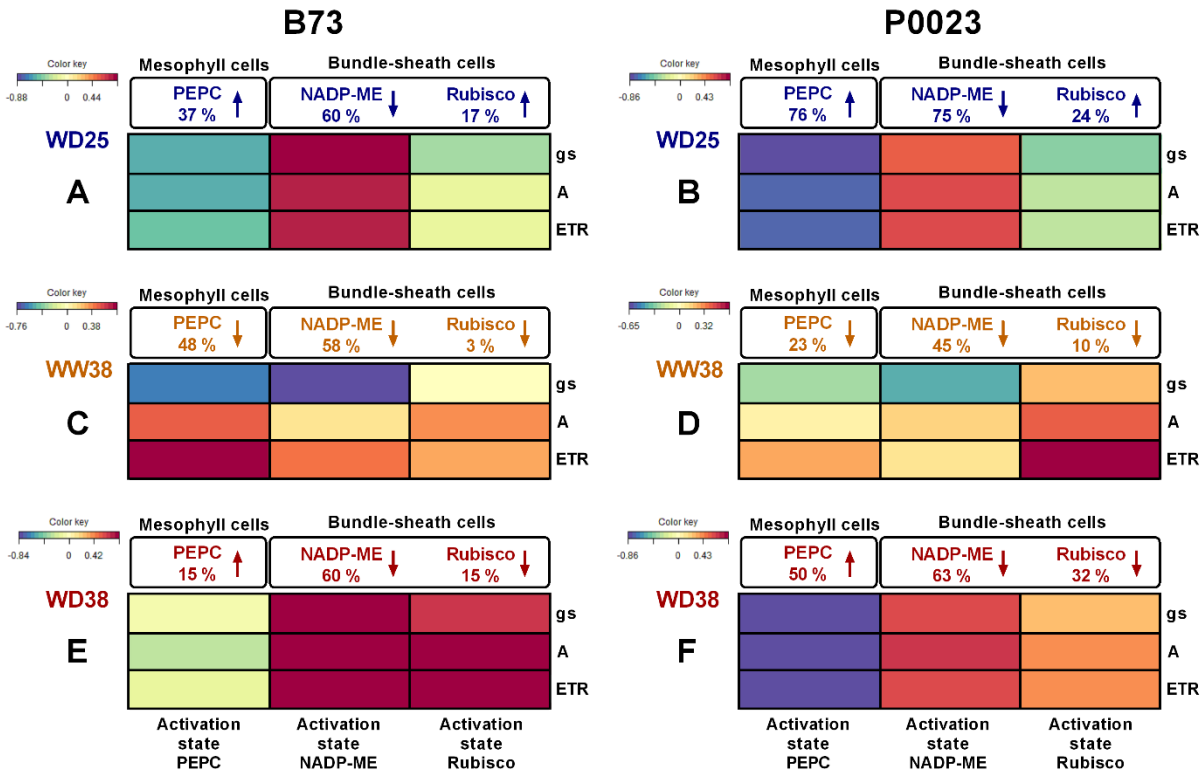

Figure 3.5 – PEPC, NADP-ME and Rubisco activation state of two maize genotypes (B73, P0023) grown under well-watered (WW) and water deficit (WD) conditions and acclimatized to 25ºC or 38ºC. Heatmap represents the correlation between the activation state of key

photosynthetic enzymes and steady-state chlorophyll *a* fluorescence or gas-exchange parameters of two maize genotypes (B73, P0023). Canonical correlations were determined according to the effect of **(A-B)** water deficit at 25 ºC (WD25), **(C-D)** high temperatures (well-watered at 38ºC, WW38) and **(E-F)** water deficit combined with high temperatures (WD38) relative to control plants (WW25). PEPC, NADP-ME and Rubisco activities, gs, A and ETR were measured in extracts or fully expanded leaves of 4-week-old plants. Differences in the catalytic activity are represented as percentages to the control activity (WW25), and arrows direction indicate activity increase or decrease. Different colours denote positive (red) or negative (blue) correlations between variables (n = 4-5 biological replicates).

The PEPC phosphorylation state was evaluated by the sensitivity of PEPC inhibition to L-malate. Overall, significantly lower sensitivity was observed in P0023 compared to B73 only in WD38, when assayed at 25 and 38ºC (Figure 3.6). Moreover, the results showed that the sensitivity to L-malate decreased with water deficit at 25ºC (Figure 3.6) and was maintained at the same level of WW25 when analyzed at 38ºC but increased when assayed at 25ºC (Figure 3.6).

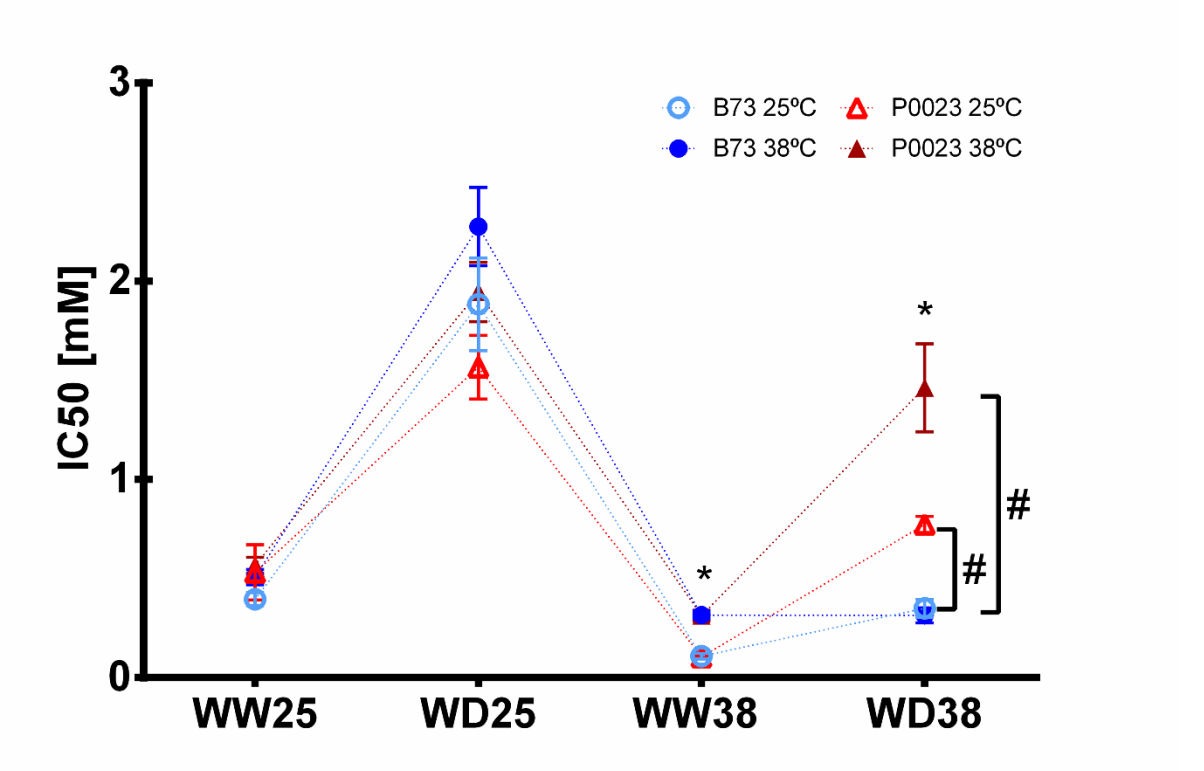

Figure 3.6 – Sensitivity of PEPC activity to the inhibitor L-malate in two maize genotypes (B73, P0023) grown under well-watered (WW) and water deficit (WD) conditions and acclimatized to 25ºC or 38ºC. The half-maximal inhibitory concentration (IC50) was measured at 25ºC (open symbols) and 38ºC (closed symbols) in extracts of fully expanded leaves from 4-week-old maize plants. Asterisks denote statistically significant differences between experimental temperature in the same genotypes and condition (t-test, $p < 0.05$), and cardinals between two genotypes in the same condition and experimental temperature (t-test, $p < 0.05$), n = 4-5 biological replicates.

3.3.5 Effects of drought and high temperature on the electron transport chain components

Chlorophyll *a* rapid chlorophyll induction was recorded and the photophysiological conditions of PSII and the electron transport chain components were evaluated by the analysis of the polyphasic induction curve (OJIP). The increase of the minimum fluorescence value O (F0), in relation to control (WW25) was observed in B73 under WW38 and WD38, but not in P0023. On the contrary, P0023 showed an increase in O under WD25 (Figure 3.7A). Both genotypes showed only minor changes in the variable fluorescence (ΔChlF) at K-step (fluorescence rise related to the inactivation of the oxygen-evolving complex (Strasser et al. 2004)), in relation to WW25 (Figure 3.7A). At the OJ-phase, reflecting QA reduction by single turnover events (Strasser et al. 2004), P0023 decreased the variable fluorescence under water deficit conditions and B73 showed a decrease at WD38 (Figure 3.7A). P0023 decreased the variable fluorescence between the JI-phase (part of the curve that corresponds to the reduction of the secondary electron acceptor (Strasser et al. 2004)) in all conditions relatively to WW25, but B73 only decreased the variable fluorescence at this level under WD38 (Figure 3.7A). The ΔChlF between I and P (induction curve attributed to the reduction of electron transporters of the PSI acceptor side (Tsimilli-Michael 2020)) decreased in both genotypes only at WD38. Overall, F0 increased in both genotypes in response to WW38. However, B73 increased J-I and P0023 maintained similar values. Under WD38 B73 highly increased F0, while P0023 maintained the same levels as WW25, and both genotypes decreased the variable fluorescence in the other steps of the polyphasic induction curve, leading to lower maximal fluorescence (Fm) (Figure 3.7A). Under high temperature conditions P023 maintained a more stable quantum yield of the electron transport flux until the PSI electron acceptors (Figure 3.7B), which is highly correlated with the maintenance of variable fluorescence at I level.

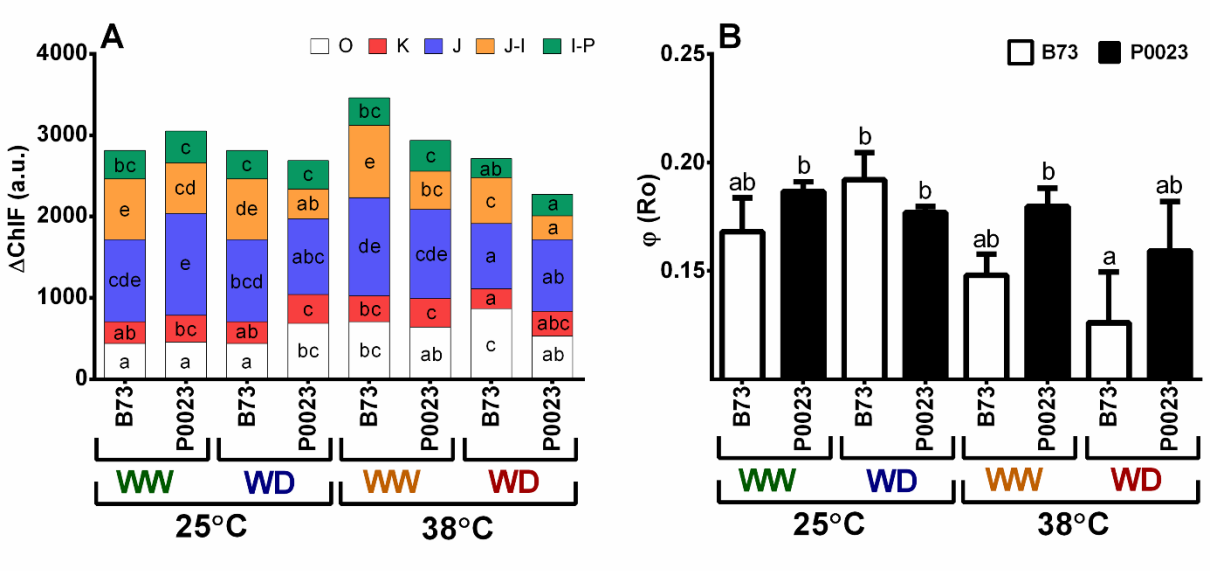

Figure 3.7 – Chlorophyll *a* fluorescence induction in two maize genotypes (B73, P0023) grown under well-watered (WW) and water deficit (WD) conditions and acclimatized to 25ºC or 38ºC. (A) The amplitude of variable fluorescence of chlorophyll *a* transient fluorescence rise (OKJIP) and **(B)** quantum yield of the electron transport flux until the PSI electron acceptors were measured in dark-adapted fully expanded leaves of maize 4-week-old plants. Different coloured bars indicate the minimal fluorescence O, (Fo, white) and changes in the amplitude of variable fluorescence intensities (ΔChlF), K (F300 µs- Fo, red), J (F2ms- Fo, blue), J-I (F30ms- F2ms, orange) and I- P (FFm- F30ms, Fm=maximal fluorescence, green). Values are means ± SEM (n = 5 biological replicates). Different letters denote statistically significant differences between treatments (Duncan analysis, $p < 0.05$).

3.3.6 Photosynthetic performance across leaf in response to drought and high temperature

Chlorophyll *a* fluorescence imaging at increasing irradiance (Rapid Light Curves, RLCs) was used to assess the topographic variation of the photosynthetic response across the leaf (L), mid-veins (MV) and area between mid-veins (BMV) when subjected to high temperature and drought (Figure 3.8A). Maximal photosynthetic electron transport rate (ETRmax) varied between leaf zones, genotypes, and growth conditions (Figure 3.8B). In B73 at WW25 ETRmax was higher at the mid-veins areas (MV ETR), with equal contribution between the MV ETR and the inner space between mid-veins (BMV ETR) to the leaf ETR (L ETR), although in P0023 in the same conditions a higher ETR and contribution to the leaf ETR was detected in BMV areas (Figure 3.8B). In WD38 both genotypes decreased the ETRmax in all zones. In WW38 a higher ETR was observed in B73 MV areas with minor contribution to leaf ETR and in P0023 all the leaf zones behaved similarly (Figure 3.8B). Under WD38, besides the ETRmax decrease in B73, the relation between the different leaf zones ETR was the same. In P0023 the difference between the three zones was less evident, but LETR showed an intermediary maximal ETR, showing similar contribution from MV and BMV to total leaf ETR

(Figure 3.8B). When measured at the growth irradiance (Figure 3.8C-D), in B73 WD25 all the areas showed the same ETR as Leaf, but P0023 showed a slightly decrease in BMV areas (Figure 3.8C-D). Under stress conditions, particularly under WD38, MV areas maintained a more stable or higher ETR than the other zones. In P0023 MV contributed more to the total leaf ETR than BMV under WD38.

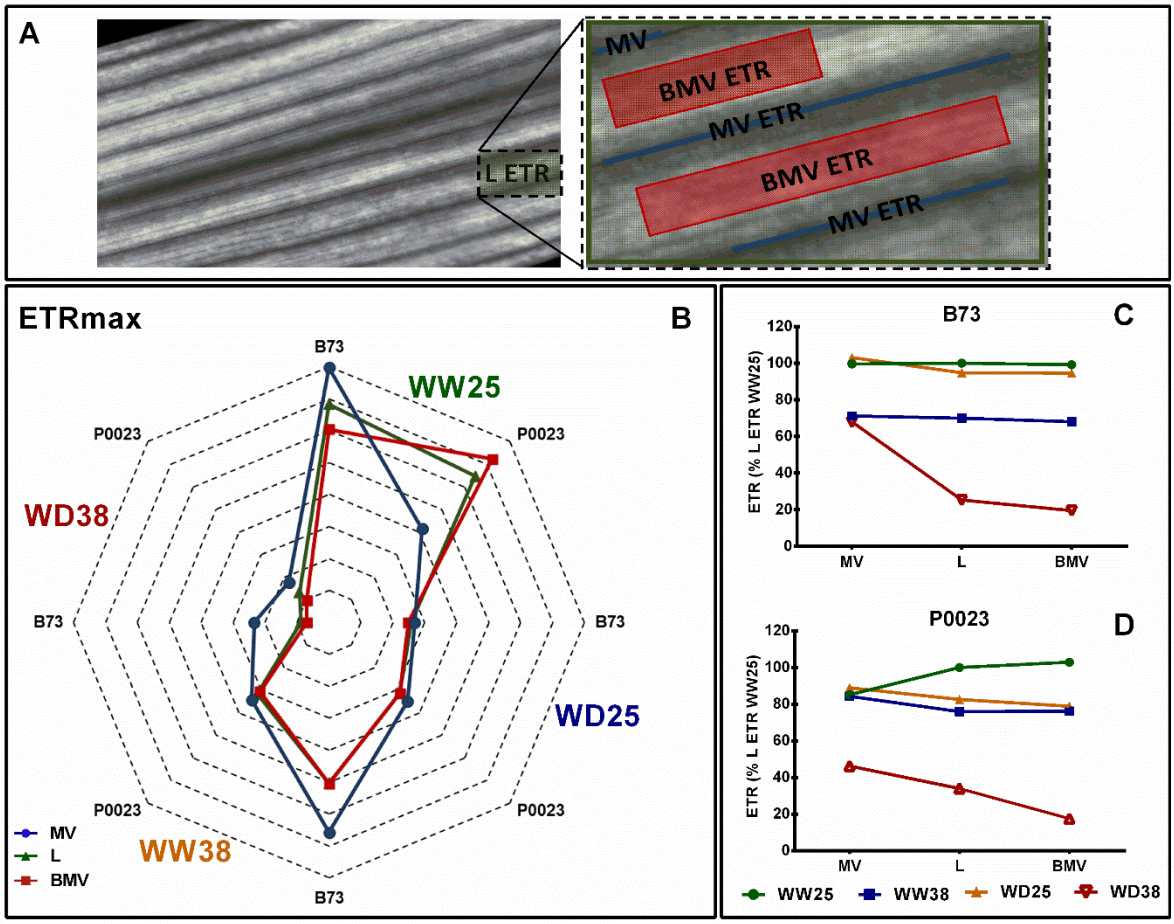

Figure 3.8 – Leaf photosynthetic heterogeny of two maize genotypes (B73, P0023) grown under well-watered (WW) and water deficit (WD) conditions and acclimatized to 25ºC or 38ºC. (A) Leaf (L), mid-vein (MV) and between consecutive mid-veins (BMV) areas of interest (AOI) from a representative chlorophyll *a* fluorescence image. **(B)** Maximal ETR and **(C-D)** growth irradiance ETR extracted from AOIs in fully expanded leaves from 4-week-old maize. ETRmax estimated from a three-parameter photosynthesis-irradiance model (Platt et al. 1982), n = 5 biological replicates, (C-D) data normalized to leaf ETR under WW25.

3.4 Discussion

Two maize genotypes, B73 and P0023, were studied for their ability to withstand water deficit and high temperatures, in isolation or combination. When well-watered plants were subjected to high temperature (WW38), both genotypes maintained near the same photosynthetic capacity (Figure 3.1A and C) and growth rate (Figure 3.2D) as control plants (WW25). However, P0023 maintained the same stomatal conductance, whereas B73

increased gs (Figure 3.1B). Concomitantly, the lower gs in P0023 was accompanied by lower transpiration rate under WW38, albeit no differences were observed between genotypes under WW25 (Figure 3.3A). Therefore, P0023 showed low transpiration rates in response to high temperature and vapour pressure deficit (VPD), since under the WW38 experimental condition, plants were exposed to constant high VPD (2.5-4.0 kPa). A broad genetic variation of the trait related to transpiration response to VPD conditions was extensively investigated by Sinclair and collaborators in several crops, including maize (Sinclair 2017, 2018; Sinclair et al. 2017). Using an experimental system that allowed precise control of VPD (VPD chamber, Gholipoor et al. 2013), it was found that some maize genotypes showed early closure of stomata as VPD increases, decreasing transpiration (TRlim) and saving soil water. The trait TRlim was considered beneficial for maize production under limited water supply and therefore was genetically incorporated in the DuPont Pioneer AQUAmax hybrids (e.g., P0023, Gaffney et al. 2015). However, TRlim was found to be thermal sensitive in maize plants grown at high temperature (32 vs 25°C, Yang et al. 2012), and in another study, some genotypes lost this characteristic when exposed for two days at 38ºC (Shekoofa et al. 2016). Our results demonstrated that reduced transpiration rate was maintained in plants of P0023 acclimated to high temperature/VPD without substantial damage to carbon assimilation. Moreover, this characteristic acted beneficially as a stress avoidance mechanism when water deficit was associated (WD38), by maintaining high leaf hydration (Figure 3.2A) and photosynthetic efficiency (Figure 3.1). Giuliani et al. (2005) found that maize lines with a greater concentration of roots in shallow soil layers had increased leaf abscisic acid concentration, causing reduced stomatal conductance. Consequently, TRlim could be associated with changes at the root system, as plants with a more robust root system can explore and obtain water from deeper soil layers (Hammer et al. 2009; Adee et al. 2016). The decrease of above-ground biomass and RGR in P0023 under WD38 (Figure 3.2C-D) besides higher photosynthetic efficiency than B73 can also suggest that photosynthetic resources in P0023 are being used in root development. Furthermore, aquaporins can also be associated with the regulation and expression of the TRlim trait (Choudhary et al. 2015), as several authors proposed aquaporins in the same way as key players in converting chemical signals (e.g. ABA) to hydraulic response and transmembrane CO_2 transport (Flexas et al. 2006; Shatil-Cohen et al. 2011; Sade et al. 2014; Moshelion et al. 2015; Grondin et al. 2015; Secchi et al. 2017; Ding et al. 2020).

A possible throwback of decreasing transpiration rate under high temperature is the potential harmful increase of leaf temperature, as usually plants use evaporative cooling to reduce it (Carmo-Silva et al. 2012, Costa et al. 2013). It is generally accepted that enzymes of the CCM and Rubisco are unaffected by changes in the range of temperatures faced by plants in our experiment (Casati et al. 1997; Crafts-Brandner and Salvucci 2002b; Salvucci

and Crafts-Brandner 2004b). However, the decrease of Rubisco activation state is usually associated with high temperatures due to an increase of catalytic misfire inhibition and decline of the regulation by heat-sensitive Rca (Salvucci and Crafts-Brandner 2004c; Carmo-Silva and Salvucci 2011). Under WW38 no significant changes on Rubisco activation state were observed (Figure 3.5C-D), which can be explained by the fact that in maize Rubisco is exclusively located in the chloroplast of BSC, surrounding the vascular tissue, that can offer a superior exposure to the evaporative cooling capacity, buffering the BSC temperature rise (Lundgren et al. 2014; Pignon et al. 2019). Another possible explanation is that the long-term acclimation to high temperature experienced by these plants allowed the expression of Rca isoforms more active under high temperature repairing catalytic misfire inhibition, as reported in other studies (Crafts-Brandner and Salvucci 2002b; Yin et al. 2014; Zhang et al. 2019; Kim et al. 2021).

On the other hand, the catalytic activity of carboxylating and decarboxylating enzymes was modulated by WW38 on both genotypes relative to WW25, but more extensively in B73 (Figure 3.4C-D and Figure 3.5C-D). A possible reason for the decrease of PEPC activation state was inhibition of physiological activity due to increased sensitivity to the inhibitor L-malate (Figure 3.6 and Figure S3.1A), known to be mainly regulated by the PEPC kinase phosphorylation (Jiao et al. 1991; Bakrim et al.1993; Nimmo 2003). Nevertheless, in B73 a strong negative correlation between PEPC maximal capacity (Vmax) and the maximum quantum yield of PSII (Fv/Fm, Figure 3.4C) and a positive correlation between PEPC activation and ETR (Figure 3.5C) can also suggest a relation to the decline of ATP production and possible reduction of PEP regeneration by Pyruvate phosphate dikinase (PPDK) in the chloroplast of mesophyll cells, that is ATP dependent (Edwards et al. 1985; Chastain et al. 2011; Chen et al. 2014). The higher NADP-ME maximal activity (Figure 3.4C-D) and lower activation state (Figure 3.5C-D) at high temperature mimics the changes in PEPC enzymatic capacities and responds to carbon supply and flux between MC and BSC (Maier et al. 2011; Wang et al. 2014). Moreover, the more considerable extent of increase of PEPC maximal capacity than NADP-ME in both genotypes (Figure 3.4C-D) can suggest that PEPC activity can be involved in the carboxylation of CO_2 from other sources than atmospheric provenance, as the recycling of CO_2 from BSC leakage or photorespiratory processes, usually associated with exposure to high temperatures (Hatch et al. 1995; Sage et al. 2010; Kromdijk et al. 2014).

Under WD38, when compared to WW25, both genotypes presented decreased Rubisco activation state, due to the lower initial activity relatively to total activity (Figure 3.5E-F, S3). This might be due to the slightly increased leaf temperature (Figure 3C), caused by the decline of gs and evaporative cooling (Figure 1B and 3), making the increase in Rubisco catalytic activity insufficient to overcome enzyme inactivation (Crafts-Brandner and Salvucci 2002b). The substantial decrease of ETR (Figure 3.1C) and the consequent decline of ADP:ATP ratio

in the chloroplast might as well have contributed to the observed decrease in Rubisco activation, as the repair of misfire inhibition by Rca is ATP dependent (Salvucci and Crafts-Brandner 2004c; Carmo-Silva and Salvucci 2011), also supported by the correlation between Rubisco activation state and ETR in B73 (Figure 3.4E). Nevertheless, P0023 increased the total activity, and B73 maintained near the same as WW25 (Figure 3.4E-F, Figure S3.3), showing a higher physiological capacity in P0023. The decrease of activation was less correlated to the reduction of net photosynthetic assimilation and ETR in this genotype than B73 (Figure 3.1A, Figure 3.5E-F). The increase in PEPC activation state in P0023 (Figure 3.5E-F) corresponds to the decrease in the sensitivity to malate (Figure 3.6), suggesting a different level of PEPC phosphorylation between genotypes and higher physiological functionality of PEPC in P0023. Nonetheless, differences between PEPC catalytic activity can be explained by other regulatory mechanisms, such as other post-translational modifications (Ruiz-Ballesta et al. 2016; Luís et al. 2016). NADP-ME maximal activity was reduced by half relative to WW38, demonstrating the negative effect of drought at 25ºC (Figure 3.4A-B) and 38ºC (Figure 3.4C-D relative to Figure 3.4E-F). Several authors reported the decrease of NADP-ME activity under water deficit (Du et al. 1996; Marques da Silva and Arrabaça 2004; Carmo-Silva et al. 2008), but to the best of our knowledge, no changes in NADP-ME activity have been previously reported in maize plants acclimatized to high temperature and subjected to water deficit. Nevertheless, the plasticity of the decarboxylating process in maize plants under stress conditions was identified by other authors (Chapman and Hatch 1981; Wingler et al. 1999; Bellasio and Griffiths 2014), and alternative decarboxylating processes, as the synthesis of aspartate as a major translocated C_4 acid, can compensate the decrease of NADP-ME decarboxylating activity under our experimental conditions (Furbank 2011; von Caemmerer and Furbank 2016).

P0023 showed a higher maximum quantum yield of PSII (Figure 3.1D) and stable quantum yield of the electron transport flux until the PSI electron acceptors (Figure 3.7B) under high temperatures and a higher contribution of the mid-veins ETR (MV ETR) to whole leaf ETR (L ETR) under WD38 (Figure 3.8C). These results demonstrated the higher efficiency in producing the chemical energy (ATP and reduction power) in this genotype under higher temperature. Maize mid-veins are anatomically characterized by highly differentiated BSC surrounded by MC, forming concentric circles around the vasculature (Lundgren et al. 2014). ATP and reduction power are cofactors of most photosynthetic enzymes, and reduction power is moved from MC to BSC through malate decarboxylation (Furbank 2011) and the shuttle of 3-PGA and triose phosphate (Hatch 1987; Bräutigam and Weber 2010). Thus, the observed superior ETR stability in these zones (MV) and the maintenance of the physical integrity components of the photosynthetic apparatus in MC and BSC can be regarded as crucial for successful acclimation of photosynthesis to high temperature conditions. Moreover, reduction

of stomatal conductance under high temperature as a water-saving mechanism in P0023 and maintenance of hydraulic conductance can also act preventing desiccation and maintenance of highly productive MC and BSC surrounding the vascular tissues (Figure 3.1B and Figure 3.8D) (Sunita et al. 2014; Sade et al. 2014; Moshelion et al. 2015).

In summary, the limited transpiration rate under high temperature/VPD, together with higher efficiency in the regulation of the CO_2 concentration mechanism contributed to the maintenance of a better physiological status in P0023 under high temperature and/or extended drought. These characteristics can allow water conservation in initial periods of soil drying, without substantial crop production damage. Genotypes with the same traits may be suitable for crop production in environments with high temperature that experience regular water shortage periods. Furthermore, high throughput screening of maize hybrids under similar experimental settings can select genotypes with the same characteristics and potential to a more stable production in warmer and drier conditions helping to overcome future throwbacks in food production.

3.5 Supplementary data

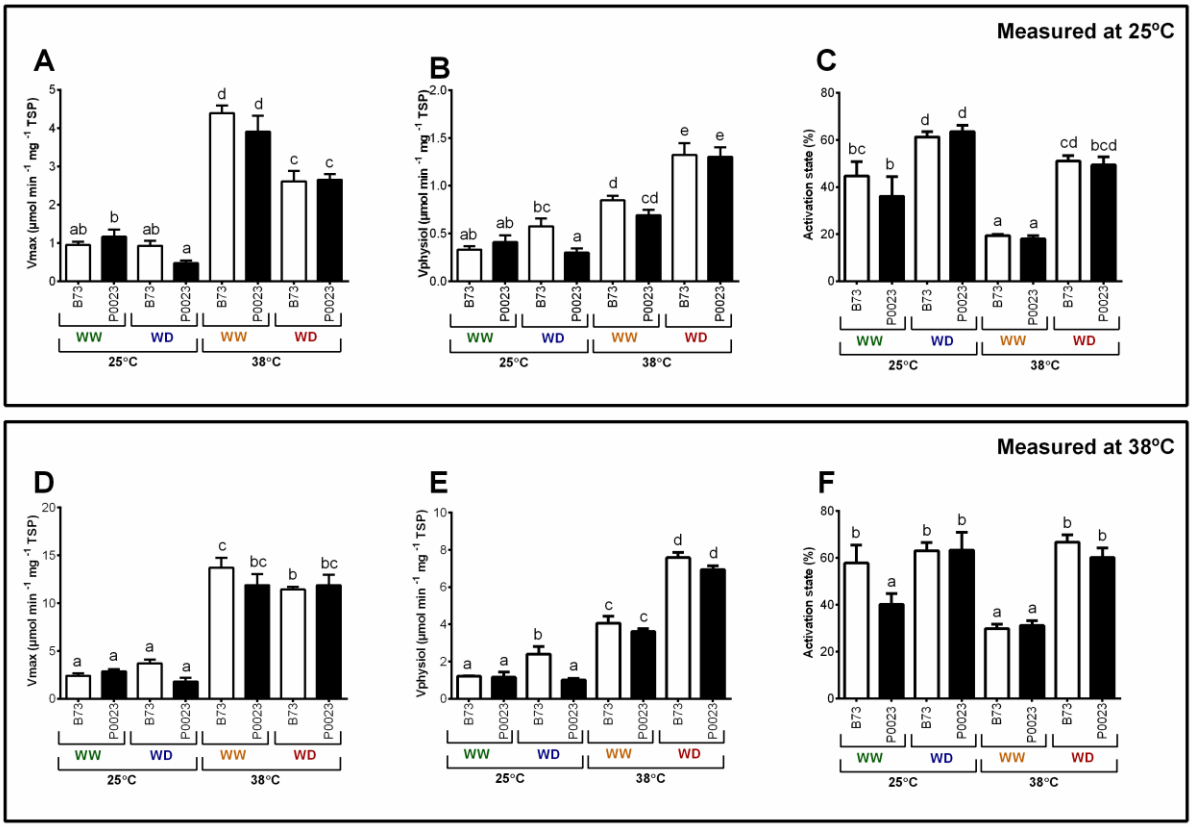

Figure S3.1– Effect of high temperature and drought on PEPC activity (expressed by total soluble protein, TSP) and activation state in two maize genotypes, B73 and P0023. (A–C) Maximal (Vmax) and physiological (Vphysiol) activities and activation state were measured at 25°C and **(D–F)** at 38°C in extracts of fully expanded leaves from 4-week-old maize plants under well-watered (WW) and water deficit (WD) conditions and exposed to control (25°C) and high temperature conditions (38°C). **(A and D)** Vmax, **(B and E)** Vphysiol, **(C and F)** activation state. Values are means ± sd (n = 4–5 biological replicates). Different letters denote statistically significant differences between treatments (Duncan analysis, $p < 0.05$)

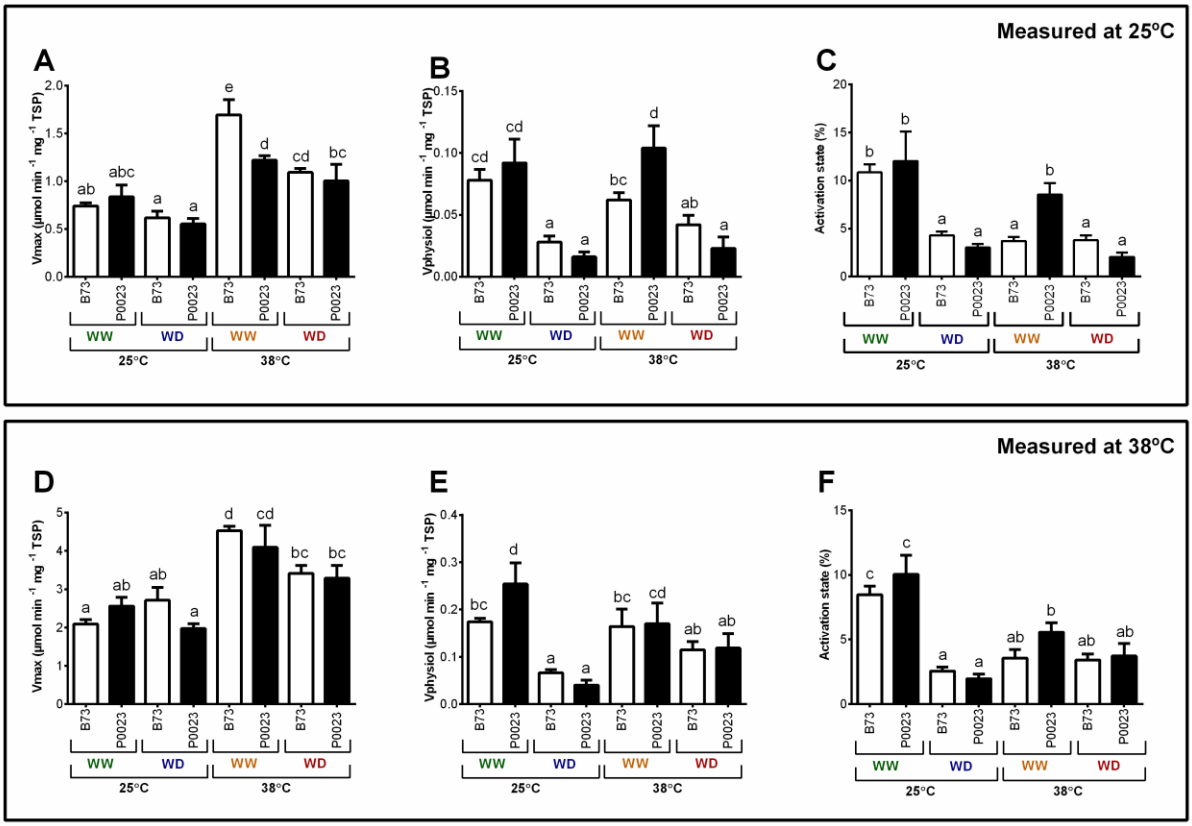

Figure S3.2 – Effect of high temperature and drought on NADP-ME activity (expressed by total soluble protein, TSP) and activation state in two maize genotypes, B73 and P0023. (A–C) Maximal (Vmax) and physiological (Vphysiol) activities and activation state were measured at 25°C and **(D–F)** at 38°C in extracts of fully expanded leaves from 4-week-old maize plants under well-watered (WW) and water deficit (WD) conditions and exposed to control (25°C) and high temperature conditions (38°C). **(A and D)** Vmax), **(B and E)** Vphysiol, **(C and F)** activation state. Values are means ± sd (n = 4–5 biological replicates). Different letters denote statistically significant differences between treatments (Duncan analysis, $p < 0.05$).

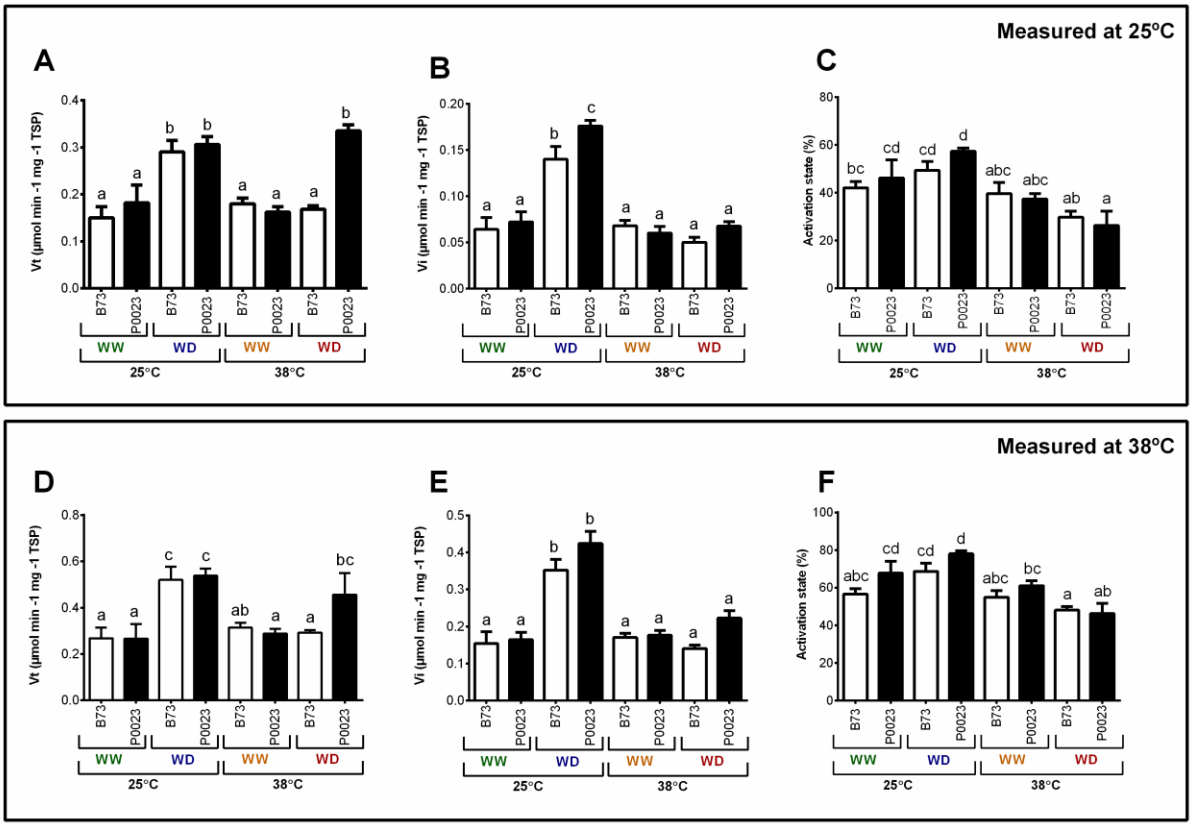

Figure S3.3 – Effect of high temperature and drought on Rubisco activity (expressed by total soluble protein, TSP) and activation state in two maize genotypes, B73 and P0023. (A–C) Rubisco initial (Vi) and total (Vt) activities and activation state were measured at 25°C and **(D–F)** at 38°C in extracts of fully expanded leaves from 4-week-old maize plants under well-watered (WW) and water deficit (WD) conditions and exposed to control (25°C) and high temperature conditions (38°C). **(A and D)** Total activity (Vi), **(B and E)** initial activity (Vt), **(C and F)** activation state. Values are means ± sd (n = 4–5 biological replicates). Different letters denote statistically significant differences between treatments (Duncan analysis, $p < 0.05$)

3.6 References

Adee E, Roozeboom K, Balboa GR, et al (2016) Drought-Tolerant Corn Hybrids Yield More in Drought-Stressed Environments with No Penalty in Non-stressed Environments. Front Plant Sci 7:1534. https://doi.org/10.3389/fpls.2016.01534

Arrivault S, Obata T, Szecówka M, et al (2017) Metabolite pools and carbon flow during C_4 photosynthesis in maize: 13CO 2 labeling kinetics and cell type fractionation. J Exp Bot 68:283–298. https://doi.org/10.1093/jxb/erw414

Bellasio C, Griffiths H (2014) The operation of two decarboxylases, transamination, and partitioning of C_4 metabolic processes between mesophyll and bundle sheath cells allows light capture to be balanced for the maize C4 pathway. Plant Physiol 164:466–480. https://doi.org/10.1104/pp.113.228221

Bradford MM (1976) A rapid and sensitive method for the quantitation of microgram quantities of protein utilizing the principle of protein-dye binding. Anal Biochem 72:248–254. https://doi.org/10.1016/0003-2697(76)90527-3

Bräutigam A, Weber APM (2010) Chapter 11 Transport Processes: Connecting the Reactions of C_4 Photosynthesis. In: Raghavendra, Sage RF (eds) C_4 Photosynthesis and Related CO_2 Concentrating Mechanisms. Advances in Photosynthesis and Respiration. Springer, Dordrecht, pp 199–219

Carmo-Silva AE, Bernardes da Silva A, Keys AJ, et al (2008) The activities of PEP carboxylase and the C_4 acid decarboxylases are little changed by drought stress in three C_4 grasses of different subtypes. Photosynth Res 97:223–233. https://doi.org/10.1007/s11120-008-9329-7

Carmo-Silva AE, Gore MA, Andrade-Sanchez P, et al (2012) Decreased CO 2 availability and inactivation of Rubisco limit photosynthesis in cotton plants under heat and drought stress in the field. Environ Exp Bot 83:1–11. https://doi.org/10.1016/j.envexpbot.2012.04.001

Carmo-Silva AE, Salvucci ME (2011) The activity of Rubisco's molecular chaperone, Rubisco activase, in leaf extracts. Photosynth Res 108:143–155. https://doi.org/10.1007/s11120-011-9667-8

Carmo-Silva E, Scales JC, Madgwick PJ, Parry MAJ (2015) Optimizing Rubisco and its regulation for greater resource use efficiency. Plant, Cell Environ 38:1817–1832. https://doi.org/10.1111/pce.12425

Carmo-Silva E (2008) Photosynthesis and Photorespiration in Three C_4 Grasses of Different Metabolic Sub-Types, Under Water Stress. 217

Casati P, Spampinato CP, Andreo CS (1997) Characteristics and physiological function of NADP-malic enzyme from wheat. Plant Cell Physiol 38:928–934. https://doi.org/10.1093/oxfordjournals.pcp.a029253

Čatský J (1960) Determination of water deficit in disks cut out from leaf blades. Biol Plant 2:76–78. https://doi.org/10.1007/BF02920701

Chapman K, Hatch M (1981) Aspartate Decarboxylation in Bundle Sheath Cells of Zea mays and Its Possible Contribution to C_3 Photosynthesis. Funct Plant Biol 8:237. https://doi.org/10.1071/pp9810237

Chastain CJ, Failing CJ, Manandhar L, et al (2011) Functional evolution of C 4 pyruvate, orthophosphate dikinase. J. Exp. Bot. 62:3083–3091

Chaves MM, Maroco JP, Pereira JS (2003) Understanding plant responses to drought — from genes to the whole plant. Funct Plant Biol 30:239. https://doi.org/10.1071/FP02076

Chen J, Xu W, Velten J, et al (2012) Characterization of maize inbred lines for drought and heat tolerance. J Soil Water Conserv 67:354–364. https://doi.org/10.2489/jswc.67.5.354

Chen YB, Lu TC, Wang HX, et al (2014) Posttranslational modification of maize chloroplast pyruvate orthophosphate dikinase reveals the precise regulatory mechanism of its enzymatic activity. Plant Physiol 165:534–549. https://doi.org/10.1104/pp.113.231993

Choudhary S, Sinclair TR, Messina CD, et al (2015) Inhibitor screen for limited-transpiration trait among maize hybrids. Environ Exp Bot 109:161–167. https://doi.org/10.1016/j.envexpbot.2014.07.015

Cooper M, Gho C, Leafgren R, et al (2014) Breeding drought-tolerant maize hybrids for the US corn-belt: discovery to product. J Exp Bot 65:6191–6204. https://doi.org/10.1093/jxb/eru064

Costa JM, Grant OM, Chaves MM (2013) Thermography to explore plant-environment interactions. J. Exp. Bot. 64:3937–3949

Crafts-Brandner SJ, Salvucci ME (2002a) Sensitivity of Photosynthesis in a C_4 Plant, Maize, to Heat Stress. Plant Physiol 129:

Crafts-Brandner SJ, Salvucci ME (2002b) Sensitivity of photosynthesis in a C_4 plant, maize, to heat stress. Plant Physiol 129:1773–1780. https://doi.org/10.1104/pp.002170

Ding L, Milhiet T, Couvreur V, et al (2020) Modification of the expression of the aquaporin ZmPIP2;5 affects water relations and plant growth. Plant Physiol 182:2154–2165. https://doi.org/10.1104/PP.19.01183

Du YC, Kawamitsu Y, Nose A, et al (1996) Effects of water stress on carbon exchange rate and activities of photosynthetic enzymes in leaves of sugarcane (Saccharum sp.). Aust J Plant Physiol 23:719–726. https://doi.org/10.1071/PP9960719

Duque AS, de Almeida AM, Bernardes da Silva A, et al (2013) Abiotic Stress Responses in Plants: Unraveling the Complexity of Genes and Networks to Survive. In: Abiotic Stress - Plant Responses and Applications in Agriculture. InTech

Duvick DN, Smith JSC, Cooper M (2010) Long-Term Selection in a Commercial Hybrid Maize Breeding Program. In: Plant Breeding Reviews. John Wiley & Sons, Inc., Oxford, UK, pp

109–151

Dwyer SA, Ghannoum O, Nicotra A, Von Caemmerer S (2007) High temperature acclimation of C_4 photosynthesis is linked to changes in photosynthetic biochemistry. Plant, Cell Environ 30:53–66. https://doi.org/10.1111/j.1365-3040.2006.01605.x

Edwards GE, Franceschi VR, Voznesenskaya E V. (2004) Single-cell C_4 photosynthesis versus the dual-cell (Kranz) paradigm. Annu. Rev. Plant Biol. 55:173–196

Edwards GE, Furbank RT, Hatch MD, Osmond CB (2001) What does it take to be C_4? Lessons from the evolution of C_4 photosynthesis. Plant Physiol 125:46–49. https://doi.org/10.1104/pp.125.1.46

Edwards GE, Nakamoto H, Burnell JN, Hatch MD (1985) Pyruvate,Pi Dikinase and NADP-Malate Dehydrogenase in C_4 Photosynthesis: Properties and Mechanism of Light/Dark Regulation. Annu Rev Plant Physiol 36:255–286. https://doi.org/10.1146/annurev.pp.36.060185.001351

Flexas J, Ribas-Carbó M, Hanson DT, et al (2006) Tobacco aquaporin NtAQP1 is involved in mesophyll conductance to CO 2 in vivo. Plant J 48:427–439. https://doi.org/10.1111/j.1365-313X.2006.02879.x

Foyer CH, Valadier MH, Migge A, Becker TW (1998) Drought-induced effects on nitrate reductase activity and mRNA and on the coordination of nitrogen and carbon metabolism in maize leaves. Plant Physiol 117:283–292. https://doi.org/10.1104/pp.117.1.283

Furbank RT (2011) Evolution of the C 4 photosynthetic mechanism: Are there really three C 4 acid decarboxylation types? J. Exp. Bot. 62:3103–3108

Gaffney J, Schussler J, Löffler C, et al (2015) Industry-Scale Evaluation of Maize Hybrids Selected for Increased Yield in Drought-Stress Conditions of the US Corn Belt. Crop Sci 55:1608. https://doi.org/10.2135/cropsci2014.09.0654

Genty B, Briantais JM, Baker NR (1989) The relationship between the quantum yield of photosynthetic electron transport and quenching of chlorophyll fluorescence. Biochim Biophys Acta - Gen Subj 990:87–92. https://doi.org/10.1016/S0304-4165(89)80016-9

Ghannoum O, Evans JR, von Caemmerer S (2010) Chapter 8 Nitrogen and Water Use Efficiency of C_4 Plants. In: Raghavendra A, Sage R (eds) C_4 Photosynthesis and Related CO_2 Concentrating Mechanisms. Advances in Photosynthesis and Respiration. Springer, Dordrecht, pp 129–146

Gholipoor M, Choudhary S, Sinclair TR, et al (2013) Transpiration Response of Maize Hybrids to Atmospheric Vapour Pressure Deficit. J Agron Crop Sci 199:155–160. https://doi.org/10.1111/jac.12010

Giuliani S, Sanguineti MC, Tuberosa R, et al (2005) Root-ABA1, a major constitutive QTL, affects maize root architecture and leaf ABA concentration at different water regimes. J Exp Bot 56:3061–3070. https://doi.org/10.1093/jxb/eri303

Grondin A, Rodrigues O, Verdoucq L, et al (2015) Aquaporins contribute to ABA-triggered stomatal closure through OST1-mediated phosphorylation. Plant Cell 27:1945–1954. https://doi.org/10.1105/tpc.15.00421

Hammer GL, Dong Z, McLean G, et al (2009) Can changes in canopy and/or root system architecture explain historical maize yield trends in the U.S. corn belt? Crop Sci 49:299–312. https://doi.org/10.2135/cropsci2008.03.0152

Hatch MD (1987) C_4 photosynthesis: a unique elend of modified biochemistry, anatomy and ultrastructure. BBA Rev. Bioenerg. 895:81–106

Hatch MD, Agostino A, Jenkins CL (1995) Measurement of the leakage of CO_2 from bundle-sheath cells of leaves during C_4 photosynthesis. Plant Physiol 108:173–181. https://doi.org/10.1104/pp.108.1.173

IPCC (2014) 2014: Climate Change 2014: Synthesis Report. Contribution of Working Groups I, II and III to the Fifth Assessment Report of the Intergovernmental Panel on Climate Change. Gian-Kasper Plattner, Geneva, Switzerland

Jiao JA, Vidal J, Echevarría C, Chollet R (1991) In vivo regulatory phosphorylation site in C_4-leaf phosphoenolpyruvate carboxylase from maize and sorghum. Plant Physiol 96:297–301. https://doi.org/10.1104/pp.96.1.297

Jiao Y, Peluso P, Shi J, et al (2017) Improved maize reference genome with single-molecule technologies. Nature 546:524–527. https://doi.org/10.1038/nature22971

Khoshravesh R, Stata M, Adachi S, et al (2020) Evolutionary Convergence of C_4 Photosynthesis: A Case Study in the Nyctaginaceae. Front Plant Sci 11:2. https://doi.org/10.3389/fpls.2020.578739

Kim SY, Slattery RA, Ort DR (2021) A role for differential Rubisco activase isoform expression in C_4 bioenergy grasses at high temperature. GCB Bioenergy 13:211–223. https://doi.org/10.1111/gcbb.12768

Kromdijk J, Ubierna N, Cousins AB, Griffiths H (2014) Bundle-sheath leakiness in C_4 photosynthesis: A careful balancing act between CO_2 concentration and assimilation. J. Exp. Bot. 65:3443–3457

Lawson T, Terashima I, Fujita T, Wang Y (2018) Coordination Between Photosynthesis and Stomatal Behavior. pp 141–161

Lopes MS, Araus JL, Van Heerden PDR, Foyer CH (2011) Enhancing drought tolerance in C 4 crops. J. Exp. Bot. 62:3135–3153

Luís IM, Alexandre BM, Oliveira MM, Abreu IA (2016) Selection of an appropriate protein extraction method to study the phosphoproteomeof maize photosynthetic tissue. PLoS One 11:e0164387. https://doi.org/10.1371/journal.pone.0164387

Lundgren MR, Osborne CP, Christin PA (2014) Econstructing Kranz anatomy to understand C_4 evolution. J. Exp. Bot. 65:3357–3369

Maier A, Zell MB, Maurino VG (2011) Malate decarboxylases: Evolution and roles of NAD(P)-ME isoforms in species performing C 4 and C 3 photosynthesis. J. Exp. Bot. 62:3061–3069

Marques da Silva J, Arrabaça MC (2004) Photosynthetic enzymes of the C 4 grass Setaria sphacelata under water stress: A comparison between rapidly and slowly imposed water deficit. Photosynthetica 42:43–47. https://doi.org/10.1023/B:PHOT.0000040568.58103.ca

Meierhoff K, Westhoff P (1993) Differential biogenesis of photosystem II in mesophyll and bundle-sheath cells of monocotyledonous NADP-malic enzyme-type C_4 plants: the non-stoichiometric abundance of the subunits of photosystem II in the bundle-sheath chloroplasts and the translational. Planta 191:23–33. https://doi.org/10.1007/BF00240892

Moshelion M, Halperin O, Wallach R, et al (2015) Role of aquaporins in determining transpiration and photosynthesis in water-stressed plants: Crop water-use efficiency, growth and yield. Plant, Cell Environ. 38:1785–1793

Nimmo HG (2003) Control of the phosphorylation of phosphoenolpyruvate carboxylase in higher plants. Arch. Biochem. Biophys. 414:189–196

Nunes C, Araújo S., Silva JM, et al (2009) Photosynthesis light curves: a method for screening water deficit resistance in the model legume *Medicago truncatula*. Ann Appl Biol 155:321–332. https://doi.org/10.1111/j.1744-7348.2009.00341.x

Omoto E, Kawasaki M, Taniguchi M, Miyake H (2009) Salinity induces granal development in bundle sheath chloroplasts of NADP-Malic Enzyme Type C_4 plants. Plant Prod Sci 12:199–207. https://doi.org/10.1626/pps.12.199

Osborne CP, Sack L (2012) Evolution of C_4 plants: A new hypothesis for an interaction of CO_2 and water relations mediated by plant hydraulics. Philos Trans R Soc B Biol Sci 367:583–600. https://doi.org/10.1098/rstb.2011.0261

Parry MAJ, Andralojc PJ, Parmar S, et al (1997) Regulation of Rubisco by inhibitors in the light. Plant, Cell Environ 20:528–534. https://doi.org/10.1046/j.1365-3040.1997.d01-85.x

Perdomo JA, Capó-Bauçà S, Carmo-Silva E, Galmés J (2017) Rubisco and Rubisco Activase Play an Important Role in the Biochemical Limitations of Photosynthesis in Rice, Wheat, and Maize under High Temperature and Water Deficit. Front Plant Sci 8:490. https://doi.org/10.3389/fpls.2017.00490

Petolino JF, Cowen NM, Thompson SA, Mitchell JC (1990) Gamete Selection for Heat-stress Tolerance in Maize. J Plant Physiol 136:219–224. https://doi.org/10.1016/S0176-1617(11)81669-X

Pignon CP, Lundgren MR, Osborne CP, Long SP (2019) Bundle sheath chloroplast volume can house sufficient Rubisco to avoid limiting C 4 photosynthesis during chilling. J Exp

Bot 70:357–365. https://doi.org/10.1093/jxb/ery345

Platt T, Harrison WG, Irwin B, et al (1982) Photosynthesis and photoadaptation of marine phytoplankton in the arctic. Deep Sea Res Part A, Oceanogr Res Pap 29:1159–1170. https://doi.org/10.1016/0198-0149(82)90087-5

Portis AR (2003) Rubisco activase - Rubisco's catalytic chaperone. Photosynth. Res. 75:11–27

Rao X, Dixon RA (2016) The differences between NAD-ME and NADP-ME subtypes of C_4 photosynthesis: More than decarboxylating enzymes. Front. Plant Sci. 7:1525

Ruiz-Ballesta I, Baena G, Gandullo J, et al (2016) New insights into the post-translational modification of multiple phosphoenolpyruvate carboxylase isoenzymes by phosphorylation and monoubiquitination during sorghum seed development and germination. J Exp Bot 67:3523–3536. https://doi.org/10.1093/jxb/erw186

Sade N, Shatil-Cohen A, Attia Z, et al (2014) The Role of Plasma Membrane Aquaporins in Regulating the Bundle Sheath-Mesophyll Continuum and Leaf Hydraulics. Plant Physiol 166:1609–1620. https://doi.org/10.1104/pp.114.248633

Sage RF (2004) The evolution of C_4 photosynthesis. New Phytol. 161:341–370

Sage RF, Kocacinar F, Kubien DS (2010) Chapter 10 C_4 Photosynthesis and Temperature. Springer, Dordrecht, pp 161–195

Sage RF, Kubien DS (2007) The temperature response of C_3 and C_4 photosynthesis. Plant, Cell Environ 30:1086–1106. https://doi.org/10.1111/j.1365-3040.2007.01682.x

Salvucci ME, Crafts-Brandner SJ (2004a) Inhibition of photosynthesis by heat stress: the activation state of Rubisco as a limiting factor in photosynthesis. Physiol Plant 120:179–186. https://doi.org/10.1111/j.0031-9317.2004.0173.x

Salvucci ME, Crafts-Brandner SJ (2004b) Relationship between the heat tolerance of photosynthesis and the thermal stability of Rubisco activase in plants from contrasting thermal environments. Plant Physiol 134:1460–1470. https://doi.org/10.1104/pp.103.038323

Salvucci ME, Crafts-Brandner SJ (2004c) Mechanism for deactivation of Rubisco under moderate heat stress. Physiol Plant 122:513–519. https://doi.org/10.1111/j.1399-3054.2004.00419.x

Schnable PS, Ware D, Fulton RS, et al (2009) The B73 Maize Genome: Complexity, Diversity, and Dynamics. Science (80-) 326:1112–1115. https://doi.org/10.1126/science.1178534

Secchi F, Pagliarani C, Zwieniecki MA (2017) The functional role of xylem parenchyma cells and aquaporins during recovery from severe water stress. Plant Cell Environ. 40:858–871

Shatil-Cohen A, Attia Z, Moshelion M (2011) Bundle-sheath cell regulation of xylem-mesophyll water transport via aquaporins under drought stress: A target of xylem-borne ABA? Plant

J 67:72–80. https://doi.org/10.1111/j.1365-313X.2011.04576.x

Shekoofa A, Sinclair TR, Messina CD, Cooper M (2016) Variation among maize hybrids in response to high vapor pressure deficit at high temperatures. Crop Sci 56:392–396. https://doi.org/10.2135/cropsci2015.02.0134

Silsbe G, Malkin SY (2015) Package "phytotools" Type Package Title Phytoplankton Production Tools

Bernardes da Silva A., Arrabaça MC, Marques da Silva J. (2001). Effect of Rapid Dehydration on the Activity of PEPC from the C_4 Grass *Paspalum dilatatum*. In: PS2001 – Proceedings of the 12th International Congress on Photosynthesis, S17-023: 1-4, CSIRO Publishing, Collingwood.

Sinclair TR (2018) Effective Water Use Required for Improving Crop Growth Rather Than Transpiration Efficiency. Front Plant Sci 9:1442. https://doi.org/10.3389/fpls.2018.01442

Sinclair TR (2017) Water-Conservation Traits to Increase Crop Yields in Water-deficit Environments. Springer International Publishing, Cham

Sinclair TR, Devi J, Shekoofa A, et al (2017) Limited-transpiration response to high vapor pressure deficit in crop species. Plant Sci. 260:109–118

Stirbet A, Govindjee (2011) On the relation between the Kautsky effect (chlorophyll *a* fluorescence induction) and Photosystem II: Basics and applications of the OJIP fluorescence transient. J Photochem Photobiol B Biol 104:236–257. https://doi.org/10.1016/J.JPHOTOBIOL.2010.12.010

Strasser RJ, Tsimilli-Michael M, Srivastava A (2004) Analysis of the Chlorophyll *a* Fluorescence Transient. In: Papageorgiou G.C., Govindjee (eds) Chlorophyll *a* Fluorescence. Advances in Photosynthesis and Respiration. Springer, Dordrecht., pp 321–362

Sunita C, Sinclair TR, Messina CD, Cooper M (2014) Hydraulic Conductance of Maize Hybrids Differing in Transpiration Response to Vapor Pressure Deficit. Crop Sci 54:1147–1152. https://doi.org/10.2135/cropsci2013.05.0303

Tsimilli-Michael M (2020) Special issue in honour of Prof. Reto J. Strasser - Revisiting JIP-test: An educative review on concepts, assumptions, approximations, definitions and terminology. Photosynthetica 58:275–292. https://doi.org/10.32615/ps.2019.150

Tsimilli-Michael M, Strasser RJ (2008) In vivo assessment of stress impact on plant's vitality: Applications in detecting and evaluating the beneficial role of mycorrhization on host plants. In: Mycorrhiza: State of the Art, Genetics and Molecular Biology, Eco-Function, Biotechnology, Eco-Physiology, Structure and Systematics (Third Edition). Springer-Verlag Berlin Heidelberg, pp 679–703

von Caemmerer S, Farquhar GD (1981) Some relationships between the biochemistry of photosynthesis and the gas exchange of leaves. Planta 153:376–387.

https://doi.org/10.1007/BF00384257

von Caemmerer S, Furbank RT (2016) Strategies for improving C_4 photosynthesis. Curr Opin Plant Biol 31:125–134. https://doi.org/10.1016/j.pbi.2016.04.003

Walker GH, Izawa S (1979) Photosynthetic Electron Transport in Isolated Maize Bundle Sheath Cells. Plant Physiol 63:133–138. https://doi.org/10.1104/pp.63.1.133

Wang Y, Long SP, Zhu XG (2014) Elements required for an efficient NADP-malic enzyme type C_4 photosynthesis. Plant Physiol 164:2231–2246. https://doi.org/10.1104/pp.113.230284

Wingler A, Walker RP, Chen ZH, Leegood RC (1999) Phosphoenolpyruvate carboxykinase is involved in the decarboxylation of aspartate in the bundle sheath of maize. Plant Physiol 120:539–545. https://doi.org/10.1104/pp.120.2.539

Woo KC, Anderson JM, Boardman NK, et al (1970) Deficient Photosystem II in Agranal Bundle Sheath Chloroplasts of C_4 Plants. Proc Natl Acad Sci 67:18–25. https://doi.org/10.1073/pnas.67.1.18

Yang L, Fountain JC, Ji P, et al (2018) Deciphering drought-induced metabolic responses and regulation in developing maize kernels. Plant Biotechnol J 16:1616–1628. https://doi.org/10.1111/pbi.12899

Yang Z, Sinclair TR, Zhu M, et al (2012) Temperature effect on transpiration response of maize plants to vapour pressure deficit. Environ Exp Bot 78:157–162. https://doi.org/10.1016/j.envexpbot.2011.12.034

Yin Z, Zhang Z, Deng D, et al (2014) Characterization of Rubisco activase genes in maize: An σ-isoform gene functions alongside a β-isoform gene. Plant Physiol 164:2096–2106. https://doi.org/10.1104/pp.113.230854

Zhang Y, Zhou Y, Sun Q, et al (2019) Genetic determinants controlling maize Rubisco activase gene expression and a comparison with rice counterparts. BMC Plant Biol 19:351. https://doi.org/10.1186/s12870-019-1965-x

Zhao C, Liu B, Piao S, et al (2017) Temperature increase reduces global yields of major crops in four independent estimates. Proc Natl Acad Sci U S A 114:9326–9331. https://doi.org/10.1073/pnas.1701762114

Chapter IV

Functional high-throughput phenotyping for wheat resilience to high temperature and water deficit

Data presented in this chapter was included in the following work:

Correia PMP, Westergaard JC, da Silva AB, Roitsch T, Carmo-Silva E, Marques da Silva J, (2021) Functional high-throughput phenotyping for wheat resilience to high temperature and water deficit - being prepared for submission to the Journal of Experimental Botany

Table of Contents Chapter IV

Abstract

Interannual and local fluctuations in wheat crop yield are majorly explained by abiotic constraints, being heatwaves and drought among the top stressors. Moreover, these stresses commonly co-occur, and their frequency is increasing with global climate change. This work optimized high-throughput methods to phenotype wheat plants under controlled water deficit and high temperature, with the aim to identify the phenotypic traits conferring adaptative stress responses. Ten wheat genotypes were characterized and classified on their water use and growth dynamics, to ultimately understand the regulatory mechanisms on the primary carbohydrate and antioxidant metabolisms under these stress conditions. Wheat plants were grown in a fully automated plant facility under 25/18ºC day/night for 30 days, and then the temperature was increased for seven days (38/31ºC day/night) while maintaining half of the plants well irrigated and half at 30% field capacity. Thermal and multispectral images and pot weights were registered twice daily. At the end of the experiment, key metabolites and enzyme activities from the carbohydrate and antioxidant metabolisms were quantified. Regression machine learning models were successfully established to predict plant biomass by image-extracted parameters. Leaf temperature and evapotranspiration traits expressed significant genotype-environment interactions (GxE) when acclimatization to stress was continuously monitored. Low leaf number and transpiration efficiency were identified as traits essential to maintain the balance between water-saving strategies and biomass production in wheat genotypes growing under water deficit and high temperature. Tolerance to these stresses included changes in the carbohydrate metabolism, particularly in the sucrolytic (cytINV) and the glycolytic pathways (HXK, PFK), and in the antioxidant metabolism (POX and phenolic compounds). The observed genetic differences in sensitivity to high temperature and water deficit can be exploited in breeding programs to improve wheat resilience to climate change.

4.1 Introduction

Wheat is a major staple food in numerous regions worldwide (FAO, 2017). Around 40% of the global wheat yield fluctuations are explained by environmental constraints, being heatwaves and drought among the top stressors (Deryng et al. 2014; Zampieri et al. 2017). Moreover, several wheat-growing regions are characterized by hot and dry summers, where drought is likely to coincide with elevated temperatures (Araus 2002; Tricker et al. 2018). Understanding the interaction between drought and high temperature on crop production is challenging, as plant responses to simultaneous stresses is more complicated than the sum of individual effects (Rizhsky et al. 2004; Tricker et al. 2018). Furthermore, such response integrates several phenological and physiological processes under multigenic controls, and depends on the individual sensitivity to the microenvironment (Parent et al. 2017). As a result, continuous monitoring of plants response to controlled stress conditions is essential to understand plant-environment interactions. High-throughput phenotyping methods appeared as the solution to compensate the otherwise labour-intensive and time-consuming classic methods of systematic plant phenotyping (Fiorani and Schurr 2013; Fahlgren et al. 2015; Tardieu et al. 2017; Roitsch et al. 2019).

Crop production is intimately dependent on carbon uptake by photosynthesis, and open stomata are vital for carbon capture. However, in response to water shortage, higher plants close stomata to limit water losses by transpiration (Chaves et al. 2003; Nunes et al. 2009; Duque et al. 2013) and when subjected to high temperatures, plants usually use evaporative cooling to reduce leaf temperature, which could otherwise be detrimental to several physiological processes (Carmo-Silva et al. 2012; Costa et al. 2013; Lawson et al. 2018). An optimal balance between risk avoidance and performance is critical to crop production under water deficit and high-temperature conditions (Tardieu 2012; Moshelion 2020). When photosynthetic performance and plant growth are challenged by water shortage and elevated temperatures, remobilization of the carbohydrate metabolism through adjustment of source-sink relations is crucial to tolerate stress and accelerate recovery to reduce yield fluctuations (El Habti et al. 2020; Chapter II).

Several carbohydrate metabolism enzymes demonstrated fundamental functions in drought stress tolerance (Albacete et al. 2011, 2015; Pinheiro and Chaves 2011; Secchi and Zwieniecki 2016; Antonio Cuesta-Seijo et al. 2019; Shokat et al. 2020), although little is known about their role in drought at high temperature. Furthermore, stress exposure usually leads to excessive accumulation of reactive oxygen species (ROS), causing damage to plasma membranes, proteins and pigments, and if the capacity of scavenging and repairing mechanisms is exceeded, photosynthesis and crop performance are constrained (Foyer and Noctor 2005; Tricker et al. 2018). Antioxidant capacity was associated with tolerance to

drought or heat stress in wheat (Sairam et al. 2000; Lascano et al. 2001; Zhang et al. 2017), although the importance of ROS scavenging, both enzymatically and/or by the production of several antioxidant compounds, in combined stresses is unknown.

In this study, we continuously monitored biomass allocation and plant-water relations in ten genotypes with heterogeneous performance under water deficit and high temperature conditions. Including some of the best available elite advanced lines (check lines), selected based on their superior performance and verified in multi-year yield trials at the International Maize and Wheat Improvement Center (CIMMYT) breeding site (Reynolds et al. 2017). Physiological Trait lines (PT lines), the outline of a breeding strategy where crosses were designed to complement "source" (biomass) with "sink" traits (harvest-index, kernel weight, grains per spike) (Reynolds et al. 2017) and parental lines used for trait-based crossing (Reynolds et al. 2007; Manès et al. 2012). The contrasting levels of tolerance to drought and heat of the ten wheat genotypes were explored to (1) optimize high-throughput methods to phenotype wheat plants under drought and high temperature; (2) profile the plant-water-environment relationship of each genotype under these conditions; (3) understand the regulatory mechanisms of the primary carbohydrate and antioxidant metabolisms associated with plants' response to drought at high temperature. The effects of long-term (7 day) growth under high temperature (WW38) and water deficit at high temperature (WD38) on traits related to water use and biomass accumulation were assessed in a high-throughput phenotyping station and linked to the carbohydrate and antioxidant metabolism regulation.

4.2 Materials and Methods

4.2.1 Germplasm and growth conditions

Ten spring wheat (*Triticum aestivum* L.) genotypes were selected based on their heterogenous performance under water deficit or high temperature conditions (Table 4.1). BORLAUG, SOKOLL and BAJ are check lines; PASTOR and SOKWB_1 were included in the Stress Adapted Trait Yield Nurseries trial (SATYN, CIMMYT) and highly performed in drought-stressed areas (SATYN series with odd numbers); PUBWB and SOKWB_2 showed outstanding performance in SATYN under heat stress conditions (SATYN series with even numbers); CMH82 and KSPA are parental lines; PARAGON is a traditional UK spring wheat elite cultivar (Moore 2015; Pennacchi et al. 2019), with good tolerance to water deficit and high temperature when characterized alongside SOKOLL in chapter II.

Plants were grown from seeds for 15 days (DAS 15) in 1 L well-watered pots containing horticultural substrate (SW Horto AB, Hammenhög) plus 10% perlite in a greenhouse at 25/18ºC (day/night), 50% relative humidity (RH) and a photoperiod of 16 hours. Plants were then moved to the phenotyping greenhouse (Phenolab, PLEN UCPH), automated for plant care and movement, with the same climatic conditions and well-watered (WW>90% field capacity). After 15 days (30 DAS), the temperature was changed to 38/31ºC (day/night), and the plants were randomly assigned to two different irrigation treatments: five plants per cultivar were maintained WW (WW38), and five plants were subject to water deficit (WD38) for seven days. WD was established by withholding watering and sustaining a minimum of 30% field capacity. The soil water content was determined gravimetrically by automatically weighing the pots twice a day, and irrigation was provided to compensate for evapotranspiration and keep the soil water content in the WW and WD pots. Pots containing only soil were maintained at the same watering regime and weighed to estimate non-transpirational water loss under WW38 and WD38 treatments. Leaf samples for biochemical analyses were collected at the end of the experiment (DAS 37), 5-7 h after the beginning of the photoperiod, frozen into liquid nitrogen and stored at -80°C.

Table 4.1– List of the ten wheat genotypes used in the study.

GenotypeID*	Cross Name	Infor-mation	GID CIMMYT	Source (tested)
PASTOR	W15.92/4/PASTOR//HXL7573/2*BAU/3/WBLL1	PT Line	5865676	CIMMYT (7^{th} SATYN)
SOKWB_1	SOKOLL/WBLL1	PT Line	6056139	CIMMYT (7^{th} SATYN)
BOR-LAUG100	BORLAUG100 F2014	Check	7806808	CIMMYT (7^{th}, 8^{th} SATYN)
CMH82	CMH82.575/CMH82.801	Parental	1187021	CIMMYT (Reynolds et al. 2007)

PUBWB	PUB94.15.1.12/WBLL1	PT Line	6056064	CIMMYT (8th SATYN)
SOKWB_2	SOKOLL/WBLL1	PT Line	6056140	CIMMYT (8th SATYN)
SOKOLL	SOKOLL	Check Parental	3825355	CIMMYT (7th, 8th SATYN)
KSPA	KS940935.7.1.2/2*PASTOR	Parental	5865910	CIMMYT (Manès et al. 2012)
BAJ	BAJ #1	Check	5106304	CIMMYT (7th, 8th SATYN)
PARAGON	CSW1724-19-5-68//Axona/Tonic	UK elite line	NA	LEC, UK (Chapter II)

* ID adopted for this study based on the cross name simplification

4.2.2 High-throughput data acquisition and extraction

Multispectral images were automatically acquired by a top centred CCD camera (PhenoLab, Videometer) at ten spectral bands (365, 460, 525, 570, 645, 670, 700, 780, 890, 970 nm) twice a day from 15 to 37 DAS. A hemisphere setup (PhenoLab, Videometer) was used to assure homogeneous and diffuse illumination of the plants by high power narrow banded LEDs. Thermal images were obtained using a thermal camera (Flir A65, FLIR Systems Inc.). Multispectral images consisting of stacked consecutive photos, each with a specific spectral band, were analysed via a supervised classification method (normalized Canonical Discriminant Analysis, nCDA) in the software VideometerLab (version 3.0.33, Videometer). Based on this procedure, crop coverage (plant exposed area) was automatically calculated from segmented transformed images and pixel reflectance intensities extracted from the same region of interest (ROI). Thermal data extraction from images was individually supervised by applying an h-dome morphological transformation and threshold segmentation. The temperature of each plant was extracted from a ROI consisting of the plant exposed area. Evapotranspiration was calculated from the gravimetric data obtained at the irrigation time as the water loss per hour between consecutive measurements (mg H_2O h^{-1}). As all the pots in each treatment were in the same conditions (soil, capacity and water availability), randomly distributed, automatically reorganized and measured twice-a-day, differences in evapotranspiration between them can be attributed to variations in plant transpiration.

4.2.3 Plant harvesting and biomass prediction

At the end of the experiment (37 DAS), plants were harvested to measure aboveground and roots fresh weight (FW) and dry weight (DW). Roots were separated from the soil by manual washing with water, and shoots were harvested by cutting at immediately above ground level. FW was directly measured in an electronic scale, and DW was measured after oven drying samples at 70°C for 52 h. The number of leaves and tillers was also assessed

prior to harvesting. Predictive models were constructed based on sixteen machine-learning regression methods implemented in the predMod module of the HTPmod Shiny application (Chen et al. 2018a) and tested to predict plant biomass (FW and DW) from image-extracted features (37 DAS), as applied in Chen et al. (2018b). A 10-fold cross-validation strategy was adopted to check the prediction power of each regression model. The dataset was randomly divided into a training set (70% of plants) and a testing set (30% of plants). The trained model, based on the training data, was then applied to predict biomass for the testing set of plants. Models were considered for further application if the following criteria for the prediction performance were satisfied: (1) Pearson correlation coefficient of determination (R^2) between the predicted values and the observed values >0.7; (2) root mean squared relative error of cross-validation (MRSRE) <0.3; (3) predictive bias between the predicted and observed values (μ) <0.05. A Linear Support Vector Machine model (svm-linear, *caret* R package (Kuhn 2008)) was then used to predict FW and DW from 15 until 37 DAS from image-derived features.

4.2.4 Growth modelling

Ten different mechanistic models implemented in the growMod module of the HTPmod Shiny application (Chen et al. 2018a) were tested to model plant growth and applied as described in Chen et al. (2014). Models were considered if the following criteria for the fitting quality were satisfied: (1) R^2>0.7; (2) P<0.05. The time point of maximum biomass (Tmax), maximum final vegetative biomass (biomass at Tmax) and the intrinsic growth rate (GR), which measures the speed of growth, were extracted from the models. The water use efficiency (WUE) from 30 to 37 DAS of each plant, as per the biomass produced per water transpiration, was calculated as:

$$\mathrm{WUE} = (\mathrm{DW}_2 - \mathrm{DW}_1)/(\mathrm{TH}_2\mathrm{O}),$$

where DW_1 is the DW estimated at the time point of stress imposition (30 DAS), DW_2 is biomass at Tmax and TH_2O is the total water supplied to each pot from 30 DAS to 37 DAS excluding the non-transpirational water loss (water loss in pots only with soil under the same irrigation regime). Comparison of plant growth between WW38 and WD38 conditions was accessed through a number of specific stress tolerance indices (Fischer and Maurer 1978; Bouslama and Schapaugh 1984; Grzesiak et al. 2012) calculated with the parameters extracted from the growth models:

$$\text{Mean productivity} = (\text{Biomass at Tmax}_{\mathrm{WW38}} + \text{Biomass at Tmax}_{\mathrm{WD38}})/2;$$

$$\text{Biomass reduction} = \text{Biomass at Tmax}_{\mathrm{WD38}} \,/\, \text{Biomass at Tmax}_{\mathrm{WW38}};$$

$$\text{Inflection point stability} = \mathrm{Tmax}_{\mathrm{WW38}} - \mathrm{Tmax}_{\mathrm{WD38}}.$$

$$\mathrm{GR\ ratio} = \mathrm{GR}_{\mathrm{WD38}} \,/\, \mathrm{GR}_{\mathrm{WW38}};$$

$$\mathrm{WUE\ ratio} = \mathrm{WUE}_{\mathrm{WD38}} \,/\mathrm{WUE}_{\mathrm{WW38}};$$

4.2.5 Enzymes extraction

Frozen wheat leaf samples were homogenized in liquid nitrogen with 1% (w/v) insoluble polyvinylpyrrolidone (PVP). Total protein was extracted from samples (0.5 g FW) in ice-cold extraction medium containing 40 mM TRIS-HCl pH 7.6, 3 mM $MgCl_2$, 1 mM ethylenediaminetetraacetic acid (EDTA), 0.1 mM phenylmethylsulfonyl fluoride (PMSF), 1 mM benzamidine, 14 mM β-mercaptoethanol, 24 µM nicotinamide adenine dinucleotide phosphate ($NADP^+$), following the protocol described in Jammer et al. (2015). Total soluble protein (TSP) content was determined according to the Bradford method (Bradford 1976) using BSA Fraction V as standard protein. Extracts were aliquoted, frozen in liquid nitrogen and stored at -20°C.

4.2.6 Activity of carbohydrate metabolism enzymes

The activity of nine enzymes from the carbohydrate metabolism was measured in thawed leaf extracts using a semi-high-throughput protocol in 96-well microtiter plates as described in Jammer et al. (2015) (Figure S4.1), with variable extract volume (1-5 µL), and monitoring absorbance at 30°C (ELx808, BioTek Instruments, Inc.). Briefly, Aldolase (Ald, EC 4.1.2.13) and Phosphofructokinase (PFK, EC 2.7.1.11) activities were measured by coupling the reactions with a Glycerol-3-phosphate dehydrogenase (GPDH) NADH-dependent reaction and recording the decrease in absorbance at 340 nm due to conversion of NADH to NAD^+. ADP-glucose pyrophosphorylase (AGPase, EC 2.7.7.27), Glucose-6-phosphate dehydrogenase (G6PDH, EC 1.1.1.49), Hexokinase (HXK, EC 2.7.1.1), Phosphoglucoisomerase (PGI, EC 5.3.1.9) and Phosphoglucomutase (PGM, EC 5.4.2.2) activities were assayed by linking the reactions with a G6PDH NADP-dependent reaction and recording the increase in absorbance at 340 nm due to conversion of $NADP^+$ to NADPH. Cytoplasmic Invertase (cytINV, EC 3.2.1.26) and vacuolar Invertase (vacINV, EC 3.2.1.26) activities were measured in an end-point assay, and the amount of liberated glucose was determined by measurement of absorbance at 405 nm. All reactions were carried out in triplicates alongside control reactions (in the absence of substrate), and enzyme activity was expressed relative to the amount of TSP in each sample.

4.2.7 Quantification of carbohydrates

Carbohydrates were extracted from frozen leaf samples homogenized in liquid nitrogen (0.1 g FW) by homogenization in ethanol (80% v/v) for 5 minutes at 80ºC and then centrifuged at 20,000*g* for 5 min. The supernatant was collected, allowed to evaporate overnight at 60ºC, diluted in dH_2O and used to quantify sucrose, glucose and fructose by an enzymatic method (kit AK00201, NZYTech) in a miniaturized protocol in 96-well microtiter plates following the

manufacturer recommendations. The pellet was used to quantify starch by the same method after acidic hydrolysis in 30% HCl (v/v) at 90ºC for 15min.

4.2.8 Activity of antioxidant enzymes

The activity of four enzymes from the antioxidant metabolism was measured in thawed samples using a semi-high-throughput protocol in 96-well microtiter plates as described in Fimognari et al. (2020), with variable extract volume (1-5 µL), by monitoring absorbance at 30°C (ELx808, BioTek Instruments, Inc.). Briefly, Ascorbate peroxidase (APX, EC 1.11.1.11) activity was measured by recording oxidation of ascorbate at 290 nm. Catalase (CAT, EC 1.11.1.6) activity was assayed by recording the decomposition of H_2O_2 at 240 nm. Peroxidase (POX, EC 1.11.1.7) activity was measured by recording the formation of tetraguaiacol at 450 nm. Superoxide dismutase (SOD, EC 1.15.1.1) activity was measured by recording the inhibition of the oxidation of cytochrome c at 550 nm. All reactions were carried out in triplicates alongside control reactions (in the absence of substrate), and enzyme activity was expressed relative to the amount of TSP.

4.2.9 Quantification of antioxidant capacity and metabolites

Antioxidant metabolites were extracted from frozen leaf samples homogenized in liquid nitrogen (0.4 g FW) by homogenization in pure methanol overnight in the dark at 4ºC and then centrifuged at 20,000 *g* for 5 min. The supernatant was aliquoted and stored at -20°C. Antioxidant metabolites and capacities were quantified in thawed samples using a miniaturized protocol in 96-well microtiter plates and monitoring absorbance (Synergy HTX, BioTek Instruments Inc.). Trolox equivalents antioxidant capacity (TEAC) and ferric reducing antioxidant power (FRAP) were quantified as described in Correia et al. (2020). Total phenolic content was determined by the Folin-Ciocalteu method (Singleton et al. 1999) by recording the absorbance at 765 nm. Galic acid standards in ddH_2O were measured alongside the samples and used to prepare the respective calibration curves. The total phenolic content of the extract was expressed as mg Galic acid equivalents per gram of leaf (mg g^{-1} FW). The total flavonoids content was determined by the $AlCl_3$ method (Zhishen et al. 1999) by recording the absorbance at 510 nm. Catechin was used as a standard for the calibration curve. The total flavonoids content of the extract was expressed as mg catechin equivalents per gram of sample (mg g^{-1} FW). Anthocyanins content was assessed by the pH-differential method (Giusti and Wrolstad 2001) and expressed as cyanidin-3-glucoside equivalents (mg g^{-1} FW).

4.2.10 Data pre-processing and analysis

Traits extracted from the images and gravimetrical measurements were divided in 4 classes: (1) geometrical; (2) evapotranspiration (evap); (3) thermal; (4) reflectance (reflect). Pre-processing of data for outlier detection, trait reproducibility and collinearity assessment was conducted using the same approach as Chen et al. (2014). Briefly, Grubbs' test (Grubbs 1950) was used to detect outliers in replicated plants in each genotype at the same condition and data point, outliers were deleted and missing values were imputed (missForest R package, Stekhoven & Bühlmann, 2012). Traits were considered as highly reproducible if the following criteria were satisfied in at least one treatment condition: (1) the median correlation coefficient over genotypes was larger than 0.7; (2) the coefficients were significantly higher in replicates than in random plant pairs (Welch's t-test $P < 0.05$). To reduce the excessive correlation among explanatory variables (multicollinearity), a stepwise variable selection using variance inflation factors (VIFs) was applied, traits were considered if VIF < 5. The observed variance in phenotypic traits, enzymatic activities and metabolites amounts was partitioned into components attributable to different sources of variation, the variation of genotype (G), environment (E), and their interaction (GxE), using the same approach as Chen et al. (2014). Briefly, a linear model was applied to determine the likelihood of genotype-to-phenotypes linkage for each trait measured in each day, *P*-values were corrected for multiple comparisons with the Benjamini-Hochberg false discovery rate method (fdr), the LOD scores (log of odds) were calculated, as the -log probability (corrected *P*-value, fdr) (Joosen et al. 2013). A heat map representation and hierarchical clustering were applied to the matrix of LOD scores or tolerance indices. ANOVA and post-hoc comparison (Duncan test, $P < 0.05$) were also used to dissect the statistical significance of individual trait variation between genotypes. A t-test ($P < 0.05$) was used for comparison between two treatments (WD38 and WW38) within the same genotype. A partial least squares-discriminant analysis (PLS-DA) was performed to classify and discriminate plants into treatments (WW38, WD38) and genotypes for each treatment and to identify the key variables that drive such discrimination (MixOmics R package, Rohart et al., 2017).

4.3 Results

4.3.1 Phenotypic descriptors reflecting the response to water deficit and high temperature

Traits with low reproducibility and high collinearity were filtered and extracted from the data set to avoid redundant or low-quality descriptors of the ten wheat genotypes (Table 4.1). A total of 16 traits reflecting the four trait classes were maintained (*Figure 4.1*), two traits

reflecting leaf temperature (Thermal, orange), three traits associated with the evapotranspiration processes (Evap., blue), the aboveground plant area exposed (geometrical, green) and ten traits reflecting the multispectral signature (Reflect, light grey). The statistical significance on phenotypic variance (LOD score) was determined to identify the traits that could reflect an effect of genotype (G), treatment (E, environment) and their interaction (GxE) for each measurement day (Table S4.1). All traits increased LOD scores for G effect when stress was imposed (30-32 DAS, Figure 4.1A), but a gradual decrease of differences in multispectral traits was observed until the end of the experiment (37 DAS). Interestingly, at 30 DAS, it was possible to discriminate between different groups: check lines (BAJ, BORLAUG), PT lines (PASTOR, PUBWB, SOKWB_1, SOKWB_2) and the other genotypes (Figure S4.2A-B). At 37 DAS, the genotypes' distribution was more uniform and centralised horizontally under WD38 (Figure S4.2C) and vertically under WW38 (Figure S4.2D). At this stage, most of the traits exhibited similar LOD scores, except for the aboveground area exposed, that after a quick increase of LOD scores at 30-31 DAS, stabilised until the end of the experiment (Figure 4.1A, Table S4.1). The Environment effect (E) altered thermal, evapotranspiration and biomass traits progressively after stress imposition and until the end (Figure 4.1B). Although, a slower reaction was observed for the thermal traits that only changed after 31 DAS and to a lesser extent for the aboveground area (Figure 4.1B and Table S4.2). Multispectral traits showed a distinct dynamic after stress imposition (Figure 4.1B and Table S4.2). No change was observed for UVA and Blue (365-460nm). On the other hand, green, yellow and reds (525-700 nm) decreased LOD sores, showing a similar behaviour in G effect, and NIR (700-970) LOD scores increased after 35 DAS. All traits were observed to have significant GxE effects when the temperature increased from 25 to 38ºC (30 DAS; Figure 4.1C, Table S4.3). On the other hand, only the traits related to leaf temperature and evapotranspiration expressed significant GxE differences until the end of the experiment (37 DAS), indicating a strong influence of high temperature and extended drought on genetic factors related to these traits.

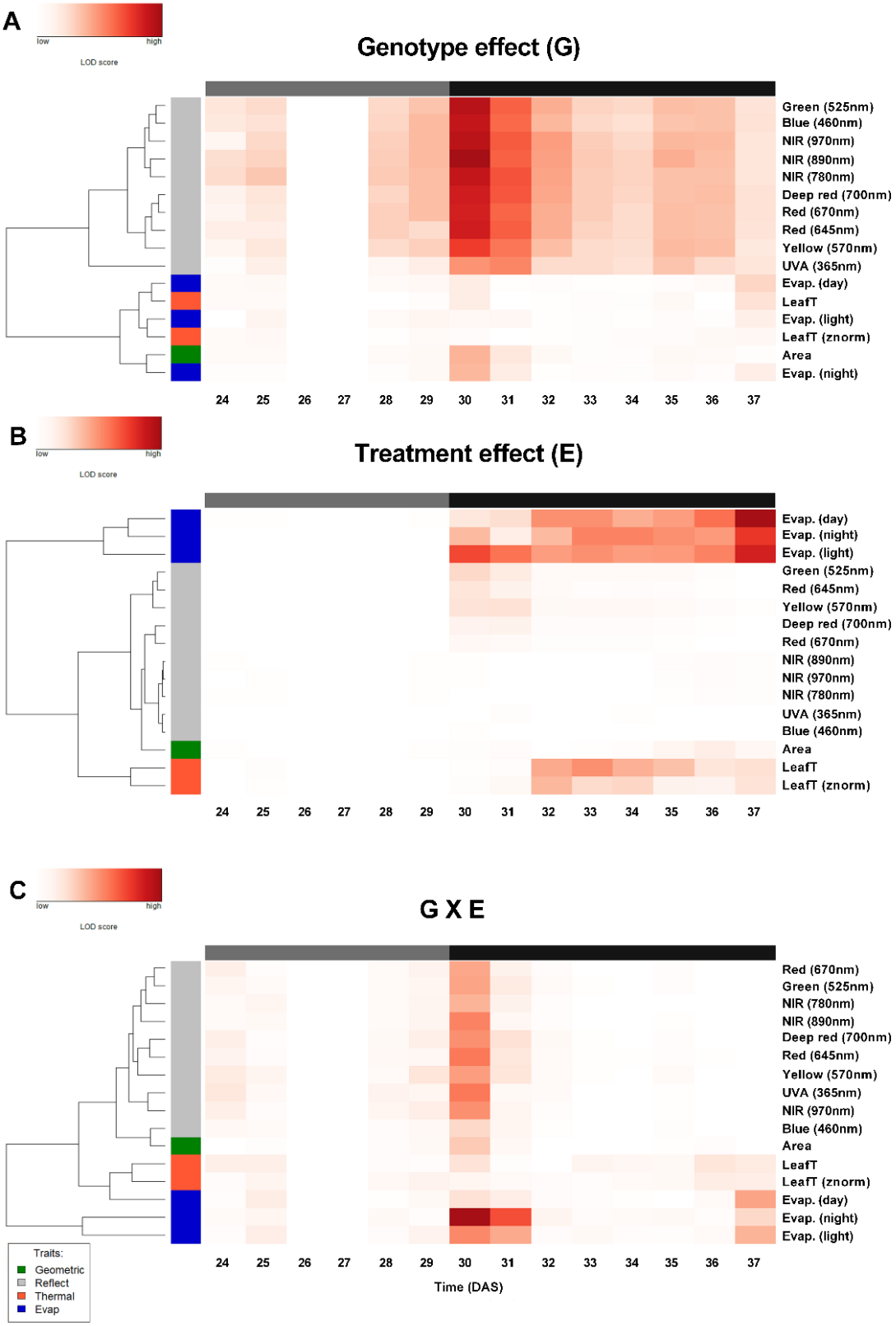

Figure 4.1– Phenotypic variation over-time of wheat plants exposed to high temperature (WW38) or water deficit at high temperature (WD38). (A) Statistical significance of genotype effect, **(B)** treatment effect (WW38 vs WD38), and **(C)** their interaction effect (GxE) for each phenotype trait measured in each day. The shading plot indicates the significance level

(Bonferroni corrected P values) in LOD scores (-log probability). Hierarchical clustering was applied to the LOD scores matrix rows (phenotypic traits). Grey-balck bars along the top reflect the stress imposition; Dark grey bar, before stress imposition, all plants were well-watered at 25ºC (DAS <30); Black bar, after stress imposition (DAS>30), WW38 and WD38. Coloured bars along the left indicate the corresponding trait class, geometrical (green), reflectance (light grey), thermal (orange) and evapotranspiration (blue).

4.3.2 Indicators of water status and evaporative colling

Genotype-environment effects changed significantly phenotypic variance of traits related to evapotranspiration and leaf temperature over the period when plants were exposed to high temperature and water deficit. Daily evapotranspiration (Evap. (day)) and leaf temperature (LeafT) data were explored in more detail to understand the relevance of these adjustments, generally related to the water status and evaporative cooling. Evapotranspiration increased with temperature, although when plants were exposed to water deficit (WD38), water availability rapidly decreased and under these conditions evapotranspiration decreased after stress imposition in all genotypes (Figure 4.2A-J). Only CMH82 (Figure 4.2C), PARAGON (Figure 4.2E) and SOKWB_1 (Figure 4.2I) did not show a significant difference between treatments at 30 DAS. Under WD38 conditions (Figure 4.2K), KSPA, PASTOR and SOKWB_2 showed low evapotranspiration, while BORLAUG100, CMH82, PARAGON and SOKOLL displayed high values. When only exposed to high temperatures (WW38, Figure 4.2L), BAJ, BORLAUG, SOKOLL showed the highest values and CMH82, KSPA and SOKWB_1 the lowest. At the end of stress exposition (37 DAS, Figure 4.2M-N) under WD38 conditions (Figure 4.2M), KSPA, SOKOLL and SOKWB_1 showed low values of evapotranspiration, contrasting PUBWB and BORLAUG100 with high values. Under WW38 (Figure 4.2N), KSPA showed low levels of evapotranspiration and PARAGON high levels (Figure 4.2N).

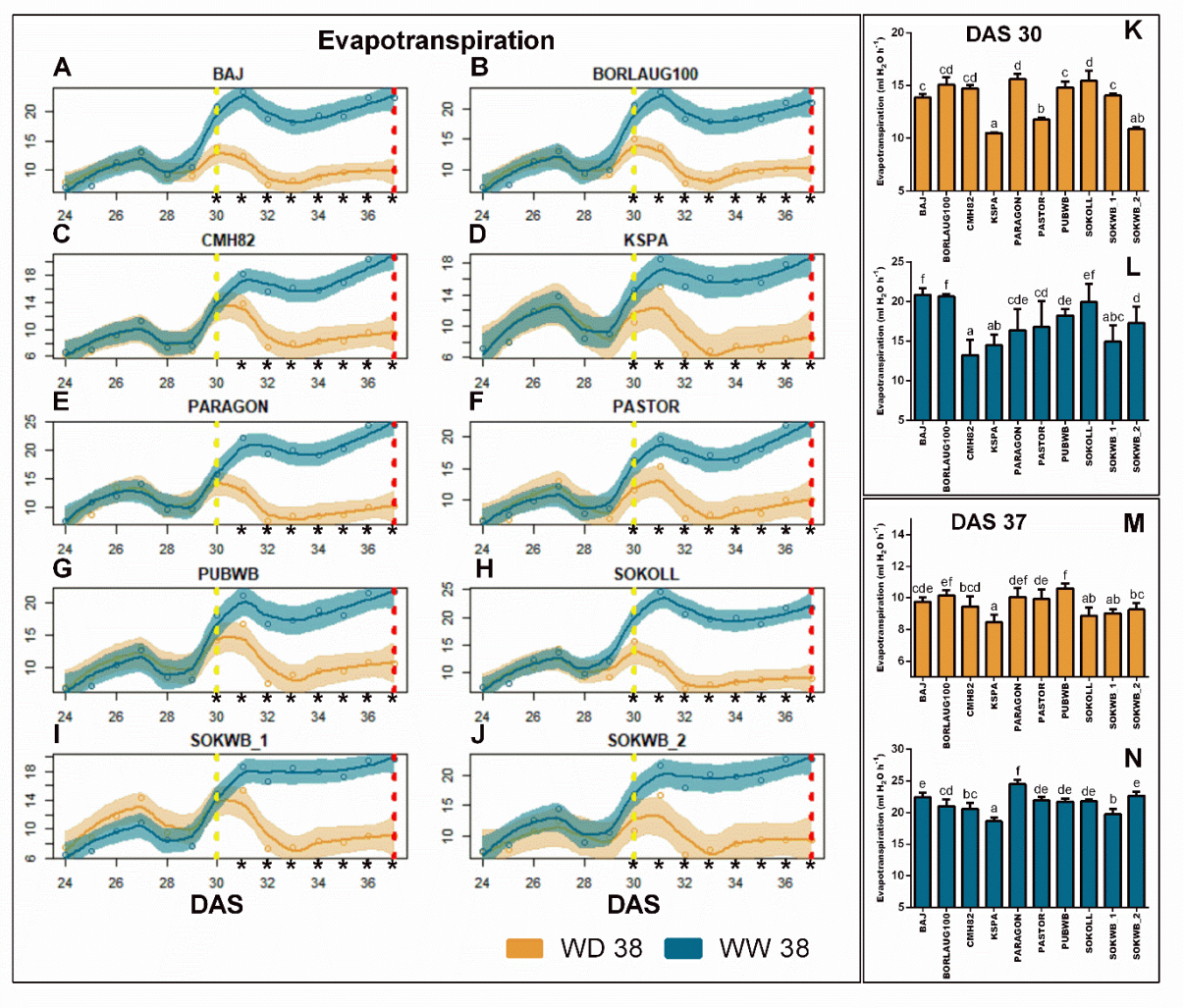

Figure 4.2 – Evapotranspiration over-time of wheat plants exposed to high temperature (WW38) or water deficit at high temperature (WD38). (A-J) Measurements taken continuously throughout the experiment for each genotype in plants under WW38 and WD38. **(K,L)** Comparison of genotypes at the start of the stress imposition (30 DAS). **(M,N)** Comparison of genotypes at the end of the experiment (37 DAS). Blue lines and bars represent WW38 plants; yellow solid lines and bars represent WD38 plants. Shaded areas represent 95% confidence intervals. Yellow dashed lines denote stress imposition (30 DAS) and red dashed lines the end of the experiment (37 DAS). Asterisks denote significant differences between treatments in each genotype (t-test, $P<0.05$, A-J). Bar charts show mean values ± SEM (n = 5 biological replicates). Different letters denote significant differences between genotypes (Duncan analysis, $P<0.05$).

Most genotypes only showed differences in leaf temperature between treatments at 32 DAS (Figure 4.3A-J), expect for SOKWB_1 and SOKWB_2 with differences from 30 DAS (Figure 4.3I-J). On the first day of stress, all genotypes in both conditions showed average leaf temperature inferior to 30ºC (Figure 4.3K-L). At the end of the experiment under WW38, PARAGON, PASTOR and SOKWB_2 showed statistically significant differences in leaf temperature between treatments (Figure 4.3E, F and J), still, in average only PARAGON

showed temperatures less than 30ºC (Figure 4.3M-N), significantly colder than the majority of the genotypes. At the end of the experiment under WD38, SOKOLL exhibited the highest temperature and PARAGON the lowest (Figure 4.3M). Under WW38, most genotypes maintained leaf temperature around 30ºC, only PARAGON maintained a cooler temperature (Fig. 3N).

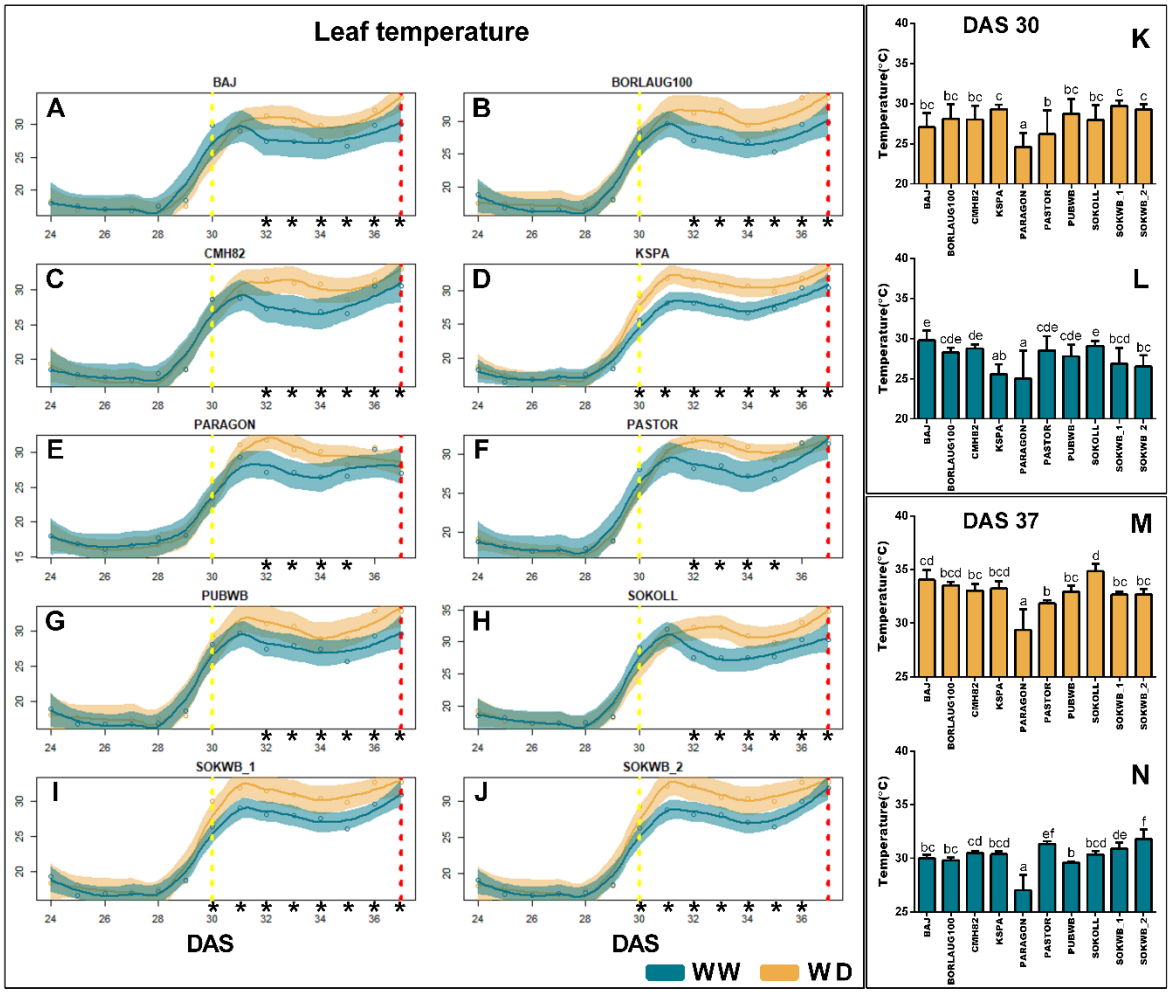

Figure 4.3 – Leaf temperature variation over-time (24-37 DAS) of wheat plants exposed to high temperature (WW38) or water deficit at high temperature (WD38). (A-J) Measurements taken continuously throughout the experiment for each genotype in plants under WW38 and WD38. **(K,L)** Comparison of genotypes at the start of the stress imposition (30 DAS). **(M,N)** Comparison of genotypes at the end of the experiment (37 DAS). Blue lines and bars represent WW38 plants; yellow solid lines and bars represent WD38 plants. Shaded areas represent 95% confidence intervals. Yellow dashed lines denote stress imposition (30 DAS) and red dashed lines the end of the experiment (37 DAS). Asterisks denote significant differences between treatments in each genotype (t-test, P<0.05, A-J). Bar charts show mean values ± SEM (n = 5 biological replicates). Different letters denote significant differences between genotypes (Duncan analysis, P<0.05).

Under WD38, a positive correlation between the ratio of evapotranspiration to aboveground biomass (Evap/AerialDW) and evapotranspiration was observed (Figure 4.4), as well as between the number of leaves and leaf temperature. SOKOLL showed the highest number of leaves and temperature, while Paragon displayed the cooler temperature and fewer leaves for the same root mass fraction (Figure 4.3M, Figure S4.3). Under WW38, aboveground biomass correlated positively with evapotranspiration (Figure 4.4), and the ratio of evapotranspiration to root biomass (Evap/RootDW) correlated positively with leaf temperature (Figure 4.4).

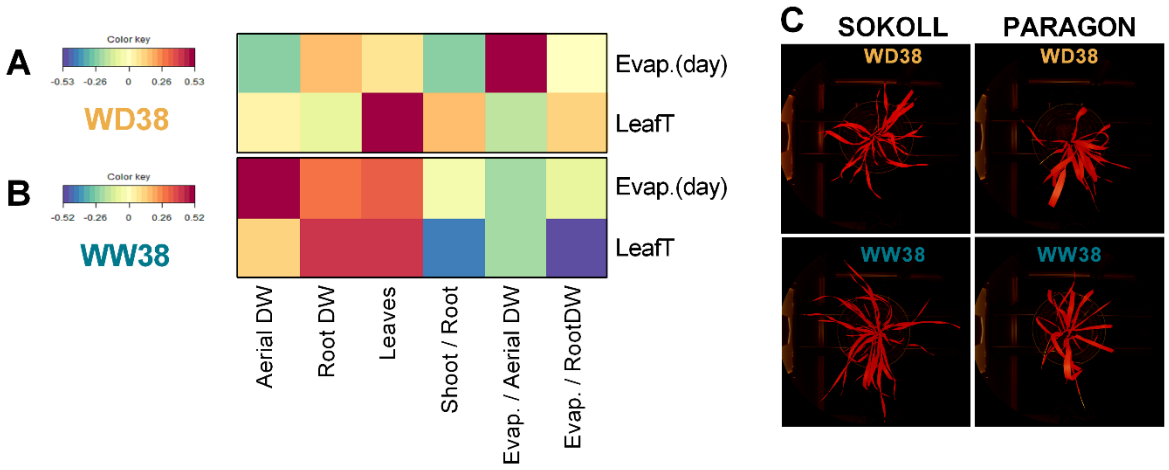

Figure 4.4 – Relative importance of biomass and architecture traits to evapotranspiration and leaf temperature at DAS 37 of wheat plants exposed to high temperature (WW38, A) or water deficit at high temperature (WD38, B). Heatmap represents a canonical correlation between evapotranspiration, leaf temperatures and traits related to biomass and plants architecture. Evap: evapotranspiration; LeafT: plant mean leaf temperature, Evap/RootDW: evapotranspiration normalized to root dry biomass; Evap/AerialDW: evapotranspiration normalized to aboveground dry biomass; Shoot/Root: shoot to root mass fraction; Leaves: number of leaves per plant, Root DW: roots dry biomass; Aerial DW: aboveground dry biomass. (C) Representative segmented images of SOKOLL and PARAGON, leaves shown in red.

4.3.3 Biomass prediction from images and plant growth modelling

Regression models were developed to quantify the ability of geometrical traits to predict the aboveground biomass (DW, FW), measured at 37 DAS, in order to investigate the relationship between the image-extracted parameters and plant biomass. From the sixteen tested machine-learning regression models implemented in predMod (Chen et al. 2018a), nine passed the defined criteria for model selection: R^2 >0.7; MRSRE <0.3; μ <0.05 (Figure 4.5). Linear Support Vector Machine (SVM-linear) was selected as the best model due to the low predictive bias (μ) and similar results for the other parameters (Figure 4.5).

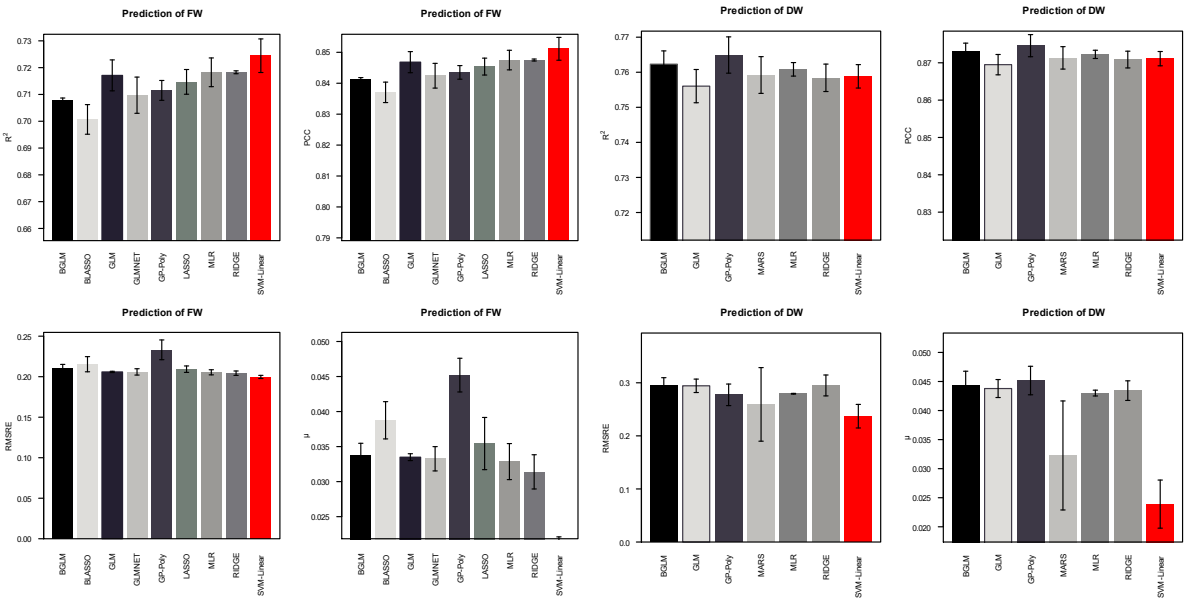

Figure 4.5 – Performance of nine machine-learning regression models considered for predicting plant biomass (FW and DW) by image-extracted parameters (37 DAS). Models: (1) BGLM: Bayesian Generalized Linear Model; (2) BLASSO: Bayesian Lasso; (3) GLM: Generalized Linear Model; (4) GLMNET: Lasso and Elastic-Net Regularized Generalized Linear Models; (5) GP-Poly: Gaussian Process with Polynomial Kernel; (6) LASSO: Lasso Model; (7) MLR: Multivariate Linear Regression; (8) RIDGE: Ridge Regression; (9) SVM-Linear: Support Vector Machines with Linear Kernel. R^2: Pearson correlation coefficient of determination between the predicted values and the observed values; PCC: Pearson correlation coefficient; MRSR: root mean squared relative error of cross-validation; (3) μ: predictive bias between the predicted and observed values.

The geometrical traits area exposed (area.low) and pyramidical plant volume (volumepyr, calculated from the area and plant height) showed high predictive power, and the model constructed with the two parameters showed slightly higher accuracy to predict DW and FW, under WD38 and WW38 conditions, compared to the best single trait model, only with area.low (Figure 4.6). FW predicted with the SVM-linear regression model constructed with area.low and volumepyr showed the best correlation to FW observed and concomitant correlation to DW (Figure 4.6A), and was used as a proxy of plant aboveground biomass to model plant growth from 15 DAS until the forecasted 41 DAS (Figure 4.7).

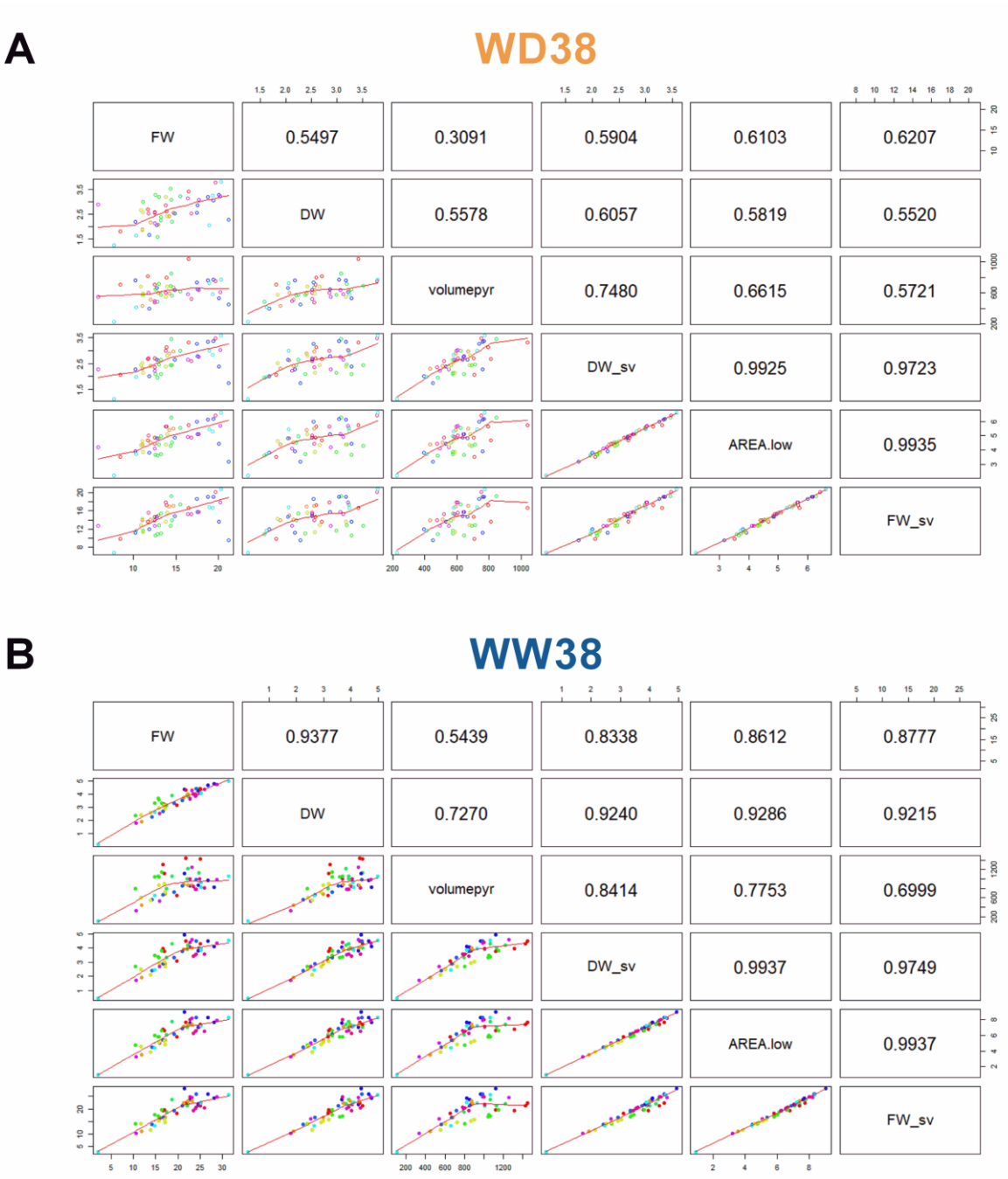

Figure 4.6 – Pearson correlation matrix between manual measurements, image-derived features, and model-predicted data from plants growing at WW38 (A) and WD38 (B). Values are correlation coefficients (r). FW: aboveground fresh biomass; DW: aboveground dry biomass; FW_sv: predicted fresh biomass (SVM-linear); DW_sv: predicted dry biomass (SVM-linear); AREA.low: exposed leaf area extracted from images; volumepyr: plant pyramidal volume calculated based on image-derived features. Different coloured dots represent genotypes.

To determine the best model for biomass accumulation in wheat plants subjected to WW38 and WD38, ten different mechanistic models implemented in growMod (Chen et al. 2018a) were tested. A Bell shape model satisfied the previously established criteria (R^2>0.7, P<0.05)

for all genotypes in WW38 and WD38 conditions, with the best fit (R^2) for all the genotypes under WD38 and comparable results to the logistic model in WW38, thus being selected to represent plant growth (Figure 4.7). Different dynamics were observed between genotypes and stress conditions. The maximum biomass prediction (Biomass at Tmax) under WW38 was extracted from the growth model of Sokoll at 37 DAS (23.5 g, Figure 4.7H) and the lowest for CMH82 at 36 DAS (12.9 g, Figure 4.7C). Under WD38, the highest value was observed in SOKWB_2 at 36 DAS (16.5 g, Figure 4.7E) and the smallest in CMH82 at 35 DAS (12.7 g, Figure 4.7C).

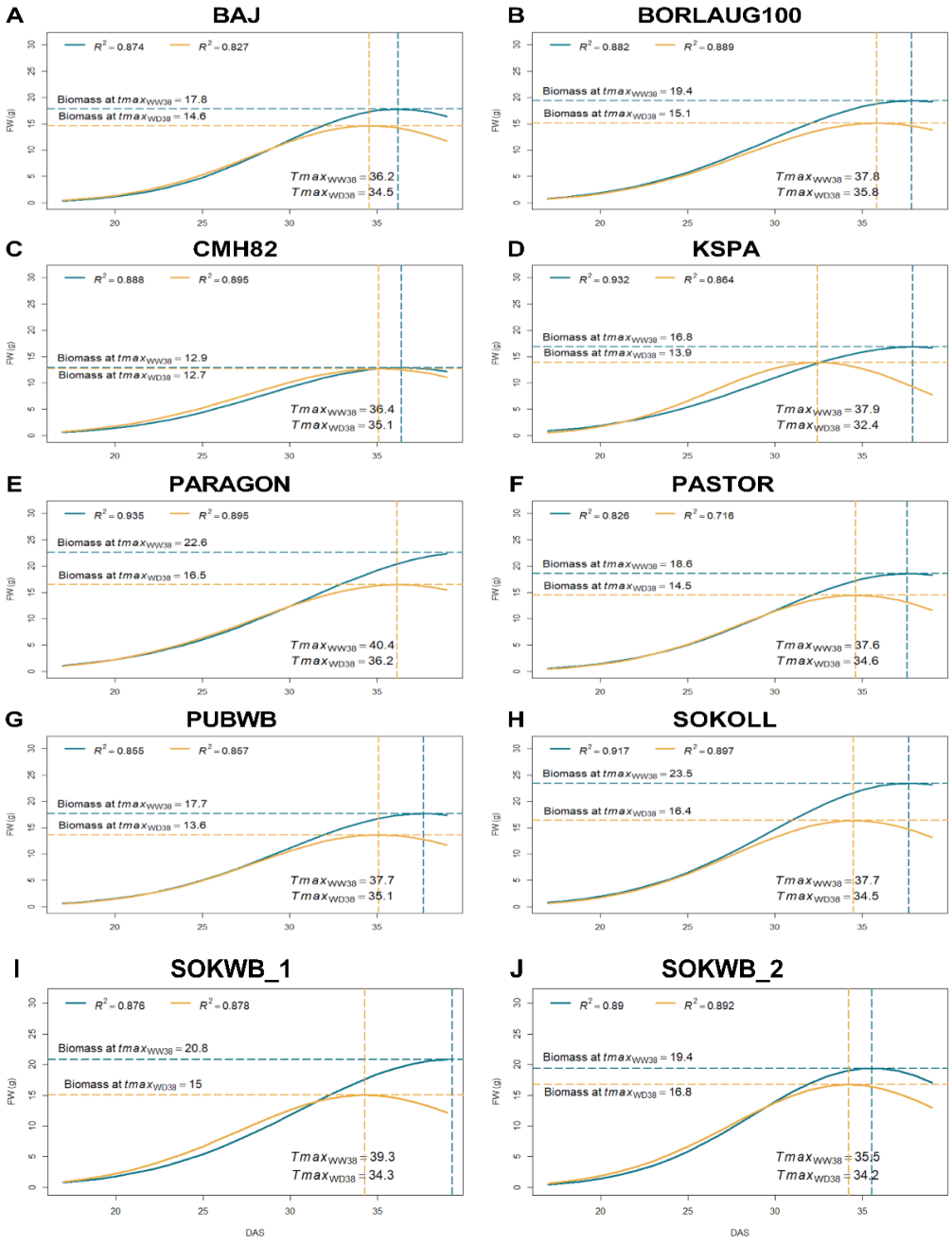

Figure 4.7 – Modelling plant growth in ten wheat genotypes exposed to high temperature (WW38) or water deficit at high temperature (WD38). Growth models are based on

fitting predicted biomass values from 24 to 41 DAS using a bell shape model. Blue lines represent WW38 plants and yellow lines represent WD38 plants. Quality of fit (R^2) of each model, the time point of maximum biomass (Tmax, vertical dashed lines) and maximum growth capacity (Biomass at Tmax, horizontal dashed lines) are indicated.

4.3.4 Tolerance indices revealing stress symptoms

To characterise and classify the genotypes according to their growth dynamics under WW38 and WD38, stress tolerance indices were calculated with the parameters extracted from the growth models and the genotypes clustered accordingly (Figure 4.8). CMH82 showed a distinct behaviour with high biomass stability, low productivity, minor changes in GR between conditions and elevated WUE under WD38 (Figure 4.7C and Figure 4.8). KSPA and SOKWB_1 showed a premature inflection point (Tmax) under WD38 relative to WW38, the highest reduction in the GR and WUE ratio (Figure 4.7D, I and Figure 4.8). However, SOKWB_1 showed higher productivity and biomass reduction, whereas KSPA was the only genotype with a higher WUE under WW38 than WD38 (Figure 4.7D, I and Figure 4.8). PARAGON and SOKOLL revealed the highest mean productivity (MP) and high biomass reduction (BRR), although PARAGON showed a less accentuated reduction of GR and higher WUE under WD38 (Figure 4.7E and H and Figure 4.8). BAJ, BORLAUG100, PASTOR and PUBWB demonstrated a similar behaviour with average values (Figure 4.7 A,B,F,G and Figure 4.8), the only emphasis was on the higher value of WUE in BORLAUG100, due to the elevated productivity and inflection point stability (Figure 4.7B and Figure 4.8). SOKWB_2 showed high MP, more akin to SOKWB_1 (Figure 4.8). However, similarly to BAJ and BORLAUG100, it exhibited a high inflection point stability (Figure 4.7H, A, B and Figure 4.8).

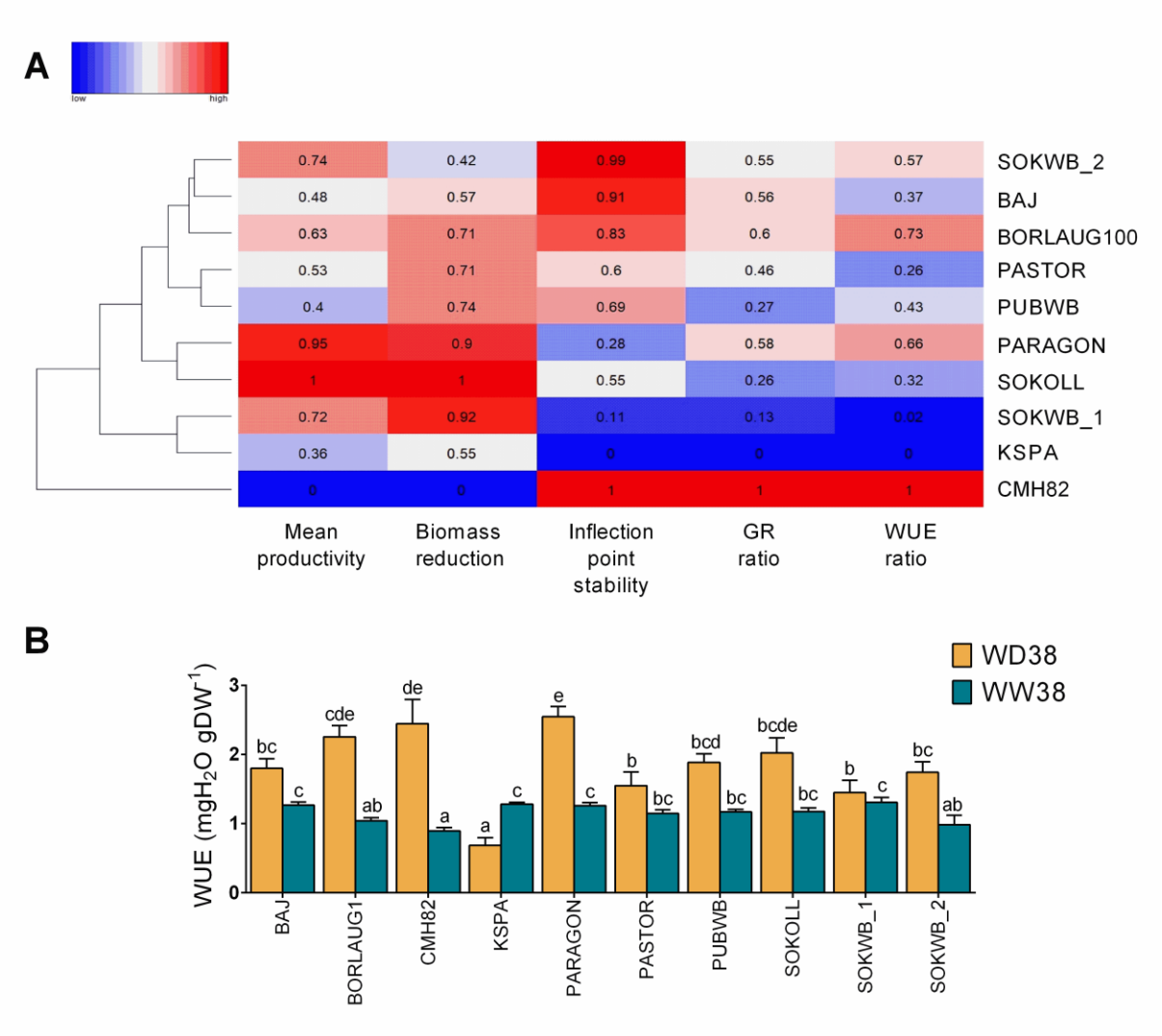

Figure 4.8 – Stress tolerance indices of ten wheat genotypes when exposed to high temperature (WW38) or water deficit at high temperature (WD38). (A) Heat map representation of rescaled values (0-1) of Mean productivity, Biomass reduction, Inflection point stability, growth rate (GR) and water use efficiency (WUE) ratios of WD38 to WW38. Blue cells represent low values and red cells high values. Hierarchical clustering was applied to the matrix rows. **(B)** Water use efficiency, as biomass produced per water transpiration. Different letters denote statistically significant differences between genotypes (Duncan analysis, $P<0.05$).

4.3.5 Impact of WD38 and WW38 on phenotypic traits and adjustment of carbohydrate and antioxidant metabolism

Significance of variance associated with genotype (G), treatment (E) and their interaction was evaluated for phenotypic traits including the activity of key enzymes and metabolites from the carbohydrate and antioxidant metabolism to dissect the components relevant to the response to water deficit under high temperature. CAT, POX, cytINV, AGPase, vacINV activities, antioxidant capacities (TEAC and FRAP), phenols and starch content revealed the

strongest G effects (Figure 4.9A). On the other hand, anthocyanins, flavonoids, phenols, fructose content, VacINV, PFK activities, FRAP and the number of leaves displayed the highest environmental effects (Figure 4.9A). CytINV, vacINV, HXK, PFK, Aldolase, AGPase, POX activities, TEAC, FRAP and phenols content expressed significant genotype-environment interactions (GxE) (Figure 4.9A). The traits that expressed significant GxE differences at the end of the experiment were linked to the carbohydrate and antioxidant metabolism and were explored in more detail to understand the regulatory mechanisms linked to WD38 and WW38. Except for KSPA, PASTOR and SOKOLL, all the genotypes experienced changes in cytINV or vacINV activities. From those, only CMH82 demonstrated an increase of cytINV activity under WD38. PUBWB only showed significant differences in vacINV and SOKWB_2 in cytINV, despite the high activity under both conditions in cytINV and vacINV (Figure 4.9B). CMH82 showed the strongest activity of HXK under WD38 concomitantly with significant changes in PARAGON and PUBWB. Excluding KSPA and BORLAUG100, all the other genotypes exhibited significantly higher activity under WW38. BORLAUG100, CMH82, KSPA, PASTOR, PUBWB, SOKOLL and SOKWB_2 demonstrated a significantly elevated activity of PFK under WD38. SOKOLL showed a robust activity of Aldolase under WD38, CMH82 exhibited differences in a minor scale, and KSPA revealed high intrinsic activity despite no differences between conditions. CMH82 showed elevated activity of AGPase under WD38, and to a lesser extent, BAJ, PARAGON and PUBWB showed a significantly higher activity under the same condition. On the other hand, significant increases in the antioxidant capacity and activity occur only under WD38 (Figure 4.9C-D). BAJ, KSPA, PARAGON, SOKOLL and SOKWB_2 exhibited changes in all the traits. BORLAUG only showed differences in POX activity and SOKWB_1 in phenols amount (Figure 4.9C-D).

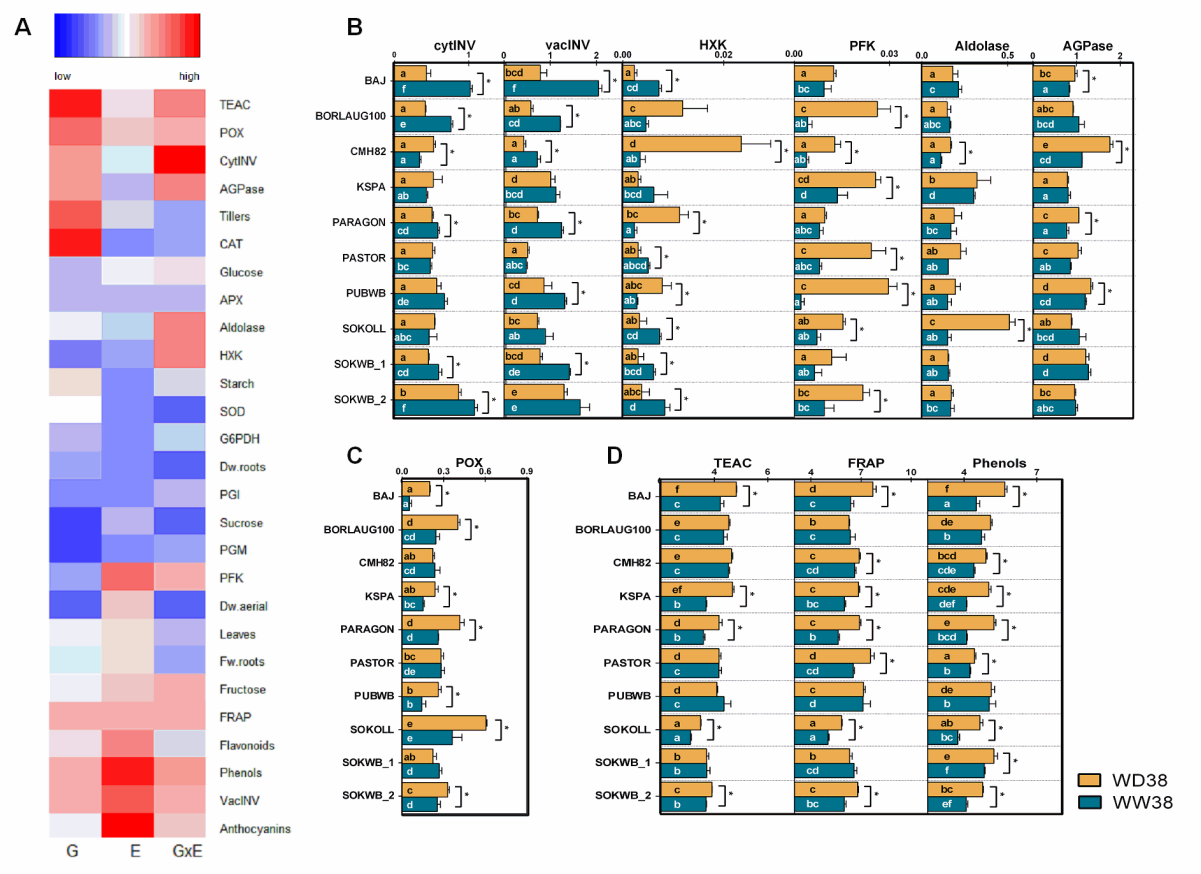

Figure 4.9 – Phenotypic and metabolic acclimatization of wheat when exposed to high temperature (WW38) or water deficit at high temperature (WD38). (A) Statistical significance of genotype effect, treatment effect (WW38 vs WD38), and their interaction (GxE) for each trait measured at the end of the experiment (37 DAS). The shading plot indicates the significance level (Bonferroni corrected P values) in LOD scores (-log probability). Blue cells represent low LOD values and red cells high values. **(B-C)** Top 10 traits with highest GxE LOD scores. **(B)** Carbohydrate metabolism enzymes activity expressed relative to the amount of TSP. **(C)** Peroxidase activity expressed relative to the amount of TSP. **(D)** Antioxidant capacities and total phenols (mg/g of equivalents). Asterisks denote significant differences between treatments in each genotype (t-test, P<0.05). Bars show mean values ± SEM (n = 4-5 biological replicates), and different letters denote statistically significant differences between genotypes (Duncan analysis, P<0.05).

4.4 Discussion

The impact of water deficit at high temperature on phenotypic traits related to water use and biomass accumulation was assessed in ten spring wheat lines. The pool of genotypes with heterogeneous performance to drought stress or high temperature conditions was used to investigate genetic and environmental interaction (GxE) of trait response in a phenotyping platform with a controlled high temperature and water regime. Additionally, to understand the regulatory mechanisms of the primary carbohydrate and antioxidant metabolisms associated

with wheat response to drought at high temperature, the activities of key enzymes and metabolism associated with those pathways were analysed.

We identified an overall strong genotype reflectance signature throughout the experiment, which was intensified when temperature increased (30 DAS, Figure 4.1A). This indicates constitutive differences in pigments/secondary metabolites and leaf structure between genotypes (Merzlyak et al. 2003; Blackburn 2007). On the other hand, only NIR intensities (700-970nm) were related to the acclimatization to water deficit (LOD scores increased after 35 DAS, Figure 4.1B), consistently with the decrease of water content, as reported in previous drought experiments (Seelig et al. 2008; Chen et al. 2014; Junker et al. 2015).

Moreover, genotype-environment effects significantly changed evapotranspiration and leaf temperature throughout acclimatization to high temperature and water deficit (

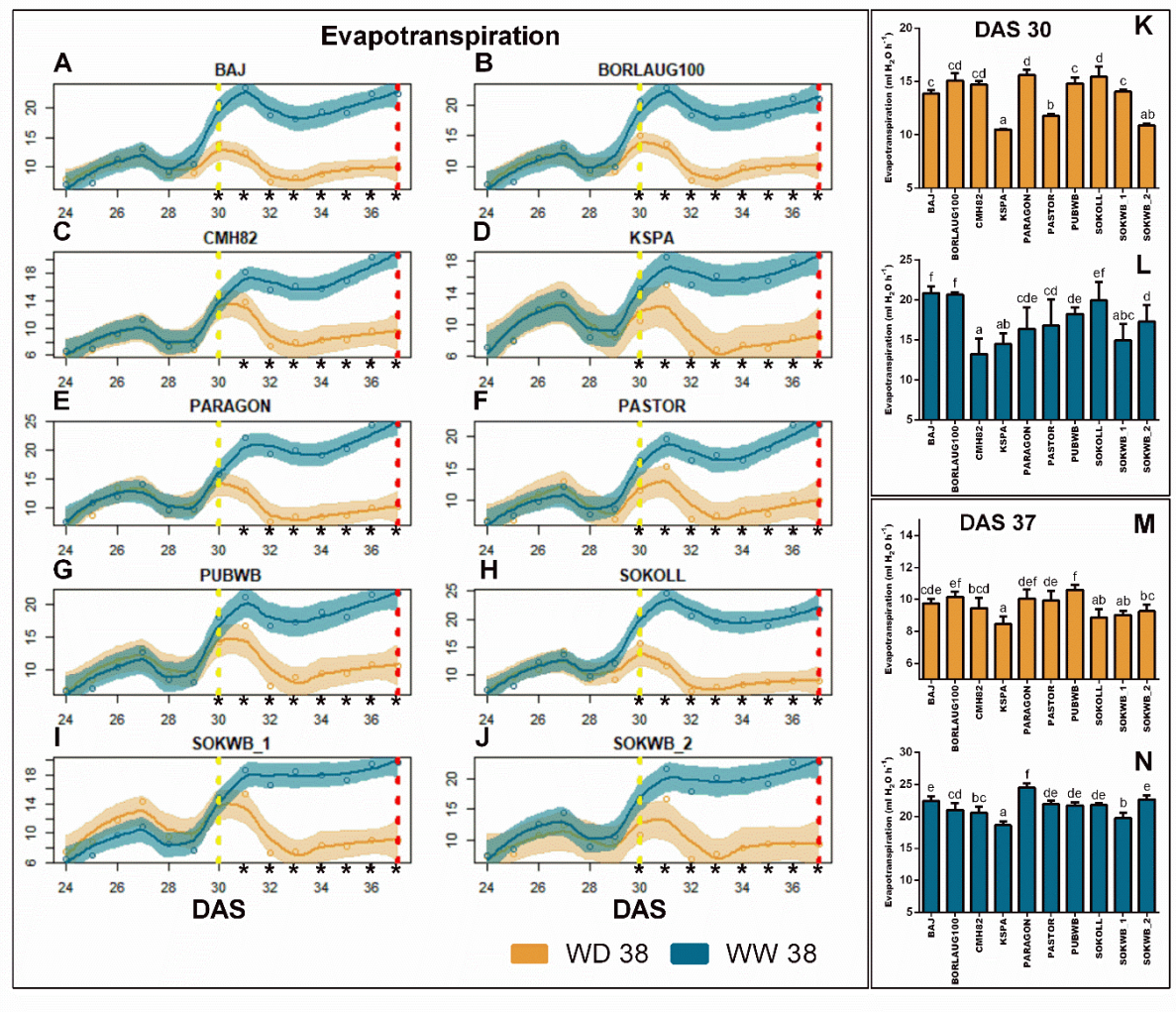

Figure 4.3). At the end of the experiment under WD38, all the genotypes decreased evapotranspiration to 40% relative to WW38, however we could identify three distinct transpiration behaviours in face of water deficit at high temperature. While CMH82, PARAGON and SOKWB_1 maintained the same evapotranspiration rate throughout the WD38 treatment; BAJ, BORLAUG and SOKOL (check lines) decreased transpiration gradually upon stress

imposition; and KSPA, PASTOR, PUBWB and SOKWB_2 decreased transpiration on the first day under WD38 (70% relatively to WW38), then maintained it stable for the following two days prior to a subsequent continuous decrease (Figure 4.2). Additionally, the data establish a correlation under WD38 between evapotranspiration and transpiration efficiency (ratio between biomass and evapotranspiration) (Figure 4.4A). On the other hand, evapotranspiration under WW38 was more related to aboveground biomass (Figure 4.4B). Schoppach et al. (2016) also identified a trade-off between night and day transpiration and biomass in wheat response to high vapour pressure deficit (VPD). Other studies associated transpiration efficiency and increased yield potential in well-watered and water-limited environments to high stomatal densities and conductance (Roche 2015; Shahinnia et al. 2016).

Despite the differences in the transpiration behaviour, all genotypes showed an effective evaporative cooling system in the first two days, except for KSPA, SOKWB_1 and 2, highlighting the dependence between transpiration and water use. Our data also showed a correlation between leaf temperature and the number of leaves under WD38 (Figure 4.4A). In WW38, the leaf temperature was correlated to the ratio between evapotranspiration and root biomass (Figure 4.4B). Low canopy temperature is usually associated to optimal root distribution to capture water for continuous evaporative cooling, which is dependent on the soil-water distribution (Lopes et al. 2012; Pinto and Reynolds 2015). As water use is essential for either drought or heat tolerance, these results suggest that traits such as low leaf number and adequate root architecture to a maximal soil moisture capture are essential to maintain the balance between evaporative cooling, water saving and photosynthesis in wheat genotypes growing under water deficit at high temperature.

We also found different growth dynamics and WUE. CMH82 was identified as highly tolerant to WD38, however this genotype also decreases the potential to biomass accumulation under WW38, showing the lowest WUE and mean productivity under both conditions. This behaviour would be advantageous under prolonged high temperature associated with very dry conditions, but most likely would have a negative effect under the more common agricultural conditions (Tardieu 2012; Parent et al. 2017). The tolerance mechanism was associated with a large modulation in the carbohydrate metabolism, with higher activity in most enzymes related to sucrolytic and glycolytic pathways (Figure 4.9). If carbohydrates are used for glycolysis in the leaves, sink strength is lost in other organs, and it is most likely that assimilates will be less available for reproductive organs and grain filling, causing yield penalties (Shokat et al. 2020; Roitsch and González 2004). Nevertheless, CMH82 showed higher activity of cytINV under WD38, which was previously associated with a faster recovery from water deficit and high temperature (Chapter II). On the other hand, KSPA showed high WUE under WW38 but high susceptibility to WD38, without major changes

in the carbohydrate metabolism. These results suggest that modulation of the carbohydrate metabolism upon water deficit at high temperature can be regarded as an essential protective mechanism. Paragon showed the best trad-off between WUE efficiency under WD38/WW38 and biomass production, demonstrating tolerance to growth under high temperature and mid-water deficit generally experienced in field conditions. Most of the genotypes with high WUE under WD38 showed higher activity of HXK under this condition. HXK is responsible for the phosphorylation of hexoses (Figure S4.1), acting as a glucose sensor to interconnect nutrient, light, and hormone signaling networks for controlling growth in response to environmental variations (Moore et al. 2003) and is associated with the acquisition of desiccation tolerance (Whittaker et al. 2001). Almost all the genotypes demonstrated high activity of PFK related to the increase of glycolysis and reallocation of carbohydrates to respiration under WD38. The increase of cytINV and vacINV activities was also observed in leaves of barley exposed to high temperature (Antonio Cuesta-Seijo et al. 2019), while tomato leaves exposed to water deficit demonstrated lower activity of cytINV and vacINV (Albacete et al. 2015). Likewise, hexoses accumulation was only observed in leaves under WD38 (Figure S4.4), showing that besides the increase of the sucrolytic activity under WW38, carbohydrates are being remobilized to other tissues.

Concerning the antioxidant enzymes evaluated, POX showed the highest genotype-environment effect, and although the different genotypes demonstrated different levels, all of them increased POX activity under WD38. These results the importance of POX activity in oxygen peroxide (H_2O_2) scavenging under water deficit and high temperature, resulting in better control of ROS levels and protection against oxidative damage. Other studies also highlighted the importance of the modulation of Peroxidases activities to ROS scavenging under drought and high temperature (Koussevitzky et al. 2008; Zandalinas et al. 2017). ROS detoxification under WD38 was also associated with a non-enzymatic antioxidant defence, demonstrated by the increase of antioxidant capacity (FRAP and TEAC) and by the production of phenolic compounds.

In summary, this study illustrates the importance of canopy architecture (namely, the number of leaves) to fine-tune transpiration to achieve an equilibrium between water-saving, leaf evaporative cooling and biomass production when water deficit occurs at high temperature, highlighting the importance of root distribution and transpiration efficiency to the maintenance of water uptake and transpiration/photosynthesis under these circumstances. Adjustments in the carbohydrate and antioxidant metabolism are essential to tolerate these stressful conditions, more specifically in the sucrolytic (cytINV), glycolytic pathways (HXK, PFK), and the ROS scavenging by POX and phenolic compounds. The integration of cell physiological phenotyping, via the semi-high-throughput determination of enzyme activity signatures and metabolites, with high-throughput phenotyping methods, proved to be an

efficient approach to quantitatively characterize genotype-environment interaction of complex traits. The application of this methodology into breeding programs will facilitate selection of promising candidates for wheat production in environments subjected to high temperature and drought.

4.5 Supplementary data

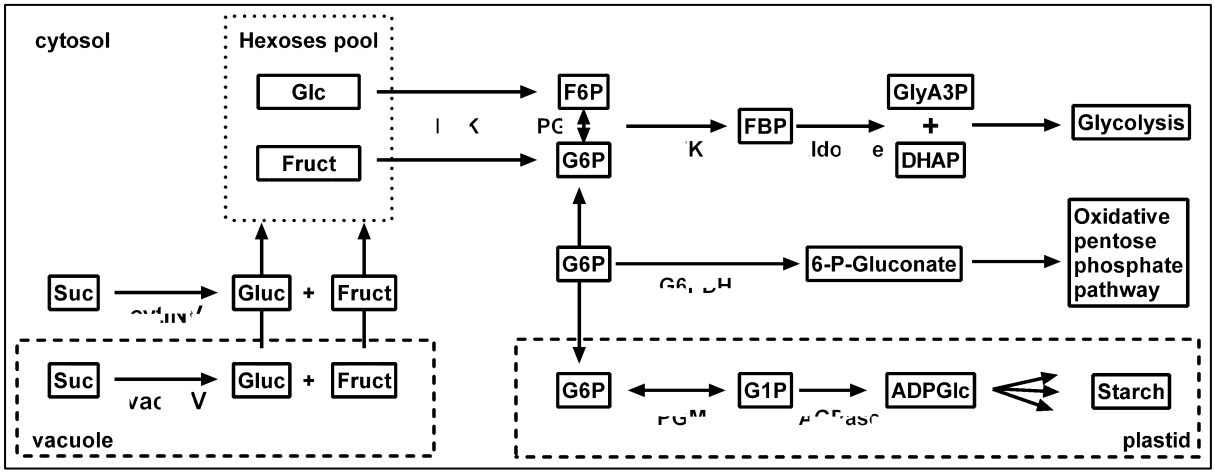

Figure S4.1 – Generalized scheme of the primary carbohydrate metabolism. Kinetic reactions of nine key enzymes are highlighted (grey). Vacuolar Invertase (vacINV) and cytoplasmic Invertase (cytINV), possess sucrolytic activity; Hexokinase (HXK), Phosphoglucoisomerase (PGI), Phosphofructokinase (PFK), and Aldolase (Ald) are important for glycolysis; ADP-glucose pyrophosphorylase (AGPase) and Phosphoglucomutase (PGM) are relevant for starch biosynthesis; Glucose-6-phosphate dehydrogenase (G6PDH) is critical for the oxidative pentose phosphate pathway. The figure is based on Jammer et al. 2015.

Table S4.1 – Lod scores table genotype effect. Statistical significance of genotype effect for each phenotype trait measured in each day. When LOD equal 0 the correspondent trait was not significative (adjusted *P*<0.05).

Genotype effect														
Traits	**LOD scores**													
AREA.low	3.82	4.59	0.00	0.00	3.91	5.62	28.00	14.88	5.11	2.13	2.28	5.65	4.72	1.64
Blue.460nm.low.reflect	13.69	17.19	0.00	0.00	20.68	27.02	64.05	44.69	27.75	19.76	17.82	24.60	25.58	16.74
Deep.red.700nm.low.reflect	10.33	15.08	0.00	0.00	20.24	25.85	61.00	48.71	30.92	22.52	20.06	25.64	26.02	16.51
EVAPT.ALL.Plant.evap	4.38	5.70	0.00	0.00	4.38	6.36	12.31	0.00	2.39	1.40	1.40	2.42	4.36	20.68
EVAPT.DAYtoNight.Plant.evap	1.76	2.10	0.00	0.00	1.70	5.34	27.83	12.52	0.00	2.71	1.98	4.27	2.28	11.69
EVAPT.Light.Plant.evap	0.00	8.65	0.00	0.00	4.45	8.48	6.26	6.67	0.00	2.07	0.00	2.90	1.98	10.80
Green.525nm.low.reflect	15.09	19.23	0.00	0.00	19.80	24.52	66.82	46.00	29.98	20.92	19.37	26.29	25.38	16.38
Leaf.therm	3.93	3.85	0.00	0.00	0.00	2.63	12.47	0.00	0.00	2.82	1.63	5.44	0.00	17.19
Leafznorm.therm	4.46	6.36	0.00	0.00	0.00	3.70	3.21	0.00	1.35	1.66	3.38	3.12	5.04	6.69
NIR.780nm.low.reflect	18.69	24.28	0.00	0.00	22.99	26.09	64.05	48.80	31.69	22.72	21.03	25.43	25.20	15.26
NIR.890nm.low.reflect	18.57	21.39	0.00	0.00	22.82	26.94	71.63	46.16	32.47	22.99	21.28	29.38	25.85	15.17
NIR.970nm.low.reflect	7.37	19.42	0.00	0.00	21.87	26.54	65.97	47.30	33.31	22.58	19.73	27.41	26.72	15.14
Red.645nm.low.reflect	11.57	11.69	0.00	0.00	22.01	18.84	61.51	46.84	30.08	20.91	18.97	25.96	25.41	16.20
Red.670nm.low.reflect	8.81	13.92	0.00	0.00	21.87	25.85	60.81	45.78	29.68	22.33	19.03	25.90	25.40	16.76
UVA.365nm.low.reflect	1.86	10.75	0.00	0.00	6.87	11.58	35.16	38.51	19.08	18.69	16.72	24.75	19.09	15.64
Yellow.570nm.low.reflect	8.02	14.48	0.00	0.00	19.08	21.74	53.48	42.11	26.25	19.17	18.14	26.55	26.00	14.18
DAS	24.00	25.00	26.00	27.00	28.00	29.00	30.00	31.00	32.00	33.00	34.00	35.00	36.00	37.00

Note: If LOD = 0 the correspondent trait was not significative (adjusted P<0.05).

Table S4.2 – Lod scores table treatment effect. Statistical significance of treatment effect for each phenotype trait measured in each day. When LOD equal 0 the correspondent trait was not significative (adjusted *P*<0.05).

Treatment effect														
Traits	**LOD scores**													
Area	0	0	0	0	0	0	2.1	4.09	0	0	2.79	9.76	13.18	7.61
Blue (460nm)	0	0	0	0	0	0	0	0	0	0	0	0	0	0
Deep red (700nm)	0	0	0	0	0	0	11.23	11.71	3.52	3.37	3.71	2.76	1.41	0
Evap. (day)	0	1.34	0	0	0	1.48	16.86	21.07	41.63	41.62	33.97	38.53	49.48	82.17
Evap. (night)	0	0	0	0	0	0	30.55	13.18	30.56	45.02	45.05	41.62	38.97	63.01
Evap. (light)	0	0	0	0	0	0	58.84	49.04	38.53	41.62	37.81	39.07	44.94	69.29
Green (525nm)	0	0	0	0	0	0	22.79	15.5	5.56	4.64	4.87	4.49	2.08	0
LeafT	0	2.13	0	0	0	0	0	2.68	34.69	41.62	33.58	29.49	17.39	20.14
LeafT (znorm)	0	0	0	0	0	0	2.17	6.52	31.25	21.44	23.72	12.24	11.5	18.82
NIR (780nm)	0	1.41	0	0	0	0	0	0	0	0	0	1.4	2.67	2.13
NIR (890nm)	0	0	0	0	0	0	0	0	0	0	0	3.04	3.45	2.38
NIR (970nm)	0	0	0	0	0	1.32	1.6	0	0	0	0	2.36	3.37	2.25
Red (645nm)	0	0	0	0	0	0	18.02	12.15	4.37	3.06	3.37	3.11	0	0
Red (670nm)	0	0	0	0	0	0	7.16	5.74	2.03	1.72	1.83	0	0	0
UVA (365nm)	0	0	0	0	0	0	0	2.13	0	0	0	0	0	0
Yellow (570nm)	0	0	0	0	0	0	18.74	19.7	6.57	6.65	6.82	5.51	3.97	1.34
DAS	**24**	**25**	**26**	**27**	**28**	**29**	**30**	**31**	**32**	**33**	**34**	**35**	**36**	**37**

Note: If LOD = 0 the correspondent trait was not significative (adjusted P<0.05).

Table S4.3 – Lod scores table GXE effect. Statistical significance of the genotype and treatment interaction effect for each phenotype trait measured in each day. When LOD equal 0 the correspondent trait was not significative (adjusted *P*<0.05).

G x E effect														
Traits	**LOD scores**													
Area	0	0	0	0	0	1.76	7.61	2.08	0	0	0	0	0	0
Blue (460nm)	1.89	1.45	0	0	0	2.08	6.48	2.41	0	0	0	0	0	0
Deep red (700nm)	3.7	0	0	0	1.88	3.65	11.8	5.52	1.81	0	0	0	0	0
Evap. (day)	0	4.03	0	0	0	1.79	5.63	3.88	0	0	0	0	0	10.44
Evap. (night)	1.47	2.38	0	0	1.7	0	23.57	16.46	2.87	0	1.51	1.86	0	6.48
Evap. (light)	0	3.85	0	0	0	3.11	12.41	9.93	0	1.78	0	0	1.49	9.25
Green (525nm)	2.5	1.47	0	0	0	2.57	10.44	4.47	0	0	0	0	0	0
LeafT	3.7	3.73	0	0	0	0	5.37	0	0	3.04	2.15	1.7	5.1	4.31
LeafT (znorm)	0	2.91	0	0	2.04	3.1	2.43	1.46	0	0	1.65	1.78	4.21	3.85
NIR (780nm)	1.47	2.71	0	0	1.46	2.86	9.27	3.34	0	0	0	0	0	0
NIR (890nm)	1.39	1.68	0	0	0	2.84	12.95	2.3	0	0	0	0	0	0
NIR (970nm)	3.65	0	0	0	2.38	3.85	11.99	2.82	0	0	0	0	0	0
Red (645nm)	3.19	0	0	0	1.94	2.22	13.52	4.88	0	0	0	0	0	0
Red (670nm)	3.65	0	0	0	1.55	3.15	10.28	3.46	0	0	0	0	0	0
UVA (365nm)	4.76	1.9	0	0	3.27	2.7	13.52	1.8	1.36	0	0	0	0	0
Yellow (570nm)	4.26	2.98	0	0	1.5	5.1	10.93	4.97	1.46	0	0	0	0	0
DAS	**24**	**25**	**26**	**27**	**28**	**29**	**30**	**31**	**32**	**33**	**34**	**35**	**36**	**37**

Note: If LOD = 0 the correspondent trait was not significative (adjusted P<0.05).

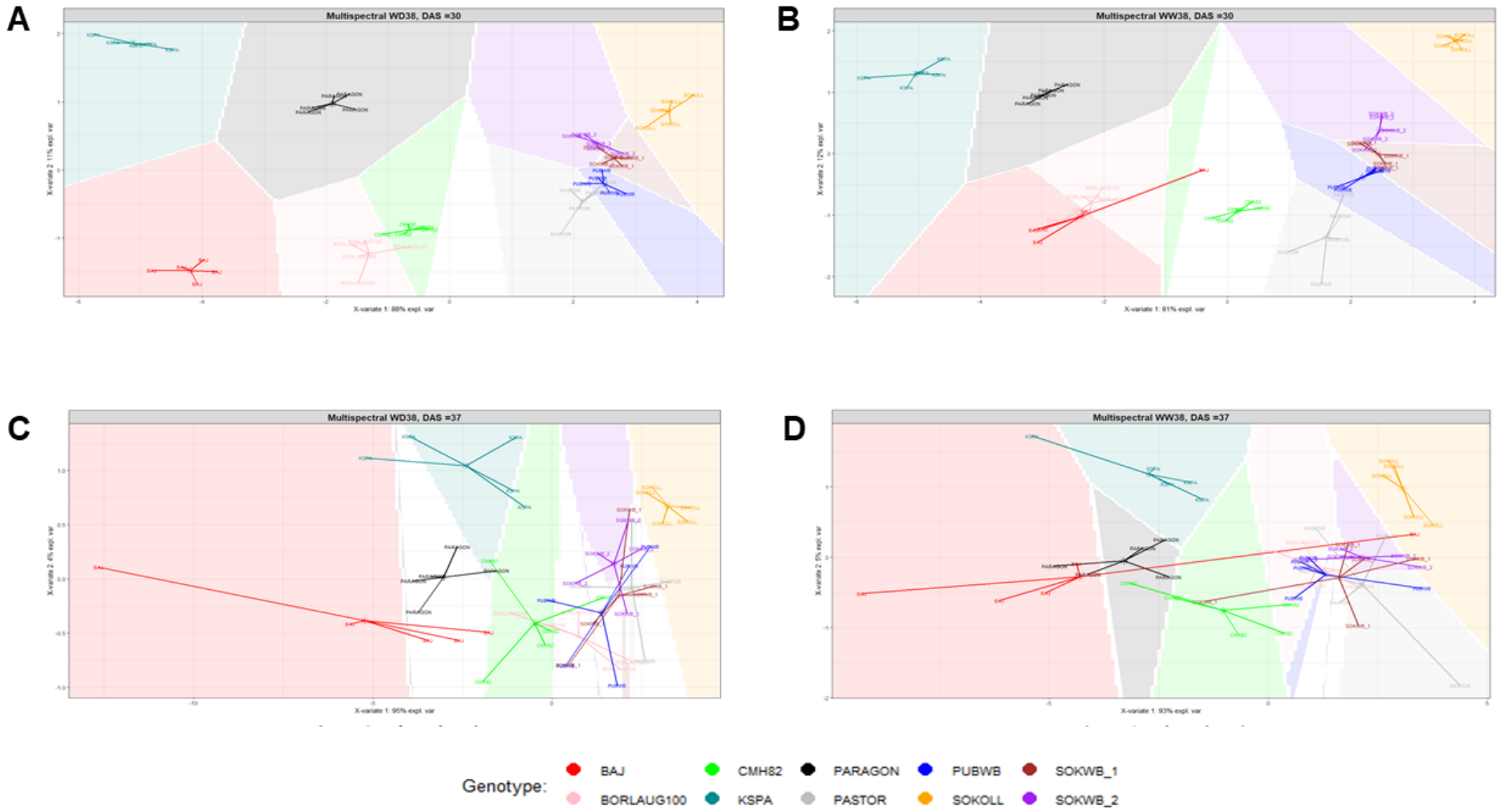

Figure S4.2 – Classification of wheat by multispectral signatures when exposed to high temperature (WW38, B and D) or water deficit at high temperature (WD38, A and C). (A-B) Partial least squares discrimination of wheat plants on the first day after stress imposition (30 DAS). **(C-D)** Discrimination at the end of the experiment (37 DAS). Background colours are predicted areas for the space representation of each genotype based on the centroid distance.

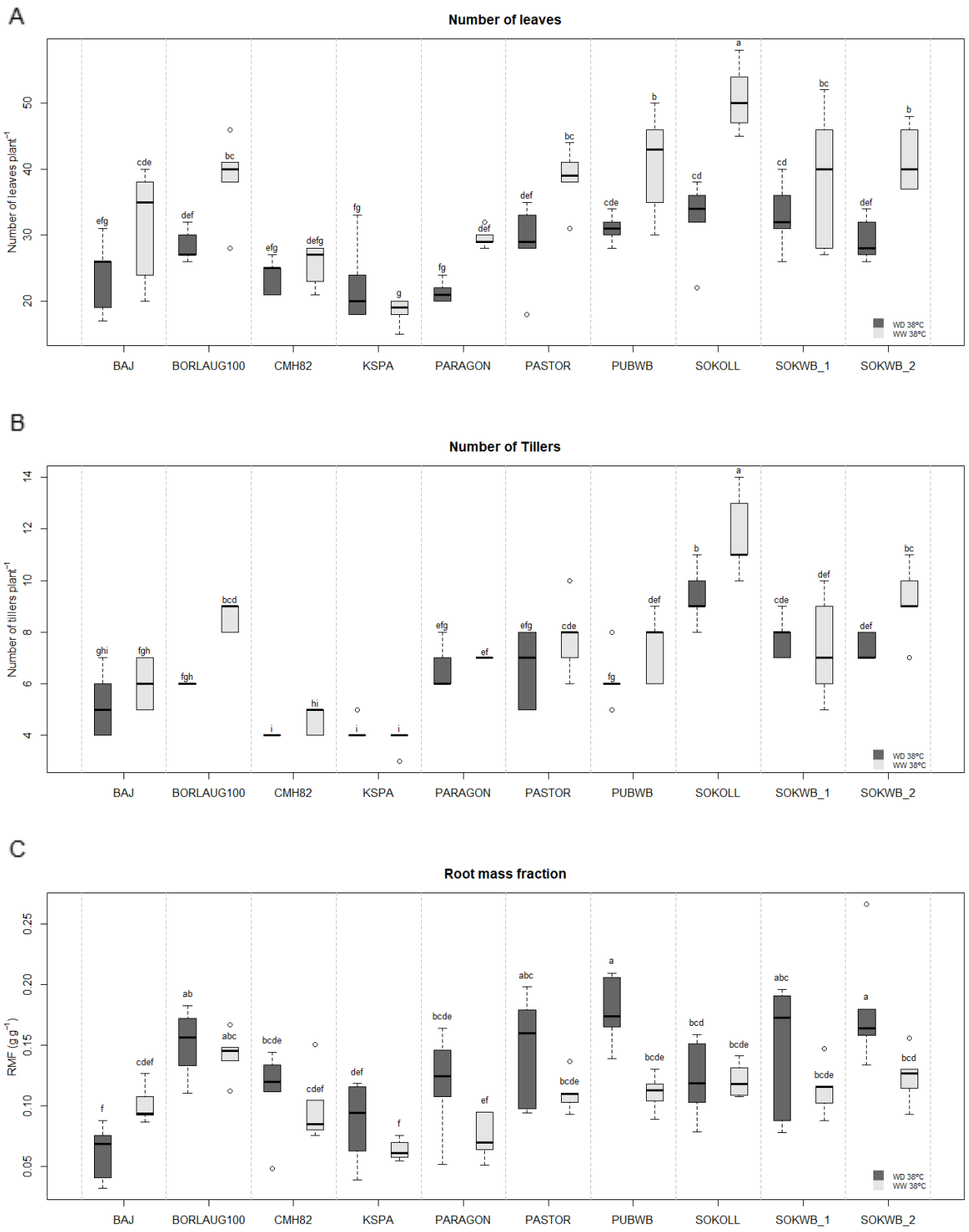

Figure S4.3 – Above ground architecture and root mass fraction of wheat when exposed to high temperature (WW38) or water deficit at high temperature (WD38). (A) The number of leaves. **(B)** The number of tillers. **(C)** Root mass fraction. Box plots show median values and interquartile range (IQR) (n = 5 biological replicates), and different letters denote statistically significant differences between genotypes (Duncan analysis, *P*<0.05).

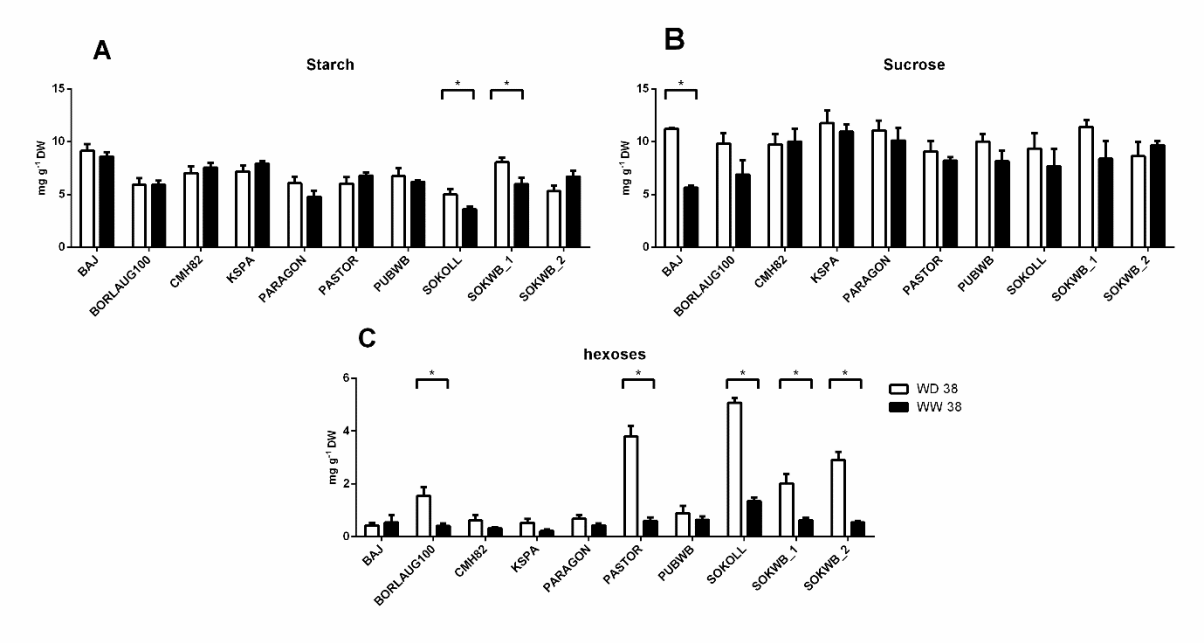

Figure S4.4 – Impact of high temperature (WW38) or water deficit at high temperature (WD38) on the (A) starch, (B) sucrose and (C) hexose content of wheat leaves. Values are means ± SEM (n = 5 biological replicates). Asterisks denote statistically significant differences between treatments in each genotype (t-test, *P*<0.05, A-C)

4.6 References

Albacete A, Cantero-Navarro E, Großkinsky DK, et al (2015) Ectopic overexpression of the cell wall Invertase gene CIN1 leads to dehydration avoidance in tomato. J Exp Bot 66:863–878. https://doi.org/10.1093/jxb/eru448

Albacete AA, Großkinsky DK, Roitsch T (2011) Trick and treat: a review on the function and regulation of plant Invertases in the abiotic stress response.

Antonio Cuesta-Seijo J, De Porcellinis AJ, Valente AH, et al (2019) Amylopectin Chain Length Dynamics and Activity Signatures of Key Carbon Metabolic Enzymes Highlight Early Maturation as Culprit for Yield Reduction of Barley Endosperm Starch after Heat Stress. Plant Cell Physiol 60:2692–2706. https://doi.org/10.1093/pcp/pcz155

ARAUS JL (2002) Plant Breeding and Drought in C_3 Cereals: What Should We Breed For? Ann Bot 89:925–940. https://doi.org/10.1093/aob/mcf049

Blackburn GA (2007) Hyperspectral remote sensing of plant pigments. J Exp Bot 58:855–867. https://doi.org/10.1093/jxb/erl123

Bouslama M, Schapaugh WT (1984) Stress Tolerance in Soybeans. I. Evaluation of Three Screening Techniques for Heat and Drought Tolerance 1 . Crop Sci 24:933–937. https://doi.org/10.2135/cropsci1984.0011183x002400050026x

Bradford MM (1976) A rapid and sensitive method for the quantitation of microgram quantities of protein utilizing the principle of protein-dye binding. Anal Biochem 72:248–254. https://doi.org/10.1016/0003-2697(76)90527-3

Carmo-Silva AE, Gore MA, Andrade-Sanchez P, et al (2012) Decreased CO 2 availability and inactivation of Rubisco limit photosynthesis in cotton plants under heat and drought stress in the field. Environ Exp Bot 83:1–11. https://doi.org/10.1016/j.envexpbot.2012.04.001

Chaves MM, Maroco JP, Pereira JS (2003) Understanding plant responses to drought — from genes to the whole plant. Funct Plant Biol 30:239. https://doi.org/10.1071/FP02076

Chen D, Fu LY, Hu D, et al (2018a) The HTPmod Shiny application enables modeling and visualization of large-scale biological data. Commun Biol 1:1–8. https://doi.org/10.1038/s42003-018-0091-x

Chen D, Neumann K, Friedel S, et al (2014) Dissecting the phenotypic components of crop plant growthand drought responses based on high-throughput image analysis w open. Plant Cell 26:4636–4655. https://doi.org/10.1105/tpc.114.129601

Chen D, Shi R, Pape JM, et al (2018b) Predicting plant biomass accumulation from image-derived parameters. Gigascience 7:1–13. https://doi.org/10.1093/gigascience/giy001

Correia PMP, da Silva AB, Roitsch T, et al (2020) Photoprotection and optimization of

sucrose usage contribute to faster recovery of photosynthesis after water deficit at high temperatures in wheat. Physiol Plant ppl.13227. https://doi.org/10.1111/ppl.13227

Costa JM, Grant OM, Chaves MM (2013) Thermography to explore plant-environment interactions. J. Exp. Bot. 64:3937–3949

Deryng D, Conway D, Ramankutty N, et al (2014) Global crop yield response to extreme heat stress under multiple climate change futures. Environ Res Lett 9:034011. https://doi.org/10.1088/1748-9326/9/3/034011

Duque AS, de Almeida AM, Bernardes da Silva A, et al (2013) Abiotic Stress Responses in Plants: Unraveling the Complexity of Genes and Networks to Survive. In: Abiotic Stress - Plant Responses and Applications in Agriculture. InTech

El Habti A, Fleury D, Jewell N, et al (2020) Tolerance of Combined Drought and Heat Stress Is Associated With Transpiration Maintenance and Water Soluble Carbohydrates in Wheat Grains. Front Plant Sci 11:1555. https://doi.org/10.3389/fpls.2020.568693

Fahlgren N, Gehan MA, Baxter I (2015) Lights, camera, action: High-throughput plant phenotyping is ready for a close-up. Curr Opin Plant Biol 24:93–99. https://doi.org/10.1016/j.pbi.2015.02.006

FAOSTAT (2019) Food and Agriculture Organization of the United Nations. http://www.fao.org/faostat/en/#data. Accessed 13 Jul 2020

Fimognari L, Dölker R, Kaselyte G, et al (2020) Simple semi-high throughput determination of activity signatures of key antioxidant enzymes for physiological phenotyping. Plant Methods 16:42. https://doi.org/10.1186/s13007-020-00583-8

Fiorani F, Schurr U (2013) Future Scenarios for Plant Phenotyping. Annu Rev Plant Biol 64:267–291. https://doi.org/10.1146/annurev-arplant-050312-120137

Fischer RA, Maurer R (1978) Drought resistance in spring wheat cultivars. I. Grain yield responses. Aust J Agric Res 29:897–912. https://doi.org/10.1071/AR9780897

Foyer CH, Noctor G (2005) Oxidant and antioxidant signalling in plants: A re-evaluation of the concept of oxidative stress in a physiological context. Plant, Cell Environ. 28:1056–1071

Giusti MM, Wrolstad RE (2001) Characterization and Measurement of Anthocyanins by UV-Visible Spectroscopy. Curr Protoc Food Anal Chem 00: https://doi.org/10.1002/0471142913.faf0102s00

Grubbs FE (1950) Sample Criteria for Testing Outlying Observations. Ann Math Stat 21:27–58. https://doi.org/10.1214/aoms/1177729885

Grzesiak MT, Marcińska I, Janowiak F, et al (2012) The relationship between seedling growth and grain yield under drought conditions in maize and triticale genotypes. Acta Physiol Plant 34:1757–1764. https://doi.org/10.1007/s11738-012-0973-3

Jammer A, Gasperl A, Luschin-Ebengreuth N, et al (2015) Simple and robust determination

of the activity signature of key carbohydrate metabolism enzymes for physiological phenotyping in model and crop plants. J Exp Bot 66:5531–5542. https://doi.org/10.1093/jxb/erv228

Junker A, Muraya MM, Weigelt-Fischer K, et al (2015) Optimizing experimental procedures for quantitative evaluation of crop plant performance in high throughput phenotyping systems. Front Plant Sci 5:1–21. https://doi.org/10.3389/fpls.2014.00770

Koussevitzky S, Suzuki N, Huntington S, et al (2008) Ascorbate peroxidase 1 plays a key role in the response of *Arabidopsis thaliana* to stress combination. J Biol Chem 283:34197–34203. https://doi.org/10.1074/jbc.M806337200

Kuhn M (2008) Building Predictive Models in R Using the caret Package. J Stat Software; Vol 1, Issue 5

Lascano HR, Antonicelli GE, Luna CM, et al (2001) Antioxidant system response of different wheat cultivars under drought: Field and in vitro studies. Aust J Plant Physiol 28:1095–1102. https://doi.org/10.1071/pp01061

Lawson T, Terashima I, Fujita T, Wang Y (2018) Coordination Between Photosynthesis and Stomatal Behavior. pp 141–161

Louis Joosen RV, Arends D, Li Y, et al (2013) Identifying genotype-by-environment interactions in the metabolism of germinating arabidopsis seeds using generalized genetical genomics. Plant Physiol 162:553–566. https://doi.org/10.1104/pp.113.216176

Manès Y, Gomez HF, Puhl L, et al (2012) Genetic yield gains of the CIMMYT International semi-arid wheat yield trials from 1994 to 2010. Crop Sci 52:1543–1552. https://doi.org/10.2135/cropsci2011.10.0574

Merzlyak MN, Gitelson AA, Chivkunova OB, et al (2003) Application of Reflectance Spectroscopy for Analysis of Higher Plant Pigments. Russ. J. Plant Physiol. 50:704–710

Moore B, Zhou L, Rolland F, et al (2003) Role of the Arabidopsis glucose sensor HXK1 in nutrient, light, and hormonal signaling. Science (80-) 300:332–336. https://doi.org/10.1126/science.1080585

Moore G (2015) Strategic pre-breeding for wheat improvement. Nat. Plants 1

Moshelion M (2020) The dichotomy of yield and drought resistance. EMBO Rep 21:e51598. https://doi.org/10.15252/embr.202051598

Nunes C, Araújo S., Silva JM, et al (2009) Photosynthesis light curves: a method for screening water deficit resistance in the model legume *Medicago truncatula*. Ann Appl Biol 155:321–332. https://doi.org/10.1111/j.1744-7348.2009.00341.x

Parent B, Bonneau J, Maphosa L, et al (2017) Quantifying wheat sensitivities to environmental constraints to dissect genotype × environment interactions in the field. Plant Physiol 174:1669–1682. https://doi.org/10.1104/pp.17.00372

Pennacchi JP, Carmo-Silva E, Andralojc PJ, et al (2019) Stability of wheat grain yields over three field seasons in the UK. Food Energy Secur 8:e00147. https://doi.org/10.1002/fes3.147

Pinheiro C, Chaves MM (2011) Photosynthesis and drought: Can we make metabolic connections from available data? J Exp Bot 62:869–882. https://doi.org/10.1093/jxb/erq340

Reynolds MP, Pask AJD, Hoppitt WJE, et al (2017) Strategic crossing of biomass and harvest index—source and sink—achieves genetic gains in wheat. Euphytica 213:257. https://doi.org/10.1007/s10681-017-2040-z

Reynolds MP, Pierre C Saint, Saad ASI, et al (2007) Evaluating Potential Genetic Gains in Wheat Associated with Stress-Adaptive Trait Expression in Elite Genetic Resources under Drought and Heat Stress. Crop Sci 47:. https://doi.org/10.2135/cropsci2007.10.0022IPBS

Rizhsky L, Liang H, Shuman J, et al (2004) When defense pathways collide. The response of arabidopsis to a combination of drought and heat stress 1[w]. Plant Physiol 134:1683–1696. https://doi.org/10.1104/pp.103.033431

Rohart F, Gautier B, Singh A, Lê Cao K-A (2017) mixOmics: An R package for 'omics feature selection and multiple data integration. PLOS Comput Biol 13:e1005752. https://doi.org/10.1371/journal.pcbi.1005752

Roitsch T, Cabrera-Bosquet L, Fournier A, et al (2019) Review: New sensors and data-driven approaches—A path to next generation phenomics. Plant Sci. 282:2–10

Roitsch T, González MC (2004) Function and regulation of plant Invertases: Sweet sensations. Trends Plant Sci. 9:606–613

Sairam RK, Srivastava GC, Saxena DC (2000) Increased antioxidant activity under elevated temperatures: A mechanism of heat stress tolerance in wheat genotypes. Biol Plant 43:245–251. https://doi.org/10.1023/A:1002756311146

Secchi F, Zwieniecki MA (2016) Accumulation of sugars in the xylem apoplast observed under water stress conditions is controlled by xylem pH. Plant Cell Environ 39:2350–2360. https://doi.org/10.1111/pce.12767

Seelig HD, Hoehn A, Stodieck LS, et al (2008) The assessment of leaf water content using leaf reflectance ratios in the visible, near-, and short-wave-infrared. Int J Remote Sens 29:3701–3713. https://doi.org/10.1080/01431160701772500

Shokat S, Großkinsky DK, Roitsch T, Liu F (2020) Activities of leaf and spike carbohydrate-metabolic and antioxidant enzymes are linked with yield performance in three spring wheat genotypes grown under well-watered and drought conditions. BMC Plant Biol 20:400. https://doi.org/10.1186/s12870-020-02581-3

Shokat S, Großkinsky DK, Roitsch T, Liu F Activity of leaf and spike carbohydrate-metabolic

and antioxidant enzymes linked with yield performance in three spring wheat genotypes grown under well-watered and drought conditions. https://doi.org/10.21203/rs.2.24180/v3

Singleton VL, Orthofer R, Lamuela-Raventós RM (1999) Analysis of total phenols and other oxidation substrates and antioxidants by means of folin-ciocalteu reagent. Methods Enzymol 299:152–178. https://doi.org/10.1016/S0076-6879(99)99017-1

Stekhoven DJ, Bühlmann P (2012) Missforest-Non-parametric missing value imputation for mixed-type data. Bioinformatics 28:112–118. https://doi.org/10.1093/bioinformatics/btr597

Tardieu F (2012) Any trait or trait-related allele can confer drought tolerance: Just design the right drought scenario. J Exp Bot 63:25–31. https://doi.org/10.1093/jxb/err269

Tardieu F, Cabrera-Bosquet L, Pridmore T, Bennett M (2017) Plant Phenomics, From Sensors to Knowledge. Curr Biol 27:R770–R783. https://doi.org/10.1016/j.cub.2017.05.055

Tricker PJ, Elhabti A, Schmidt J, Fleury D (2018) The physiological and genetic basis of combined drought and heat tolerance in wheat. J. Exp. Bot. 69:3195–3210

Whittaker A, Bochicchio A, Vazzana C, et al (2001) Changes in leaf Hexokinase activity and metabolite levels in response to drying in the desiccation-tolerant species Sporobolus stapfianus and Xerophyta viscosa. J Exp Bot 52:961–969. https://doi.org/10.1093/jexbot/52.358.961

Zampieri M, Ceglar A, Dentener F, Toreti A (2017) Wheat yield loss attributable to heat waves, drought and water excess at the global, national and subnational scales. Environ Res Lett 12:. https://doi.org/10.1088/1748-9326/aa723b

Zandalinas SI, Balfagón D, Arbona V, Gómez-Cadenas A (2017) Modulation of Antioxidant Defense System Is Associated with Combined Drought and Heat Stress Tolerance in Citrus. Front Plant Sci 8:953. https://doi.org/10.3389/fpls.2017.00953

Zhang G, Zhang M, Zhao Z, et al (2017) Wheat TaPUB1 modulates plant drought stress resistance by improving antioxidant capability. Sci Rep 7:1–13. https://doi.org/10.1038/s41598-017-08181-w

Zhishen J, Mengcheng T, Jianming W (1999) The determination of flavonoid contents in mulberry and their scavenging effects on superoxide radicals. Food Chem 64:555–559. https://doi.org/10.1016/S0308-8146(98)00102-2

Chapter V

General Discussion and Future Perspectives

Heat and drought are environmental pressures limiting crop productivity worldwide, accounting for a major share of the global inter-annual yield fluctuations in some of the most produced crops. Moreover, climatic models predict that global temperature will increase along this century and episodes of extreme temperatures associated with periods of water shortage will be more frequent in some regions, causing additional damage to crop production. Those challenges on food security prospects will cause devastating economic and social impacts if new strategies to reduce crop losses are not applied. Therefore, this emphasises the need to develop crops more resilient to high temperature and water deficit. However, the tolerance to drought at high temperature is highly intricate, compared with the tolerance to single heat or drought stresses, involving crosstalk between co-activated pathways at different levels, and the interplay between the two stresses has been less studied than the response to the individual stresses.

The main goal of this work was to improve the understanding of crop physiological responses involved in tolerance to high temperature in co-occurrence with drought. To achieve this, two of the most produced crops, wheat and maize, with contrasting photosynthetic mechanisms, were investigated under these environmental conditions. This discussion provides an integrated overview of the major findings reported in the previous chapters, including additional research directions to complement or follow up the present work, with the aim to contribute to further improve research in this topic.

5.1 Impact of drought at high temperature on wheat physiology

In spite of the distinct geographical provenience of two of the studied spring wheat cultivars, Paragon (UK cultivar) and Sokoll (Mexican synthetic-derived cultivar), under our experimental conditions, in the absence of water deficit, both genotypes successfully acclimatised to high temperature. Some authors argued that most of the modern wheat cultivars are heat tolerant when water is available (Parent et al. 2017; Tricker et al. 2018). Our results reinforce the idea that to improve wheat tolerance to the projected climatic condition, where precipitation will be scarce and water less available to maintain irrigation systems, plants must be studied under combined conditions (Parent et al. 2017; Tricker et al. 2018). Furthermore, Paragon was photosynthetically more efficient under water deficit. However, the combination of conditions was equally deleterious for ETR and carbon assimilation rate in both genotypes, highlighting the uniqueness of combined response and the more harmful consequences.

Nevertheless, Paragon could recover photosynthetic performance faster than Sokoll when water supply was re-established, and temperature decreased to 25ºC, and this was associated with higher cytINV activity and light-energy dissipation capacity (Chapter II). The ability of crops to maintain physiological functions and recover photosynthesis faster after stress is one of the major processes contributing to the maintenance of productivity and yield under

fluctuating environmental conditions (Izanloo et al. 2008; Abid et al. 2018). To further unravel the role of the cytINV and the carbohydrate metabolism in response to high temperature, key carbohydrate enzymes were investigated in a larger pool of genotypes (chapter IV) that have previously shown diverse performance under water deficit or high temperature conditions in CIMMYT's SATYN experiments (Solís Moya and Camacho Casas 2016; Reynolds et al. 2017). Taking advantage of the genetic diversity and response to water deficit at high temperature, we found that cytINV was involved in a tolerance mechanism connected to higher WUE (CMH82). However, we also found significant differences in cytINV activity between the genotypes, and the increase of activity was also associated with a more conservative strategy, allowing these plants to tolerate stress with a possible penalty to biomass accumulation and yield under normal conditions. These results suggest that higher cytINV activity could be advantageous in more stressful conditions, and could foster recovery from intense drought and high temperature stress predicted in the future, however, its advantage in more moderate conditions needs to be established.

Additionally, most of the genotypes with higher WUE under water deficit at high temperature increased the activity of HXK. HXK, in addition to its hexoses catalytic phosphorylation activity, was previously associated with a glucose-sensing function, involved in the repression of photosynthetic genes or modulation of enzymes related to biosynthetic and energy producing pathways (Jang et al. 1997; Aguilera-Alvarado and Sanchez-Nieto 2017). Several studies demonstrated the presence of cytINV in mitochondria and plastids (Murayama and Handa 2007; Vargas et al. 2007) and HXK in plastids, mitochondria and in the nucleus (Jang et al. 1997; Zhang et al. 2010; Granot et al. 2013). Further characterisation of isoenzymes expression and localisation could help to elucidate the relevance of enzymatic activity changes, the interplay between cytINV and HXK and its relevance for growth, development and signalling under episodes of water deficit and high temperature. Some authors proposed a network involving mitochondrial bound HXK activity and mitochondrial and/or cytINV activities, where glucose originating from Invertase activity may serve as a substrate for the HXK contributing to mitochondrial ROS homeostasis (Xiang et al. 2011). Nevertheless, ROS scavenging capacity was increased under water deficit at 38ºC and related to the action of antioxidant enzymes, highlighting the pivotal role of POX in H_2O_2 scavenging and the production of phenolic compounds. A scenario in which the catalytic activity of HXK regulates phenolic compounds poll, through glucose-6-phosphate synthesis, also hypothesizes that vacuolar sugars in combination with phenolic compounds form a vacuolar redox system that acts in cytoplastic antioxidant mechanisms (Bolouri-Moghaddam et al. 2010). In parallel, authors suggested a synergistic association between the synthesis of soluble sugars and ROS scavenging potential and the ability of wheat to withstand and survive water-deficit conditions (Abid et al. 2018).

A similar system regulating ROS homeostasis in chloroplasts, as occurring in the mitochondria, involving HXK and cytINV activities was also suggested (Bolouri-Moghaddam et al. 2010; Valluru and Van den Ende 2011), but it is yet to be proven. Therefore, it would be interesting to further characterise the photoprotection mechanism involved in the response to water deficit at high temperature. It has been reported that overexpression of some NPQ components, such as the PSII subunit S (PsbS) and the enzymes involved in the xanthophylls cycle (violaxanthin de-epoxidase, zeaxanthin epoxidase) contribute to accelerate the induction and relaxation of NPQ, leading to higher radiation use efficiency, biomass and yield in tobacco plants growing in the field (Kromdijk et al. 2016) and rice in greenhouse conditions (Hubbart et al. 2018). These players were also involved in stomata control signalling, decreasing stomatal conductance and contributing to the reduction in water loss per CO_2 assimilated in tobacco plants under field conditions without water privation (Głowacka et al. 2018). Further exploration of NPQ regulation machinery and the identification of key players involved in excess energy dissipation would be essential to define the mechanisms involved in photoprotection during episodes of high temperature conjugated with drought. It would also be interesting to further elucidate the sucrose metabolism role in embolism refilling and xylem function restoration under conditions of water deficit and high temperature, and its influence on photosynthetic recovery in wheat.

We also identify phenotypic traits conferring adaptative stress responses by monitoring and comparing the performance of 10 wheat genotypes during the acclimatisation under high temperature and well-watered or water deficit conditions. We found that low leaf number and transpiration efficiency was associated with a higher stress tolerance (chapter III). These results suggest that these traits were acquired through adaptation to environmental conditions as high temperature and water deficit. However, as suggested by other authors, a fine-tuning of hydraulic control via highly dense small stomata or patchy closure (Vile et al. 2012; Roche 2015; Shahinnia et al. 2016) must also be involved in this mechanism as a water deprivation avoidance strategy. Further experiments connecting anatomical (number/ size of stomata), phenological (number, shape and angle of leaves) and functional traits (stomatal conductance and transpiration rate) to stress tolerance will help to elucidate the role of each component in the adaptation to fluctuations in water deficit associated to high temperature.

5.2 Involvement of the CCM in response to water deficit at high temperature

C_4 crops, such as maize, are known to have a relatively higher temperature optimum than C_3 crops. We explored the CCM role in the tolerance of maize to water deficit under high temperature. Despite the contrasting levels of drought and heat tolerance, both maize cultivars successfully acclimatised to high temperature conditions, although with different mechanisms

(chapter III). While plants of B73 maintained photosynthetic rates by increasing gs, the more tolerant line P0023 showed limited transpiration. Under water deficit at high temperature, P0023 maintained better cellular hydration and showed higher photosynthetic activity. These characteristics can allow water conservation in initial periods of soil drying, acting beneficially as a stress avoidance mechanism when water deficit is associated with high temperature.

Even though some authors suggested that the limited transpiration trait was related to the expression and regulation of aquaporins (Shekoofa and Sinclair 2018), it is still unknown how an increase in the temperature modulates the expression of aquaporins and the involved signalling regulatory pathways warrant further study. Therefore, it would be interesting to explore the role of aquaporins in the reduction of transpiration in P0023. The simultaneous expression of adjusted root architecture, allowing a prolonged water extraction under high temperature, and limited transpiration could be beneficial to maintain the hydraulic and stomatal conductance under water deficit and high temperature. Future experiments with simultaneous phenotyping of root, biomass traits and stomatal conductance could help in the selection of genotypes with those characteristics and test the hypothesis that this would be beneficial under those co-occurring conditions and in elucidating the mechanisms involved in the expression of those traits.

The results in chapter III also suggest that the maintenance of the hydraulic continuum could buffer the increase of temperature near the vascular tissues and be correlated to the higher ETR, maintaining the activity of some enzymes and the integrity of structural components more prone to be thermaly inhibited or degraded. Testing this hypothesis in genotypes selected in the previously suggested phenotyping experiment could help to assess if there is a correlation between the maintenance of the hydraulic continuum and the functional activity of some critical components of the C_4 photosynthetic apparatus. Additionally, in P0023, higher photosynthetic activity was correlated with the regulation of PEPC – higher level of phosphorylation and activation state, under water deficit and high temperature. Recently, it has been reported that phosphorylation of the Ser419 residue of NADP-ME was also involved in tuning the CCM in the first hours of light (Bovdilova et al. 2019). The involvement of the post-translational modifications in the regulation of PEPC, NADP-ME, Rubisco and other enzymes engaged in adjusting the CCM under fluctuating conditions of high temperature and water deficit should also be further explored. In parallel, it has also been suggested that, in maize, there is an adjustment of the decarboxylating process to abiotic stresses, such as high temperature and drought, increasing the usage of other decarboxylation pathways (Furbank 2011; von Caemmerer and Furbank 2016). The prevalence of other decarboxylating pathways, alternative to NADP-ME decarboxylation, and its relevance for tolerating unfavourable environmental conditions can also be explored. Furthermore, future experiments should also investigate putative changes in ETR components in BSC and MC, notably PSII

activity, and consider its requirement for the energetic adjustment to alternative decarboxylating pathways.

5.3 Conclusion

This work contributed to a better understanding of the impact of heatwaves combined with water scarcity on crop physiological and biochemical processes, and to identify response mechanisms associated with a better performance under these conditions, predicted to increase in their co-occurrence in the future. Wheat and maize are two key crops that differ in their photosynthetic mechanism. A range of genotypes of both species were investigated under high temperature in isolation and combined with water deficit. The research also raised new questions that can be assessed in future research, as detailed above. The findings can inform selection of genotypes and traits to feed into breeding programs, aiming for the early selection of crop lines to be tested in an agricultural context and contribute to increasing crop productivity under these environmental conditions.

5.4 References

Abid M, Ali S, Qi LK, et al (2018) Physiological and biochemical changes during drought and recovery periods at tillering and jointing stages in wheat (*Triticum aestivum* L.). Sci Rep 8:1–15. https://doi.org/10.1038/s41598-018-21441-7

Bolouri-Moghaddam MR, Le Roy K, Xiang L, et al (2010) Sugar signalling and antioxidant network connections in plant cells. FEBS J. 277:2022–2037

Bovdilova A, Alexandre BM, Höppner A, et al (2019) Posttranslational modification of the NADP-malic enzyme involved in C_4 photosynthesis modulates the enzymatic activity during the day. Plant Cell 31:2525–2539. https://doi.org/10.1105/tpc.19.00406

Furbank RT (2011) Evolution of the C 4 photosynthetic mechanism: Are there really three C 4 acid decarboxylation types? J. Exp. Bot. 62:3103–3108

Głowacka K, Kromdijk J, Kucera K, et al (2018) Photosystem II Subunit S overexpression increases the efficiency of water use in a field-grown crop. Nat Commun 9:1–9. https://doi.org/10.1038/s41467-018-03231-x

Granot D, David-Schwartz R, Kelly G (2013) Hexose kinases and their role in sugar-sensing and plant development. Front. Plant Sci. 4

Hubbart S, Smillie IRA, Heatley M, et al (2018) Enhanced thylakoid photoprotection can increase yield and canopy radiation use efficiency in rice. Commun Biol 1:1–12.

https://doi.org/10.1038/s42003-018-0026-6

Izanloo A, Condon AG, Langridge P, et al (2008) Different mechanisms of adaptation to cyclic water stress in two South Australian bread wheat cultivars. J Exp Bot 59:3327–3346. https://doi.org/10.1093/jxb/ern199

Jang JC, León P, Zhou L, Sheen J (1997) Hexokinase as a sugar sensor in higher plants. Plant Cell 9:5–19. https://doi.org/10.1105/tpc.9.1.5

Kromdijk J, Głowacka K, Leonelli L, et al (2016) Improving photosynthesis and crop productivity by accelerating recovery from photoprotection. Science (80-) 354:857–861. https://doi.org/10.1126/science.aai8878

Murayama S, Handa H (2007) Genes for alkaline/neutral Invertase in rice: Alkaline/neutral Invertases are located in plant mitochondria and also in plastids. Planta 225:1193–1203. https://doi.org/10.1007/s00425-006-0430-x

Parent B, Bonneau J, Maphosa L, et al (2017) Quantifying wheat sensitivities to environmental constraints to dissect genotype × environment interactions in the field. Plant Physiol 174:1669–1682. https://doi.org/10.1104/pp.17.00372

Paulina Aguilera-Alvarado G, Sanchez-Nieto S (2017) Plant Hexokinases are Multifaceted Proteins. Plant Cell Physiol 58:1151–1160. https://doi.org/10.1093/pcp/pcx062

Reynolds MP, Pask AJD, Hoppitt WJE, et al (2017) Strategic crossing of biomass and harvest index—source and sink—achieves genetic gains in wheat. Euphytica 213:257. https://doi.org/10.1007/s10681-017-2040-z

Roche D (2015) Stomatal Conductance Is Essential for Higher Yield Potential of C_3 Crops. CRC Crit Rev Plant Sci 34:429–453. https://doi.org/10.1080/07352689.2015.1023677

Shahinnia F, Roy J Le, Laborde B, et al (2016) Genetic association of stomatal traits and yield in wheat grown in low rainfall environments. BMC Plant Biol 16:150. https://doi.org/10.1186/s12870-016-0838-9

Shekoofa A, Sinclair T (2018) Aquaporin Activity to Improve Crop Drought Tolerance. Cells 7:123. https://doi.org/10.3390/cells7090123

Solís Moya E, Camacho Casas MA (2016) Evaluation of the Stress Adaptive Trait Yield Nursery (SATYN) in irrigated wheat growing locations in Mexico during the 2015-16 growing season. Proc 2nd Int TRIGO Yield Potential 10–14

Tricker PJ, Elhabti A, Schmidt J, Fleury D (2018) The physiological and genetic basis of combined drought and heat tolerance in wheat. J. Exp. Bot. 69:3195–3210

Vargas WA, Pontis HG, Salerno GL (2007) Differential expression of alkaline and neutral Invertases in response to environmental stresses: Characterization of an alkaline isoform as a stress-response enzyme in wheat leaves. Planta 226:1535–1545. https://doi.org/10.1007/s00425-007-0590-3

Vile D, Pervent M, Belluau M, et al (2012) Arabidopsis growth under prolonged high temperature and water deficit: Independent or interactive effects? Plant, Cell Environ 35:702–718. https://doi.org/10.1111/j.1365-3040.2011.02445.x

von Caemmerer S, Furbank RT (2016) Strategies for improving C_4 photosynthesis. Curr. Opin. Plant Biol. 31:125–134

Xiang L, Le Roy K, Bolouri-Moghaddam MR, et al (2011) Exploring the neutral Invertase-oxidative stress defence connection in *Arabidopsis thaliana*. J Exp Bot 62:3849–3862. https://doi.org/10.1093/jxb/err069

Zhang ZW, Yuan S, Xu F, et al (2010) The plastid Hexokinase pHXK: A node of convergence for sugar and plastid signals in Arabidopsis. FEBS Lett 584:3573–3579. https://doi.org/10.1016/j.febslet.2010.07.024